Lehrstuhl für Fluidverfahrenstechnik
der
Technischen Universität München

Efficient Energy Storage in Liquid Desiccant Cooling Systems

Astrid Hublitz

Vollständiger Abdruck der von der Fakultät für Maschinenwesen
der Technischen Universität München zur Erlangung des akademischen Grades eines
Doktor-Ingenieurs
genehmigten Dissertation.

Vorsitzender:	Univ.-Prof. Dr.-Ing. D. Weuster-Botz
Prüfer der Dissertation:	1. Univ.-Prof. Dr.-Ing., Dr.-Ing. habil. J. Stichlmair, em.
	2. Univ.-Prof. Dr.-Ing. habil. H. Spliethoff

Die Dissertation wurde am 02.01.2008 bei der Technischen Universität München eingereicht und durch die Fakultät für Maschinenwesen am 18.07.2008 angenommen.

I dedicate this dissertation to my parents, Melitta and Bruno Hublitz,
who have always supported my adventures and endeavors.
Their love and guidance encouraged me to reach innumerable goals.
I also dedicate this dissertation to my sister, Dr. Inka Hublitz,
who has been one of my engineering role models.

Acknowledgments

First and foremost, I would like to express my deep gratitude to my major advisor Prof. Dr.-Ing. Johann Stichlmair for giving me the unique opportunity to complete my dissertation under his guidance.

I am also thankful to the members of my supervisory committee Prof. Dr.-Ing. Hartmut Spliethoff and Prof. Dr.-Ing. Dirk Weuster-Botz.

Furthermore, I am indebted to Eberhard Lävemann for sharing his great expertise and his huge amount of support and advice.

I would also like to thank Dr. Andreas Hauer and Wolfgang Schölkopf for providing the financial support for the project and for offering me the chance to participate in various national and international conferences to constantly increase my network of colleagues working in relevant fields.

I also acknowledge my colleagues from the Bavarian Center for Applied Energy Research and would especially like to thank

- Georg Storch for his enormous support and helpful suggestions,
- Wolfgang Dallmayer for teaching me applied solar engineering,
- Michael Landspersky, Ricardo Ehrenpford and Carsten Lampe for their hard work that was always greatly appreciated.

Abstract

Efficient Energy Storage in Liquid Desiccant Cooling Systems

Liquid Desiccant Cooling Systems (LDCS) are open loop sorption systems for air-conditioning that use a liquid desiccant such as a concentrated salt solution to dehumidify the outside air and cool it by evaporative cooling. Thermochemical energy storage in the concentrated liquid desiccant can bridge power mismatches between demand and supply. Low-flow LDCS provide high energy storage capacities but are not a state-of-the-art technology yet. The key challenge remains the uniform distribution of the liquid desiccant on the heat and mass transfer surfaces. The present research analyzes the factors of influence on the energy storage capacity by simulation of the heat and mass transfer processes and specifies performance goals for the distribution of the process media. Consequently, a distribution device for the liquid desiccant is developed that reliably meets the performance goals.

Effiziente Energiespeicherung in sorptionsgestützten Klimatisierungssystemen

Sorptionsgestützte Klimatisierungssysteme (SGK) entfeuchten Außenluft sorptiv und kühlen sie durch Verdunsten von Wasser. Die Entfeuchtung der Außenluft erfolgt z.B. mit einer konzentrierten Salzlösung (Sole), die sich verdünnt. Die thermochemische Speicherung von Energie in der konzentrierten Sole kann eine ungleiche Verteilung von Energiebedarf und -verfügbarkeit überbrücken. SGK mit geringen spezifischen Solemassenströmen erreichen hohe Energiespeicherdichten, sind aber noch in der Entwicklungsphase. Die größte technische Herausforderung ist die gleichmäßige Verteilung der Sole auf den Wärme- und Stoffübertragungsflächen. Durch Simulation der Wärme- und Stoffübertragungsvorgänge analysiert die vorliegende Arbeit die Einflussfaktoren auf die erreichbare Energiespeicherdichte und setzt Gütesziele für die Verteilung der Prozessmedien fest. Darauf aufbauend werden Verteilelemente für die Sole entwickelt und getestet, von denen eines sich als besonders geeignet erweist.

Contents

List of Tables

List of Figures

Nomenclature

Index of Symbols

Latin

A	m^2	area
a	m^2/m^3	specific area of a packing
a	-	constant
C_S	kg/kg	mass concentration of the salt solution
c_p	kJ/(kg K)	specific heat capacity
D	m^2/s	diffusion coefficient
d_h	m	hydraulic diameter
d_{pl}	m	distance between the exchange plates
f_{dis}	-	distribution factor
$f_{\dot{m}}$	-	mass flow factor
f_{mal}	-	maldistribution factor
$\dot{G}$	kmol/s	gas flow rate
h	m	height
h	kJ/kg	specific enthalpy
$\dot{H}$	kW	enthalpy flow
k	-	constant
$\dot{L}$	kmol/s	liquid flow rate
l_{abs}	m	length of the absorber
M	kg	mass
$\dot{M}$	kg/s	mass flow rate
$\overline{m}$	kg	mean sample mass
$\hat{M}$	kg/kmol	molar mass
MR	-	mass flow ratio of air to liquid desiccant flow
n	-	number, constant
N_{OG}	-	number of transfer units
p	Pa, bar	pressure, partial pressure
$\dot{Q}$	kW	heat flow
r	kJ/kg	enthalpy of condensation

SC	kWh/m^3	volumetric energy storage capacity
s_{pl}	m	total thickness of the exchange plate
s_{PP}	m	wall thickness of the exchange plate
T	°C, K	temperature
u	m/s	superficial velocity
U	W/(m^2 K)	overall heat transfer coefficient
V	m^3	volume
$\dot{V}$	m^3/s	volume flow rate
$\dot{v}$	m^3/(s m)	specific volume flow rate
w	m	width
X	kg/kg	humidity ratio, water content
X_{mol}	kmol/kmol	humidity ratio, water content
Y_{mol}	kmol/kmol	humidity ratio, water content
z	-	control variable, dimensionless height

Greek

α	W/(m^2 K)	convective heat transfer coefficient
β	m/s	mass transfer coefficient
η	kg/(m s)	dynamic viscosity
λ	W/(m K)	heat conductivity
ρ	kg/m^3	density, partial density
σ	N/m	surface tension
φ	-	relative humidity

Subscripts

A	air
abs	absorber, absorption
c	column
con	condensation
dil	diluted, dilution
dis	distribution
dp	dew point
ev	evaporation
ext	external
i	individual
i	inlet
L	liquid
lat	latent
m	mean

max	maximum
mal	maldistribution
min	minimum
o	outlet
pac	packing
pl	plate
S	solution
sat	saturation
sen	sensible
Slt	salt
tot	total
V	vapor
W	water
wb	wet bulb

Superscripts

*	equilibrium
°	saturation

Constants

g	9.81 m/s^2	gravitational acceleration
p_0	101.3 kPa	standard barometric pressure
T_0	273.15 K	standard temperature

Index of Abbreviations

ASME	American Society of Mechanical Engineers
COP	Coefficient of Performance
DCS	Desiccant Cooling Systems
ECES	Energy Conservation through Energy Storage
EES	Engineering Equation Solver
IA	Implementing Agreement
IEA	International Energy Agency
IPCC	Intergovernmental Panel on Climate Change
LDCS	Liquid Desiccant Cooling Systems
PCM	Phase Change Material
ZAE Bayern	Bavarian Center for Applied Energy Research

Chapter 1

Introduction

In their latest assessment report about climate change, the Intergovernmental Panel on Climate Change (IPCC) agrees that "warming of the climate system is unequivocal, as [it] is now evident from observations of increases in global average air and ocean temperatures, widespread melting of snow and ice, and rising global average sea level" [IPCC 2007]. The IPCC has been established by the United Nations Environment Programme and the World Meteorological Organization. It assesses scientific, technical and socio-economic information relevant for understanding human-induced climate change, its potential impacts and options for adaptation and mitigation. The IPCC and Al Gore were jointly awarded the Nobel Peace Prize in 2007. The report names the increased global atmospheric concentrations of carbon dioxide as main cause for global warming and includes the other greenhouse gases such as methane and nitrous oxide that also contribute to global warming. Since 1750, the carbon dioxide concentration increased by 35% from 280 ppm to 380 ppm in the year 2005. Primarily, an extensive use of fossil fuels and a change of land use provoced this rise.

The panel predicts that "continued greenhouse gas emissions at or above current rates would cause further warming and induce many changes in the global climate system during the 21st century that would very likely be larger than those observed during the 20th century. There is now higher confidence in projected patterns of warming and other regional-scale features, including changes in wind patterns, precipitation and some aspects of extremes and of ice" [IPCC 2007]. Reducing greenhouse gas emissions on a global scale and at the same time satisfying an increasing energy demand of emerging markets asks for very energy efficient technical solutions.

Space cooling is considered to be among the fastest growing sectors of new energy consumption [Waide 2004] and space cooling is estimated to account for 6.4%, of the residential electricity consumption in the 22 member countries of the International Energy Agency (IEA) in 2000. In 1990, it consumed 132.2 TWh of electricity in IEA households but this increased by 13% to 149.2 TWh in 2000. [IEA 2003]

1.1 Air-Conditioning

The expression climate control refers to the process of adjusting temperature, air humidity ratio and air quality by cooling or heating, removing or supplying humidity and filtering the air [Berliner 1976]. The term **air-conditioning** is used for applications that serve exclusively air dehumidification and cooling purposes. Currently, the world market for stationary air-conditioning is about 35 billion US $ per year and it increases rapidly [Henning 2004].

Air-conditioning equipment provides air within the indoor comfort range. The **indoor comfort range** defines an array of various conditions inside a building or a room that most persons are comfortable with. These conditions include basic physical parameters such as air temperature, air moisture, airflow, mean radiant temperature and illumination. Besides, the sensed comfort also depends on personal data such as gender, age, physique, health, clothing, activity and psychological factors [Recknagel 1997].

The most common process for air dehumidification is cooling the air below its dew point and condensing the excess humidity. Another option for removing the excess humidity is to absorb or adsorb it by a hygroscopic medium, also called **desiccant**.

The most common processes for cooling the air are vapor compression, absorption chilling and evaporative cooling. The air subsequently cools down while transferring heat directly or indirectly to liquid refrigerant that evaporates. Depending on the temperature levels of the heat transfer and the outside humidity, the evaporation of the refrigerant takes place at low pressure or at atmospheric pressure.

Latest air-conditioning concepts shift the room conditions towards higher temperatures and lower humidities. The human body senses air with 26 °C and a relative humidity of 40% colder than air with 24 °C and a relative humidity of 60% as a warmer but dryer room climate allows a better heat regulation [Steimle 2000]. A lower temperature difference between room and ambient is also sensed more comfortable and diminishes the energy required for providing the space cooling.

The majority of the installed air-conditioning units are vapor compression chillers driven by electricity. Consequently, the rising number of installed air-conditioning units leads to an increasing electricity demand on hot days. In Japan, the electricity demand for air-conditioning and other summer demands accounts for approximately 35% of the peak load in summer [TEPCO 2003]. Air-conditioning is often the single largest cause of overloaded electric transmission and distribution systems [Lowenstein *et al.* 2006]. The summer blackout in Italy in 2003 is closely linked to an unexpectedly high electricity demand for air-conditioning [Hancocks 2003]. Replacing electricity driven air-conditioning units by heat driven ones stabilizes the electric transmission and distribution systems and lowers the peak power demand.

1.2 Desiccant Cooling Systems

Desiccant Cooling Systems (DCS) are heat driven air-conditioning systems. They use a solid desiccant to dehumidify the outside air and cool the dehumidified air by cold recovery from the return air and evaporative cooling, see Figure 1.1. DCS are **open loop sorption systems** that exchange heat and water vapor with the environment. While closed loop systems allow only heat transfer between the system and the ambiance, open loop systems allow heat and mass transfer between the system and the ambiance.

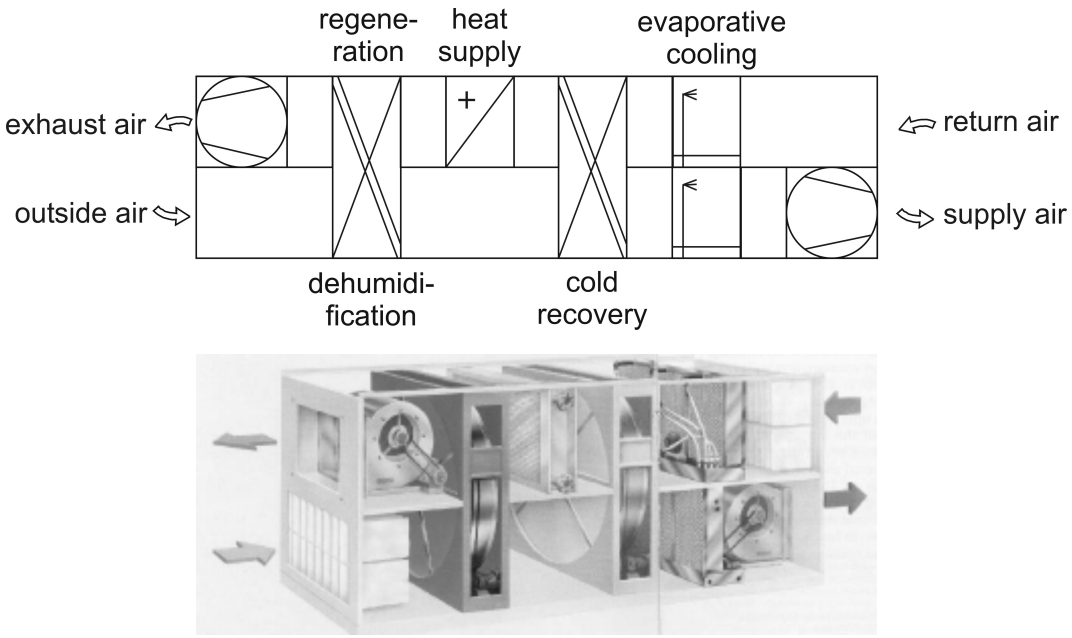

Figure 1.1: *Desiccant cooling system, adopted from [Munters 2007]*

DCS are thermally driven, mostly by natural gas. The supplied heat evaporates the water adsorbed by the solid desiccant during the air dehumidification. DCS require electricity only as auxiliary energy [Heinrich 1997]. Thus, they do not contribute to the high electricity demand in summer caused by conventional air-conditioning units driven by electricity. Cooling by evaporation and not by a chiller driven by electricity also constitutes an ecologically friendly process management [Steimle 2000].

DCS are suitable for the latest air-conditioning concepts because they can provide dehumidified air cost-efficiently. They are commercially available in the USA, Japan and Europe and especially in the USA do they gain market shares. The discussion about the indoor air quality has led to higher demanded air exchange rates that require an efficient cold recovery. DCS feature an efficient cold recovery and are therefore suitable for high air exchange rates.

Liquid Desiccant Cooling Systems (LDCS) are DCS that utilize a liquid desiccant such as a concentrated salt solution to dehumidify the outside air. Almost all available LDCS currently under development use an aqueous lithium chloride solution as liquid desiccant [Henning 2004]. The higher the salt concentration of the solution, the higher is its potential for air dehumidification. The air dehumidification process is called **absorption process** and the salt concentration decreases during this absorption of water vapor in the liquid desiccant. By supplying heat to the depleted desiccant, the absorbed water is removed and the solution reconcentrated. This process is referred to as **regeneration process**.

One main advantage of LDCS compared to DCS is that lower heat supply temperatures are sufficient for the regeneration of the desiccant. This might imply further benefits such as primary energy savings if the systems work with heat sources that are not fully exploited yet such as

- waste heat,
- district heat or
- solar heat.

The required temperature level of the heat supply depends on the desiccant and the process management. Low temperature levels of the required heat supply enhance the possibilities for using waste heat as driving force.

District heating is well used in winter but not in the summer due to few heat consumers at this time of the year. Supplying thermally driven applications with district heat during light load times leads to a higher annual efficiency of the district heating system and to better efficiencies of cogeneration plants.

An increased use of solar energy leads to a significant reduction of primary energy consumption. "Solar energy is an essentially inexhaustible source [...] and indications are that solar energy is the most promising of the unconventional energy sources" [Goswami 2000]. Solar thermal collectors provide solar heat by absorbing the incident solar radiation, converting it into heat and transferring this heat to a working fluid. A benefit from using solar thermal energy is the good seasonal match between the availability of solar radiation and the energy demand for air-conditioning. Due to the intermittent availability of solar radiation, however, solar systems always require a storage system to buffer times without irradiation.

Two alternative LDCS concepts are on the market and under development,

- LDCS with simultaneous absorption and regeneration processes and
- LDCS with energy storage and not necessarily simultaneous absorption and regeneration processes.

In LDCS with simultaneous absorption and regeneration processes, the liquid desiccant replaces the solid desiccant and the system works analogously to the DCS shown in Figure 1.1. Absorption and regeneration process take place simultaneously at different sections of a rotating sorption wheel containing the liquid desiccant solution. They can also take place in two individual apparatus - absorber and regenerator - that operate simultaneously. The depleted desiccant exiting the absorber is reconcentrated continuously in the regenerator and fed back into the absorber. Therefore, a continuous heat supply is required for the regeneration of the liquid desiccant that ultimately drives the dehumidification process in the absorber.

LDCS with energy storage are suitable for an intermittent heat supply such as a solar heat supply. Absorption and regeneration do not need to coincide and concentrated and diluted liquid desiccant are stored in separate tanks. The concentrated liquid desiccant drives the dehumidification process and ensures a continuous operation of the LDCS without the need of a further heat supply until the reservoir is exhausted. The depleted desiccant is regenerated when enough solar energy is available.

High-flow LDCS with energy storage is a state-of-the-art technology. Low-flow LDCS are not available on the market yet. Low-flow LDCS operate with a reduced liquid load in the absorber and can operate longer than high-flow systems with the same amount of concentrated desiccant. While the absorber of a low-flow system is more complex than a high-flow absorber, the regenerators of high-flow and low-flow systems can be identical in design. Figure 1.2 shows the schematic diagram of a low-flow LDSC with energy storage that is under development at the Bavarian Center for Applied Energy Research (ZAE Bayern).

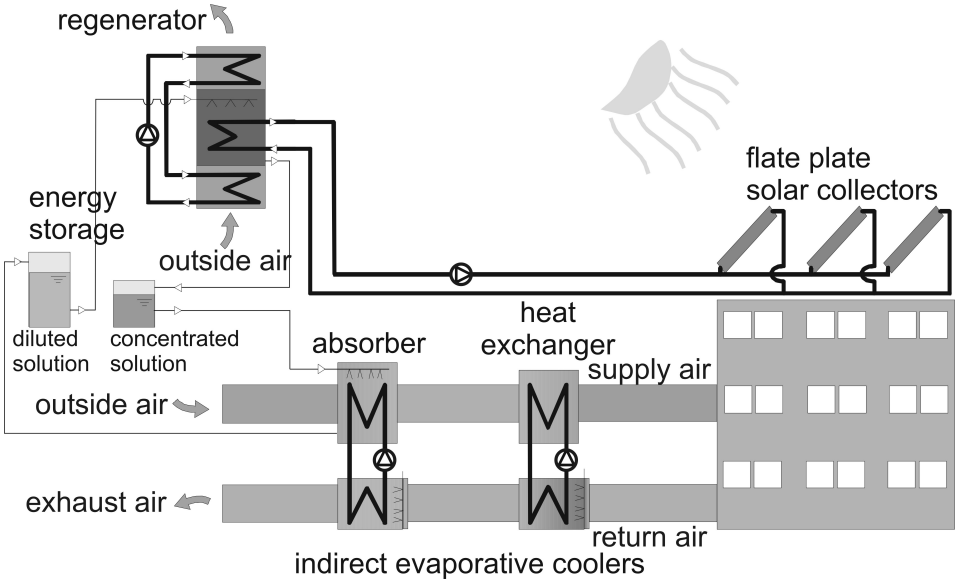

Figure 1.2: *Low-flow LDSC with energy storage driven by solar thermal energy under development at ZAE Bayern*

While there is a good seasonal match between the availability of solar radiation and the energy demand for air-conditioning, for the course of a day or a week the availability of solar radiation and the air-conditioning demand can differ greatly. The amount of stored desiccant must be sufficient to bridge this mismatch between demand and supply to ensure a continuous operation of the LDCS. As low-flow LDCS can operate longer than high-flow systems with the same amount of concentrated desiccant, the further developing of low-flow LDCS improves the storage possibilities for the discontinuous energy source solar energy and broadens the application possibilities of this heat source for air-conditioning.

Efficient energy storage in low-flow LDCS is not only relevant for solar air-conditioning but amplifies the opportunities for the use of excess heat for air-conditioning as well. This contributes to exploiting the full potential of reducing the primary energy consumption. Saving excess heat in light load times by regenerating depleted desiccant instead of rejecting the heat provides air-conditioning during thermal peak load times without further heat supply.

1.3 Energy Storage in Liquid Desiccant Cooling Systems

An important measure for the quality of the energy storage in LDCS is the **volumetric energy storage capacity**. The volumetric energy storage capacity is defined as stored energy per volume of the storage medium. The higher the volumetric energy storage capacity is, the smaller is the storage system for the same energy content. As this research only relates the stored energy to the volume of the storage medium and never to the mass of the storage medium, the term "energy storage capacity" always abbreviates the volumetric energy storage capacity.

The energy storage capacity in dehumidification applications is defined as the dehumidification energy per volume of the storage medium. In LDCS, this is the ratio of the enthalpy of removed water vapor to the volume of diluted liquid desiccant. Storing heat by means of a reversible process is called **thermochemical** heat storage.

High-flow LDCS dilute the concentrated LiCl-solution with an absorber inlet concentration of 44% to an outlet concentration of 37%, yielding an energy storage capacity of approximately 130 kWh/m^3. Low-flow LDSC have the potential of achieving even higher energy storage capacities of approximately 280 kWh/m^3 by diluting the concentrated solution to approximately 29%. Therefore, low-flow systems can operate twice the time of high-flow systems with the same amount of concentrated desiccant.

To compare the thermochemical energy storage capacity of LDCS with other energy storage options for air-conditioning, Table 1.1 lists the main energy storage options

that are in principle eligible for bridging typical mismatches between air-conditioning demand and solar power supply that last from some hours to up to three days.

Table 1.1: *Energy storage options for air-conditioning*

Storage Method	**Storage Medium**	**Operational Region**
latent heat storage	ice	0 °C
sensible heat storage	cold water	6 °C - 12° C
sensible heat storage	hot water for driving the regenerator	75 °C - 95 °C
thermochemical storage	salt solution in a high-flow system	37% - 44%
thermochemical storage	salt solution in a low-flow system	29% - 44%

Figure 1.3 compares their energy storage capacities. It plots the maximum energy storage capacities for the given operational range and does not consider the dimensions of required heat transfer equipment or of any insulation of the storage tank.

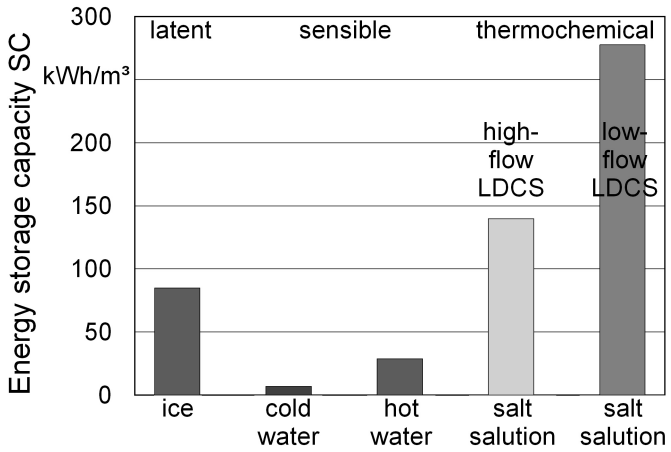

Figure 1.3: *Comparison of the energy storage capacities of the main energy storage options for air-conditioning with the boundary conditions listed in Table 1.1*

Ice is suitable for cold storage as it possesses a high energy storage capacity. Still, it requires an additional ice generator, driven by electricity. Also, the temperature of the stored cold is lower than the typical operating range of air-conditioning systems.

A cold water storage is applied as buffer in some conventional air-conditioning systems but only for very limited time spans. It operates in the narrow temperature difference of 6 K and therefore provides the lowest energy storage capacities of the listed options. It is not suitable for buffering the time spans that solar air-conditioning requires.

A hot water storage system is usually part of a solar heat supply system. The usable temperature range for this application is about 20 °C. The upper temperature is limited to approximately 95 °C by the solar collector. The lower temperature is limited by the temperature level required by the thermally driven air-conditioning process ($\approx$ 70 °C) and the temperature difference required for the heat transfer ($\approx$ 5 K).

This comparison does not reflect the complexity of the individual storage systems and their efficiency. Though the coefficient of performance (COP) of an ice generator lowers the cold output per electricity input, the energy storage capacity of the ice directly reflects the cold the melting ice provides for air-conditioning.

The COP of the conversion of the stored heat into cold lowers the cold that can be withdrawn per heat input from the storage system. If the heat drives an absorption chiller with a COP of 0.7, only 70% of the 29 kWh/m^3 stored heat are applicable as air-conditioning energy. Furthermore, the temperature of the storage medium in these storage systems is always different from the temperature of the surrounding environment. Insulating the storage tank minimizes thermal losses, but the amount of stored energy decreases over time.

Thermochemical storage is almost loss-free. As the concentrated solution only reduces its dehumidification potential by the absorption of moisture, a tight tank without any insulation keeps the solution concentrated. By definition, the LDCS energy storage capacities directly specify the applicable dehumidification energy for air-conditioning. Figure 1.3 shows that low-flow LDCS provide the highest energy storage capacities.

In summary, LDCS are suitable for latest air-conditioning concepts that shift the room conditions towards higher temperatures and lower humidities and work with higher air exchange rates. LDCS require lower regeneration temperatures and allow energy storage within the liquid desiccant. Furthermore, they can be arranged more flexible within the building because the air ducts for supply air and exhaust air do not need to be within one air handling unit as in DCS but the heat transfer between them is accomplished by water loops. As LDCS have a high potential for primary energy savings, they are investigated and further developed in many countries but low-flow LDCS are not a state-of-the-art technology yet.

1.4 Objectives

The Bavarian Center for Applied Energy Research (ZAE Bayern) is investigating a low-flow LDCS with the focus on thermochemical storage with high energy storage capacities. It has proven the technological feasibility of such systems with high thermochemical energy storage capacities in laboratory scale applications. Currently, the ZAE Bayern is working on a full-scale application that provides 12 kW of cooling to a building in Munich. While the cooling performance of the equipment is acceptable, the measured energy storage capacities that have been realized in this project lack behind the predicted ones. The key challenge remains the uniform distribution of the liquid desiccant on the heat and mass transfer surfaces inside the absorber that are schematically shown in Figure 1.4.

The objective of the present research is to increase the achievable energy storage capacity in LDCS and to contribute to the understanding of the factors of influence. Maldistribution of liquid desiccant, air and cooling water worsens the performance. The specification of reasonable performance goals for the distribution of the process media will support the effective development of proper production methods.

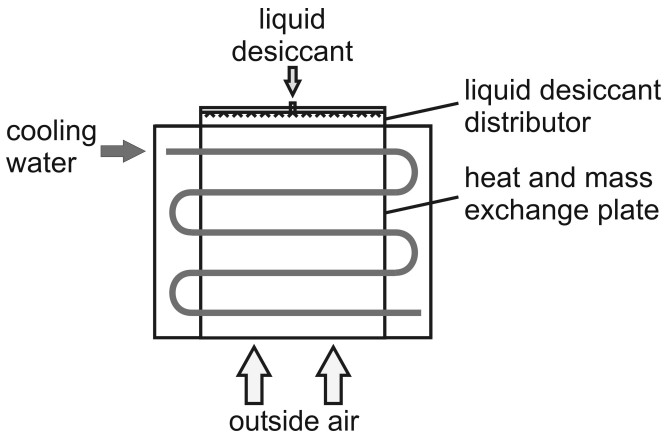

Figure 1.4: *Schematic diagram of a heat and mass transfer plate*

Previous research proved that very low desiccant flows are required for effective energy storage [Lävemann *et al.* 1993] and the uniform distribution of these small amounts is a technical challenge. Therefore, main focus is the improvement of the liquid desiccant distribution device in terms of performance and reliability. The individual tasks can be divided into theoretical simulations and experimental analysis and further development of the liquid desiccant distributors:

Theoretical Part

- development of a numerical model for the simulation of
  - air dehumidification processes with a liquid desiccant
  - regeneration processes of the liquid desiccant
  - air humidification processes in indirect evaporative coolers
- determination of the energy storage capacity for the air dehumidification in LDCS for different absorption modes
- determination of the sensitivity of the energy storage capacity to maldistribution of the cooling water flow and to simultaneous maldistribution of liquid desiccant and air flow

Experimental Part

- design and construction of a new measuring system for the distribution of the liquid desiccant
- measuring and assessing the existing liquid desiccant distributors
- development of a new liquid desiccant distributor based on the results
- improvement of the connection of the new liquid desiccant distributor to the commonly used heat and mass transfer plates or integration of the new liquid desiccant distributor into the heat and mass transfer plates

Chapter 2

State of the Art

2.1 Energy Storage in Air-Conditioning Systems

This section presents the current research in the field of energy storage in air-conditioning systems, including concepts that increase the thermal capacity of lightweight construction buildings. It excludes the analysis of a high building mass as energy storage though a high building mass can also be considered a passive form of thermal storage as it lowers the peak air-conditioning demand.

Main objectives of energy storage in air-conditioning systems are to lower the peak power demand and to save primary energy. In heat driven air-conditioning systems, disconnecting the building load from the heat availability utilizing a storage system allows to supply heat from discontinuous sources such as solar heat or waste heat.

The International Energy Agency (IEA) has increased its research activities in the field of energy storage in air-conditioning systems. The Implementing Agreement "Energy Conservation through Energy Storage" (ECES IA), established in 1978, is one of the 14 different Implementing Agreements within the R&D program "Efficient Energy End-Use Technologies". Within the ECES IA, several annexes deal with storage for air-conditioning applications including sensible, latent and thermochemical storage [Lottner 2006]. Annex 14 "Cooling with Thermal Energy Storage in all Climates" focuses especially on cooling, covering all types of thermal energy storage technologies and considering different climates. The ongoing Annex 20 "Sustainable Cooling with Thermal Energy Storage" expands the feasibility studies, design and construction of practical demonstrations of viable thermal energy storages in representative cooling applications in different climates. Main objective is to advance the prospects of cooling with thermal energy storage systems. In a project oriented approach, the sustainability of cooling with an integrated thermal energy storage system will be demonstrated and evaluated in terms of energy savings and CO_2 emission

reductions [Okumiya and Paksoy 2006]. Other IEA implementing agreements such as the "Solar Heating and Cooling Programme" also investigate advanced solutions for thermal energy storage. Task 32 "Advanced Storage Concepts for Solar Thermal Systems in Low Energy Buildings" aims at a high solar fraction of the energy supply of low energy housing by means of integrating advanced storage systems both for heating and cooling [Hardon 2006].

The 5th energy research program "Innovation and New Energy Technologies" launched by the German Federal Government in 2005 focuses on renewable energies and efficiency technologies with thermal energy storage as major R&D subject, including long term sensible storage, latent storage and thermochemical storage for heating and cooling [Wille and Lottner 2006].

2.1.1 Sensible Heat Storage

The sensible heat storage either stores cold for directly supplying the cooling coils or it stores heat for driving a heat driven air-conditioning system.

Cold Storage

The first large-scale short term cold water storage in Germany is currently built in Chemnitz to improve the efficiency of a trigeneration plant that provides electricity, heat and cold. The 3500 m^3 tank will store cold water with a temperature of 5 °C provided by an absorption chiller and supply the district cooling at peak load times. The supply and return net temperatures are 5 to 7 °C and 13 °C [Urbaneck *et al.* 2006a, Urbaneck *et al.* 2006b].

Heat Storage

The heat storage has to cover the temperature difference between supply and return of the heat driven air-conditioning system. For temperatures up to 100 °C, a market survey lists the features of 1026 commercially available storage tanks for solar systems [Solid 2006]. Heat storage systems are available for temperatures up to 400 °C. They serve applications such as solar thermal electricity generation. While storing sensible heat in the heat transfer fluid itself was common in the first solar thermal power plants, solid sensible heat storage is in development for further plants. Castable ceramics and high temperature concrete are investigated as solid storage materials. The synthetic oil used as heat transfer fluid flows through a tubular heat exchanger embedded in the solid storage material to charge or discharge the storage [Steinmann *et al.* 2005]. Storing high temperature heat allows electricity generation on demand to run electricity driven vapor compression chillers when required.

2.1.2 Latent Heat Storage

Latent heat storage systems store heat by means of a phase change of the storage material, the so-called phase change material (PCM). Available PCM storage systems apply a solid-liquid phase change as melting is characterized by a small change in the specific volume and a large phase change enthalpy if a suitable material is selected. A solid-solid phase change is not applied due to the low phase change enthalpy. Though a liquid-gas phase change has a higher phase change enthalpy, the evaporation and condensation process is not suitable for PCM storage. Evaporation at constant pressure leads to a large volume change and evaporation at constant volume leads to a large pressure change. Therefore, the liquid-gas phase change is also not applied for PCM storage systems. Due to the constant temperature during the phase change, latent heat storage systems can store heat within a small temperature interval. [Mehling and Cabeza 2007]

Incorporation of PCM into building materials reduces the temperature swings of lightweight buildings by increasing their thermal mass. Compared to a sensible storage, a latent heat storage for space heating or cooling can reduce the storage volume by a factor of three or more. Storing cold from the night air by solidifying a PCM that melts during the day is also called free cooling and this approach is very promising concerning primary energy savings. [Mehling *et al.* 2007]

Water is the by far best known PCM and ice has been used as storage material for more than 2000 years. Storing ice and snow as cold source for the summer was common before mechanical refrigeration systems were introduced. In the year 2000, the first modern snow cooling plant was built with storage volume of 60 000 m^3 for natural and artificial snow. It cools a regional hospital in Sundsvall, Sweden, and in the first operational years, the fraction of natural snow lay between 41% and 62%. [Nordell and Skogsberg 2007]

The unit "refrigeration ton" or "ton of air-conditioning" is still in use to express the cooling capacity of an air-conditioning equipment. It dates back to the times when ice was used to cool a building. Installing an air-conditioning equipment with a capacity of one ton of refrigeration (3.5 kW) lowered the daily need for ice by one ton. [Jeffus 2004]

Artificial ice generation during night time to provide cold for the day has become popular recently [Mehling *et al.* 2007]. According to MacCracken (2006) over 6000 installations world wide use off-peak cooling systems with thermal energy storage in form of ice or chilled water. The addition of storage to all buildings needing air-conditioning, can lead to a 40% peak load reduction [MacCracken 2006].

2.1.3 Thermochemical Heat Storage

Thermochemical heat storage systems store heat by means of a reversible chemical reaction, adsorption or absorption process. The energy storage capacity of thermochemical storage is higher than the one of physical changes such as phase change or sensible heating. The boundary conditions of the process that is to be supplied by the storage system specify which thermochemical storage method is the best option for supplying the process.

Equation 2.1 states a gas-solid reaction of magnesium oxide and water as example reaction.

$$Mg(OH)_2(s) \Longleftrightarrow MgO(s) + H_2O(g) \tag{2.1}$$

Further working pairs currently used for chemical reactions are MgO/H_2O, $CaCl_2/NH_3$, CaO/H_2O and metal hydrates/H_2. The choice of reaction also depends on the temperature range of the energy storage. [Kato 2007]

Zeolites and silicagels are the most common storage materials for adsorptive thermochemical storage processes and water vapor is the adsorbate. Heat input into the storage material dries it by evaporating the adsorbed water and charges the storage system. Adsorption of water vapor discharges the storage system and releases the stored heat to an air flow that is dried and heated. The water vapor can be adsorbed up to a total mass fraction of 30% to 40% of the storage material [Hauer 2007a]. For a charging temperature of 300 °C, storage systems based on zeolite have the potential of providing energy storage densities of up to 200 kWh/m^3. Energy storage densities of 120 kWh/m^3 have been realized in demonstration facilities with both, storage in silicagel and in zeolite [Hauer 2007b]. As an air flow discharges this storage system, it suits for supplying processes that require hot and dry air such as drying processes.

Hygroscopic salt solutions are the most common storage materials for absorptive thermochemical storage processes and water vapor is used as absorbate. An energy storage density of 150 kWh/m^3 has been reached in a low-flow LDCS with an aqueous lithium chloride solution developed by ZAE Bayern. Driven by district heating, it provides 12 kW of cooling to a jazz club in Munich [Lävemann *et al.* 2006]. A similar but solar driven LDCS manufactured by L-DCS Technology operating in Singapur that provides 100 kW of cooling and dehumidification achieved an energy storage density of 185 kWh/m^3 [L-DCS 2007, Hublitz *et al.* 2006].

Allowing crystallization of the salt in the desiccant increases the achievable energy storage density. The Swedish company ClimateWell developed the so-called thermochemical accumulator that crystallizes the solution on purpose and reaches an energy storage capacity of 330 kWh/m^3 [Bales *et al.* 2005, Bales 2006]. The complexity of this system exceeds the complexity of thermochemical storage without crystallization by far and increases the risk of unintended crystallization outside the storage tank.

2.2 Liquid Desiccant Cooling Systems

This section summarizes the research activities in the field of liquid desiccant cooling systems, including the search for suitable liquid desiccants, various concepts using solar heat directly within a solar collector to regenerate the desiccant, and energy storage with the liquid desiccant.

One of the first LDCS for solar air-conditioning dehumidified the air using the liquid desiccant triethylene glycol [Löf 1955a, Löf 1955b]. For the humid climate of India where high wet bulb temperatures exclude the possibility of using evaporative cooling, Kapur (1960) combined dry cooling with dehumidification by absorption. Robinson (1978a) tested a 17.6 kW solar air conditioner working with triethylene glycol as desiccant and used the concentrated glycol solution as a storage system. Though the low temperature level of 50 °C required for the regeneration of the desiccant is advantageous for solar cooling, its vapor pressure can not be neglected. In a redesign of the air conditioner, Robinson replaced the glycol desiccant by an artificially colored aqueous calcium chloride solution and investigated the reconcentration of the desiccant by direct absorption of solar radiation [Robinson 1978b]. In a 2-year field test of the solar LDCS with an aqueous calcium chloride solution as desiccant, Robinson (1983) demonstrated the technical feasibility but he did not aim at commercializing the system. Loss of the glycol desiccant and its possibly negative impact on the environment led to a discarding of the glycols as desiccants for the vast majority of open loop systems [Patnaik *et al.* 1990].

The No-Frost® System by the Niagara Blower Company (2007) is one of the few examples that still applies glycols as desiccants. Aqueous salt solutions of lithium chloride (LiCl) and calcium chloride ($CaCl_2$) replaced glycol as liquid desiccant. Almost all available LDCS and LDCS currently under development use an aqueous lithium chloride solution as liquid desiccant [Henning 2004].

With the focus on solar LDCS, Katabaev and Khandurdyev (1969), and Katabaev *et al.* (1972) investigated direct solar regeneration within a solar collector studying both forced and natural convection. They proved that in dry and hot climates the liquid desiccant can be regenerated directly in a solar collector. The sun heats the diluted desiccant in the collector and water from the diluted desiccant evaporates directly into the ambient air.

At the Solar Energy Laboratory of the Indian Institute of Technology in Madras, Mullick and Gupta (1974) and Gupta and Gandhidasan (1978) theoretically analyzed a so-called "collector-cum-desorber" unit that also directly regenerated the calcium chloride solution in a solar collector. The concept lowers the parasitic power consumption by omitting the blower for the scavenging air flow. The scavenging air required for the water vapor removal flows through the "collector-cum-desorber" due

to natural buoyancy forces. Gandhidasan *et al.* (1979) studied the buoyancy effects on the heat and mass transfer in the solar regenerator.

At the Los Alamos Scientific Laboratory of the University of California, Collier (1979) simulated and analyzed the COP (cooling provided per incident solar radiation) of an absorption system with an open loop solar regenerator. In the solar regenerator, diluted desiccant flowed over an open, flat, black surface. The overall daily cooling COP ranged from 0.09 to 0.45 for various conditions such as desiccant flow rate, collector length, and weather.

Research at the Arizona State University measured the performance of an open loop absorption refrigeration system with a prototype solar collector/regenerator consisting in a 11 m x 11 m black shingled roof. They developed simulation tools for the heat and mass transfer within the device and compared the performance differences between the unglazed collector/regenerator and a glazed one. The latter is less sensitive to varying ambient temperature and humidity. For a wide range of meteorological conditions, the model predicted the experimentally measured performance accurately [Wood *et al.* 1983a, Wood *et al.* 1983b, Novak *et al.* 1985, Novak and Wood 1985, Novak *et al.* 1986, Nelson *et al.* 1986, Nelson and Wood 1989]. While the previous open-loop absorption modeling included only the solar collection part, Siebe *et al.* (1986) evaluated the critical parameters necessary in order to have a viable LDCS and identified the potential for five system design concepts for various climate regions of the United States. Hawleder *et al.* (1993) further improved the collector/regenerator and experimentally determined regeneration efficiencies between 38% and 67%, corresponding to cooling capacities between 31 kW and 72 kW.

Peng and Howell (1981, 1984) of the University of Texas proposed and analyzed theoretically an open loop LDCS referred to as hybrid double-absorption system with low operating parasitic power requirements. A fraction of the dehumidified air mixed with the return air from the building and lowered the wet bulb temperature of the air flowing into the indirect evaporative cooler. They evaluated triethylene glycol and an aqueous lithium chloride solution as desiccant. For the regeneration of the desiccant, they compared the performance of an unglazed collector/ regenerator and the regeneration in a chamber with finned tubes. They recommended the regeneration chamber as it is more compact and less depended on the weather conditions.

Research at the Texas A&M University focused on heat and mass transfer in adiabatic counterflow packed bed absorbers with ceramic Raschig rings as packing material and a calcium chloride solution as liquid desiccant. Gandhidasan *et al.* (1985) simulated the performance of the absorber for various parameters such as concentration, temperature, humidity, and flow rates. For comparison, Gandhidasan *et al.* (1986) also evaluated Berl saddles as packing material. Based on heat and mass transfer calculations, Ullah *et al.* (1988) analyzed the absorber effectiveness of air moisture removal.

Stevens *et al.* (1989) of the Solar Energy Laboratory of the University of Wisconsin-Madison developed a model for the simulation of a packed-bed, liquid desiccant absorber for LDCS. The model predicted the exchange efficiency given as ratio of achieved conversion to achievable conversion. So'Brien and Satcunanathan (1989) designed a combined absorber-regenerator-unit that abstained from a mechanical circulation of the solution. They documented an exchange efficiency of 20% to 25%.

For the climatic conditions of Taiwan, Yang and Yan (1989) studied the aptitude of a system similar to the one described in Novak *et al.* (1986) for humid regions. As LDCS research also includes thermochemical heat storage in the concentrated liquid desiccant, Yang and Yan simulated the solar LDCS in Taiwan with thermochemical heat storage in the lithium chloride solution. The prototypes, however, yielded exchange efficiencies of only 5%, far below the 80% required for efficient energy storage. Choi and Kimura (1989) stored diluted and concentrated solution in one tank without a separating membrane. Though the density differences of the two fractions were high enough for a stratification of the solution, experimental density measurements proved a mixing of diluted and concentrated solution. Focusing on thermochemical heat storage in the concentrated liquid desiccant, Khelifa and Sizmann (1989), and Khelifa *et al.* (1990) compared the theoretical energy storage capacities of aqueous lithium chloride and calcium chloride solutions. Scalabrin and Scaltriti (1988) studied and modeled the performance of an internally cooled absorber composed of a pipe bundle that was sprayed with lithium chloride solution. Though the internally cooled configuration is suitable for low-flow technology and energy storage within the desiccant, they recirculated the solution and tested high-flow conditions. They extended their modeling and experimental analysis of the cooled absorber and presented and simulated a complete LDCS. In the proposed LDCS, the process air was adiabatically humidified in a direct evaporative cooler after exiting the cooled absorber. The solution regenerator was identical in design with the absorber and externally heated water flowed inside the tube bundle [Scalabrin and Scaltriti 1990]. Patnaik *et al.* (1990) studied a 10.5 kW solar LDCS with packed bed absorber and regenerator installed at the Solar Energy Applications Laboratory in Colorado. For the regenerator, they compared two different distribution systems for the liquid desiccant to achieve a proper wetting of the exchange surface: a gravity tray distributor and a spray nozzle system. The spray system led to a lower pressure drop within the air flow and higher cooling capacities.

Researchers of the Technion, the Israel Institute of Technology, constructed a packed column and analyzed its performance for air dehumidification and regeneration of the desiccant. They also modeled the so called air-liquid contactor. While the experiments carried out with a lithium bromide solution as desiccant agreed well with the simulated performance, the predicted performance values deviated from the experimental values for the desiccant monoethylene glycol due to problems associated with

the use of glycols. They showed that a preheating of the scavenging regeneration air significantly improves the regeneration [Factor and Grossman 1980]. Subsequent studies at the Technion focused on the combination of a closed loop absorber with an open loop regenerator. Two regenerators were analyzed and their performance modeled. One reconcentrated the solution within an solar collector and the other one brought the solution in contact with air that had previously been heated in a solar collector. Results indicated that the former showed a better performance than the latter [Haim *et al.* 1992]. Further development of the computer code to a more flexible and modular form allowed to simulate and compare the performance of various cycle configurations and different working fluids such as LiCl-H_2O solar-powered open absorption cycles, LiBr-H_2O triple-effect cycles and ammonia-water single-effect cycles [Grossman and Wilk 1994]. Further investigation focused on an open loop dehumidifier - evaporator - regenerator (DER) absorption chiller capable of utilizing low-grade heat sources. In this LDCS, the dehumidified air produced chilled water in an evaporative cooler. The previously developed modular computer code was adapted to simulate this system. An analysis of the influence of various design parameters indicated that the cycle held considerable promise but some practical problems needed to be solved [Hellmann and Grossman 1995].

Research at the ZAE Bayern experimentally and theoretically analyzed a LDCS with focus on energy storage within the lithium chloride solution as desiccant. The absorber prototype diluted the aqueous lithium chloride solution to 29.7%, resulting in an energy storage density of 204 kWh/m^3 [Lävemann *et al.* 1993, Lävemann *et al.* 1996].

Researcher of the Solar Energy and Energy Conversion Laboratory at the University of Florida measured and modeled the performance of packed bed absorbers and regenerators. The selected packings generated a low pressure drop in spite of the high desiccant flow rates of triethylene glycol as desiccant. They assessed the effectiveness of the dehumidification and the regeneration process based on the air and desiccant flow rates, air temperature and humidity, and desiccant temperature and concentration. Decisive for the performance of the regenerator are the air flow rate, and temperature and concentration of the desiccant [Martin and Goswami 1999] [Fumo and Goswami 2002]. The same analysis was carried out for an aqueous lithium chloride solution as desiccant [Öberg and Goswami 1998].

Kourouma (1998) analyzed possibilities and constraints of LDCS in tropical regions for the example of Konakri in Guinea. He simulated the application of solar energy for the regeneration and identified the range of an economic application of solar energy.

Yang and Wang (2001) simulated and compared the performance of two LDCS, one with a single-glazed collector/regenerator and one with a double-glazed collector/regenerator for a range of chilled water temperatures and daily cooling demands.

Solar LDCS were also a research topic at the Sustainable Energy Centre at the University of South Australia. Saman and Alizadeh analyzed the aptitude of a plate heat exchanger with spray nozzles as internally cooled absorber with calcium chloride as desiccant. The same type of heat exchanger with spray nozzles served as indirect evaporative cooler for cooling the absorption process. A parametric study showed that the proposed configuration could not meet the sensible and latent heat requirements as stand-alone system but needed an auxiliary cooler or more dehumidification/indirect evaporative cooling stages [Saman and Alizadeh 2001]. They investigated the performance of the absorber experimentally by testing at first only the heat transfer in the absorber without desiccant flow and subsequently the combined heat and mass transfer with desiccant flow and an internal cooling of the exchange plates by evaporative cooling. The experiments indicated that the modified heat exchanger could act as absorber. The experiments agreed well with the previously simulated performance [Saman and Alizadeh 2002]. For the regeneration of the calcium chloride solution, a solar glazed collector/regenerator was designed and tested. The rate of evaporation of water vapor was determined as function of operating and climatic conditions [Alizadeh and Saman 2002a, Alizadeh and Saman 2002b].

The National Renewable Energy Laboratory of the USA has been promoting and financially supporting LDCS research. In a review of desiccant dehumidification technology, Pesaran (1993) compared solid and liquid desiccant cooling and presented three proper dehumidification applications: a supermarket, a hotel, and an office building. Lowenstein and Dean (1992) analyzed the impact of the regenerator performance on the COP of LDCS. They showed that a single-effect packed bed regenerator provides a COP of 0.7 and that double-effect regenerators can increase the COP to values above 1.3. To reconcentrate the desiccant independently from the weather conditions, Lowenstein (1993) built a gas-fired regenerator that heated the solution in an atmospheric steam vessel and evaporated water vapor until the solution reached the required concentration. In 1994, Lowenstein (1994) filed a patent for a low-flow and internally cooled absorber that operates with a liquid load of 0.24 - 0.73 $m^3/(m^2\ h)$ and an air velocity of 2 - 4.1 m/s. The absorber was designed as part of a complete LDCS with a concentration difference between diluted and concentrated solution of 4 percentage points. To avoid crystallization, the maximum concentration for the lithium chloride solution was set to 44%. Past attempts to built an internally cooled absorber had failed because of the problem of high air-side pressure drops due to flooding of the air passages with liquid as well as leaks between the cooling and the process side [Lowenstein *et al.* 1988, Feldman *et al.* 1991]. Since carryover of liquid desiccant droplets into the process stream remained a problem, Lowenstein *et al.* (1998) identified the development of a zero-carryover water cooled or evaporatively cooled absorber as one the most important R & D tasks in the field of LDCS.

Mesquita *et al.* (2004, 2005) developed a model for the solar regeneration of the liquid desiccant in a parallel plate regenerator. They evaluated the capacity and the specific energy consumption of the regenerator for a broad range of solar collector efficiencies and hot water parameters such as inlet temperature and mass flow rate.

To increase the efficiency of the regeneration process, Lowenstein *et al.* (2005) built and tested a two-stage regenerator referred to as 1.5-effect regenerator. Natural gas drove the first stage, a 90 kW boiler, that produced a steam flow of 70 kg/h by reconcentrating the diluted desiccant. This steam provided the thermal energy for the second stage, a scavenging-air regenerator. A COP increase from 0.95 to 1.05 was predicted for an improved insulation of the 1.5-effect prototype regenerator. Complementary to the efficient 1.5-effect gas-fired regenerator, Lowenstein *et al.* (2006) built a zero-carryover liquid desiccant air conditioner for solar applications that was coupled to a single-stage regenerator. Both units operated with very low flows of liquid desiccant to avoid an entrainment of desiccant droplets by the process air. The mass flow ratio of air mass flow rate to liquid desiccant mass flow rate lay at 13 in the absorber. The desiccant flowed in thin wicks (approximately 0.5 mm) on the outer surface of the parallel plastic plates inside the conditioner and the regenerator. During the mass exchange of water, the desiccant was continually cooled or heated. Though low-flow technology was applied, this configuration did not store energy thermochemically but operated continuously. An interchange heat exchanger transfered heat from the concentrated and hot desiccant leaving the regenerator to the weak desiccant from the conditioner that entered the regenerator. As the concentration cycled between 44% and 38%, an energy storage density of 117 kWh/m^3 would be feasible in this application. AIL Research, Inc. (2007) commercializes the low-flow absorber and regenerator, and the 1.5-effect regenerator.

Chapter 3

Liquid Desiccant Cooling Systems

This chapter provides the thermodynamic fundamentals of liquid desiccant cooling systems. It characterizes moist air and liquid desiccants and it explains sorption processes with liquid desiccants and energy storage with liquid desiccants. The low-flow liquid desiccant cooling system with energy storage under development at ZAE Bayern is presented and its components are described in detail.

3.1 Thermodynamic Fundamentals

3.1.1 Psychrometrics

Psychrometrics is the science of "the determination of the properties of gas-vapor mixtures. The air-water system is by far the system most commonly encountered" [Perry 1998]. Except otherwise indicated, the definitions in this subsection are adopted from the Fundamentals Handbook of the American Society of Heating, Refrigeration and Air-Conditioning Engineers, Inc. [ASHRAE 2001].

Dry and Moist Air

Dry air is obtained by removing all water vapor and contaminants such as smoke, pollen or gaseous pollutants from atmospheric air. The binary mixture of dry air and a varying amount of water vapor is referred to as **moist air**. The state of moist air with the maximum amount of water vapor is called **saturation**. The relative amount of water vapor in moist air depends only on temperature, the absolute amount of water vapor in moist air depends on temperature and pressure.

Various physical values such as dry bulb temperature, wet bulb temperature, dew point temperature, humidity ratio and relative humidity have been defined to characterize the state of moist air. Yet, a pair of only three out of these physical values already determines the state of moist air unambiguously.

Standard Barometric Pressure

The **standard barometric pressure** p_0 is defined as the barometric pressure at sea level, $p_0 = 101.3$ kPa.

Dry Bulb Temperature

The **dry bulb temperature** T is also simply referred to as air temperature. It is a measure for the heat content of an air sample.

Humidity Ratio of Moist Air

The **humidity ratio of moist air** X_A is defined as the ratio of the mass of water vapor M_V to the mass of dry air M_A. The humidity ratio is also referred to as moisture content.

$$X_A = \frac{M_V}{M_A} \tag{3.1}$$

Partial Pressure of Water Vapor in Moist Air

The **partial pressure of the water vapor in moist air** p_V can be calculated from the humidity ratio X_A, the total pressure p and the molar masses of dry air $\tilde{M}_A$ and water $\tilde{M}_W$.

$$p_V = \frac{p}{1 + \frac{\tilde{M}_W}{X_A \cdot \tilde{M}_A}} \tag{3.2}$$

Saturation Pressure of Water Vapor

The **saturation pressure of water vapor** p° only depends on temperature. Equation 3.3 gives a good approximation for the saturation pressure of water vapor for the temperature range of 0 °C to 100 °C. This research applies this approximation proposed by Keßling (1997) that has a maximum deviation of 0.03% from the more precise but also more complex fuction given in Grigull (1989).

$$p^\circ = p_1 \cdot exp\Big(\frac{T}{C_1 + T \cdot (C_2 + T \cdot C_3)}\Big) \tag{3.3}$$

$$\begin{aligned} \text{with} \quad p_1 &= 610.8 \text{ N/m}^2 \\ C_1 &= 13.75775 \text{ °C} \\ C_2 &= 0.05714358 \\ C_3 &= 9.127117 \cdot 10^{-6} \text{ 1/°C} \end{aligned}$$

Relative Humidity of Moist Air

The **relative humidity of moist air** φ_A is defined as the ratio of the partial pressure

of the water vapor p_V to the saturation pressure of the water vapor p° at the given dry bulb temperature.

$$\varphi_A = \frac{p_V}{p^\circ(T)} \tag{3.4}$$

Dew Point Temperature

The **dew point temperature** T_{dp} is another option to specify the water content of an air sample. The dew point temperature of the sample is the temperature of moist air saturated at the same total pressure p with the same humidity ratio X_A as that of the given sample of moist air. At the dew point temperature, water vapor starts to condense out of the air.

Adiabatic-Saturation Temperature

Mixing unsaturated air with a quantity of water at the temperature T_W in an adiabatic system leads to evaporation of the water and the air temperature decreases. If the final state of the cooled and humidified air is in equilibrium with the water, T_W is the **adiabatic-saturation temperature** T_{sat}. The line relating the temperatures and humidities of this air state change is the adiabatic-saturation line. [Perry 1998]

Wet Bulb Temperature

The **wet bulb temperature** T_{wb} is "the dynamic equilibrium temperature attained by a water surface when the rate of heat transfer to the surface by convection equals the rate of mass transfer away from the surface" [Perry 1998].

Though the difference between adiabatic-saturation temperature and wet-bulb temperature increases with increasing humidity, for most engineering calculations of air-water systems, the adiabatic-saturation temperature and wet-bulb temperature are substantially equal and can be used interchangeably [Perry 1998].

Enthalpy of Moist Air

As the enthalpy of a mixture of ideal gases equals the sum of the individual partial enthalpies of the components, the enthalpy of moist air $h_{A,\text{moist}}$ with the water vapor content X_A consists of the enthalpy of dry air $h_{A,\text{dry}}$ and the enthalpy of the water vapor h_V. If not stated differently, h_A abbreviates $h_{A,\text{moist}}$.

$$h_{A,\text{moist}} = h_{A,\text{dry}} + X_A \cdot h_V \approx c_{p,A} \cdot T + X_A \cdot (c_{p,V} \cdot T + r_0) \tag{3.5}$$

Psychrometric Chart

A psychrometric chart illustrates changes of state of moist air in heating, cooling, humidification and dehumidification processes. The format for the psychrometric chart

commonly used in Europe, the so-called Mollier-diagram, plots the humidity ratio as abscissa. The lines of constant humidity ratio and therefore also constant dew point temperature run vertically. The dew point temperature is given by the saturation line. As a simplification, the present research, does not apply the Mollier-diagram to illustrate changes of state of moist air but plots psychrometric charts with the humidity ratio as abscissa and the temperature as ordinate. These psychrometric charts also include the adiabatic-saturation lines (enthalpy isolines) and the relative humidity isolines for the relative humidities 0.2, 0.4, 0.6, 0.8 and 1. In some for psychrometric charts, the enthalpy isolines are plotted at specific wet bulb temperatures.

Figure 3.1 shows the changes of state of moist air for two example cooling processes in a psychrometric chart. The air enters the cooling systems with the ARI[1] Reference Conditions for inlet air for air conditioning systems [ARI 2004], an inlet dry bulb temperature of 35 °C and an inlet relative humidity of 0.4. The two example cooling processes are a sensible air cooling process that reduces exclusively the air temperature but does not change the humidity ratio and an adiabatic air cooling process that reduces air temperature while increasing the humidity ratio.

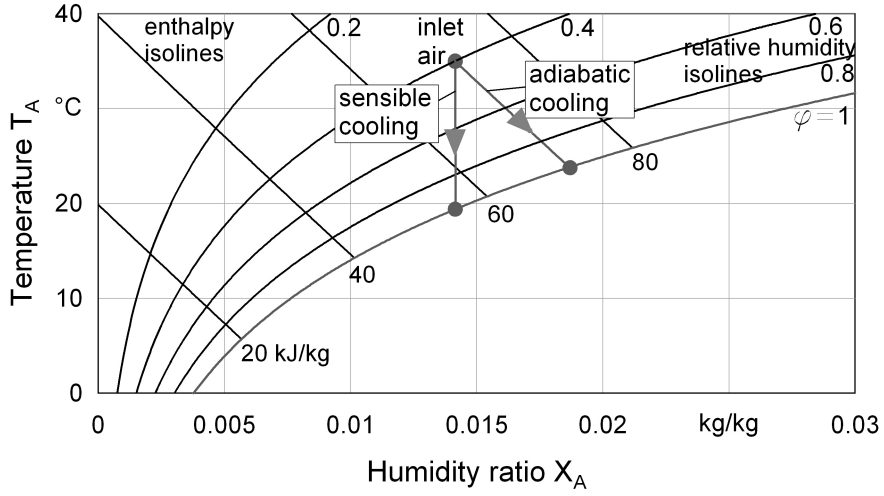

Figure 3.1: *Psychrometric chart for a sensible and an adiabatic air cooling process of air with an inlet temperature of* $T_A = 35\ °C$ *and a relative humidity of* $\varphi_A = 0.4$

Cooling Load

The determination of the required cooling load is the first step in designing an air-conditioning system. The knowledge of the following boundary conditions and heat gains within the confined space is required: design conditions including ventilation, solar heat gain, heat transmission, heat gain from occupants, heat gain from appliances, infiltration, and duct heat gain [Jeffus 2004]. Main fractions of the cooling load are the sensible heat load and the latent heat load [ASHRAE 2001].

[1] Air-Conditioning and Refrigeration Institute

Sensible Heat Load

The sensible heat load $\dot{H}_{\text{sensible load}}$ is the rate of energy consumption due to the cooling of the incoming air mass flow $\dot{M}_A$ from the outdoor air temperature $T_{A,\text{outside}}$ to the defined supply air temperature $T_{A,\text{supply}}$.

$$\dot{H}_{\text{sensible}} = \dot{M}_A \cdot c_{p,A} \cdot (T_{A,\text{outside}} - T_{A,\text{supply}}) \tag{3.6}$$

Latent Heat Load

The latent heat load $\dot{H}_{\text{latent load}}$ is the rate of energy consumption due to the modification of the moisture content of the incoming air mass flow $\dot{M}_A$. $\dot{M}_V$ is the mass flow of water vapor that has to be removed.

$$\dot{M}_V = \dot{M}_A \cdot (X_{A,\text{outside}} - X_{A,\text{supply}}) \tag{3.7}$$

Neglecting the energy associated with any condensate and the sensible temperature change of the water vapor, equation 3.8 states the latent load with the specific enthalpy of evaporation of water $h_{W,\text{evap}}$.

$$\dot{H}_{\text{latent}} = \dot{M}_V \cdot h_{W,\text{evap}} \tag{3.8}$$

3.1.2 Characteristics and Properties of Liquid Desiccants

The term liquid desiccant refers to a liquid with hygroscopic properties, such as aqueous salt solutions. The present research utilizes exclusively a solution of lithium chloride in water as liquid desiccant. The composition of the salt solution is characterized by the concentration of the solution C_S or the water content X_{Slt}.

Concentration of the Aqueous Salt Solution

The **mass concentration of the aqueous salt solution** C_S is defined as the ratio of the mass of dissolved salt M_{Slt} to the mass of solution M_S consisting of the mass of the solvent water M_W and the mass of the solute salt M_{Slt}.

$$C_S = \frac{M_{Slt}}{M_S} = \frac{M_{Slt}}{M_{Slt} + M_W} \tag{3.9}$$

Water Content of the Salt

The **water content of the salt** X_{Slt} is defined as the ratio of the solvent water M_W to the mass of the solute salt M_{Slt}.

$$X_{Slt} = \frac{M_W}{M_{Slt}} = \frac{1 - C_S}{C_S} \tag{3.10}$$

Vapor Pressure Reduction

Dissolved salts lead to a reduction of the vapor pressure of the solution in comparison to the vapor pressure of pure solvent. The vapor pressure generally increases with increasing temperature and decreases with increasing concentration of the solution. Previous research at ZAE Bayern determined the vapor-liquid-equilibrium data for lithium chloride solutions experimentally [Lävemann *et al.* 1993]. Equations 3.11 and 3.12 state the numerical fit of the measured equilibrium dew point temperature of moist air T^*_{dp} above the lithium chloride solution as function of the concentration and the temperature.

$$T^*_{dp} = \frac{T + T_0}{1.4321 \cdot k^3} - T_0 \tag{3.11}$$

$$k = \frac{2.3226 \cdot C_S}{1 + 1.3226 \cdot C_S} \tag{3.12}$$

For the temperature range of 10 °C to 80 °C and a concentration range of 0% to 45%, Figure 3.2 shows the numerical fit of the vapor-liquid-equilibrium data relatively to the vapor pressure of pure water. Equation 3.3 states the calculation for the vapor pressure from the equilibrium dew point temperature.

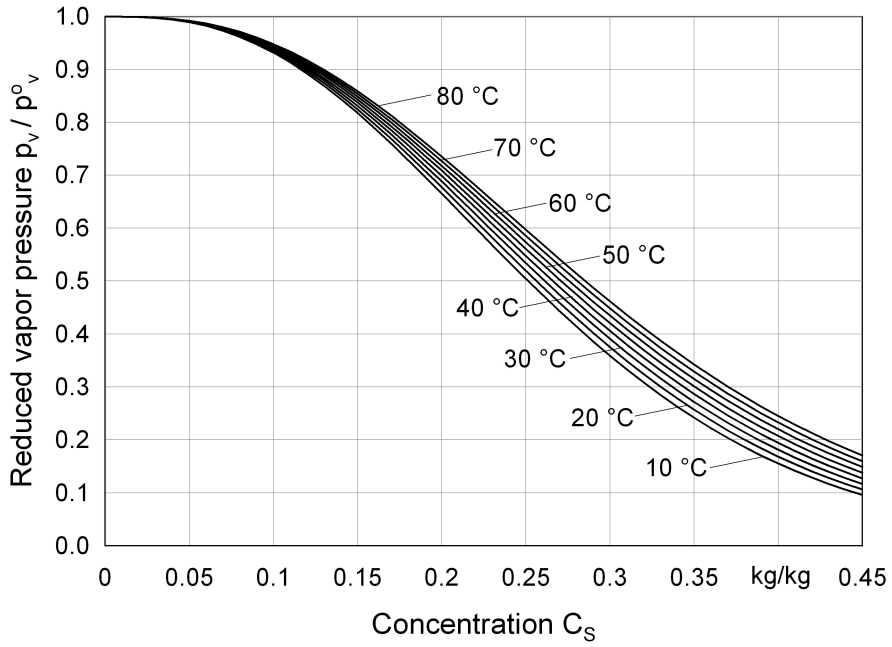

Figure 3.2: *Relative vapor pressure of the aqueous lithium chloride solution as function of the salt concentration and for different temperatures of the salt solution*

Enthalpy of Absorption and Enthalpy of Dilution

Due to the reduced vapor pressure of the salt solution compared to the pure solvent water, the concentrated salt solution absorbs air humidity and this process releases the enthalpy of absorption. This enthalpy of absorption released during the absorption of water vapor in the salt solution is higher than the enthalpy of condensation that would have been released if the vapor had been solely condensed. The enthalpy of dilution accounts for the difference. The specific enthalpy of dilution h_{dil}, the heat released per mass unit of absorbed water vapor, can be deduced from experimental data. The necessary steps for the determination of the enthalpy of dilution are

- determination of the enthalpy of absorption as function of concentration and temperature,
- determination of the enthalpy of condensation as function of temperature, and
- determination of the enthalpy of dilution as difference between absorption and condensation enthalpy.

Equation 3.13 states the Clausius-Clapeyron approximation that allows the deduction of the absorption enthalpy Δh_{abs} from data sets of the vapor pressure p_V as function of temperature [Atkins 1994].

$$\Delta h_{abs} = -R_{H_2O} \cdot \frac{d \ln p_V}{d(1/T)} \tag{3.13}$$

Figure 3.3 plots the logarithmic vapor pressure as function of the inverse absolute temperature for various concentrations. The bold line represents pure water.

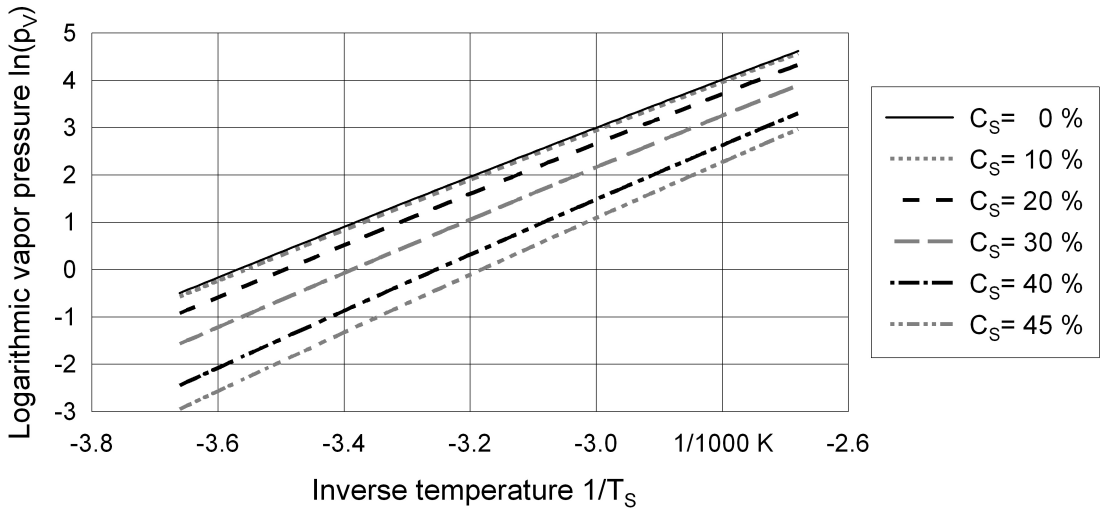

Figure 3.3: *Logarithmic vapor pressure as function of the inverse absolute temperature for various concentrations of the solution*

Figure 3.4 plots the absorption enthalpy calculated from the data in Figure 3.3 with equation 3.13.

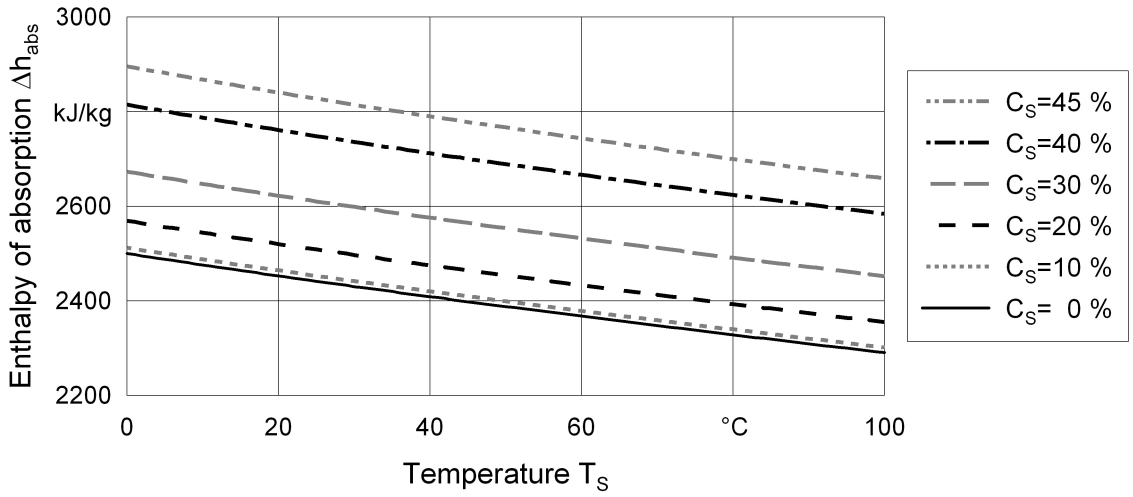

Figure 3.4: *Enthalpy of absorption as function of temperature for various concentrations of the solution*

The enthalpy of condensation $r(T_S)$ for water vapor at a certain temperature and pressure is accurately quantified [Grigull 1989]. Consequently, the enthalpy of dilution $h_{dil}(C_S, T_S)$ is given by the difference between the enthalpy of absorption and the enthalpy of condensation.

$$h_{dil}(C_S, T_S) = \Delta h_{abs}(C_S, T_S) - r(T_S) \tag{3.14}$$

The bold line in Figure 3.4 plots the absorption enthalpy of a solution with the concentration $C_S = 0\%$, i.e. pure water and therefore this line represents the enthalpy of condensation values that have to be subtracted from the other ones to yield the enthalpy of dilution.

Figure 3.5 plots the enthalpy of dilution as function of the temperature and the concentration of the solution. It clearly shows that the enthalpy of dilution highly depends on the concentration while dependency on the temperature is minor.

Enthalpy of the Salt Solution

In isobar systems without technical work, the enthalpy balance directly leads to the required heat supply or cooling loads. Therefore, thermodynamical data sets with the enthalpy as function of temperature and concentration of the liquid desiccant are advantageous for the design of liquid desiccant systems. The present research deducts a formulation of the enthalpy of aqueous lithium chloride solutions as function of concentration and temperature.

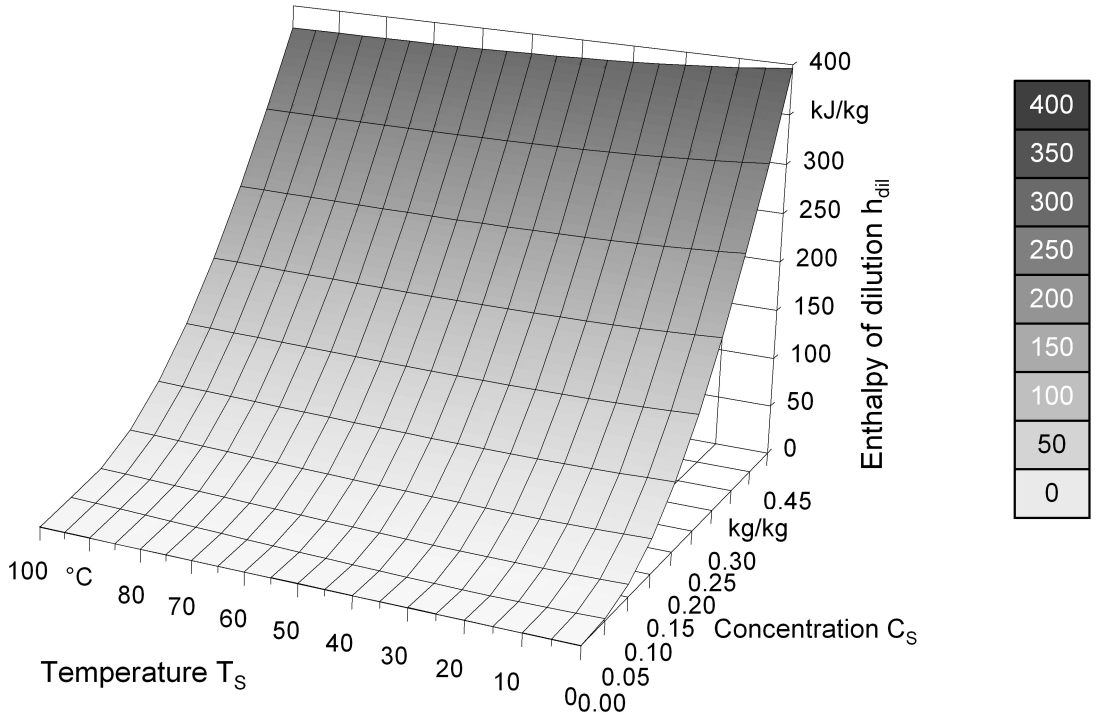

Figure 3.5: *Enthalpy of dilution as function of the temperature and the concentration of the solution*

The specific enthalpy of a pure substance depends only on temperature and is given by:

$$h = \int_{T_0}^{T} c_p \, dT \tag{3.15}$$

The definition of the specific enthalpy of the salt solution h_S consists of terms for the water fraction and the salt fraction and it includes a term that accounts for the enthalpy of dilution: $C_S \cdot h_{Slt}$ with $h_{Slt} = f(h_{dil})$. As the heat of dilution is released during the absorption of water vapor, it is defined positive.

$$h_S = (1 - C_S) \cdot c_{p,W} \cdot (T_S - T_0) + C_S \cdot c_{p,Slt} \cdot (T_S - T_0) + C_S \cdot h_{Slt}(C_S) \tag{3.16}$$

For this deduction, the specific enthalpy of the pure substances are set to 0 kJ/kg at the lower integration limit of 273.15 K.

In the following, a numerical expression for h_{Slt} as function of the enthalpy of dilution h_{dil} and consequently the concentration C_S is deduced. As h_{dil} highly depends on concentration but its dependency on the temperature is minor, see Figure 3.5, the temperature dependence of h_{dil} is neglected in this approximation.

The enthalpy of the salt solution is deducted for a steady state absorption process without heat losses to the ambiance or further media. Figure 3.6 shows the diagram with the corresponding flows and variables for the deduction of the enthalpy of the salt solution.

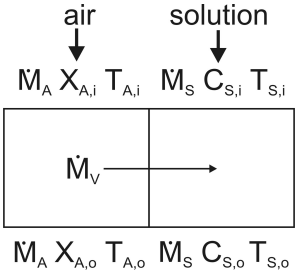

Figure 3.6: *Diagram for the deduction of the enthalpy of the salt solution: steady state absorption without heat losses to the ambiance or further media*

Due to the reduced vapor pressure of the salt solution compared to the pure solvent water, the concentrated salt solution flow $\dot{M}_{S,i}$ with the inlet concentration $C_{S,i}$ absorbs the water vapor flow $\dot{M}_V$ and is diluted to the solution flow $\dot{M}_{S,o}$ with the outlet concentration $C_{S,o}$.

$$\dot{M}_{S,i} \cdot (1 - C_{S,i}) - \dot{M}_{S,o} \cdot (1 - C_{S,o}) + \dot{M}_V = 0 \tag{3.17}$$

The inlet humidity ratio $X_{A,i}$ of the air flow $\dot{M}_A$ decreases to the outlet humidity ratio $X_{A,o}$.

$$\dot{M}_A \cdot (X_{A,i} - X_{A,o}) - \dot{M}_V = 0 \tag{3.18}$$

Equation 3.19 states the balance of absorbed water and

$$\dot{M}_A \cdot (X_{A,i} - X_{A,o}) + \dot{M}_{S,i} \cdot (1 - C_{S,i}) - \dot{M}_{S,o} \cdot (1 - C_{S,o}) = 0 \tag{3.19}$$

equation 3.20 states the enthalpy balance for the steady state absorption process.

$$\Delta\dot{H}_A + \Delta\dot{H}_S = 0 \tag{3.20}$$

Applying the enthalpy definition for moist air in equation 3.5 and the specific enthalpy of 0 kJ/kg at 0 °C leads to the air enthalpy flow $\Delta\dot{H}_A$.

$$\Delta\dot{H}_A = \dot{M}_A \cdot \left(c_{p,A} \cdot (T_{A,i} - T_{A,o}) + X_{A,i} \cdot (c_{p,V} \cdot T_{A,i} + r_0) - X_{A,o} \cdot (c_{p,V} \cdot T_{A,o} + r_0)\right) \tag{3.21}$$

Expansion and addition of $X_{A,i} \cdot c_{p,V} \cdot T_{A,o} - X_{A,i} \cdot c_{p,V} \cdot T_{A,o} = 0$ leads to

$$\begin{aligned}\Delta\dot{H}_A &= \dot{M}_A \cdot \big(c_{p,A} \cdot (T_{A,i} - T_{A,o}) + X_{A,i} \cdot c_{p,V} \cdot T_{A,o} - X_{A,i} \cdot c_{p,V} \cdot T_{A,o} + \\ &\quad + X_{A,i} \cdot c_{p,V} \cdot T_{A,i} + X_{A,i} \cdot r_0 - X_{A,o} \cdot c_{p,V} \cdot T_{A,o} - X_{A,o} \cdot r_0\big). \end{aligned} \tag{3.22}$$

Summarization of the equations terms and combination with equation 3.18 yields

$$\begin{aligned}\Delta\dot{H}_A &= \dot{M}_A \cdot \big(c_{p,A} \cdot (T_{A,i} - T_{A,o}) + X_{A,i} \cdot c_{p,V} \cdot (T_{A,i} - T_{A,o}) + \\ &\quad + (X_{A,i} - X_{A,o}) \cdot r_0 + (X_{A,i} - X_{A,o}) \cdot c_{p,V} \cdot T_{A,o}\big) = \\ &= \dot{M}_A \cdot \big((c_{p,A} + X_{A,i} \cdot c_{p,V}) \cdot (T_{A,i} - T_{A,o}) + \\ &\quad + (X_{A,i} - X_{A,o}) \cdot (c_{p,V} \cdot T_{A,o} + r_0)\big) = \\ &= \dot{M}_A \cdot (c_{p,A} + X_{A,i} \cdot c_{p,V}) \cdot (T_{A,i} - T_{A,o}) + \\ &\quad + \dot{M}_A \cdot (X_{A,i} - X_{A,o}) \cdot (c_{p,V} \cdot T_{A,o} + r_0) = \\ &= \dot{M}_A \cdot (c_{p,A} + X_{A,i} \cdot c_{p,V}) \cdot (T_{A,i} - T_{A,o}) + \dot{M}_V \cdot (c_{p,V} \cdot T_{A,o} + r_0). \end{aligned} \tag{3.23}$$

Applying the enthalpy definition for the salt solution in equation 3.16 leads to the enthalpy flow of the salt solution $\Delta\dot{H}_S$.

$$\begin{aligned}\Delta\dot{H}_S &= \dot{M}_{S,i} \cdot (1 - C_{S,i}) \cdot c_{p,W} \cdot T_{S,i} - \dot{M}_{S,o} \cdot (1 - C_{S,o}) \cdot c_{p,W} \cdot T_{S,o} + \\ &\quad + \dot{M}_{S,i} \cdot C_{S,i} \cdot c_{p,Slt} \cdot T_{S,i} - \dot{M}_{S,o} \cdot C_{S,o} \cdot c_{p,Slt} \cdot T_{S,o} + \\ &\quad + \dot{M}_{S,i} \cdot C_{S,i} \cdot h_{Slt,i} - \dot{M}_{S,o} \cdot C_{S,o} \cdot h_{Slt,o} \end{aligned} \tag{3.24}$$

To shorten the following transformations, equation 3.25 defines an abbreviation term for the enthalpy flow due to the released heat of absorption.

$$\Delta\dot{H}_{Slt} = \dot{M}_{S,i} \cdot C_{S,i} \cdot h_{Slt,i} - \dot{M}_{S,o} \cdot C_{S,o} \cdot h_{Slt,o} \tag{3.25}$$

Addition of $\dot{M}_{S,i} \cdot (1 - C_{S,i}) \cdot c_{p,W} \cdot T_{S,o} - \dot{M}_{S,i} \cdot (1 - C_{S,i}) \cdot c_{p,W} \cdot T_{S,o} = 0$ and summarization of the equations terms yields

$$\begin{aligned}\Delta\dot{H}_S &= \dot{M}_{S,i} \cdot (1 - C_{S,i}) \cdot c_{p,W} \cdot T_{S,i} - \dot{M}_{S,i} \cdot (1 - C_{S,i}) \cdot c_{p,W} \cdot T_{S,o} + \\ &\quad + \dot{M}_{S,i} \cdot (1 - C_{S,i}) \cdot c_{p,W} \cdot T_{S,o} - \dot{M}_{S,o} \cdot (1 - C_{S,o}) \cdot c_{p,W} \cdot T_{S,o} + \\ &\quad + \dot{M}_{S,i} \cdot C_{S,i} \cdot c_{p,Slt} \cdot T_{S,i} - \dot{M}_{S,o} \cdot C_{S,o} \cdot c_{p,Slt} \cdot T_{S,o} + \Delta\dot{H}_{Slt} = \\ &= \dot{M}_{S,i} \cdot (1 - C_{S,i}) \cdot c_{p,W} \cdot (T_{S,i} - T_{S,o}) + \\ &\quad + \big(\dot{M}_{S,i} \cdot (1 - C_{S,i}) - \dot{M}_{S,o} \cdot (1 - C_{S,o})\big) \cdot c_{p,W} \cdot T_{S,o} + \\ &\quad + \dot{M}_{S,i} \cdot C_{S,i} \cdot c_{p,Slt} \cdot T_{S,i} - \dot{M}_{S,o} \cdot C_{S,o} \cdot c_{p,Slt} \cdot T_{S,o} + \Delta\dot{H}_{Slt}. \end{aligned} \tag{3.26}$$

Addition of $\dot{M}_{S,i} \cdot C_{S,i} \cdot c_{p,Slt} \cdot T_{S,o} - \dot{M}_{S,i} \cdot C_{S,i} \cdot c_{p,Slt} \cdot T_{S,o} = 0$ and summarization of the equations terms leads to

$$\begin{aligned}
\Delta\dot{H}_S &= \dot{M}_{S,i}\cdot(1-C_{S,i})\cdot c_{p,W}\cdot(T_{S,i}-T_{S,o})+\\
&\quad +\big(\dot{M}_{S,i}\cdot(1-C_{S,i})-\dot{M}_{S,o}\cdot(1-C_{S,o})\big)\cdot c_{p,W}\cdot T_{S,o}+\\
&\quad +\dot{M}_{S,i}\cdot C_{S,i}\cdot c_{p,Slt}\cdot T_{S,i}-\dot{M}_{S,o}\cdot C_{S,o}\cdot c_{p,Slt}\cdot T_{S,o}+\Delta\dot{H}_{Slt}+\\
&\quad +\dot{M}_{S,i}\cdot C_{S,i}\cdot c_{p,Slt}\cdot T_{S,o}-\dot{M}_{S,i}\cdot C_{S,i}\cdot c_{p,Slt}\cdot T_{S,o}=\\
&= \dot{M}_{S,i}\cdot(1-C_{S,i})\cdot c_{p,W}\cdot(T_{S,i}-T_{S,o})+\\
&\quad +\big(\dot{M}_{S,i}\cdot(1-C_{S,i})-\dot{M}_{S,o}\cdot(1-C_{S,o})\big)\cdot c_{p,W}\cdot T_{S,o}+\\
&\quad +\dot{M}_{S,i}\cdot C_{S,i}\cdot c_{p,Slt}\cdot(T_{S,i}-T_{S,o})+\\
&\quad +(\dot{M}_{S,i}\cdot C_{S,i}-\dot{M}_{S,o}\cdot C_{S,o})\cdot c_{p,Slt}\cdot T_{S,o}+\Delta\dot{H}_{Slt}. \qquad (3.27)
\end{aligned}$$

With the simplification $\dot{M}_{S,i}\cdot C_{S,i}-\dot{M}_{S,o}\cdot C_{S,o}=\dot{M}_{Slt}-\dot{M}_{Slt}=0$ and combination with equation 3.17 yields

$$\begin{aligned}
\Delta\dot{H}_S &= \dot{M}_{S,i}\cdot\big((1-C_{S,i})\cdot c_{p,W}+C_{S,i}\cdot c_{p,Slt}\big)\cdot(T_{S,i}-T_{S,o})-\\
&\quad -\dot{M}_V\cdot c_{p,W}\cdot T_{S,o}+\Delta\dot{H}_{Slt}. \qquad (3.28)
\end{aligned}$$

Thus, the enthalpy balance in equation 3.20 can be stated as in equation 3.29.

$$\begin{aligned}
\Delta\dot{H}_A+\Delta\dot{H}_S &= \dot{M}_A\cdot(c_{p,A}+X_{A,i}\cdot c_{p,V})\cdot(T_{A,i}-T_{A,o})+\dot{M}_V\cdot(c_{p,V}\cdot T_{A,o}+r_0)+\\
&\quad +\dot{M}_{S,i}\cdot\big((1-C_{S,i})\cdot c_{p,W}+C_{S,i}\cdot c_{p,Slt}\big)\cdot(T_{S,i}-T_{S,o})-\\
&\quad -\dot{M}_V\cdot c_{p,W}\cdot T_{S,o}+\Delta\dot{H}_{Slt}=\\
&= \dot{M}_A\cdot(c_{p,A}+X_{A,i}\cdot c_{p,V})\cdot(T_{A,i}-T_{A,o})+\\
&\quad +\dot{M}_{S,i}\cdot\big((1-C_{S,i})\cdot c_{p,W}+C_{S,i}\cdot c_{p,Slt}\big)\cdot(T_{S,i}-T_{S,o})+\\
&\quad +\dot{M}_V\cdot(c_{p,V}\cdot T_{A,o}+r_0-c_{p,W}\cdot T_{S,o})+\Delta\dot{H}_{Slt} \qquad (3.29)
\end{aligned}$$

Addition of $c_{p,V}\cdot T_{S,o}-c_{p,V}\cdot T_{S,o}=0$ and summarization of the equations terms yields an enthalpy balance that can be split up into the terms for sensible and latent changes.

$$\begin{aligned}
\Delta\dot{H}_A+\Delta\dot{H}_S &= \dot{M}_A\cdot(c_{p,A}+X_{A,i}\cdot c_{p,V})\cdot(T_{A,i}-T_{A,o})+\\
&\quad +\dot{M}_{S,i}\cdot\big((1-C_{S,i})\cdot c_{p,W}+C_{S,i}\cdot c_{p,Slt}\big)\cdot(T_{S,i}-T_{S,o})+\Delta\dot{H}_{Slt}\\
&\quad +\dot{M}_V\cdot(c_{p,V}\cdot T_{A,o}+r_0-c_{p,W}\cdot T_{S,o}+c_{p,V}\cdot T_{S,o}-c_{p,V}\cdot T_{S,o}) \qquad (3.30)
\end{aligned}$$

$$\begin{aligned}
0 &= \dot{M}_A\cdot(c_{p,A}+X_{A,i}\cdot c_{p,V})\cdot(T_{A,i}-T_{A,o})+\\
&\quad +\dot{M}_{S,i}\cdot\big((1-C_{S,i})\cdot c_{p,W}+C_{S,i}\cdot c_{p,Slt}\big)\cdot(T_{S,i}-T_{S,o})+\Delta\dot{H}_{Slt}\\
&\quad +\dot{M}_V\cdot\big(c_{p,V}\cdot(T_{A,o}-T_{S,o})+r_0-(c_{p,W}-c_{p,V})\cdot T_{S,o}\big) \qquad (3.31)
\end{aligned}$$

The change in air temperature reflects the sensible change of the air enthalpy $\Delta\dot{H}_{A,sen}$.

$$\Delta\dot{H}_{A,sen}=\dot{M}_A\cdot(c_{p,A}+X_{A,i}\cdot c_{p,V})\cdot(T_{A,i}-T_{A,o}) \qquad (3.32)$$

The change in solution temperature reflects the sensible change of the solution enthalpy $\Delta\dot{H}_{S,sen}$.

$$\Delta\dot{H}_{S,sen} = \dot{M}_{S,i} \cdot \big((1 - C_{S,i}) \cdot c_{p,W} + C_{S,i} \cdot c_{p,Slt}\big) \cdot (T_{S,i} - T_{S,o}) \tag{3.33}$$

Equation 3.34 states the sensible change of the water vapor enthalpy $\Delta\dot{H}_{V,sen}$ assuming that the water vapor temperature adjusts to the air outlet temperature before the vapor is absorbed.

$$\Delta\dot{H}_{V,sen} = \dot{M}_V \cdot c_{p,V} \cdot (T_{A,o} - T_{S,o}) \tag{3.34}$$

The term $\Delta\dot{H}_{abs}$ summarizes the latent changes. As the absorption of water vapor by the aqueous lithium chloride solution is an exothermic process, it releases this heat flow during the absorption.

$$\Delta\dot{H}_{abs} = \dot{M}_V \cdot \big(r_0 - (c_{p,W} - c_{p,V}) \cdot T_{S,o}\big) + \Delta\dot{H}_{Slt} \tag{3.35}$$

$\Delta\dot{H}_{abs}$ splits up into the enthalpy of condensation $\Delta\dot{H}_{con}$

$$\Delta\dot{H}_{con} = \dot{M}_V \cdot \big(r_0 - (c_{p,W} - c_{p,V}) \cdot T_{S,o}\big) \tag{3.36}$$

and $\Delta\dot{H}_{Slt}$, see equation 3.25, accounts for the enthalpy of dilution.

The specific enthalpy of dilution h_{dil} states the heat released per mass unit of absorbed water vapor and is a function of C_S. Yet, the definition of specific enthalpy of the salt solution requires an expression for h_{Slt} that relates the heat of absorption to the mass of salt in the solution. This derivation of h_{Slt} starts with the mean specific enthalpy of dilution $h_{dil,\text{mean}}$ representing the mean enthalpy of dilution between the concentrations $C_{S,i}$ and $C_{S,o}$.

$$\begin{aligned} h_{dil,\text{mean}} &= \frac{\Delta\dot{H}_{Slt}}{\dot{M}_V} = \frac{\dot{M}_{S,i} \cdot C_{S,i} \cdot h_{Slt,i} - \dot{M}_{S,o} \cdot C_{S,o} \cdot h_{Slt,o}}{\dot{M}_V} = \\ &= \frac{\dot{M}_{Slt} \cdot h_{Slt,i} - \dot{M}_{Slt} \cdot h_{Slt,o}}{\dot{M}_{S,o} - \dot{M}_{S,i}} = \frac{\dot{M}_{Slt} \cdot (h_{Slt,i} - h_{Slt,o})}{\dot{M}_{Slt} \cdot \frac{\dot{M}_{S,o}}{\dot{M}_{Slt}} - \dot{M}_{Slt} \cdot \frac{\dot{M}_{S,i}}{\dot{M}_{Slt}}} = \\ &= \frac{\dot{M}_{Slt} \cdot (h_{Slt,i} - h_{Slt,o})}{\dot{M}_{Slt} \cdot (\frac{1}{C_{S,o}} - \frac{1}{C_{S,i}})} = \frac{h_{Slt,i} - h_{Slt,o}}{\frac{1}{C_{S,o}} - \frac{1}{C_{S,i}}} \end{aligned} \tag{3.37}$$

$$h_{Slt,i} - h_{Slt,o} = h_{dil,\text{mean}} \cdot (\frac{1}{C_{S,o}} - \frac{1}{C_{S,i}}) \tag{3.38}$$

While h_{dil} gives the enthalpy of dilution as function of C_S, $h_{dil,\text{mean}}$ is the mean enthalpy of dilution between the concentrations $C_{S,i}$ and $C_{S,o}$. The mean function value

of a certain interval can be calculated by integrating the function in the considered interval and dividing the result by the difference of the both end points,

$$h_{dil,\text{mean}} = \frac{1}{C_{S,o} - C_{S,i}} \cdot \int_{C_{S,i}}^{C_{S,o}} h_{dil}\ dC_S \tag{3.39}$$

leading to the following expression for $h_{Slt,i} - h_{Slt,o}$.

$$h_{Slt,i} - h_{Slt,o} = \frac{1}{C_{S,o} - C_{S,i}} \cdot (\frac{1}{C_{S,o}} - \frac{1}{C_{S,i}}) \cdot \int_{C_{S,i}}^{C_{S,o}} h_{dil}\ dC_S \tag{3.40}$$

Simplification of equation 3.40

$$h_{Slt,o} - h_{Slt,i} = \frac{1}{C_{S,o} \cdot C_{S,i}} \cdot \int_{C_{S,i}}^{C_{S,o}} h_{dil}\ dC_S \tag{3.41}$$

and limit approach with $C_{S,i} \to C_S, C_{S,o} \to C_S + dC$ and $dC \to 0$ leads to

$$\frac{dh_{Slt}(C_S)}{dC_S} \cdot dC_S = \frac{1}{{C_S}^2} \cdot h_{dil}(C_S) \cdot dC_S \tag{3.42}$$

$$\frac{dh_{Slt}(C_S)}{dC_S} = \frac{1}{{C_S}^2} \cdot h_{dil}(C_S). \tag{3.43}$$

Integration of equation 3.43 leads to an expression for the specific salt enthalpy h_{Slt} as function of C_S. It includes $h_{dil}(C_S)$, the enthalpy of dilution plotted in Figure 3.5, that can be deduced from experimental data.

$$h_{Slt}(C_S) = \int_0^{C_S} \Big(\frac{1}{{C_S}^2} \cdot h_{dil}(C_S)\Big) dC_S \tag{3.44}$$

This simplified approach neglects the temperature dependency of the enthalpy of dilution and equation 3.45 states the proposed fit function for h_{dil}.

$$h_{dil} = a_4 \cdot {C_S}^4 + a_3 \cdot {C_S}^3 + a_2 \cdot {C_S}^2 \tag{3.45}$$

It includes no constant term because $h_{dil}(C_S = 0) = 0$ and no liner term because $h_{Slt}(C_S = 0) = 0$

$$h_{dil} \cdot \frac{1}{{C_S}^2} = a_4 \cdot {C_S}^2 + a_3 \cdot C_S + a_2 \tag{3.46}$$

$$h_{Slt}(C_S) = \int \Big(h_{dil} \cdot \frac{1}{{C_S}^2}\Big)\ dC_S = a_4 \cdot \frac{{C_S}^3}{3} + a_3 \cdot \frac{{C_S}^2}{2} + a_2 \cdot C_S + a_1 \tag{3.47}$$

with $a_1 = 0$.

A numerical fit of the data for h_{dil} at 20 °C yields

$$h_{Slt,fit}(C_S) = -1980.3744 \cdot {C_S}^3 + 2277.68505 \cdot {C_S}^2 + 1059.288 \cdot C_S. \tag{3.48}$$

Thus, this research applies the approximation for the enthalpy of aqueous lithium chloride solutions as function of concentration and temperature stated in equation 3.49.

$$\begin{aligned} h_S =&(1 - C_S) \cdot c_{p,W} \cdot T_S + C_S \cdot c_{p,Slt} \cdot T_S - \\ &- 1980.3744 \cdot {C_S}^4 + 2277.68505 \cdot {C_S}^3 + 1059.288 \cdot {C_S}^2 \end{aligned} \tag{3.49}$$

3.1.3 Sorption Processes with Liquid Desiccants

In industry, liquid desiccants are also utilized to absorb another substance in the liquid desiccant and the term **absorption process** refers to this technical process. The subsequent exsorption of the previously absorbed substance is called **regeneration process** of the liquid desiccant.

In this research focusing on efficient energy storage in liquid desiccant cooling systems, absorption exclusively refers to the absorption of water vapor from the air humidity in the salt solution and regeneration relates to the reconcentration of the salt solution by evaporating water vapor out of the solution.

Absorption Process

Liquid desiccant cooling systems apply an absorption process for the dehumidification of the supply air for a building. A concentrated salt solution with the inlet concentration $C_{S,con}$ absorbs water vapor from the air humidity and is diluted to the outlet concentration $C_{S,dil}$. Simultaneously, the humidity ratio of the inlet air decreases from the moist outside humidity ratio $X_{A,\text{outside}}$ to the required supply humidity ratio $X_{A,\text{supply}}$.

Figure 3.7 illustrates two absorptive air dehumidification processes, an adiabatic and a cooled one. To illustrate the changes in state, the psychrometric chart in Figure 3.7 also includes salt concentration isolines as dotted lines. For a constant salt concentration of the solution, they plot the equilibrium humidity ratio of the air above the salt solution in relation to the temperature.

The two example air dehumidification processes in Figure 3.7 visualize the advantage of a simultaneous cooling of the absorption process to lower the humidity ratio of the supply air provided by an LDCS. In both cases, the adiabatic and the cooled one, the

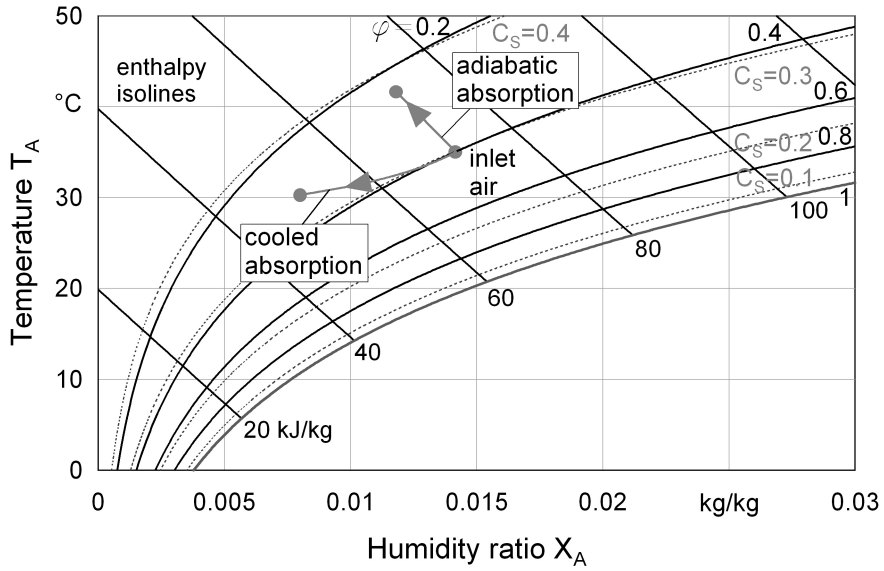

Figure 3.7: *Psychrometric chart for an adiabatic and a cooled air dehumidification process, inlet air temperature:* $T_A = 35\ °C$*, relative humidity:* $\varphi_A = 0.4$*, inlet concentration of the LiCl-solution:* $C_{S,con} = 44\%$

driving force for the dehumidification is an aqueous lithium chloride solution with an inlet concentration of 44%.

The adiabatic process shows that without cooling the temperature of the air rises because of the heat of absorption that is released during the absorption process, see subsection 3.1.2. As the heat of absorption does not only include the heat of condensation but also the heat of dilution that leads to a temperature increase, the line plotting this change of state is steeper than an enthalpy isoline. Both, air and solution temperature rise. For the same concentration, the equilibrium humidity ratio of the solution increases with temperature. Therefore, a rise in the solution temperature causes a decrease of the driving force for the dehumidification process.

The line plotting the cooled dehumidification process ends at a state of air with a lower air temperature and a lower humidity ratio. Withdrawing heat from the system during the absorption process maintains the temperature level of the salt solution. This prevents the decrease of the driving force for the dehumidification due to the increase of the solution temperature. The cooling options are not limited to withdrawing only the heat of absorption.

Regeneration Process

The regeneration process reconcentrates the diluted solution from the absorption process with the concentration $C_{S,dil}$ to its initial concentration $C_{S,con}$ by evaporating

the water that has been absorbed. Heat drives the regeneration process and in open sorption systems, this water vapor directly evaporates into ambient air.

3.1.4 Energy Storage in Liquid Desiccants

As the dehumidification process is driven by the concentrated solution only and without further thermal energy supply, the concentrated solution can serve as storage medium for the driving energy for the dehumidification process. Comparable to thermal storage systems with the temperature difference between inlet and outlet temperature as measure for the stored thermal energy, in LDCS, the concentration difference between concentrated and diluted solution is a measure for the stored energy. The higher the concentration difference is, the higher is the amount of stored energy. Storing energy by means of a concentration difference belongs to the storage method **thermochemical storage**.

The volumetric energy storage capacity SC quantifies the stored energy per volume of the storage medium. As this research only relates the stored energy to the volume of the storage medium and never to the mass of the storage medium, the abbreviation energy storage capacity always refers to the volumetric energy storage capacity.

In dehumidification applications, SC is defined as the ratio of the dehumidification energy to the volume of the storage medium, i.e. the enthalpy of removed water vapor per volume of diluted solution $V_{S,dil}$.

$$\text{volumetric energy storage capacity } SC = \frac{\text{dehumidification energy}}{\text{volume of diluted solution}} \tag{3.50}$$

This dehumidification energy can be calculated from the latent heat load given in equation 3.8 that includes the heat of evaporation and the mass of absorbed water vapor ΔM_V. By definition, the energy storage capacity of a LDCS specifies the directly applicable dehumidification energy for air-conditioning. As during the regeneration process, the heat of dilution has to be supplied additionally to the heat of evaporation, the energy input into the regenerator is about 10% higher than the applicable dehumidification energy.

Keßling (1998) deduced an equation for the energy storage capacity in liquid desiccants for air dehumidification that includes the concentrations of the concentrated solution $C_{S,con}$ and the diluted solution $C_{S,dil}$. It expresses the mass of absorbed water vapor ΔM_V by these concentrations and the mass of diluted solution $M_{S,dil}$.

$$\Delta M_V = M_{S,dil} \cdot C_{S,dil} \cdot \left(\frac{1 - C_{S,dil}}{C_{S,dil}} - \frac{1 - C_{S,con}}{C_{S,con}} \right) \tag{3.51}$$

This leads to the expression for the volumetric energy storage capacity SC of a LDCS.

$$\begin{aligned} SC &= \frac{M_{S,dil} \cdot C_{S,dil}}{V_{S,dil}} \cdot \left(\frac{1 - C_{S,dil}}{C_{S,dil}} - \frac{1 - C_{S,con}}{C_{S,con}} \right) \cdot r_0 = \\ &= \rho_{S,dil} \cdot C_{S,dil} \cdot \left(\frac{1 - C_{S,dil}}{C_{S,dil}} - \frac{1 - C_{S,con}}{C_{S,con}} \right) \cdot r_0 \end{aligned} \tag{3.52}$$

Thus, the concentrations of the diluted and the concentrated solution and the density of the diluted solution allow an assessment of the energy storage potential of the system. The solubility boundary limits the concentration of the concentrated solution and the solubility boundary lies at 45.2% at 19 °C [Conde 2004]. To definitely prevent crystallization in the tank, the reference concentration is set to 44%. Figure 3.8 plots the energy storage capacity as function of the concentration of the diluted solution and the reference concentrated solution of 44%.

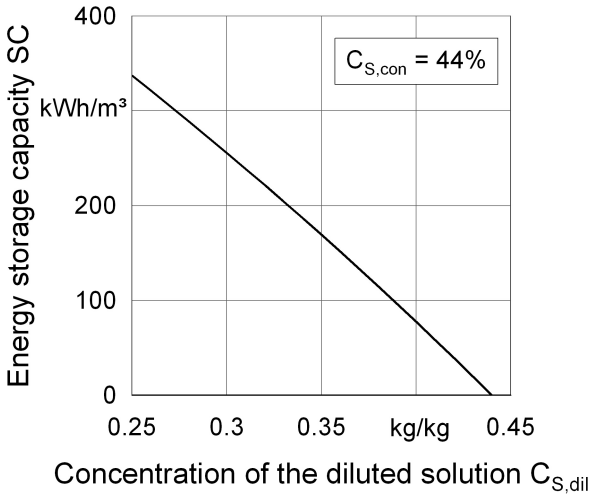

Figure 3.8: *Energy storage capacity SC as function of the concentration of the diluted solution, concentration of the concentrated solution* $C_{S,con} = 44\%$

The solubility of the lithium chloride provides the upper limit for the concentration of the concentrated solution. The theoretical lower limit for the concentration of the diluted solution is defined by the thermodynamical equilibrium. Yet, in LDCS, the operating conditions of the absorption process preset the concentration of the diluted solution. Main influence factor on the diluted concentration is the ratio of air flow to solution flow. One option for quantifying this relation is the mass flow ratio of air to liquid desiccant flow MR. MR ranges between 0.5 and 80.

$$MR = \frac{\dot{M}_A}{\dot{M}_S} \tag{3.53}$$

The more common option for quantifying the relation between the two flows is the

liquid to gas ratio $\dot{L}/\dot{G}$. $\dot{L}/\dot{G}$ ranges between 0.015 and 2.4.

$$\dot{L}/\dot{G} = \frac{\tilde{M}_A}{\tilde{M}_S} \cdot \frac{1}{MR} \tag{3.54}$$

Figure 3.9 plots the dehumidification and the energy storage capacity as function of the liquid to gas ratio for the case of an ideally cooled absorption.

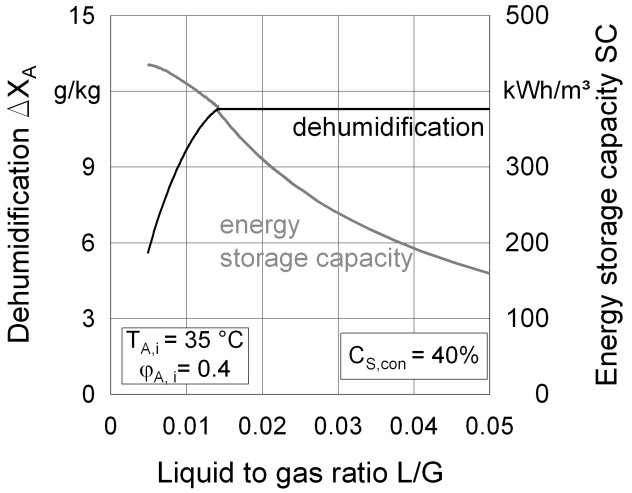

Figure 3.9: *Air dehumidification and energy storage capacity as function of the liquid to gas ratio for the case of ideally cooled absorption, inlet air temperature 35 °C, relative humidity: 40%, inlet concentration of the LiCl-solution: 40%*

Figure 3.9 shows that for the case of an ideally cooled absorption, the obtainable dehumidification is limited by the equilibrium data and a further increase of the liquid to gas ratio does not improve the dehumidification. Yet, for this example, values of $\dot{L}/\dot{G}$ below 0.014 lead to a decrease of the obtainable dehumidification. The solution flow does not provide enough capacity to absorb the water vapor from the air. Lowering the liquid to gas ratio leads to a better dilution of the solution as less solution absorbs the same amount of water vapor. Therefore, the energy storage capacity increases with a decreasing liquid to gas ratio.

While providing dehumidified supply air is the prime demand for an LDCS, the energy storage capacity can also play an important role, especially for LDCS driven by a discontinuous energy supply such as solar energy. The storage bridges the mismatch between energy demand and supply. The optimum operating point that still ensures the required dehumidification and aims at a high energy storage capacity lies at $MR \approx 80$, i.e. $\dot{L}/\dot{G} \approx 0.015$. This research focuses on LDSC operating in this mass flow range, referred to as **low-flow** LDCS. **High-flow** LDCS operate in the mass flow range of 0.5 to 1. See section 4.3 for a comparison of both systems.

3.2 Low-Flow Liquid Desiccant Cooling System with Energy Storage

Figure 3.10a shows the schematic of the low-flow LDCS with energy storage under development at the ZAE Bayern. Figure 3.10b illustrates the air state changes in a psychrometric chart that includes enthalpy isolines for specific wet bulb temperatures.

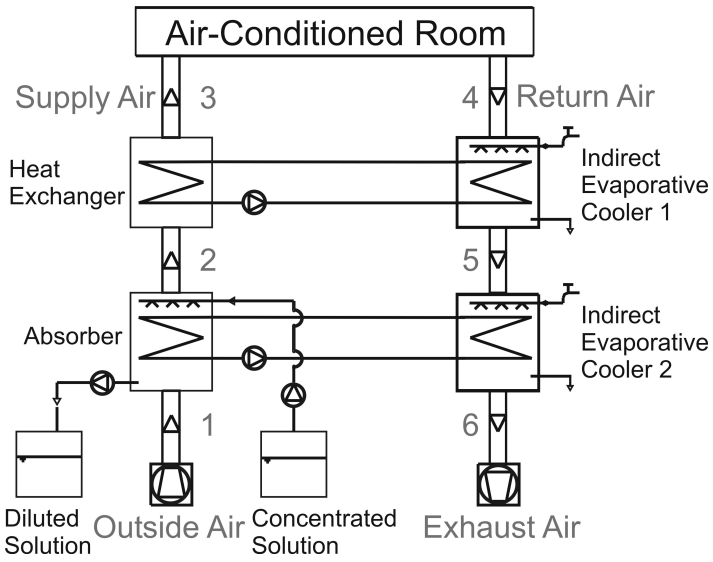

(a)

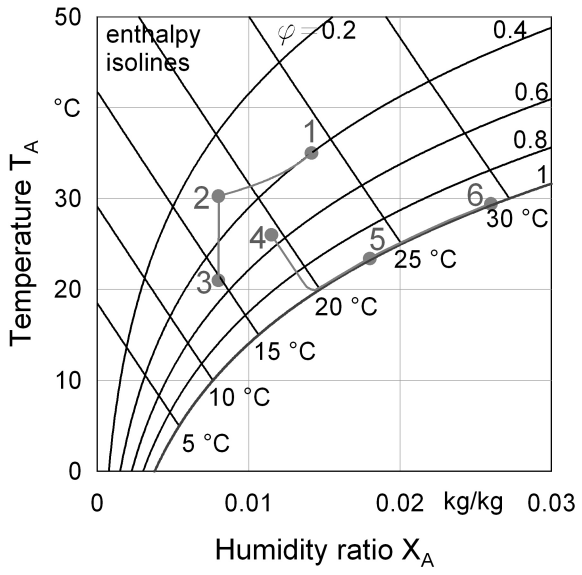

(b)

Figure 3.10: *Low-flow liquid desiccant cooling system with energy storage (a) schematic diagram (b) psychrometric chart*

The absorber dehumidifies the inlet air with ARI-conditions (dry bulb temperature of 35 °C and a relative humidity of 0.4) to the pre-determined supply air humidity ratio, in this example $X_{A,\text{supply}} = 8$ g/kg. A subsequent heat exchanger cools the air to the pre-determined supply air temperature of $T_{A,\text{supply}} = 21$ °C for this example. In the room, the air takes up humidity and its temperature increases.

Only 80% of the supply air flow are withdrawn as return air to prevent infiltration of untreated outside air. The return air conditions are $T_{A,\text{return}} = 26$ °C and $X_{A,\text{return}} = 11.5$ g/kg. As the wet bulb temperature of the return air from the air-conditioned room lies at $T_{wb,\text{return}} = 19.3$ °C, it is suitable for providing cold for the absorber and the heat exchanger by evaporative cooling. The wet bulb temperature of the outside reference conditions only lies at $T_{wb,\text{outside}} = 24$ °C. Therefore, in two subsequent indirect evaporative coolers, water is evaporated into the return air cooling it down. Simultaneously, heat is transferred from the heat exchanger and the absorber further enhancing the evaporation. The exhaust air has a lower temperature than the outside air but it is saturated and its cooling potential therefore depleted.

3.3 Components of Liquid Desiccant Cooling Systems

This section characterizes the main components of the low-flow LDCS this research focuses on: absorber, regenerator and indirect evaporative cooler.

3.3.1 Absorber

The absorber is the most critical part of the system in terms of performance. To ensure high energy storage capacities, it has to operate with a low liquid to gas ratio. For a simultaneous cooling of the absorption process, it has to provide a cooled exchange surface for the heat and mass transfer. Thus, the interior of the absorber is filled with a structured packing of parallel vertical plates as shown in Figure 3.11. Internally cooled packings formed of corrugated sheets cause a high pressure drop and therefore require high performance blowers that are more expensive than conventional components for air-conditioning systems. Therefore, parallel plates in a vertical alignment form the structured packing inside the absorber.

Structured packing in the absorber

The following dimensions define the absorber packing: height h_{pl}, width w_{pl} and thickness s_{pl} of the exchange plates and the distance between the exchange plates d_{pl}.

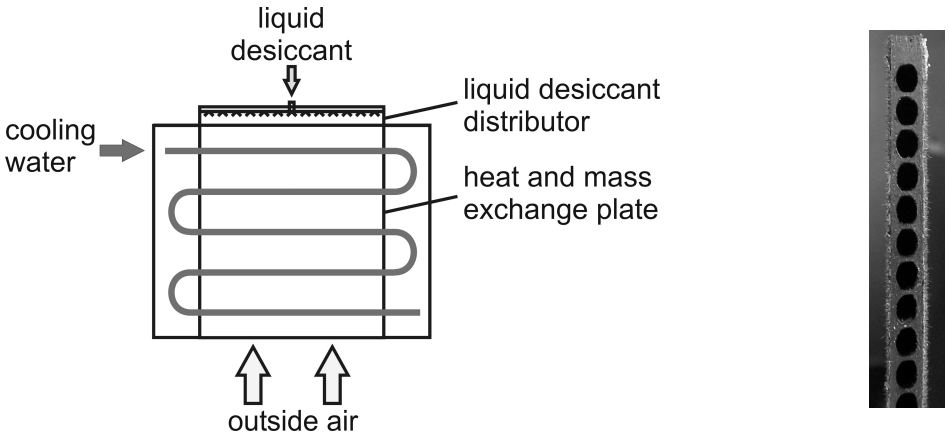

Figure 3.11: *Heat and mass transfer plate (a) schematic diagram (b) detail of the cooling water channels, side view of the plate*

Table 3.1 lists the reference values for the packing dimensions. For the considered absorber design, the height of the packing h_{pac} is equal to the height of the exchange plate h_{pl} and the width of the packing w_{pac} is equal to the width of the exchange plate w_{pl}.

Table 3.1: *Dimensions of the structured packing inside the absorber*

Parameter	**Variabel**	**Reference Value**
height of the exchange plate	h_{pl}	0.8 m
width of the exchange plate	w_{pl}	1 m
thickness of the exchange plate	s_{pl}	0.004 m
distance of the exchange plates	d_{pl}	0.004 m
height of the packing	h_{pac}	0.8 m
width of the packing	w_{pac}	1 m
thickness of the packing	s_{pac}	1 m

Equation 3.55 defines the cross sectional area of the packing

$$A_{pac} = s_{pac} \cdot w_{pl} \tag{3.55}$$

and equation 3.56 specifies the number of exchange plates in the packing n_{pl}.

$$n_{pl} = \frac{s_{pac} + d_{pl}}{s_{pl} + d_{pl}} \tag{3.56}$$

As the thickness of the packing s_{pac} exceeds the thickness of the exchange plate s_{pl} by far, simplifying equation 3.56 yields

$$n_{pl} = \frac{s_{pac}}{s_{pl} + d_{pl}}. \tag{3.57}$$

Equation 3.58 deducts the specific area of the packing a given by the exchange surface per volume unit of the packing.

$$a = \frac{2 \cdot n_{pl} \cdot h_{pl} \cdot w_{pl}}{s_{pac} \cdot h_{pac} \cdot w_{pac}} = \frac{2 \cdot s_{pac} \cdot h_{pl} \cdot w_{pl}}{(s_{pl} + d_{pl}) \cdot s_{pac} \cdot h_{pl} \cdot w_{pl}} = \frac{2}{s_{pl} + d_{pl}} \tag{3.58}$$

Thus, the specific area of the packing a only depends on the thickness of the exchange plates s_{pl} and their distance d_{pl}.

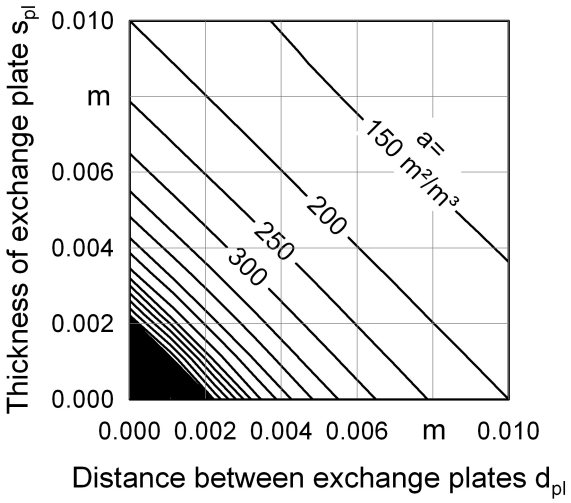

Figure 3.12: *Specific area of the structured packing in the absorber*

Figure 3.12 shows the range of the specific area of the structured packing as function of the thickness of the exchange plates s_{pl} and their distance d_{pl}. The reference dimensions, a thickness of the exchange plates of $s_{pl} = 4$ mm and a distance of the exchange plates of $d_{pl} = 4$ mm, lead to a number of 125 plates per meter absorber length and a specific area of the packing of 250 m^2/m^3 absorber volume. These dimensions provide optimal exchange area per absorber volume and yet allow sufficient cooling of the exchange plate through the internal cooling water channels of the exchange plate.

Air flow in the absorber

Experiments detected a carry-over of solution droplets into the air flow for an air velocity u_A in the gap above 4.4 m/s [Kapfhammer 1997]. To prevent this carry-over, the air velocity is set to 3 m/s. The air velocity and the cross sectional area of the gap between the exchange plates A_{gap} given by equation 3.59

$$A_{\text{gap}} = d_{pl} \cdot w_{pl} \tag{3.59}$$

determine the volume flow of air per gap $\dot{V}_{A,\text{gap}}$.

$$\dot{V}_{A,\text{gap}} = u_A \cdot A_{\text{gap}} \tag{3.60}$$

This volume flow of air per gap $\dot{V}_{A,\text{gap}}$ and the number of gaps n_{gaps} define the total volume flow of air $\dot{V}_A$ in the absorber.

$$\dot{V}_A = n_{\text{gap}} \cdot \dot{V}_{A,\text{gap}} = (n_{pl} - 1) \cdot A_{\text{gap}} \cdot u_A = \left(\frac{s_{pac}}{s_{pl} + d_{pl}} - 1 \right) \cdot d_{pl} \cdot w_{pl} \cdot u_A \tag{3.61}$$

For the further calculations, also the air mass flow rate $\dot{M}_A$ and the gas flow rate $\dot{G}$ are defined.

$$\dot{M}_A = \rho_A \cdot \dot{V}_A \tag{3.62}$$

$$\dot{G} = \frac{\dot{M}_A}{\tilde{M}_A} \tag{3.63}$$

Solution flow in the absorber

While the air flow depends mainly on the cooling and dehumidification load of the building, the solution flow additionally depends on the requirements for the energy storage capacity. The higher the intended energy storage capacity, the lower the solution flow may be, see Figure 3.9. A mass flow ratio of air flow to solution flow of $MR \approx 80$ provides an optimum between the best energy storage capacity for yet best dehumidification performance. Thus, the air mass flow $\dot{M}_A$ and the mass flow ratio MR define the solution mass flow $\dot{M}_S$ according to Equation 3.53.

The solution volume flow $\dot{V}_S$ is determined by the density of the solution ρ_S and the solution mass flow $\dot{M}_S$. The number of gaps n_{gaps} defines the solution volume flow per gap $\dot{V}_{S,\text{gap}}$. As this solution volume flow per gap flows down on both sides of the channel, the solution volume flow per side of the exchange plate is half the solution volume flow per gap $\dot{V}_{S,\text{gap}}$. Both sides of each exchange plate provide a surface for the heat and mass transfer and the solution distributor at the top of each exchange plate also provides solution for both sides of the exchange plate. Consequently, the solution flow that the solution distributor has to distribute is equal to the solution volume flow per gap $\dot{V}_{S,\text{gap}}$.

The key parameter for the distributor is the specific volume flow of solution $\dot{v}_S$. It is defined as the solution flow that the distributor has to distribute evenly on each side of the exchange plate per width of the exchange plate. Equation 3.64 states the

equation for $\dot{v}_S$.

$$\begin{aligned} \dot{v}_S &= \frac{1}{2} \cdot \frac{\dot{V}_{S,\mathrm{gap}}}{w_{pl}} = \frac{1}{2} \cdot \frac{\dot{M}_{S,\mathrm{gap}}}{w_{pl} \cdot \rho_S} = \frac{1}{2} \cdot \frac{\dot{M}_{A,\mathrm{gap}}}{w_{pl} \cdot \rho_S \cdot MR} = \frac{1}{2} \cdot \frac{\dot{V}_{A,\mathrm{gap}} \cdot \rho_A}{w_{pl} \cdot \rho_S \cdot MR} = \\ &= \frac{1}{2} \cdot \frac{u_A \cdot A_{\mathrm{gap}} \cdot \rho_A}{w_{pl} \cdot \rho_S \cdot MR} = \frac{1}{2} \cdot \frac{u_A \cdot d_{pl} \cdot w_{pl} \cdot \rho_A}{w_{pl} \cdot \rho_S \cdot MR} = \frac{1}{2} \cdot d_{pl} \cdot \frac{\rho_A}{\rho_S} \cdot \frac{u_A}{MR} \end{aligned} \tag{3.64}$$

Thus, the specific volume flow of solution $\dot{v}_S$ depends on packing geometry, i.e. distance between the exchange plates, thermodynamical data, i.e. density of air and solution, and on operating conditions, i.e. air velocity and the mass flow ratio of air flow to solution flow. The reference conditions for the energy storage capacity demand a mass flow ratio MR of 80. Thus, the distributor has to distribute the specific volume flow $\dot{v}_S = 0.23$ l/(h m)$= 6.5 \cdot 10^{-8}$ m^3/(s m) evenly on each side of the plate.

Comparison of liquid load in the low-flow absorber with the recommended minimum liquid load for packed columns

The liquid load of a packed column $\dot{V}_L/A_c$ is the volume flow of liquid per cross sectional area of the packed column A_c. The liquid load can also be expressed as superficial velocity of the liquid u_L.

Figure 3.13 shows the typical operating region for structured packings and the common operational range of liquid distributors. It includes the operating point for the reference conditions. While the gas load is in the typical operating region for structured packings, the liquid load is by far lower than the common operating conditions for structured packings and liquid distributors.

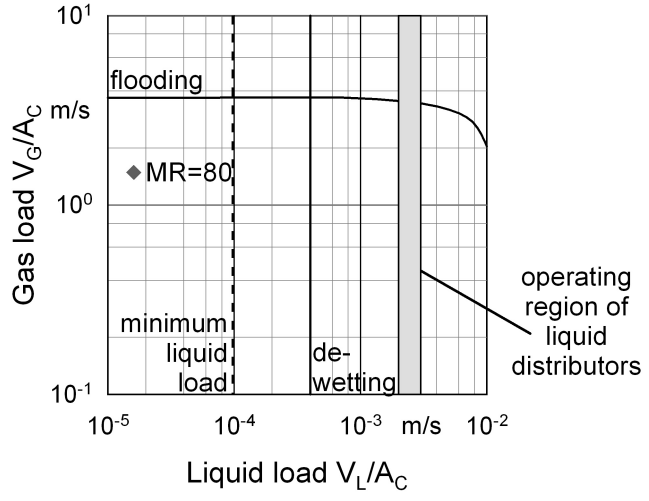

Figure 3.13: *Operating region of structured packings and liquid distributors, adopted from Stichlmair and Fair (1998)*

The position of the dewetting-line in Figure 3.13 depends on the thermodynamical properties of the liquid that has to be distributed. The dewetting-line plots the minimum liquid load for the specific liquid and equation 3.65 is suitable for estimating this minimum liquid load [Stichlmair and Fair 1998].

$$u_{L,min} = 7.7 \cdot 10^{-6} \cdot \left(\frac{\rho_L \cdot \sigma^3}{\eta_L^4 \cdot g} \right)^{2/9} \cdot \left(\frac{g}{a} \right)^{1/2} \tag{3.65}$$

Applying equation 3.65 and including the thermodynamical properties of the concentrated solution such as density $\rho_L = 1.28 \cdot 10^3$ kg/m^3, surface tension $\sigma = 9.86 \cdot 10^{-2}$ N/m and dynamic viscosity $\eta_L = 5.58 \cdot 10^{-3}$ kg/(m s), the specific area of the packing $a = 250$ m^2, and the acceleration due to gravity $g = 9.81$ m/s^2 yields the minimum superficial velocity of $u_{L,min} = 9.67 \cdot 10^{-5}$ m/s and the minimum liquid load for the absorber $\dot{V}_L/A_c = 0.348$ m^3/(m^{2}h).

Combining equations 3.55, 3.57, and 3.64, equation 3.66 deducts the liquid load in the low-flow absorber as function of packing geometry, thermodynamical data, and operating conditions.

$$\dot{V}_L/A_c = \frac{\dot{V}_S}{A_{pac}} = \frac{\dot{v}_S \cdot w_{pl} \cdot n_{pl} \cdot 2}{A_{pac}} = \frac{d_{pl}}{s_{pl} + d_{pl}} \cdot \frac{\rho_A}{\rho_S} \cdot \frac{u_A}{MR} \tag{3.66}$$

For the reference dimensions of the absorber packing, Figure 3.14 shows the recommended minimum liquid load and the liquid load in the low-flow absorber as function of the mass flow ratio air to solution MR and the liquid to gas ratio $\dot{L}/\dot{G}$. For a mass flow ratio of $MR = 80$, the liquid load lies at $\dot{V}_L/A_c = 0.0578$ m^3/(m^{2}h) and the superficial velocity lies at $u_{L,min} = 1.61 \cdot 10^{-5}$ m/s.

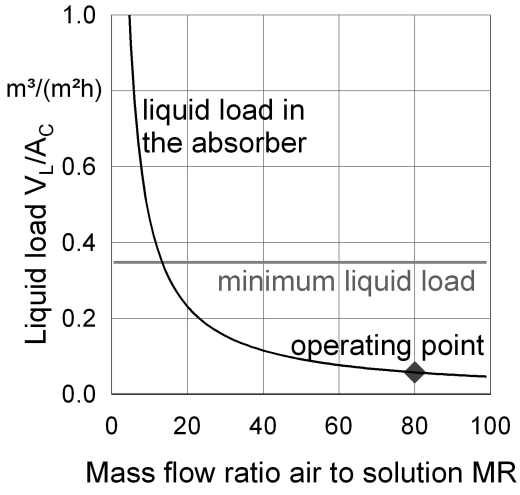

Figure 3.14: *Minimum liquid load and liquid load in the absorber of low-flow LDCS as function of the mass flow ratio air to solution*

Cooling water flow in the absorber

The cooling water has to withdraw the heat of absorption that is released during the dehumidification process and possibly provide a further pre-cooling of the air. The cooling water flows inside the heat and mass transfer plates shown in Figure 3.15 and passes the absorber in a cross current flow. The cooling water mass flow $\dot{M}_W$ that is required to provide the preset cooling can be calculated with the conventional heat balances for heat exchangers.

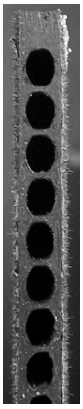

Figure 3.15: *Side view of a heat and mass transfer plate with cooling water channels*

3.3.2 Regenerator

Regenerator and absorber can be identical in design. While the absorber operates in a very limited operating region because it has to meet two requirements at the same time, dehumidifying the air to the supply air humidity ratio and providing a good energy storage capacity by diluting the solution to a low outlet concentration, the regenerator can operate in a broader operating range. It only has to reconcentrate the solution to 44%. The change in humidity of the air that passes the regenerator does not have to meet strict specifications. Yet, the air velocity is also limited to 3 m/s to prevent any carryover of solution. In principle, the mass flow ratio *MR* in the regenerator can vary in a broad range and the optimal *MR* depends on the temperature level of the heat supply. A regenerator that is identical in its dimensions with the absorber presented in subsection 3.3.1 and that is supplied by heating water with a temperature level of 70 °C reconcentrates the solution with an inlet concentration of 29% to the required outlet concentration of 44% operating with a *MR* of 18 in the regenerator. Figure 3.16a shows that for higher heating water inlet temperatures, the optimal *MR* decreases, i.e. the solution mass flow rate can be increased. Preheating the inlet air also decreases *MR*. Compared to the cooling and dehumidification power provided by the absorber, the relative power of a regenerator

with identical dimension is significantly higher. Figure 3.16b plots the regeneration power as function of the heating water inlet temperature relative to the cooling power provided by the absorber presented in subsection 3.3.1 with identical dimensions.

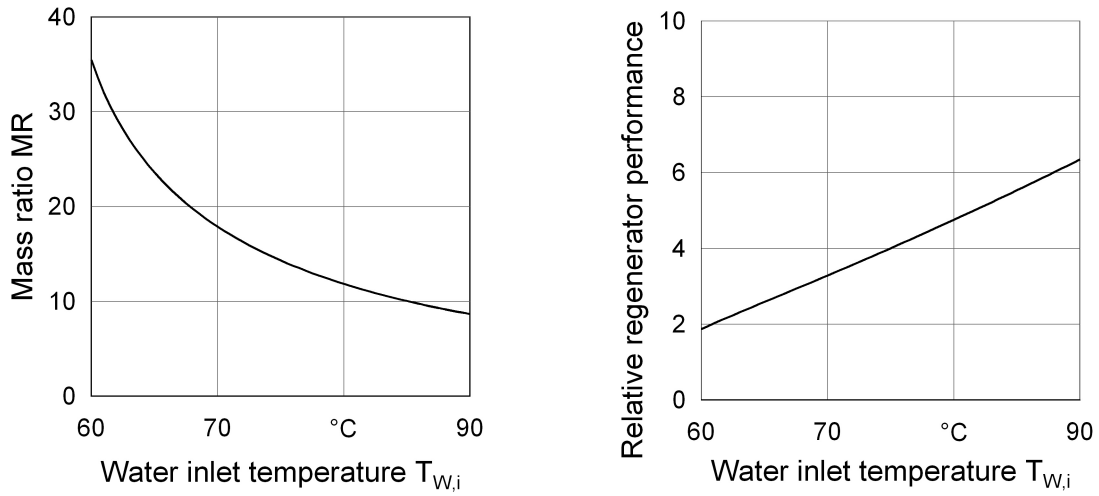

(a) (b)

Figure 3.16: *Influence of the heating water inlet temperature on (a) the mass flow ratio MR and (b) the regenerator performance relative to an absorber of the same size*

The material properties of the PP-plates limit the possible heating water inlet temperature. Though increasing the inlet temperature from 70 °C to 90 °C almost doubles the regenerator performance, the lack of stability of PP at high temperatures does not allow such high temperatures for the structured PP-packing. Another challenge for the regenerator design is that maldistribution of the solution in the regenerator can lead to local crystallization of the salt. Crystals that remain in the regenerator lead to a lower outlet concentration of the solution after the regeneration process. Therefore, alternative concepts for the regenerator are under development.

3.3.3 Indirect Evaporative Cooler

The indirect evaporative cooler cools circuit water by evaporative cooling. It consists of a conventional finned air-water-heat-exchanger that is sprayed with water. The fins are coated with a hydrophilic material. Figure 3.17 shows a schematic diagram of an indirect evaporative cooler, a detail of the fins and one of a spray nozzle. The air that flows through the indirect evaporative cooler saturates with water and cools down towards its wet bulb temperature. Simultaneously, the circuit water can transfer heat to the air, enhance the evaporation process and cool down itself. 30% of the water that is sprayed is evaporated, the rest elutriates the fins and is recirculated.

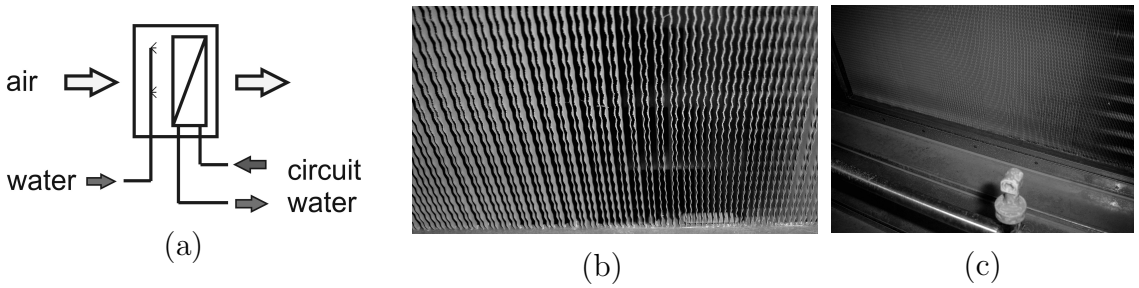

Figure 3.17: *Indirect evaporative cooler (a) schematic diagram (b) detail of the fins (c) spray nozzle*

3.3.4 Storage Tank

The required volume of the storage tank depends on the energy storage capacity. Theoretically, diluted and concentrated solution can be stored in the same tank, separated by a membrane. The volume of the solution increases during the absorption due to the absorbed water and therefore the storage tank has to embrace a volume that corresponds to the volume if all solution is diluted.

Common oil storage technology can be applied for the tank that can be a plastic tank or a steel tank with plastic liner. Plastic material is also appropriate for the piping. As the energy storage is accomplished thermochemically, the storage tank does not need any insulation.

Chapter 4

Modeling of Liquid Desiccant Cooling Systems

This chapter characterizes the development of a numerical model for simulating the components of liquid desiccant cooling systems. It presents the simulation of a low-flow and a high-flow LDCS and compares the energy storage potential of both systems.

4.1 Model Development

The objective of the model development was to create a numerical model for simulating the main components of the LDCS. According to the selected media and the flow directions, it simulates

- the air dehumidification process with a liquid desiccant
- the regeneration process of the liquid desiccant or
- the air humidification process in the indirect evaporative coolers.

Figure 4.1 shows the schematic for the model development. A one-dimensional steady state analysis describes the physical processes that take place between the three media air, solution and cooling or heating water, respectively. In this section, the three media involved in the processes are always referred to as air, solution and water though the solution is replaced by water for the case of the air humidification process in the indirect evaporative coolers.

All flow directions are defined positive according to the arrows in Figure 4.1 and a direction term adjusts the actual flow direction of solution and water. A negative direction term indicates counter-current flow of solution or water related to the direction of the air flow.

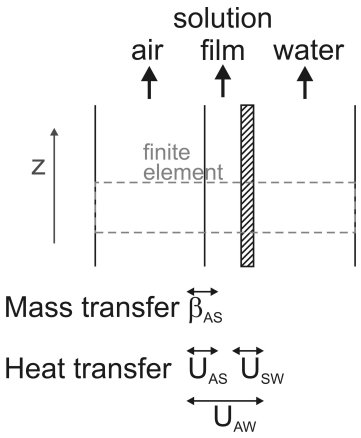

Figure 4.1: *Schematic for the model development: heat transfer takes place between air, solution and water, mass transfer takes place between air and solution*

4.1.1 Boundary Conditions and Assumptions

Boundary conditions for the heat and mass transfer

The exchange surface A is not completely wetted by the solution but splits into a fraction of wetted exchange surface A_{SW} and into a fraction of non-wetted exchange surface A_{AW} with $A = A_{SW} + A_{AW}$.

Heat transfer takes place between

- air and solution through the fraction of wetted exchange surface,
- solution and water through the fraction of wetted exchange surface, and
- air and water through the fraction of non-wetted exchange surface.

Mass transfer, i.e. transfer of water vapor, takes place between air and solution through the fraction of wetted exchange surface.

Assumptions for the heat and mass transfer

The model is based on the following assumptions:

- The absorption is steady-state and one-dimensional. For each medium, gradients of temperature, concentration or humidity ratio occur only in flow direction.
- The heat and mass transfer coefficients are constant along the z-axis.
- The total pressure is constant as the pressure drop in all media is negligible.

4.1.2 Mass and Enthalpy Balances

Table 4.1 lists the state variables for the process and Figure 4.2 shows them in the finite volume element for the model development. Figure 4.2 also includes the further variables that are required for the derivation of the heat and mass balances over the finite volume element and Table 4.2 characterizes them. z is a dimensionless control variable with $0 \leq z \leq 1$. It paces the exchange surface A with $dA = A \cdot dz$. z defines the positive air flow direction and the other flow directions are also defined positive. A direction term adjusts the actual flow direction of solution and water.

Table 4.1: *State variables of the process*

Variable	**Unit**	**Notation**
$T_A(z)$	°C	air temperature
$T_S(z)$	°C	solution temperature
$T_W(z)$	°C	water temperature
$X_A(z)$	kg/kg	air humidity ratio
$X_{Slt}(z)$	kg/kg	water content of the salt
$\dot{M}_A$	kg/s	mass flow of dry air
$\dot{M}_{Slt}$	kg/s	mass flow of salt
$\dot{M}_W$	kg/s	mass flow of water

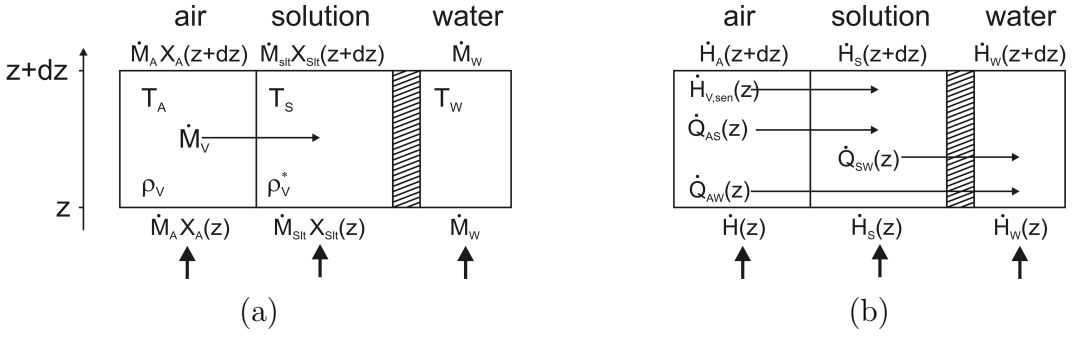

Figure 4.2: *Finite volume element with (a) mass flows (b) enthalpy flows*

Equations 4.1 to 4.3 state the heat transfer with a difference of temperatures as driving force and equation 4.4 states the mass transfer with a difference of partial densities as driving force.

Heat transfer

$$\dot{Q}_{AS}(z) = U_{AS} \cdot \Big(T_A(z) - T_S(z)\Big) \cdot A_{AS} \cdot dz \tag{4.1}$$

$$\dot{Q}_{SW}(z) = U_{SW} \cdot \Big(T_S(z) - T_W(z)\Big) \cdot A_{SW} \cdot dz \tag{4.2}$$

$$\dot{Q}_{AW}(z) = U_{AW} \cdot \Big(T_A(z) - T_W(z)\Big) \cdot A_{AW} \cdot dz \tag{4.3}$$

Mass transfer

$$\dot{M}_V(z) = \beta_{AS} \cdot \Big(\rho_V(z) - \rho_V^*(z)\Big) \cdot A_{AS} \cdot dz \tag{4.4}$$

Table 4.2: *Process variables*

Variable	Unit	Notation
$\dot{M}_V(z)$	kg/s	mass flow of water vapor transferred from the air to the solution
$\dot{H}_{V,sen}(z)$	kW	enthalpy flow that is released due to the absorption of the water vapor
$\dot{Q}_{AS}(z)$	kW	heat flow between air and solution
$\dot{Q}_{SW}(z)$	kW	heat flow between solution and water
$\dot{Q}_{AW}(z)$	kW	heat flow between air and water
U_{AS}	kW/(m^2 K)	heat transfer coefficient between air and solution
U_{SW}	kW/(m^2 K)	heat transfer coefficient between solution and water
U_{AW}	kW/(m^2 K)	heat transfer coefficient between air and water
β_{AS}	m/s	mass transfer coefficient between air and solution
$\rho_V(z)$	kg/m^3	partial density of water vapor
$\rho_V^*(z)$	kg/m^3	equilibrium partial density of water vapor

Mass Balances

The solution absorbs the water vapor removed from the air completely,

$$\dot{M}_A \frac{dX_A(z)}{dz} + \dot{M}_{Slt} \frac{dX_{Slt}(z)}{dz} = 0 \tag{4.5}$$

and the solution mass flow $\dot{M}_S(z)$ increases with the mass flow of absorbed water vapor $\dot{M}_V(z)$. This direction of the mass flow of water vapor has been defined in equation 4.4, i.e. from the air to the solution.

$$\frac{d\dot{M}_S(z)}{dz} = \dot{M}_V(z) \tag{4.6}$$

Enthalpy Balances

Equation 4.7 states the enthalpy balance for the air.

$$\frac{d\dot{H}_A(z)}{dz} - \dot{H}_V(z) - \dot{Q}_{AS}(z) - \dot{Q}_{AW}(z) = 0 \tag{4.7}$$

$$\dot{H}_V(z) = \dot{M}_V(z) \cdot \Big(c_{p,V} \cdot \big(T_A(z) - T_S(z) \big) + r_0 \Big) \tag{4.8}$$

Equation 4.9 states the enthalpy balance for the solution.

$$\frac{d\dot{H}_S(z)}{dz} + \dot{H}_V(z) + \dot{Q}_{AS}(z) - \dot{Q}_{SW}(z) = 0 \tag{4.9}$$

$$\dot{H}_S(z) = \dot{M}_S \cdot h_S\big(C_S(z), T_S(z)\big) \tag{4.10}$$

$H_S(z)$ is the enthalpy function of the solution. It comprises the sensible and latent changes in the enthalpy due to changes in temperature and concentration. A detailed deduction of $h_S\big(C_S(z), T_S(z)\big)$ is given in subsection 3.1.2.

4.1.3 Heat and Mass Transfer Coefficients

The heat and mass transfer coefficients can be estimated applying the thermodynamic data of the media and the dimensions and material properties of the heat and mass transfer plates. The equivalent thermal circuit concept is a useful tool for the development of the one dimensional steady state transfer model. The thermal resistance is defined as the ratio of the temperature difference to the corresponding heat transfer rate. The heat transfer coefficients are calculated according to VDI (1997) and Incropera *et al.* (2007).

Heat Transfer Coefficient U_{AW}

Through the fraction of non-wetted exchange surface A_{AW}, the air transfers heat to the cooling water. Figure 4.3 depicts the modes of heat transfer and states the equivalent thermal resistance circuit.

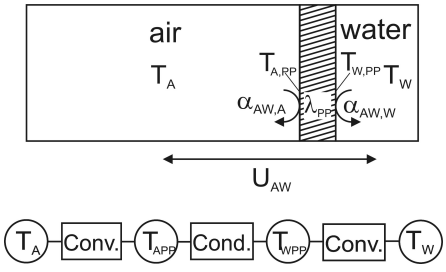

Figure 4.3: *Heat transfer and thermal resistance circuit for the non-wetted surface*

The heat transfer includes the following steps. First convection heat transfer takes place between the air and the plate outside, then heat is transferred by conduction through the PP-plate of the thickness s_{PP}. Heat transfer between the inner surface of the plate and the cooling water occurs due to convection. Due to the partitions between the cooling water channels, the inner surface of the PP-plate that can transfer heat to the cooling water is only 5/6 of A_{AW}. The individual heat transfer coefficients add up to U_{AW}.

$$\frac{1}{U_{AW}} = \frac{1}{\alpha_{AW,A}} + \frac{s_{PP}}{\lambda_{PP}} + \frac{1}{\frac{5}{6} \cdot \alpha_{AW,W}} \tag{4.11}$$

Equation 4.12 states the hydraulic diameter of the parallel-plate channel $d_{h,A}$ that is required to determine the air side heat transfer coefficient $\alpha_{AW,A}$ for forced convection.

$$d_{h,A} = 2 \cdot d_{pl} \tag{4.12}$$

Besides the hydraulic diameter $d_{h,A}$, the air velocity u_A, the dynamic viscosity η_A and the density ρ_A define the Reynolds number Re.

$$Re = u_A \cdot \frac{d_{h,A} \cdot \rho_A}{\eta_A} \tag{4.13}$$

For the boundary conditions given in section 3.3.1, the Reynolds number is below 2300 and therefore the flow is classified to be laminar. Equation 4.14 yields the mean Nusselt number Nu_m for a hydrodynamically fully developed flow in a parallel-plate channel.

$$Nu_m = \left(114.9 + 6.240 \cdot Re \cdot Pr_A \cdot \frac{d_{h,A}}{H_{pl}}\right)^{\frac{1}{3}} \tag{4.14}$$

Equation 4.14 includes the Prandtl number Pr that provides a measure of the relative effectiveness of momentum and energy transport by diffusion. Pr combines the fluid properties dynamic viscosity η, specific heat capacity cp and heat conductivity λ.

$$Pr = \frac{\eta \cdot c_p}{\lambda} \tag{4.15}$$

The mean Nusselt number Nu_m, hydraulic diameter and heat conductivity define the air side convective heat transfer coefficient $\alpha_{AW,A}$.

$$\alpha_{AW,A} = Nu_m \cdot \frac{\lambda_A}{d_h} \tag{4.16}$$

The water side convective heat transfer coefficient $\alpha_{AW,W}$ can be calculated analogously as the flow within the cooling water channels is also laminar.

For the boundary conditions given in section 3.3.1, Table 4.3 lists the convective and the conductive heat transfer coefficients that add up to $U_{AW} = 0.019\,\mathrm{kW/(m^2\,K)}$. The air side convective heat transfer coefficient $\alpha_{AW,A}$ has the lowest value and dominates the overall heat transfer from the air to the cooling water.

Table 4.3: *Individual heat transfer coefficients and overall heat transfer coefficient U_{AW} based on the boundary conditions for the absorber (see subsection 3.3.1)*

Heat Transfer Mode	**Variable**	**Value**	**Unit**
convection	$\alpha_{AW,A}$	0.021	$\mathrm{kW/(m^2\,K)}$
conduction	s_{PP}/λ_{PP}	0.22	$\mathrm{kW/(m^2\,K)}$
convection	$\alpha_{AW,W}$	1.0	$\mathrm{kW/(m^2\,K)}$
combined	U_{AW}	0.019	$\mathrm{kW/(m^2\,K)}$

A sensitivity analysis identifies the influence of a change of the distance of the exchange plates d_{pl} or of a variation of air velocity u_A or cooling water velocity u_W. Figure 4.4 plots $\alpha_{AW,A}$ and U_{AW} for varying operating conditions and shows that U_{AW} is more sensitive to a change of the distance of the exchange plates than to a varying air velocity or cooling water velocity. In Figure 4.4a, the air mass flow rate is kept constant and the velocity varies due to the varying distance of the exchange plates. In Figure 4.4b, the distance of the exchange plates is kept constant and the air mass flow rate varies due to the varying velocity. In Figure 4.4c, the dimensions are kept constant and the water mass flow rate varies due to the varying velocity.

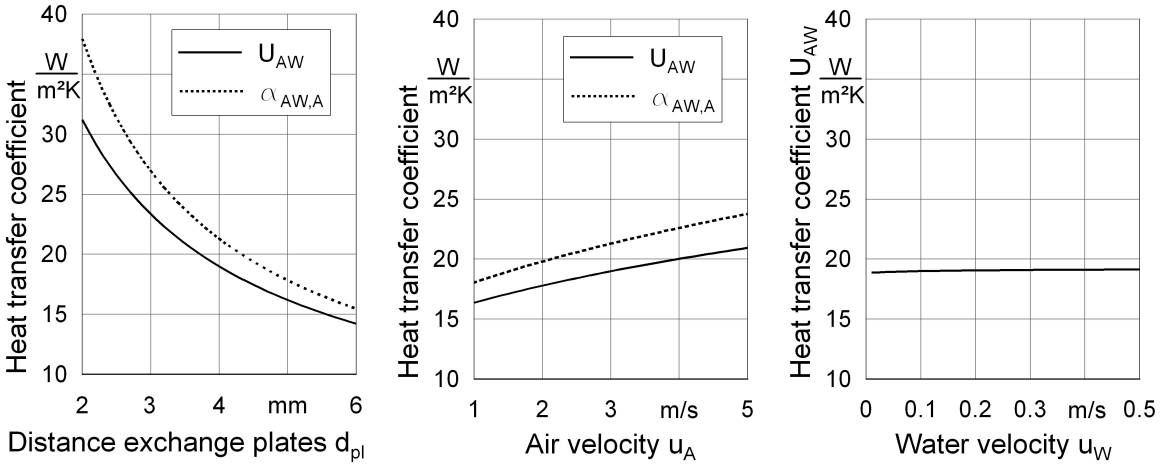

Figure 4.4: *Heat transfer coefficients as function of the distance of the exchange plates and the air and the cooling water velocity*

Heat Transfer Coefficient U_{SW}

Through the fraction of wetted exchange surface A_{SW}, the solution transfers heat to the cooling water. The determination of the heat transfer coefficient U_{SW} is similar to the determination of U_{AW} as the heat transfer includes the same steps. Figure 4.5 depicts the modes of heat transfer and states the equivalent thermal resistance circuit.

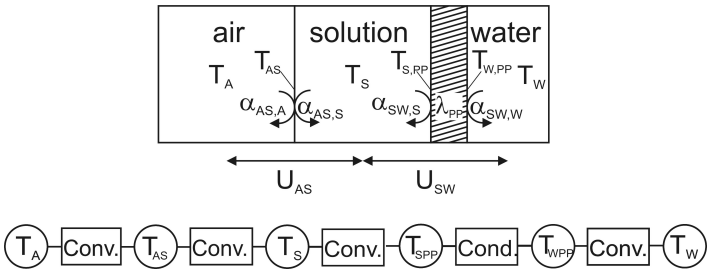

Figure 4.5: *Heat transfer and thermal resistance circuit for the wetted surface*

Convective heat transfer takes place between the solution and the plate outside, then heat is transferred by conduction through the PP-plate. Heat transfer between the inner surface of the plate and the cooling water occurs due to convection and $\alpha_{SW,W} = \alpha_{AW,W}$.

$$\frac{1}{U_{SW}} = \frac{1}{\alpha_{SW,S}} + \frac{s_{PP}}{\lambda_{PP}} + \frac{1}{\frac{5}{6} \cdot \alpha_{SW,W}} \tag{4.17}$$

The surface of the exchange plates is coated with PP fibers that are approximately perpendicular to the surface. They form a flock-coating of a thickness of 0.5 mm that improves the spreading of the solution. Therefore, a reasonable estimate for the

thickness of the laminar solution film on the exchange surface is also 0.5 mm. This boundary condition and the ones given in section 3.3.1 yield $\alpha_{SW,S} = 2.7$ kW/(m^2 K). This value is very high and afflicted with uncertainties. Yet, the exact value is of minor importance since $\alpha_{SW,S}$ does not dominate the overall heat transfer from the solution to the cooling water. The highest heat transfer resistance lies in the conductive heat transfer through the PP-plate. The thermodynamic properties of the aqueous lithium chloride solution are taken from Conde (2004). Table 4.4 lists the convective and conductive heat transfer coefficients in that add up to $U_{SW} = 0.17$ kW/(m^2 K).

Table 4.4: *Individual heat transfer coefficients and overall heat transfer coefficient U_{SW} based on the boundary conditions for the absorber (see subsection 3.3.1)*

Heat Transfer Mode	Variable	Value	Unit
convection	$\alpha_{SW,S}$	2.7	kW/(m^2 K)
conduction	s_{PP}/λ_{PP}	0.22	kW/(m^2 K)
convection	$\alpha_{SW,W}$	1.0	kW/(m^2 K)
combined	U_{SW}	0.17	kW/(m^2 K)

Heat Transfer Coefficient U_{AS}

Through the fraction of wetted exchange surface A_{SW}, the air transfers heat to the solution. Figure 4.5 depicts the modes of heat transfer and states the equivalent thermal resistance circuit. The determination of the heat transfer coefficient U_{AS} is similar to the determination of U_{AW} and U_{SW}, yet without a conductive heat transfer step. Convection heat transfer takes place between the air and the solution with $\alpha_{AS,S} = \alpha_{SW,S}$.

$$\frac{1}{U_{SW}} = \frac{1}{\alpha_{AS,A}} + \frac{1}{\alpha_{AS,S}} \tag{4.18}$$

As the solution is assumed to flow within the flock-coating, any effect of the solution film on the air flow is neglected and $\alpha_{AS,A} \approx \alpha_{AW,A}$. As this air side convective heat transfer coefficient dominates the overall heat transfer from the air to the solution, the value of $\alpha_{AS,S}$ is of minor importance again for the overall heat transfer coefficient $U_{AS} = 0.021$ kW/(m^2 K).

Table 4.5: *Individual heat transfer coefficients and overall heat transfer coefficient U_{AS} based on the boundary conditions for the absorber (see subsection 3.3.1)*

Heat Transfer Mode	Variable	Value	Unit
convection	$\alpha_{AS,A}$	0.021	kW/(m^2 K)
convection	$\alpha_{AS,S}$	1.4	kW/(m^2 K)
combined	U_{AS}	0.021	kW/(m^2 K)

Mass Transfer Coefficient β_{AS}

The Lewis number Le is relevant to any situation involving simultaneous heat and mass transfer by convection as the Lewis number relates the heat and mass transfer coefficients.

$$Le^{1-n} = \frac{\alpha_{AS,A}}{\beta_{AS} \cdot \rho \cdot c_p} \tag{4.19}$$

For laminar flow, the exponent n in equation 4.19 equals 0. The Lewis number Le can be deduced from thermodynamic data.

$$Le = \frac{\lambda}{\rho \cdot c_p \cdot D} \tag{4.20}$$

The diffusion coefficient D depends on the media. For the total pressure p in [kp/m^2] and the temperature in [K], equation 4.21 yields the diffusion coefficient $D_{\mathrm{H_2O,Air}}$ in [m^2/h] for water vapor in air [Gröber *et al.* 1988].

$$D_{\mathrm{H_2O,Air}} = \frac{805}{p} \cdot \frac{T}{T_0}^{1.80} \tag{4.21}$$

For the mean temperature in the absorber and the boundary conditions given in subsection 3.3.1, Le is 0.865 and β_{AS} is 0.021 m/s.

As the transfer coefficients depend on the temperatures of the media and the regenerator operates at higher temperatures, the heat and mass transfer coefficients are analogously determined. Table 4.6 summarizes the heat and mass transfer coefficients for the regenerator that differ only slightly from the values calculated for the absorber. Figure 4.6 shows the temperature dependency of $\alpha_{AS,A}$ and β_{AS}.

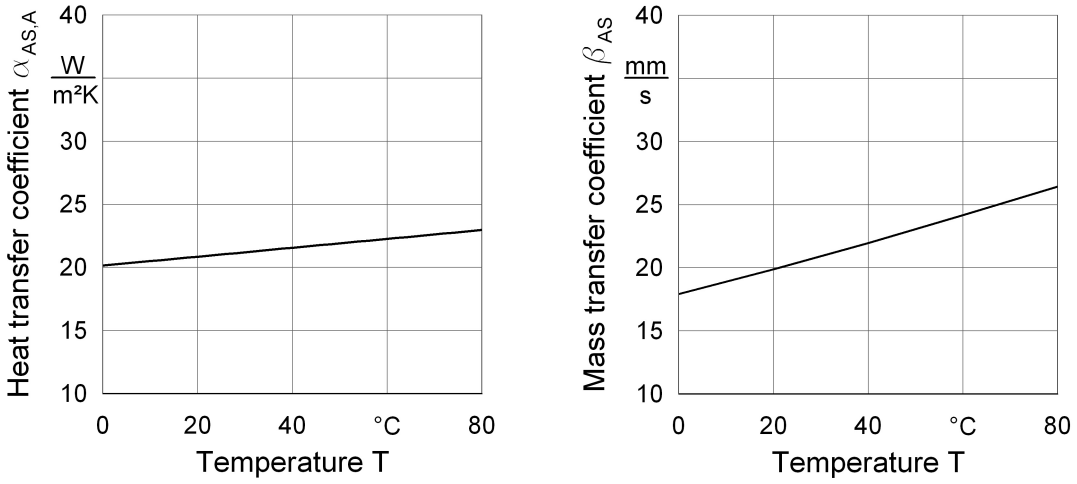

Figure 4.6: *Temperature dependency of $\alpha_{AS,A}$ and β_{AS}*

Table 4.6: *Heat and mass transfer coefficients in the regenerator*

Variable	Value	Unit
U_{AW}	0.019	kW/(m^2 K)
U_{SW}	0.17	kW/(m^2 K)
U_{AS}	0.022	kW/(m^2 K)
β_{AS}	0.022	m/s

4.1.4 Analytical Testing of the Model

The program *EES* (Engineering Equation Solver) by f-Chart Software was chosen as simulation environment because it provides a broad database of the thermodynamic properties of the working fluids moist air, water and steam. For this research, the properties of the aqueous lithium chloride solution as working fluid have been added to the database.

To verify the model, heat transfer processes between two media have been simulated with the new model and with subroutines available in *EES* to simulate heat exchangers. Both models yield the same results within the computational accuracy and this test was carried out for three different setups: (a) completely wetted exchange surface and exclusive heat transfer between air and solution, (b) completely wetted exchange surface and exclusive heat transfer between solution and water, and (c) completely dry exchange surface and exclusive heat transfer between air and water.

The mass transfer has been verified by simulating an indirect evaporative cooling process (cf. Figure 3.17) and comparing the result with the air humidification and circuit water cooling curves obtained by simulating the same process by an approximation procedure explained in [Berliner 1979]. This approximation procedure calculates the changes in state of air and circuit water in a counter-current indirect evaporative cooler by dividing the process in individual steps. Figure 4.7 shows the results of the approximation process and the changes in state of air and circuit water obtained by the new model. To understand the method of the approximation process, it is shortly outlined. Circuit water with an inlet temperature $T_{W,i} = 34$ °C is cooled to the outlet temperature $T_{W,o} = 22$ °C in a counter-current indirect evaporative cooler by ambient air with a temperature $T_{A,i} = 32$ °C and a humidity ratio of $X_{A,i} = 4.0$ g/kg. Assuming an efficiency of the cooler of 82%, the enthalpy change of the air is 48 kJ/kg. The enthalpy change of the air is divided into 6 steps of 8 kJ/kg each and the temperature change of the circuit water is divided into 3 steps of 4 °C each. To approximate the changes in state of air and circuit water during the evaporation process, the saturation humidity ratios for the water temperatures are also determined. Table 4.7 summarizes the fixed inlet and outlet conditions, the auxiliary values for the approximation and the calculated values for the air humidification process.

Table 4.7: *Temperatures and humidity ratios for the approximation: bold print = fixed inlet and outlet conditions, italic print = auxiliary values for the approximation, normal print = values obtained by the approximation*

Index i	**Air**	**Temp.** $T_{A,i}$ °C	**Hum. Rat.** $X_{A,i}$ g/kg	**Ent.** $h_{A,i}$ kJ/kg	**Water**	**Temp.** $T_{W,i}$ °C	**Sat. Hum. Rat.** $X_{W,sat,i}$ g/kg	**Ent.** $h_{W,sat,i}$ kJ/kg
0	inlet	**32**	**4.0**	*42.4*	outlet	**22**	*16.9*	*65.0*
1		28.3	8.6	*50.4*		-	-	-
2		27.7	12.0	*58.4*		*26*	*21.6*	*81.3*
3		27.1	15.4	*66.4*		-	-	-
4		27.8	18.2	*74.4*		*30*	*27.6*	*101*
5		28.5	21.1	*82.4*		-	-	-
6	outlet	29.6	23.7	*90.4*	inlet	**34**	*35.0*	*124*

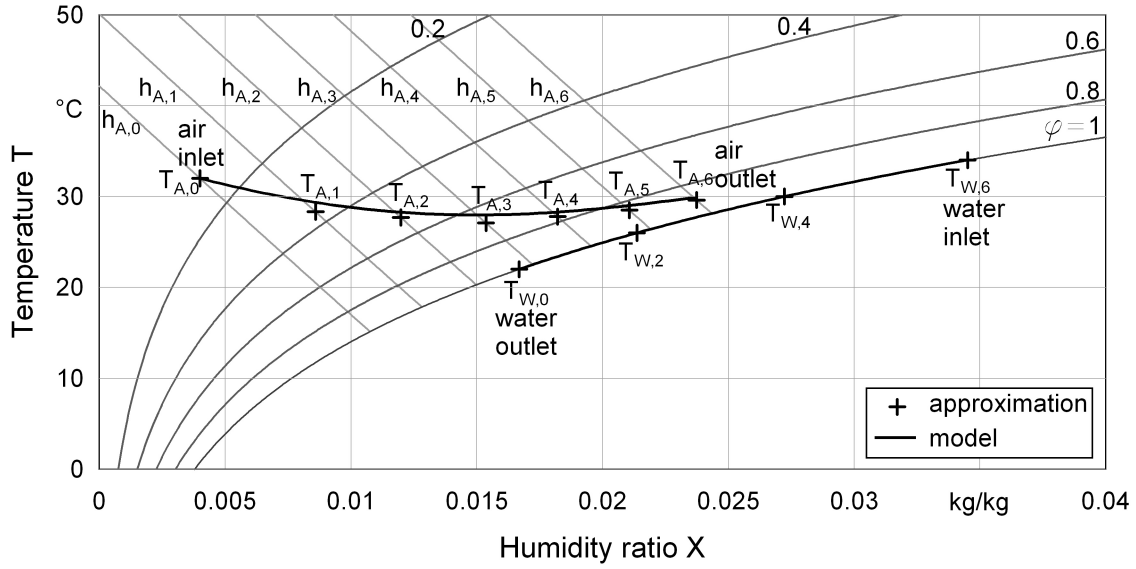

Figure 4.7: *Comparison of the changes of state of air and cooling water: results of the approximation process and of the new model*

Air inlet ($h_{A,0}/X_{A,0}$), water inlet ($h_{W,sat,6}/X_{W,sat,6}$) and water outlet ($h_{W,sat,0}/X_{W,sat,0}$) are plotted into a psychrometric chart. The state of air ($h_{A,1}/X_{A,1}$) has to lie on the connecting line between ($h_{A,0}/X_{A,0}$) and ($h_{W,sat,0}/X_{W,sat,0}$). As the enthalpy step for each step is set to 8 kJ/kg and $h_{A,0} = 42.4$ kJ/kg, the state of air ($h_{A,1}/X_{A,1}$) also has to lie on the enthalpy isoline for 50.4 kJ/kg. $X_{A,1}$ and all $X_{A,i}$ with odd index i can be calculated by equation 4.22.

$$X_{A,i} = X_{A,(i-1)} + \frac{h_{A,i} - h_{A,(i-1)}}{h_{W,sat,(i-1)} - h_{A,(i-1)}} \cdot (X_{W,sat,(i-1)} - X_{A,(i-1)}) \tag{4.22}$$

The state of air $(h_{A,2}/X_{A,2})$ has to lie on the connecting line between $(h_{A,1}/X_{A,1})$ and $(h_{W,sat,2}/X_{W,sat,2})$ and on the the enthalpy isoline for 58.4 kJ/kg. The humidity ratio $X_{A,2}$ can be calculated by equation 4.23. Equation 4.23 is valid for all $X_{A,i}$ with even index i.

$$X_{A,i} = X_{A,(i-1)} + \frac{h_{A,i} - h_{A,(i-1)}}{h_{W,sat,i} - h_{A,(i-1)}} \cdot (X_{W,sat,i} - X_{A,(i-1)}) \tag{4.23}$$

The state of air $(h_{A,3}/X_{A,3})$ is approximated to also lie on the connecting line between $(h_{A,1}/X_{A,1})$ and $(h_{W,sat,2}/X_{W,sat,2})$, yet on the enthalpy isoline for 66.4 kJ/kg.

The state of air $(h_{A,4}/X_{A,4})$ lies on the connecting line between $(h_{A,3}/X_{A,3})$ and $(h_{W,sat,4}/X_{W,sat,4})$ and on the enthalpy isoline for 74.4 kJ/kg.

The state of air $(h_{A,5}/X_{A,5})$ is approximated to also lie on the connecting line between $(h_{A,3}/X_{A,3})$ and $(h_{W,sat,4}/X_{W,sat,4})$, yet on the enthalpy isoline for 82.4 kJ/kg.

The state of the outlet air $(h_{A,6}/X_{A,6})$ lies on the connecting line between $(h_{A,5}/X_{A,5})$ and $(h_{W,sat,6}/X_{W,sat,6})$ and on the enthalpy isoline for 90.4 kJ/kg. Figure 4.7 shows the air and circuit water temperatures obtained by the six nodes approximation and the changes of state of air and circuit water obtained by the new model with 100 nodes.

4.2 Modeling of the System Components

This section explains the application of the model to simulate the performance of the components. Absorber and regenerator are modeled for their reference conditions and the indirect evaporative cooler for common return air conditions. Figure 4.8 depicts the mass and heat flows in the components. The flow directions are preset in the programmed subroutines for the component but they can be changed if necessary.

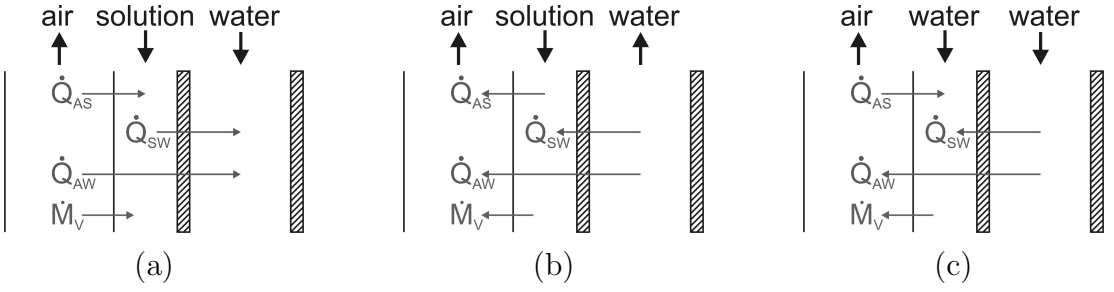

Figure 4.8: *Mass and heat flows in the components (a) absorber (b) regenerator (c) indirect evaporative cooler*

4.2.1 Absorber

In the absorber, solution and cooling water flow counter-currently to the air flow. Table 4.8 lists the reference inlet conditions for air, solution and cooling water in the low-flow absorber. Figure 4.9 shows the psychrometric chart of the changes of state taking place in the absorber including the solution and the cooling water. The solution line shows the equilibrium humidity ratio of the solution and the cooling water line plots the temperature of the cooling water on the saturation line.

Table 4.8: *Inlet conditions of the process media and boundary conditions for the reference absorption process*

Condition	**Value**	**Unit**
inlet temperature air	35	°C
inlet humidity ratio air	14.5	g/kg
inlet temperature salt solution	28	°C
inlet concentration salt solution	44	%
inlet temperature cooling water	24	°C
mass flow ratio air flow to solution flow	80	-
required outlet humidity ratio air	8	g/kg

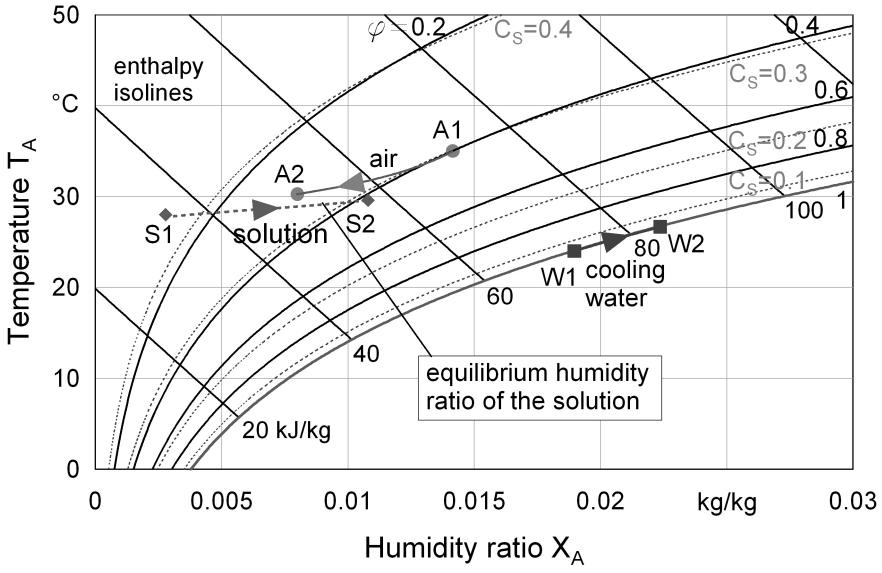

Figure 4.9: *Psychrometric chart of the changes of state taking place inside the absorber, 1=inlet, 2=outlet*

4.2.2 Regenerator

Figure 4.8 shows that in the regenerator the solution also flows counter-currently to the air flow while the heating water flows co-currently to the air flow. Table 4.9 lists the reference inlet conditions for air, solution and heating water in the regenerator. They and the transfer coefficients given in Table 4.6 were applied for the simulations. Figure 4.10 shows the psychrometric chart of the changes of state taking place in the regenerator. The regenerator in this example is identical in its dimensions with the absorber presented in subsection 3.3.1 and it does not include any heat recovery of the air. The heating water exits the regenerator with a temperature of 63 °C and it is not plotted in Figure 4.10 due to its high temperatures. The inlet temperature of the solution is of minor importance as it heats up quickly due to its small capacity. To simplify the changes in state of the solution, the plot omits this heating up step.

Table 4.9: *Inlet conditions of the process media and boundary conditions for the reference regeneration process*

Condition	**Value**	**Unit**
inlet temperature air	35	°C
inlet humidity ratio air	14.5	g/kg
inlet temperature salt solution	28	°C
inlet concentration salt solution	29	%
inlet temperature heating water	70	°C
mass flow ratio air flow to solution flow	18	-
required outlet concentration salt solution	44	%

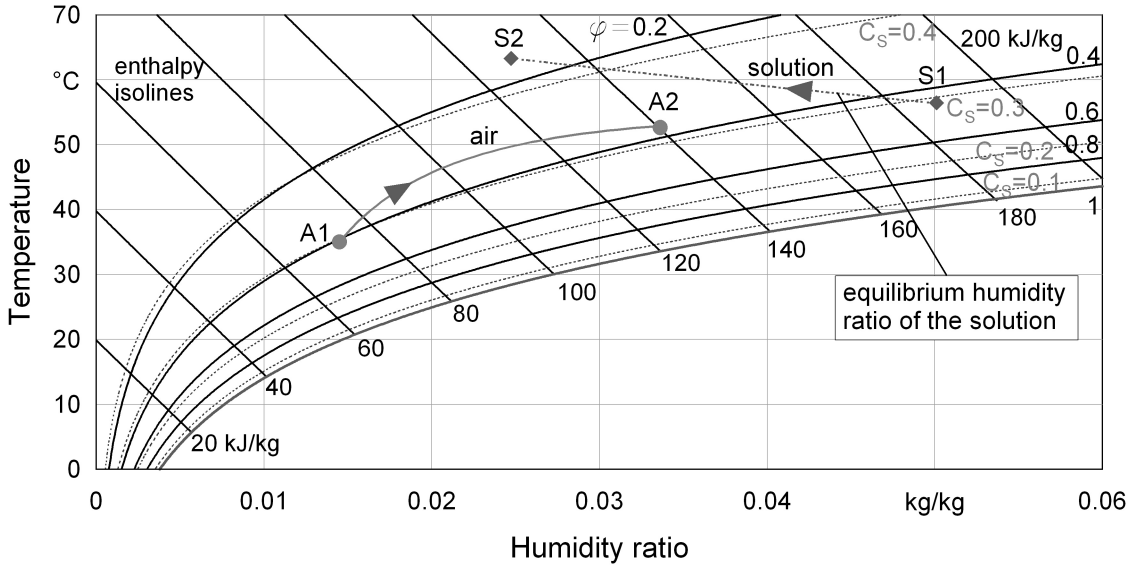

Figure 4.10: *Psychrometric chart of the changes of state taking place inside the regenerator without heat recovery from the air, 1=inlet, 2=outlet*

4.2.3 Indirect Evaporative Cooler

Figure 4.8 shows that the water is sprayed in flow direction into the air flow while the heating water flows counter-currently to the air flow. Figure 4.10 shows as example for the modeling of the changes of state in indirect evaporative coolers the psychrometric chart of the two subsequent indirect evaporative coolers of the low-flow LDSC in Figures 3.10 and 4.12a. Table 4.10 lists the main inlet and outlet conditions for this example. Due to the small capacity of the sprayed water, its temperature is of minor importance. The air inlet conditions into the first indirect evaporative cooler IEC1 are the ARI return air conditions. As the outlet air from IEC1 directly enters IEC2, the air inlet conditions into IEC2 are the air outlet conditions from IEC1.

Table 4.10: *Process media conditions and boundary conditions for the two subsequent indirect evaporative coolers of the low-flow LDSC in Figures 3.10 and 4.12a*

IEC	Condition	Value	Unit
IEC1	inlet temperature air	26.7	°C
	inlet humidity ratio air	11.5	g/kg
	inlet temperature heating water	25.5	°C
	outlet temperature heating water	20.2	°C
IEC2	inlet temperature air	23.1	°C
	inlet humidity ratio air	17.7	g/kg
	outlet temperature air	29.4	°C
	outlet humidity ratio air	26.6	g/kg
	inlet temperature heating water	31.8	°C
	outlet temperature heating water	26.2	°C

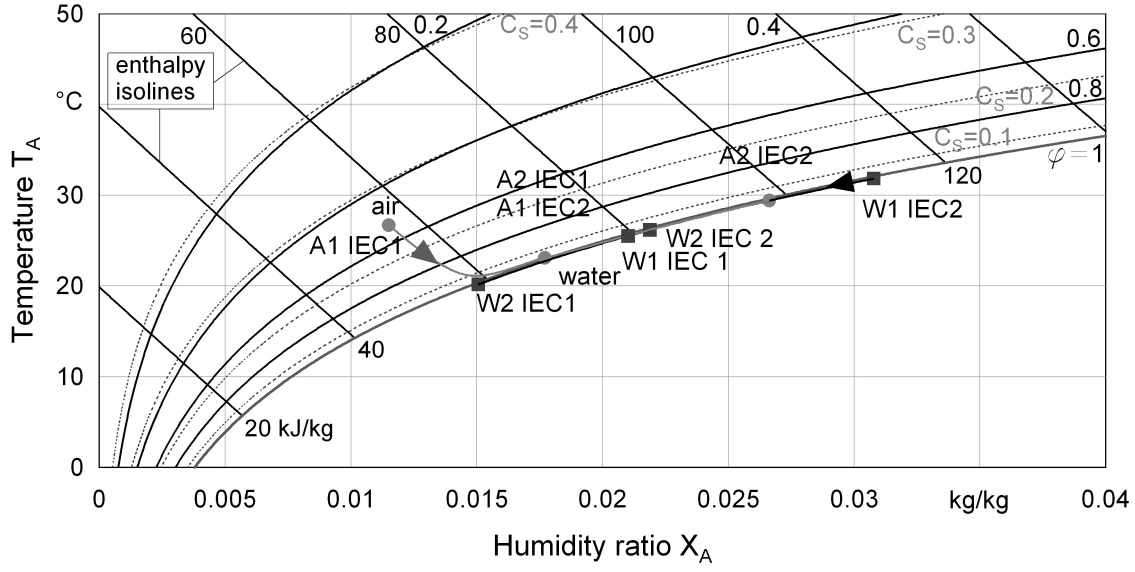

Figure 4.11: *Psychrometric chart of the changes in state taking place inside the indirect evaporative coolers, 1=inlet, 2=outlet*

4.3 Modeling of Liquid Desiccant Cooling Systems

To model the performance of liquid desiccant cooling systems, the subroutines for the components are combined in the flow chart of one program that models all components simultaneously. This section describes the two most common LDCS alternatives in detail, the innovative low-flow LDCS and the conventional high-flow LDCS that is available on the market. The model is applied to simulate their performance and to compare their energy storage capacities. The analysis is performed for reference conditions for supply air and return air and two sets of ambient temperature and humidity conditions, representing moderate and tropical climates.

Figure 4.12 shows the schematic diagrams of both configurations that consist of absorber, two indirect evaporative coolers, heat exchangers and storage tanks for the concentrated and the diluted salt solution. In both cases, the regenerator is identical in design with the absorber. The alternatives differ in the range of the liquid to gas ratio $\dot{L}/\dot{G}$ in absorber. $\dot{L}/\dot{G}$ ranges between 0.015 and 0.03 for the low-flow systems and between 1.2 and 2.4 for the high-flow systems.

In the absorber, the liquid desiccant dehumidifies outside air to the supply air humidity ratio. The dehumidified air is cooled to the demanded supply air temperature in the subsequent heat exchanger, which is cooled by means of indirect evaporative cooler 1. The indirect evaporative cooler 2 withdraws the heat that is released during the absorption process. This cooling is integrated into the absorber in low-flow systems or done by the external heat exchanger 2 in high-flow systems.

The external liquid to gas ratio $\dot{L}_{ext}/\dot{G}$ is defined as ratio of the concentrated liquid flow from the tank to the air flow. $\dot{L}_{ext}/\dot{G}$ depends on air-conditioning requests and outside air conditions, i.e. the humidity that has to be removed in the absorber.

4.3.1 Low-Flow Liquid Desiccant Cooling Systems

The liquid to gas ratio $\dot{L}/\dot{G}$ of the one-pass absorber of low-flow systems is equal to the external liquid to gas ratio $\dot{L}_{ext}/\dot{G}$. As explained in section 3.2, the absorption process is cooled simultaneously in low-flow systems. The separate cooling medium water removes the heat of absorption directly within the absorber. Consequently, the absorber can operate in the optimum operating range for energy storage and the value for $\dot{L}/\dot{G}$ lies below 0.03. The absorber outlet concentration of the salt solution is much lower than the absorber inlet concentration. Low-flow systems do not need a recirculation-pump for the solution and consume significantly less electricity than high-flow systems.

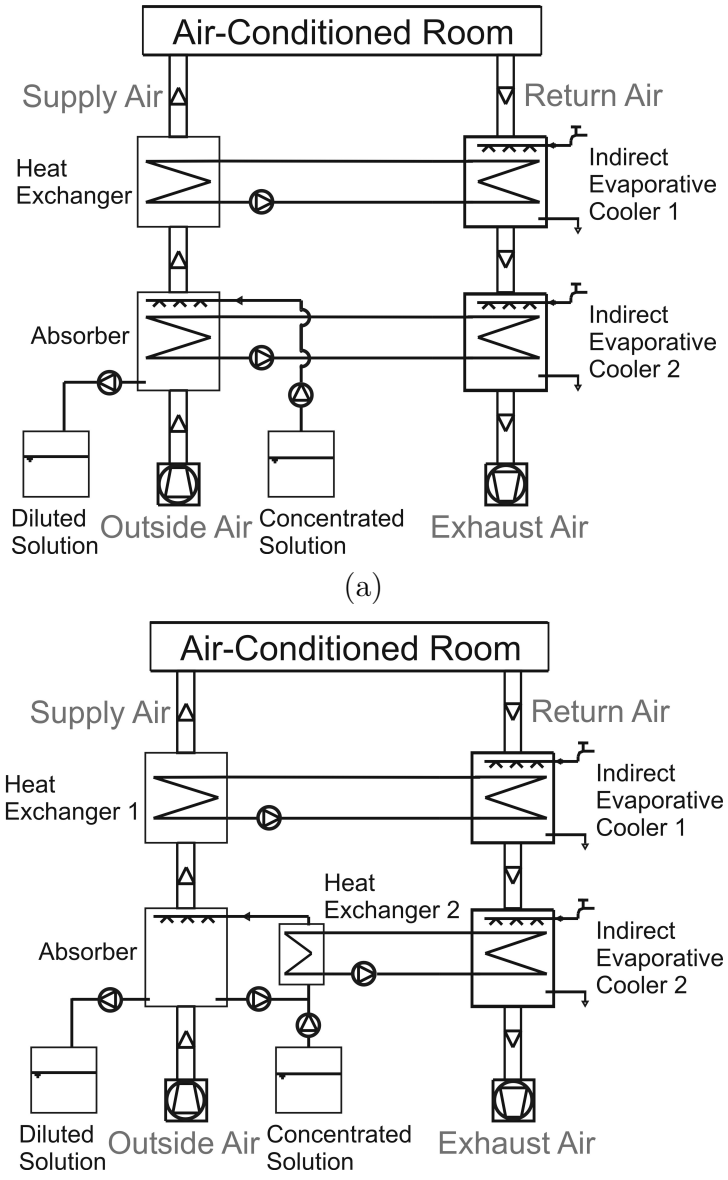

Figure 4.12: *Schematic diagram of (a) a low-flow LDCS (b) a high-flow LDCS*

4.3.2 High-Flow Liquid Desiccant Cooling Systems

In high-flow systems, the solution itself removes the heat of absorption from the absorber. This requires a high mass flow of liquid desiccant in the absorber and the value for $\dot{L}/\dot{G}$ lies above 1. As a result, the salt solution exits the absorber with an outlet concentration only slightly lower than the inlet concentration. Figure 4.12b shows that high-flow systems operate with a loop-type absorber. Only a small fraction of the absorber outlet solution is withdrawn and replaced with concentrated solution while the main fraction of the absorber outlet solution is cooled down in heat exchanger 2 and fed back into the absorber.

As the media can be selected individually in the numerical model, the high-flow absorber is simulated by choosing no cooling water flow within the absorber and an exclusive heat and mass transfer between air and solution.

4.3.3 Comparison of the Energy Storage Potential

This subsection presents the results of the numerical study that compares the energy storage potential of both configurations. To determine the energy storage potential, the study simulates the discharging of the thermochemical storage, i.e. driving an air conditioning process by the concentrated salt solution. The charging of the storage system, i.e. reconcentrating the diluted salt solution, is not simulated. As the reference concentration of the concentrated solution it set to 44%, the regeneration method has no influence on the energy storage potential of the system.

The performance of both configurations is simulated for two sets of reference air conditions representing moderate and tropical climates. Table 4.11 provides the predetermined air conditions that differ in the humidity ratio of the outside air and in the supply air temperature. These conditions represent the most common air conditioning requirements and allow to compare the energy storage potential of high-flow and low-flow systems under various operating conditions.

Table 4.11: *Reference air conditions*

Climate	**Air**	**Temperature**	**Humidity Ratio**
moderate	outside air	35 °C	14.5 g/kg
	supply air	21 °C	8 g/kg
	return air	26.7 °C	11.5 g/kg
tropical	outside air	35 °C	24 g/kg
	supply air	22 °C	8 g/kg
	return air	26.7 °C	11.5 g/kg

The air mass flow is the same for all simulations. This value influences the size of the LDCS components and the costs of the system but not the specific properties of the dehumidification and cooling processes. All other flows are given relatively to this flow. Only 80% of the supply air flow is withdrawn as return air, leading to a slight overpressure inside the building. This prevents infiltration of untreated outside air.

The energy storage capacity depends on the performance of the absorber as well as on the performance of the other LDCS components. To ensure equal conditions for both systems and that the performance of heat exchangers or indirect evaporative coolers does not limit the overall performance, they are simulated of the same size for both configurations. Table 4.12 lists the main results of the simulation, i.e. the absorber outlet concentrations and the energy storage capacities.

Table 4.12: *Results of the simulation*

Climate	**System**	**Absorber Outlet Concentration**	**Energy Storage Capacity**
moderate	low-flow	26.7%	317 kWh/m^3
	high-flow	32.4%	219 kWh/m^3
tropical	low-flow	27.6%	300 kWh/m^3
	high-flow	36.9%	137 kWh/m^3

For moderate conditions and the boundary conditions of this simulation, the low-flow system provides an absorber outlet concentration C_{dil} of 26.7%, a by far lower value than the 32.4% provided by the high-flow system. Therefore, the energy storage potential of the low-flow system is 45% higher than the one of the high-flow system.

The difference between the low-flow and the high-flow system is still higher for tropical conditions. While the low-flow system is not sensitive to the outside conditions and the outlet concentration increases by only one percentage point, the performance of the high-flow system depends strongly on the outside humidity. C_{dil} of the high-flow system is 4.5 percentage points higher for tropical conditions than for moderate ones. This leads to the low energy storage capacity for high-flow systems of 137 kWh/m^3, compared to 300 kWh/m^3 for low-flow systems. Thus, for tropical conditions, low-flow systems can provide air conditioning twice as long as high-flow systems from the same amount of stored concentrated solution. Figure 4.13 compares the energy storage capacities for both systems and both sets of reference conditions.

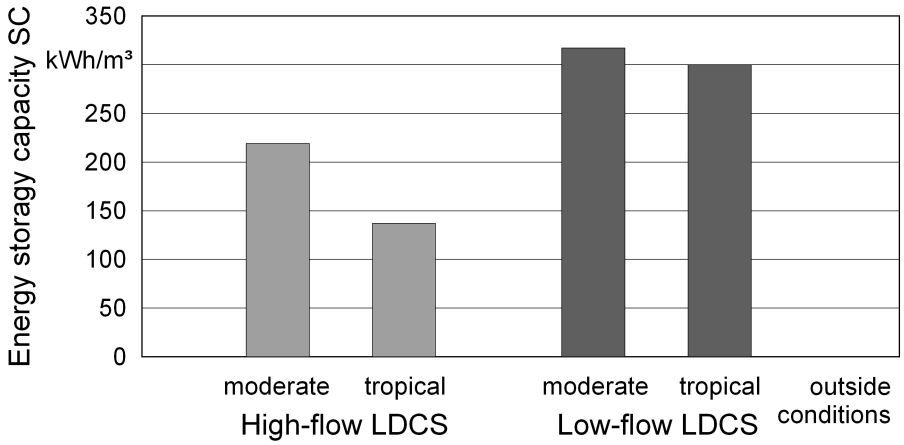

Figure 4.13: *Energy storage capacities for low-flow and high-flow LDCS for moderate and tropical reference conditions*

Compared to high-flow systems, low-flow systems provide higher energy storage capacities, omit the separate solution-water heat exchanger by integrating the withdrawal of the heat of absorption into the absorber and they consume significantly less auxiliary electricity by avoiding the recirculation-pump for the solution.

Chapter 5

Effects of Maldistribution in Low-Flow Liquid Desiccant Cooling Systems

After defining maldistribution and providing a measure for it, this chapter explains the extend of maldistribution of the process media occurring in the absorber of low-flow liquid desiccant cooling systems. It analyzes the effects of the maldistributed process media on the performance of this device and identifies the process medium that - if maldistributed - has the worst impact on the performance of absorber.

5.1 Fundamentals

5.1.1 Ideal Distribution and Maldistribution

Ideal distribution of a medium signifies a uniform flow of this medium. Ideal distribution of a liquid process medium over the surface of a heat and mass transfer plate means that the fraction of the process media that flows over a certain part of the exchange plate surface corresponds with the surface fraction of this part, e.g. a fraction of 10% of the liquid always flows over 10% of the exchange plate surface and a fraction of 20% of the liquid always flows over 20% of the exchange plate surface.

An uneven local distribution of a process media within a component is referred to as **maldistribution**. The present research applies two maldistribution measures, the mass flow factor $f_{\dot{m}}$ and the maldistribution factor f_{mal}, to characterize maldistribution and to determine the effects of maldistribution. Small-scale maldistribution has a minor effect on the total performance of a device but large scale maldistribution leads to significant performance losses. To estimate this worst case, this research calculationally combines sections with small-scale maldistribution to one larger one.

The **mass flow factor** $f_{\dot{m}}$, defined in Equation 5.1, is a dimensionless parameter that specifies the extend of local maldistribution. A mass flow factor $f_{\dot{m}} = 1$ signifies a uniform flow. The mass flow within a certain part of a device matches with the design mass flow within this part of the device. Values for the mass flow factor different from 1 indicate a non-uniform flow. The local mass flow differs from the local design mass flow.

$$f_{\dot{m}} = \frac{\text{actual local mass flow}}{\text{design local mass flow}} \tag{5.1}$$

The **maldistribution factor** f_{mal} is a dimensionless parameter that specifies the extend of maldistribution within a device. Various definitions and ranges for the maldistribution factor can be found in the literature. Commonly, $f_{mal} = 0$ signifies that no maldistribution occurs in the device at all. Values of the maldistribution factor f_{mal} greater than 0 show the extend of maldistribution. In most cases, the upper limit for the maldistribution factor is defined as $f_{mal} \to 1$ or $f_{mal} \to \infty$. In the present research, $f_{mal} = 0$ also signifies ideal distribution and the upper limit for the maldistribution factor is 1.

Table 5.1 summarizes the measures of the maldistribution of the process media, including their possible values.

Table 5.1: *Measures for the maldistribution of process media*

Notation	**Value**			**Meaning**
mass flow factor		$f_{\dot{m}}$	$= 0$	no mass flow
	$0 \leq$	$f_{\dot{m}}$	< 1	mass flow below design mass flow
		$f_{\dot{m}}$	$= 1$	ideal distribution
		$f_{\dot{m}}$	> 1	mass flow above design mass flow
maldistribution factor		f_{mal}	$= 0$	ideal distribution
	$0 <$	f_{mal}	< 1	medium is maldistributed
		f_{mal}	$= 1$	upper limit for maldistribution

Defining $f_{mal} = 1$ as upper limit for the maldistribution factor has the advantage of a simple correlation between the maldistribution factor and the distribution factor f_{dis}.

$$f_{mal} = 1 - f_{dis} \tag{5.2}$$

The **distribution factor** f_{dis} is defined as the ratio of real distribution to ideal distribution. The distribution factor can easily be determined experimentally and the maldistribution factor is deduced from it by applying equation 5.2.

Experimental determination of the distribution factor

In order to determine the distribution factor f_{dis} experimentally, for example for the distribution of a liquid on a surface, the surface is divided into n vertical sections and the liquid passing each vertical section is collected as sample. The duration of the experiment depends on the size of the sample tubes as the experiment ends once the first sample tube is filled with liquid. The individual sample masses m_i are determined by weighing each test tube. Summing up the masses of the individual samples leads to the total mass of the collected liquid m_{tot}.

$$m_{tot} = \sum_{i=1}^{n} m_i \tag{5.3}$$

The mean sample mass $\overline{m}$ is given by the total mass of the liquid m_{tot} and the number of samples n

$$\overline{m} = \frac{m_{tot}}{n} \tag{5.4}$$

Once measured, the masses of the individual samples m_i are classified and rearranged in ascending order. The original sample numbers i become irrelevant, the samples are renumbered (i'). As each sample represents a vertical section of the exchange plate and thus a fraction of the total width W of the exchange plate, the masses of the rearranged samples $m_{i'}$ can be given as function of a dimensionless exchange plate width w.

$$w(i') = \frac{i'}{n} \tag{5.5}$$

Adding the masses of the rearranged samples $m_{i'}$ up to a certain sample number i' and consequently up to a certain width $w_{i'}$ of the exchange plate, determines the amount of liquid $m(w_{i'})$ that has been collected up to this certain width $w_{i'}$ of the exchange plate.

$$m(w_{i'}) = \sum^{i'} m_{i'} \tag{5.6}$$

Dividing the added masses $m(w_{i'})$ by the total mass of the liquid m_{tot} leads to the fraction of liquid that has been collected on the surface as function of the dimensionless exchange plate width. Plotting this relation allows a fast grading of the quality of the distribution as it clearly illustrates the real distribution of the liquid compared to an ideal distribution of the liquid on the surface. The area under this curve is defined as A_{real}; the area of an ideal distribution as A_{ideal}, whereas A_{ideal} always equals 0.5.

Finally, calculating the area A_{real} and dividing it by the area of an ideal distribution A_{ideal}, determines the distribution factor defined as the ratio of real distribution to ideal distribution, i.e. A_{real} to A_{ideal}.

$$f_{dis} = \frac{A_{\text{real}}}{A_{\text{ideal}}} = \frac{\int_0^W \frac{m(w_{i'})}{m_{tot}}}{0.5} = \frac{\int_0^W \sum_{i'=0}^{w_{i'}} m'_i}{0.5 \cdot m_{tot}} = \frac{\int_0^W \int_0^W m'_i}{0.5 \cdot m_{tot}} \tag{5.7}$$

For two examples, Figure 5.1 lists the individual steps for deducing the distribution factor from the experimental data of m_i. One of these examples has an ideal distribution of the liquid, in the other one the liquid is maldistributed with a distribution factor of 66.5%.

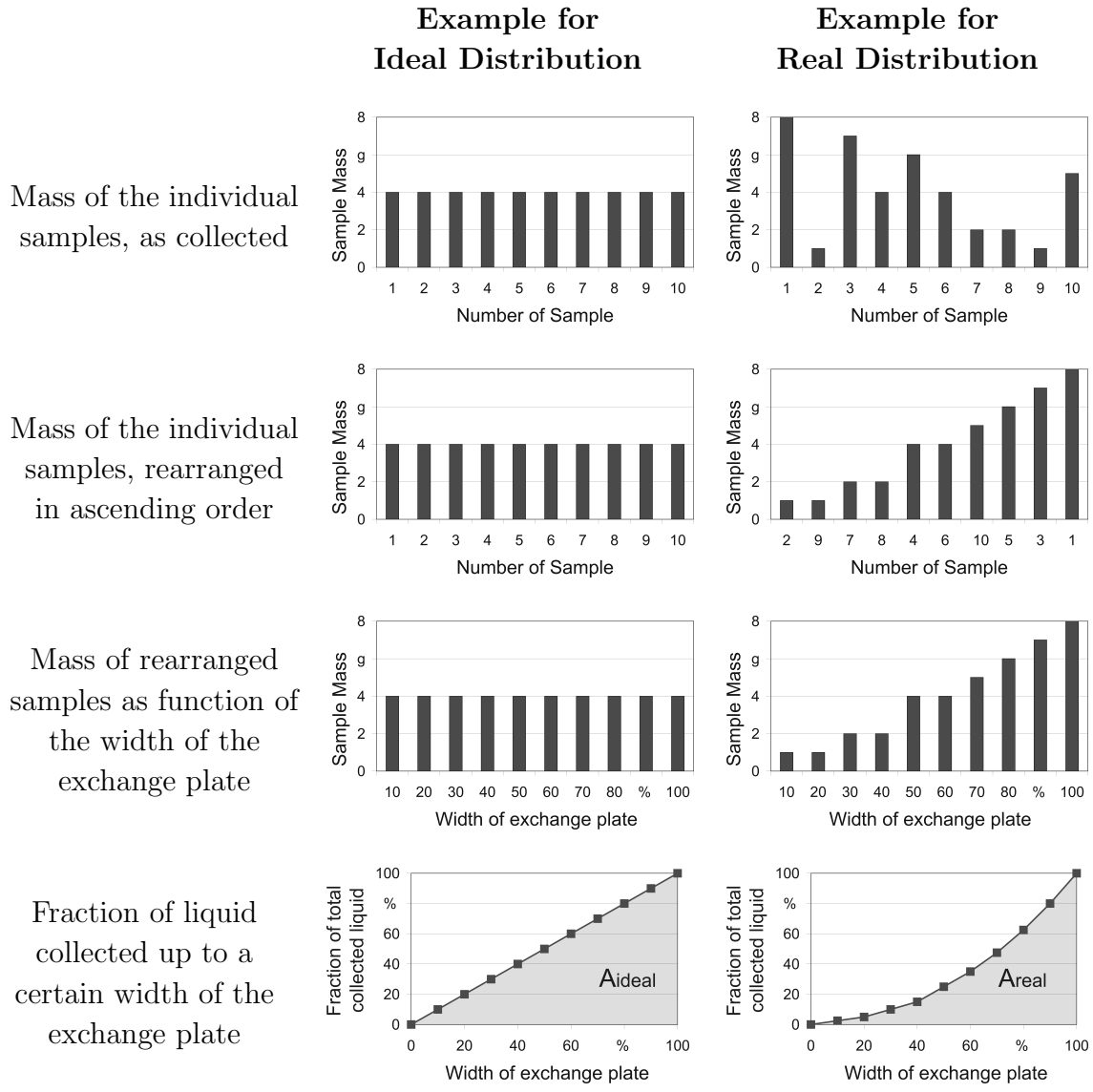

Figure 5.1: *Determination of the distribution factor*

5.1.2 Calculation of the Effects of Maldistribution on the Performance

The maldistribution of a process medium always leads to increased local mass flows in some sections of the device ($f_{\dot{m}} > 1$) and to decreased local mass flows in other sections of the device ($f_{\dot{m}} < 1$), resulting in a better and in a worse local performance of the device, respectively. As those local performance effects can compensate for each other, maldistribution does not immediately cause dramatic output losses. Some processes, however, are more sensitive to maldistribution than others. Consequently, understanding the effects of maldistribution on the performance of a technical device is important for the optimal designing of the device. The effects of maldistribution are calculated according to Kammermaier (2008).

For the case of the absorption device of a low-flow liquid desiccant cooling system described in section 3.3.1 and a cooled air dehumidification process with an aqueous LiCl-solution, this subsection describes how the effect of maldistribution on the performance of a device is identified and explains the necessary steps:

- Definition of a reference system with ideal distribution of the process media
- Calculation of the performance of the reference system
- Division of the exchange plate into sections and definition of the local mass flows caused by maldistribution of the process media
- Calculation of the performance of the individual sections of the system with the local mass flows
- Determination of the overall performance of the system by combining the performances of the individual sections of the system

Concerning the calculation of the performance of individual sections and the determination of the overall performance of the system, two approaches are possible:

- Calculation of the outlet conditions of the device with maldistribution while keeping the reference dimensions of the device constant
- Calculation of the required dimensions of the device with maldistribution while keeping the reference outlet conditions for the device constant

Definition of a reference system with ideal distribution

Figure 5.2 shows a schematic diagram of the reference system of this case, the absorption device for low-flow liquid desiccant air dehumidification, explained in section 3.3.1. At the design point, the exchange plates for the absorption operate with

an ideal distribution of the cooling water flow, the air flow and the solution flow over the exchange surface. Table 5.2 lists the inlet conditions of the process media and the boundary conditions for the reference system.

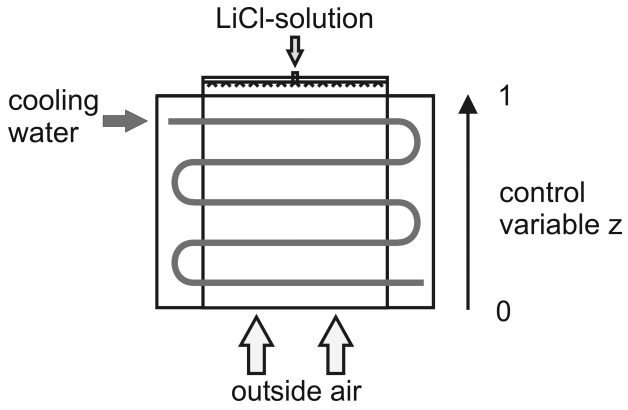

Figure 5.2: *Reference system for the cooled air dehumidification process*

Table 5.2: *Boundary conditions and inlet conditions of the process media for the reference absorption process*

Medium	**Condition**	**Value**	**Unit**
	mass flow ratio air flow to solution flow	80	-
air	required outlet humidity ratio	8	g/kg
	inlet temperature	35	°C
	inlet humidity ratio	14.5	g/kg
solution	inlet temperature	28	°C
	inlet concentration	44	%
water	inlet temperature	24	°C

Calculation of the performance of the reference system

The model described in chapter 4 is applied to calculate the design point performance of the reference system. In order to lower the inlet humidity ratio of 14.5 g/kg to the requested outlet humidity ratio of 8 g/kg, only 1.5 transfer units are necessary and a total height of the absorption device of 0.45 m. Thus, the height of a transfer unit is 0.31 m in the reference case. The height of the individual exchange plates corresponds with the total height of the absorption device ($h_{pl} = 0.45$ m).

The ideal distribution of cooling water flow, air flow and solution flow in the reference system leads to a simulated outlet concentration of 29% and an energy storage capacity of 278 kWh/m^3. Figure 5.3 displays the sensible and the latent changes of the process media in the absorber as function of the control variable z, the dimensionless height of the absorber plates.

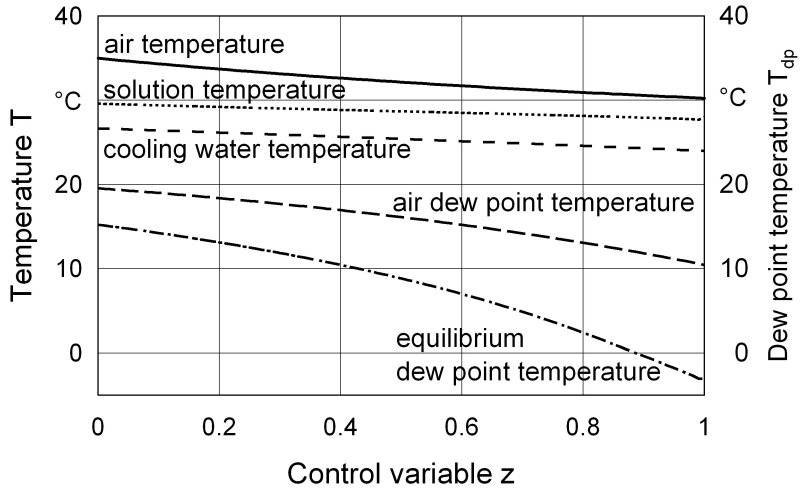

Figure 5.3: *Simulated air, salt solution and cooling water temperature profile and air dew point and equilibrium dew point temperature profile for the design point of the reference system with an ideal distribution of solution, air and cooling water flow ($f_{\dot{m},S} = 1$, $f_{\dot{m},A} = 1$, $f_{\dot{m},W} = 1$)*

Figure 5.4 plots these temperature and humidity data in a McCabe-Thiele diagram that includes the graphical determination of the number of equilibrium steps n. The number of transfer units N_{OG} is determined according to Stichlmair and Fair (1998) by integrating between the equilibrium and the operating line in the McCabe-Thiele diagram.

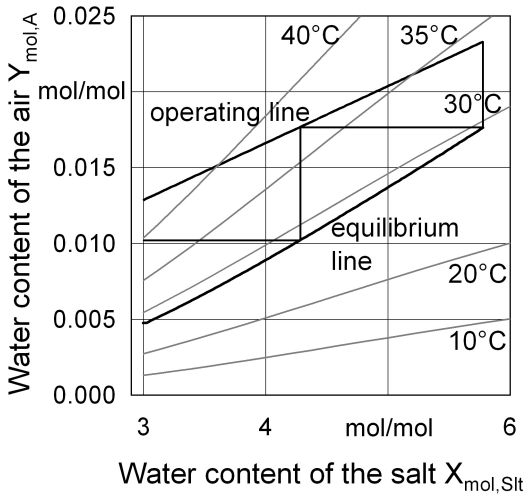

Figure 5.4: *McCabe-Thiele diagram for the design point of the reference system showing the temperature isolines and the equilibrium stages*

Division of the exchange plate into sections and definition of the local mass flows caused by maldistribution of the process media

In this example, the exchange surface (with $h_{pl} = 0.45$ m) is divided into two equal halves, section I and section II. For each medium, the mass flow factors $f_{\dot{m},I}$ and $f_{\dot{m},II}$ interdepend. In case of an ideal distribution, i.e. $f_{\dot{m},I} = 1$ and $f_{\dot{m},II} = 1$ for all media, 50% of each medium flow over each half of the exchange plate.

To simplify matters, this case considers only a maldistribution of the salt solution. Air flow and cooling water flow are distributed ideally. In this example, 25% of the total solution flow over section I, i.e. $f_{\dot{m},S,I} = 0.5$, and 75% of the total solution flow over section II, i.e. $f_{\dot{m},S,II} = 1.5$.

Calculation of the performance of the individual sections of the system with the local mass flows

The performance of both sections of the exchange plate has been calculated with the numerical model described in chapter 4. Figures 5.5a and 5.5b show the McCabe-Thiele digrams for the individual sections of the exchange plate.

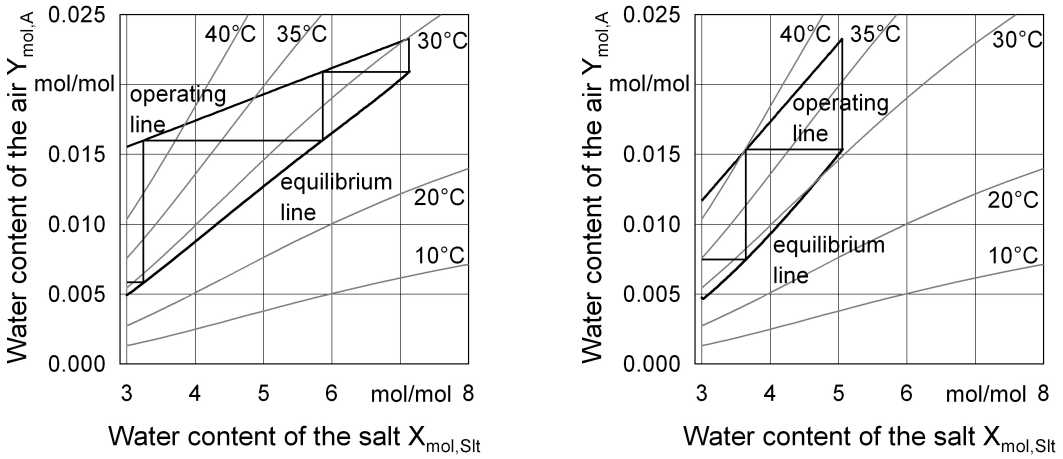

Figure 5.5: *McCabe-Thiele diagrams for the individual sections of the cooled air dehumidification process, showing the temperature isolines and the equilibrium stages with maldistribution of the solution (a) section I: $f_{\dot{m},S,I} = 0.5$, (b) section II: $f_{\dot{m},S,II} = 1.5$*

Determination of the overall performance of the system

Both, the outlet air humidity ratio and the energy storage capacity that results from the outlet salt concentration define the overall performance of the system. Combining the individual performances of both halves of the exchange plate, section I and section II, allows to determine the overall performance of the plate.

This is done by reuniting the corresponding outlet flows of both sections and calculating the outlet properties of the corresponding mixtures. Table 5.3 summarizes the outlet properties and performance values for the individual sections and the combined performance of both sections. For comparison, it lists the performance values of the reference system, i.e. the same exchange plate with an ideal distribution of the solution flow.

Table 5.3: *Performance with and without maldistribution of the salt solution flow*

Condition	**Unit**	**Section I** $f_{\dot{m},S,I} = 0.5$ half plate	**Section II** $f_{\dot{m},S,II} = 1.5$ half plate	**Sections I+II** $f_{\dot{m},S,I} = 0.5$ $f_{\dot{m},S,II} = 1.5$ whole plate	**Sections I+II** $f_{\dot{m},S} = 1$ whole plate
inlet humidity ratio	g/kg	14.5	14.5	14.5	14.5
outlet humidity ratio	g/kg	9.7	7.3	8.5	8.0
inlet concentration	kg/kg	0.44	0.44	0.44	0.44
outlet concentration	kg/kg	0.25	0.32	0.30	0.29
storage capacity	kWh/m^3	347	230	266	278

5.2 Effects of Maldistribution in the Absorber

Applying the method described in subsection 5.1.2, this subsection calculates the effects of maldistribution on the performance for wider ranges of the mass flow factors of the media in the absorber of low-flow LDCS. Three approaches are applied in succession. To deduce the general trends, at first the division of the exchange surface into two equal sections is kept for clearness and also the height of the absorption device is constant. Subsequently, the outlet humidity is kept constant and the required height of the absorption device is determined for various maldistribution cases. In a further step, also the dimensions of the two sections vary.

5.2.1 Maldistribution of the Liquid Desiccant Flow

The distribution of the liquid desiccant in the absorber depends on the distribution device on top of the exchange surface. If the distribution device does not work properly, parts of the exchange plate have a higher liquid load than others or some parts of the exchange surface even fall dry and do not participate in the air dehumidification process at all. To explain these effects, the case described in section 5.1.2 is extended to a wider range of the solution mass flow factors and to varying dimensions and surface wettings of the sections I and II.

Division of the exchange plate with reference height into equal halves

In the first calculation, the exchange plate with reference height is divided into two equal halves. The solution mass flow factor for section I varies between 0 and 1 ($0 < f_{\dot{m},S,I} < 1$) and the solution mass flow factor for section II varies between 1 and 2 ($1 < f_{\dot{m},S,I} < 2$). As previously explained, $f_{\dot{m},S,I}$ and $f_{\dot{m},S,II}$ interdepend according to $f_{\dot{m},S,I} = 2 - f_{\dot{m},S,II}$.

Figure 5.6 shows the performance of the individual sections and the combined performance of both sections as function of the solution mass flow factor $f_{\dot{m},S,II}$. For comparison, it includes the reference performance of the same exchange plate with ideal distribution of the solution flow.

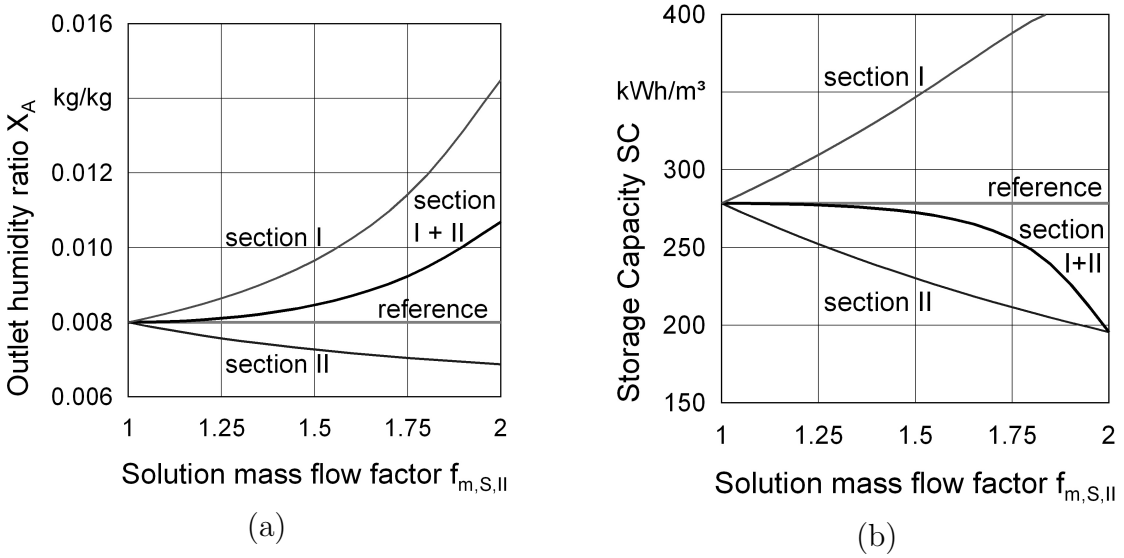

Figure 5.6: *Effects of maldistribution of the solution flow in the absorber: performance of the individual sections of the exchange plate and the combined performance of the exchange plate (a) outlet humidity ratio (b) energy storage capacity*

Figure 5.6a proves that the outlet humidity ratio increases significantly with solution mass flow factors below 1 (section I) and decreases slightly with solution mass flow factors above 1 (section II). The combination of section I with section II demonstrates that those effects do not compensate. The outlet humidity ratio resulting from the plate with maldistribution increases with increasing maldistribution. The required outlet humidity ratio of 8 g/kg, the supply air humidity ratio, is not achieved for $f_{\dot{m},S,I} < 0.75$ ($f_{\dot{m},S,II} > 1.25$).

Figure 5.6b shows the effects of maldistribution on the energy storage capacity. The energy storage capacity increases with solution mass flow factors below 1 (section I) and decreases with solution mass flow factors above 1 (section II). Those effects compensate each other for a wide range of mass flow factors ($0.5 < f_{\dot{m},S,I} < 1$,

$1 < f_{\dot{m},S,II} < 1.5$). Thus the resulting energy storage capacity is almost equal to the one for a plate without maldistribution. For $f_{\dot{m},S,I} < 0.5$ ($f_{\dot{m},S,II} > 1.5$), however, the resulting energy storage capacity decreases rapidly. For the limits of this example with $f_{\dot{m},S,I} = 0$ ($f_{\dot{m},S,II} = 2$), the combined energy storage capacity of both sections is 30% lower than the reference energy storage capacity with $f_{\dot{m},S} = 1$ for both sections.

Division of the exchange plate into equal halves and variation of the exchange plate height to meet the reference outlet humidity ratio

The outlet air humidity ratio is a strict boundary condition for the absorption process, regardless of maldistribution. Yet, Figure 5.6a shows that in case of maldistribution, the requested outlet humidity ratio might not be met. Consequently, the height of the exchange plate has to be increased to offer more exchange surface to the media until the outlet air meets the required humidity ratio. Figure 5.7 shows the required height of the exchange plate as function of the maldistribution of the solution flow.

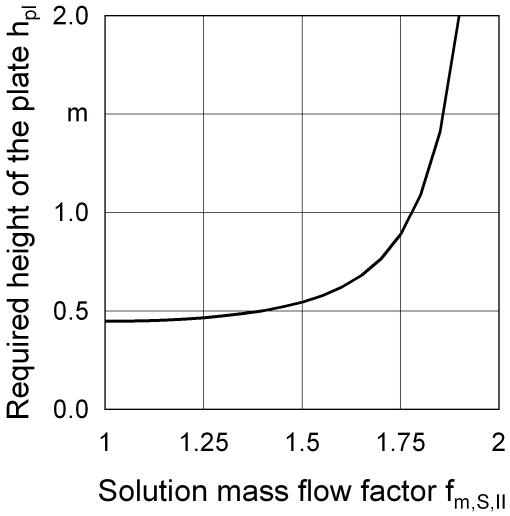

Figure 5.7: *Height of the absorption plate required to provide the reference outlet humidity ratio as function of the maldistribution of the solution flow in the absorber*

For solution mass flow factors $f_{\dot{m},S,I} > 0.5$ ($f_{\dot{m},S,II} < 1.5$), the required height increases only slightly. Yet for solution mass flow factors $f_{\dot{m},S,I} < 0.25$ ($f_{\dot{m},S,II} > 1.75$), the required height increases dramatically. For $f_{\dot{m},S,I} < 0.19$ ($f_{\dot{m},S,II} > 1.81$), for example, the required height is three times the reference height.

Division of the exchange plate into a section without any solution flow and one with the total solution flow and variation of the exchange plate height to meet the reference outlet humidity ratio

The previous calculations base on the assumption that - unless $f_{\dot{m},S,I} = 0$ - the distribution device always distributes some solution evenly on section I. In reality, however, parts of the exchange surface are not wetted at all by the solution and remain dry during the absorption process. Therefore, in a further step, the division of the exchange surface was not based on geometry (division into equal halves) but on the quality of the surface wetting:

- section I: completely dry fraction of the exchange surface
  heat transfer only between air flow and cooling water flow
- section II: completely wetted fraction of the exchange surface
  heat transfer between solution flow and cooling water flow
  heat and mass transfer between air flow and solution flow

The fraction of dry surface specifies the solution maldistribution factor $f_{mal,S}$, defined in section 5.1.1. While areas without any salt solution on the exchange surface are very common and parts without cooling also, parts of the exchange surface without any air flow at all are highly improbable. Therefore, in the present research the maldistribution factor f_{mal} can only be applied to the maldistribution of the solution flow and the cooling water flow.

Figure 5.8 shows how the required height of the exchange plates increases with an increasing maldistribution factor $f_{mal,S}$.

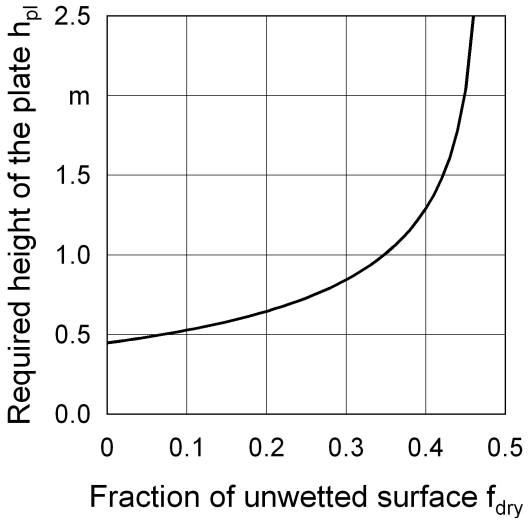

Figure 5.8: *Required height of the exchange plates as function of the solution maldistribution factor $f_{mal,S}$, i.e. the fraction of unwetted exchange surface f_{dry}*

For maldistribution factors above 46%, the absorption device cannot provide air with the required outlet humidity any more. Figure 5.9 shows the corresponding McCabe-Thiele diagram.

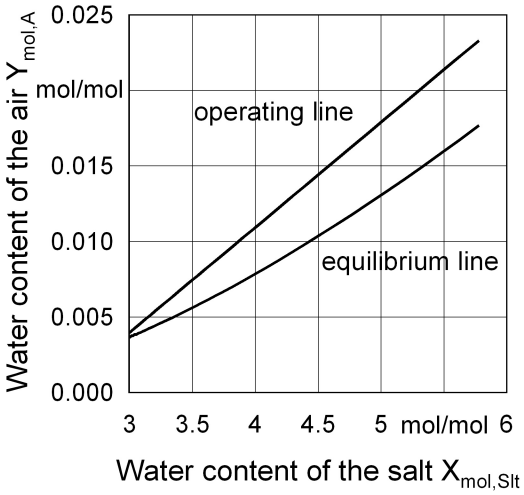

Figure 5.9: *McCabe-Thiele diagram for section II with* $f_{mal} = 0.46$

This division into only one dry and only one wet section corresponds to a worst case estimation. For every $f_{mal,S}$, the combined performance of the sections resulting from this division is always worse than the combined performance resulting from a division into various dry sections surrounded by wet sections with the same $f_{mal,S}$. As in reality the dry areas can be distributed over the exchange surface or they can form one big area, the worst case estimation allows to give the theoretical performance minimum resulting from a certain maldistribution $f_{mal,S}$.

5.2.2 Maldistribution of the Air Flow

While the distribution of the liquid desiccant depends on the distribution device on top of the exchange surface, the distribution of the air flow depends mainly on the pressure drop in the air channel. Deformation of the exchange plates locally changes the cross section of the air channel and leads to maldistribution of the air flow.

Analogously to the calculations in subsection 5.2.1, this subsection at first calculates the effects of a maldistribution of the air flow for the reference dimensions of the absorption device and the same boundary conditions as in the previous example. It subsequently determines the height of the exchange plate that is required to provide air with the requested outlet humidity ratio as function of the maldistribution of the air flow, expressed as air mass flow factor $f_{\dot{m},A}$. The solution flow is ideally distributed and sufficiently cooled in these cases.

Division of the exchange plate with reference height into equal halves

The exchange plate with reference height is divided into two equal halves. The air mass flow factor for section I varies between 0 and 1 ($0 < f_{\dot{m},A,I} < 1$) and the air mass flow factor for section II varies between 1 and 2 ($1 < f_{\dot{m},A,I} < 2$). $f_{\dot{m},A,I}$ and $f_{\dot{m},A,II}$ interdepend according to $f_{\dot{m},A,I} = 2 - f_{\dot{m},A,II}$.

Figure 5.10 shows the performance of the individual sections and the combined performance of both sections as function of the air mass flow factor $f_{\dot{m},A,II}$. For comparison, it includes the reference performance of the same exchange plate with ideal distribution of the air flow.

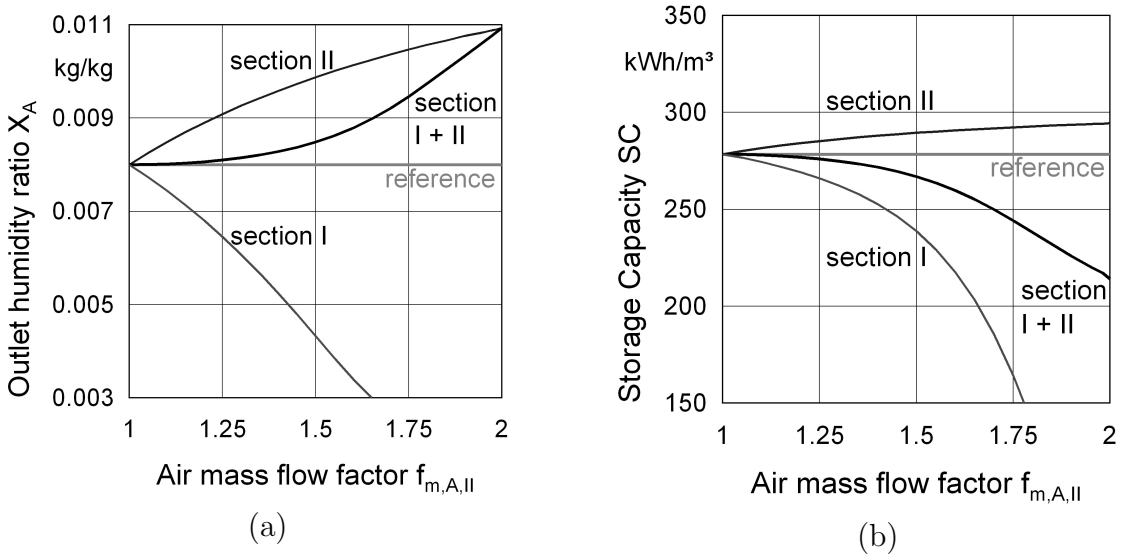

Figure 5.10: *Effects of maldistribution of the air flow in the absorber: performance of the individual sections of the exchange plate and the combined performance of the exchange plate: (a) outlet humidity ratio (b) energy storage capacity*

Figure 5.10a proves that the outlet humidity ratio decreases with decreasing air mass flow factors because the same amount of liquid desiccant dehumidifies a decreasing air flow (section I). Consequently, the outlet humidity ratio increases with an increasing air flow (section II). Combining section I and section II demonstrates that those effects compensate up to $f_{\dot{m},A,I} > 0.75$ ($f_{\dot{m},A,II} < 1.25$) so that the required outlet humidity ratio of 8 g/kg is still achieved for a minor maldistribution of the air flow.

Figure 5.10b demonstrates the effects of maldistribution of the air flow on the energy storage capacity. As the increasing air mass flow in section II provides more absolute humidity to absorb, the outlet concentration of section II decreases and the energy storage capacity increases (section II). In section I, the air flow diminishes and thus provides less absolute humidity to absorb. The outlet concentration of section I increases, leading to a decreasing energy storage capacity (section I). Those effects also

outweigh each other to a certain extend. For the limits of this example with $f_{\dot{m},A,I} = 0$ and $f_{\dot{m},A,II} = 2$, the combined energy storage capacity of both sections is 23% lower than the reference energy storage capacity with $f_{\dot{m},A} = 1$ for both sections.

Division of the exchange plate into equal halves and variation of the exchange plate height to meet the reference outlet humidity ratio

As in section 5.2.1, the height of the absorption plate that is necessary to provide air with the requested outlet humidity has been determined as function of the maldistribution of the air flow. Figure 5.11 shows how the required height of the absorption plate increases with an increasing air mass flow factor $f_{\dot{m},A,II}$.

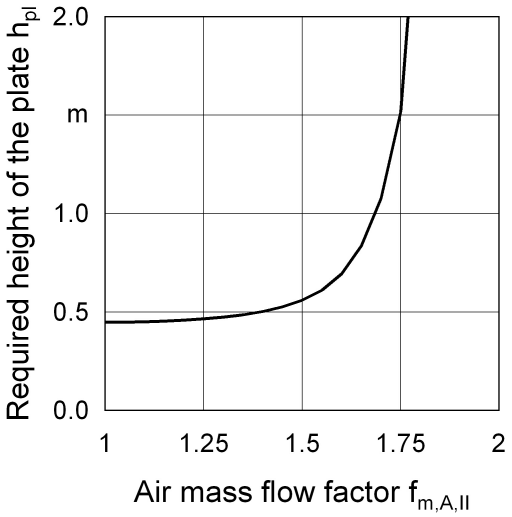

Figure 5.11: *Required height of the absorption plate as function of the maldistribution of the air flow in the absorber*

As previously explained, parts of the exchange surface without any air flow at all are highly improbable and therefore no calculation with a division of the exchange plate into a section without air flow and a section with the complete air flow has been carried out.

5.2.3 Maldistribution of the Cooling Water Flow

While air and salt solution flow in the same channel between the exchange plates and influence each other, the cooling water flows in separate channels inside the exchange plate. The cooling water flow passes the exchange plate in a cross-counter flow pattern with four direction changes as shown in figure 5.2. In case of an ideal distribution of the cooling water, the capacity of the cooling water is always sufficient to cool the salt solution even if the salt solution is maldistributed.

As a division of the exchange plate into two halves with varying mass flow factors $f_{\dot{m},W,I}$ and $f_{\dot{m},W,II}$ does not represent the cross-counter flow pattern of the cooling water, the maldistribution of the cooling water $f_{mal,W}$ is expressed as fraction of uncooled surface f_{uncooled}, analogously to the fraction of unwetted surface f_{dry} in subsection 5.2.1.

Yet a division of the exchange plate into only two sections, one coherent section without any cooling and one coherent section with sufficient cooling, does also not represent the cross-counter flow pattern of the cooling water. Therefore, the exchange plate is divided into various sections with alternating cooling characteristics. Because of the four direction changes of the cooling water, the exchange plate is divided into five sections with two subsections each that have alternating cooling characteristics. As the number of direction changes of the cooling water defines the division into the sections, all five sections have the same size.

The subdivision of each section into a cooled subsection and an uncooled subsection agrees with the fraction of uncooled surface. The cooling water passes through the first, third, fifth, seventh and ninth subsection and no cooling water flows through the second, fourth, sixth, eighth and tenth subsection. Figure 5.12 shows the alternating water cooling characteristics for the examples $f_{\text{uncooled}} = 0.2$ and $f_{\text{uncooled}} = 0.6$.

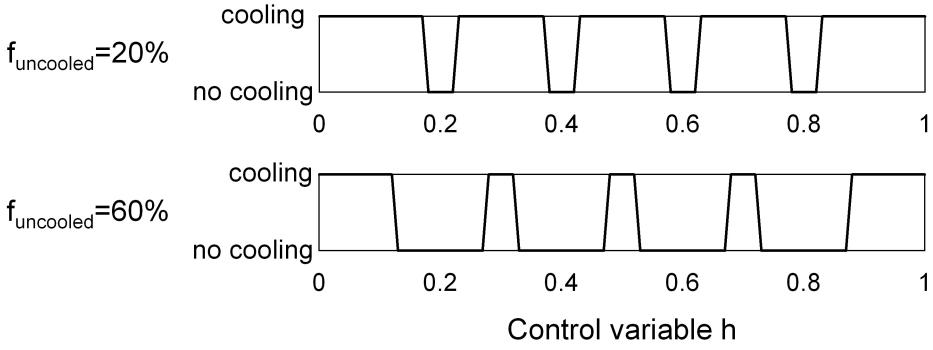

Figure 5.12: *Division of the exchange plate into subsections with alternating water cooling characteristics, examples for* $f_{uncooled} = 20\%$ *and* $f_{uncooled} = 60\%$

The lack of water cooling leads to an increase of the solution temperature and consequently to an increase of the equilibrium dew point temperature. For a case with 20% uncooled surface, Figure 5.13 displays the simulated air, solution and cooling water temperatures and the corresponding dew point temperatures. Figure 5.14 plots these temperature and humidity data in a McCabe-Thiele diagram. Though the outlet humidity is lower and the outlet concentration is higher than the reference case with 100% cooled surface, the number of transfer units for this process is also 1.5 transfer units.

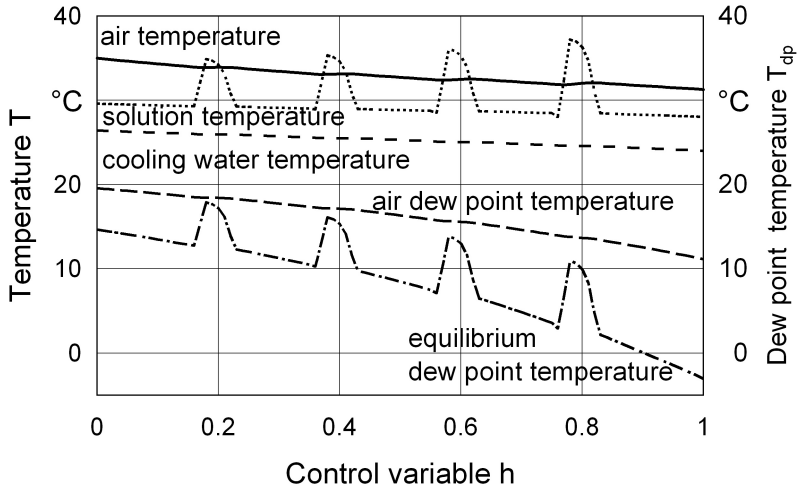

Figure 5.13: *Simulated temperature and dew point temperature sequences for* $f_{uncooled} = 20\%$ *and an ideal distribution of solution flow and air flow*

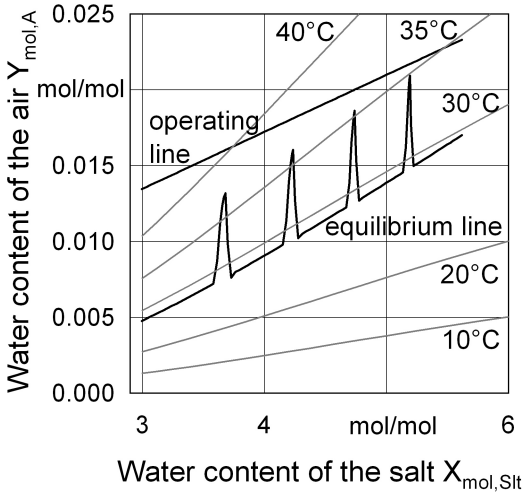

Figure 5.14: *McCabe-Thiele diagram for* $f_{uncooled} = 20\%$ *and an ideal distribution of solution flow and air flow*

Similar to the calculations in subsection 5.2.1 and subsection 5.2.2, this subsection at first calculates the effects of a reduced cooling ($f_{\text{uncooled}} > 0$) for the reference dimensions of the exchange plate. It subsequently determines the required height of the exchange plate to provide air with the requested outlet humidity ratio in case of reduced cooling. Air and solution flow are ideally distributed in these cases.

Reduced cooling of the exchange plate with reference height

In the first calculation, the fraction of unwetted surface varies between $f_{\text{uncooled}} = 0$, i.e. ideal cooling, and $f_{\text{uncooled}} = 1$, i.e. adiabatic absorption process without cooling, for the exchange plate with reference height.

Figure 5.15 shows the effect of improper cooling on the outlet temperatures of air, solution and cooling water and the outlet dew point temperature. It proves that the water cooling has a high impact on the air dehumidification. The air outlet dew point increases instantly with $f_{\text{uncooled}} > 0$.

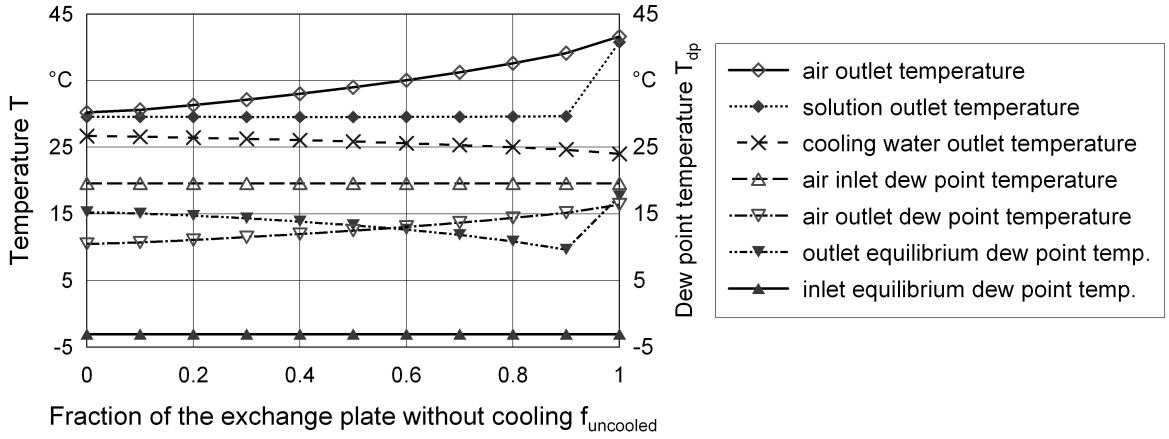

Figure 5.15: *Outlet temperatures of air, solution and cooling water and inlet and outlet dew point temperatures as function of the fraction of uncooled surface* $f_{uncooled}$

The outlet equilibrium dew point temperature reflects the concentration of the solution. An outlet equilibrium dew point temperature that decreases with increasing f_{uncooled} indicates an increasing outlet concentration of the solution and therefore a lower energy storage capacity. The impact of f_{uncooled} is shown in Figure 5.16.

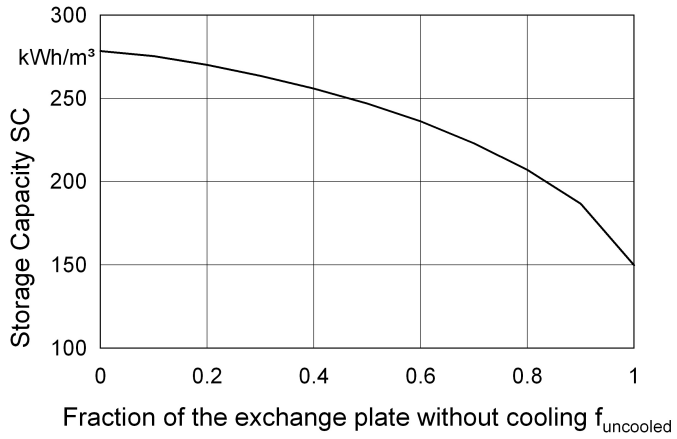

Figure 5.16: *Storage capacity as function of the fraction of uncooled surface* $f_{uncooled}$

Reduced cooling of the exchange plate and variation of the exchange plate height to meet the reference outlet humidity ratio

As in the previous sections, the height of the exchange plate that is necessary to provide air with the requested outlet humidity has been determined as function of

the maldistribution of the cooling water flow. Figure 5.17 shows how the required height of the exchange plate increases with an increasing f_{uncooled}.

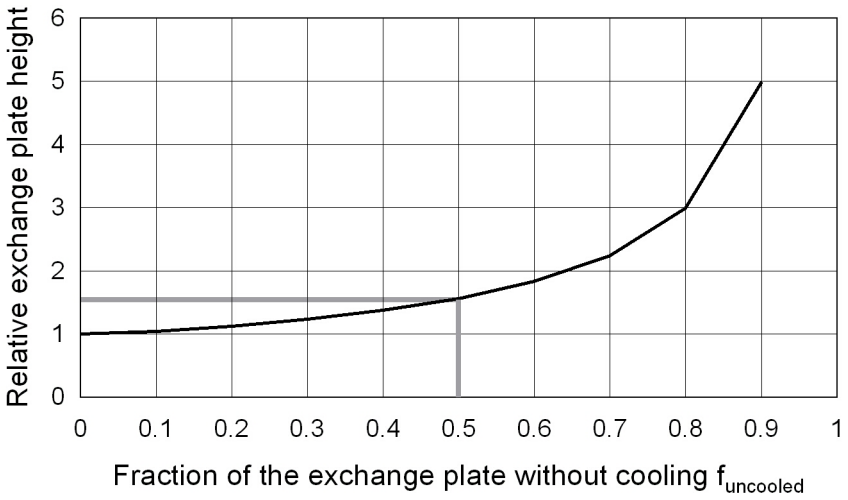

Figure 5.17: *Relative required height of the absorption plate as function of the fraction of uncooled surface* $f_{uncooled}$

For low fractions of the exchange plate without cooling water flow, the lack of water cooling can easily be compensated by an increase of the height of the exchange plate that roughly corresponds with the fraction of uncooled surface. For $f_{\text{uncooled}} = 0.5$, e.g., the required height is 1.57 times the reference height. With increasing f_{uncooled}, however, the requested outlet humidity ratio is harder to obtain. For $f_{\text{uncooled}} = 0.8$, an exchange plate three times the height of the reference height is required. Without cooling, an exchange plate with more than ten times the reference height is required to provide the requested outlet humidity ratio with the given reference conditions.

Consequently, a different absorption approach is more suitable to provide the requested outlet humidity ratio without cooling the solution during the absorption process. The inlet solution itself has to provide a cooling capacity and thus the solution has to enter the absorber with a lower temperature and a higher capacity, i.e. a higher solution flow. As explained in section 3.2, low-flow LDCS request cooling of the desiccant during the absorption process.

Experiments show that the fraction of uncooled surface in low-flow LDCS commonly ranges between 15% and 20% and therefore by far lower than the previously mentioned $f_{\text{uncooled}} = 0.5$. Due to the cross-counter flow pattern of the cooling water, the cooling water always cools parts of the solution. An exclusive combination of a dry and cooled surface on one part of the exchange plate with a wetted and uncooled surface on the other part of the exchange plate is not possible. To compensate for the maldistribution of the cooling water, thus, the height of the reference exchange plate has to be increased according to the expected or experimentally determined maldistribution of the cooling water flow.

5.2.4 Simultaneous Maldistribution of Liquid Desiccant and Air Flow

In the absorber of a liquid desiccant system, air flow, liquid desiccant flow and cooling water flow can be maldistributed simultaneously. The maldistribution of air flow and solution flow is correlated and it can be co-correlated or anti-correlated. Both are not correlated to the maldistribution of the cooling water flow because of the different flow patterns. Air and solution flow in counter flow pattern, the cooling water flow in cross counter pattern.

As the lack of cooling can easily be compensated for by increasing the height of the exchange plate according to the expected or experimentally determined maldistribution of the cooling water flow, this subsection analyzes only the simultaneous maldistribution of air flow and solution flow. It applies the previously employed method to determine the effects of a simultaneous maldistribution of air flow and solution flow.

Again, for the deduction of the general trends, the division of the exchange surface into two equal halves is kept for clearness at first. Then, the the exchange plate is divided into one dry and one wet section with varying dimensions of the sections as explained in subsection 5.2.1.

Division of the Exchange Plate with Reference Height into Equal Halves

The possibilities for combined maldistribution are limited and only two alternatives have to be considered:

- **Case A: co-correlation**
  Section I: Air $0 < f_{\dot{m},A,I} < 1$, Solution $0 < f_{\dot{m},S,I} < 1$
  Section II: Air $1 < f_{\dot{m},A,II} < 2$, Solution $1 < f_{\dot{m},S,II} < 2$
- **Case B: anti-correlation**
  Section I: Air $0 < f_{\dot{m},A,I} < 1$, Solution $1 < f_{\dot{m},S,I} < 2$
  Section II: Air $1 < f_{\dot{m},A,II} < 2$, Solution $0 < f_{\dot{m},S,II} < 1$

Case A: co-correlation of the maldistribution of air flow and solution flow

In case A, section I has a reduced gas load and a reduced liquid load. The mass flow factors of air and solution for section I are smaller than 1 and thus section I contributes only to a smaller extend to the total dehumidification process. Gas load and liquid load of section II are higher than in the reference case. The mass flow factors of air and solution for section II are greater than 1 and the main part of the total dehumidification process takes place on this section.

Figure 5.18 shows the individual outlet humidity ratios for section I and II and the combined performance of both sections and Figure 5.19 the according storage capacities.

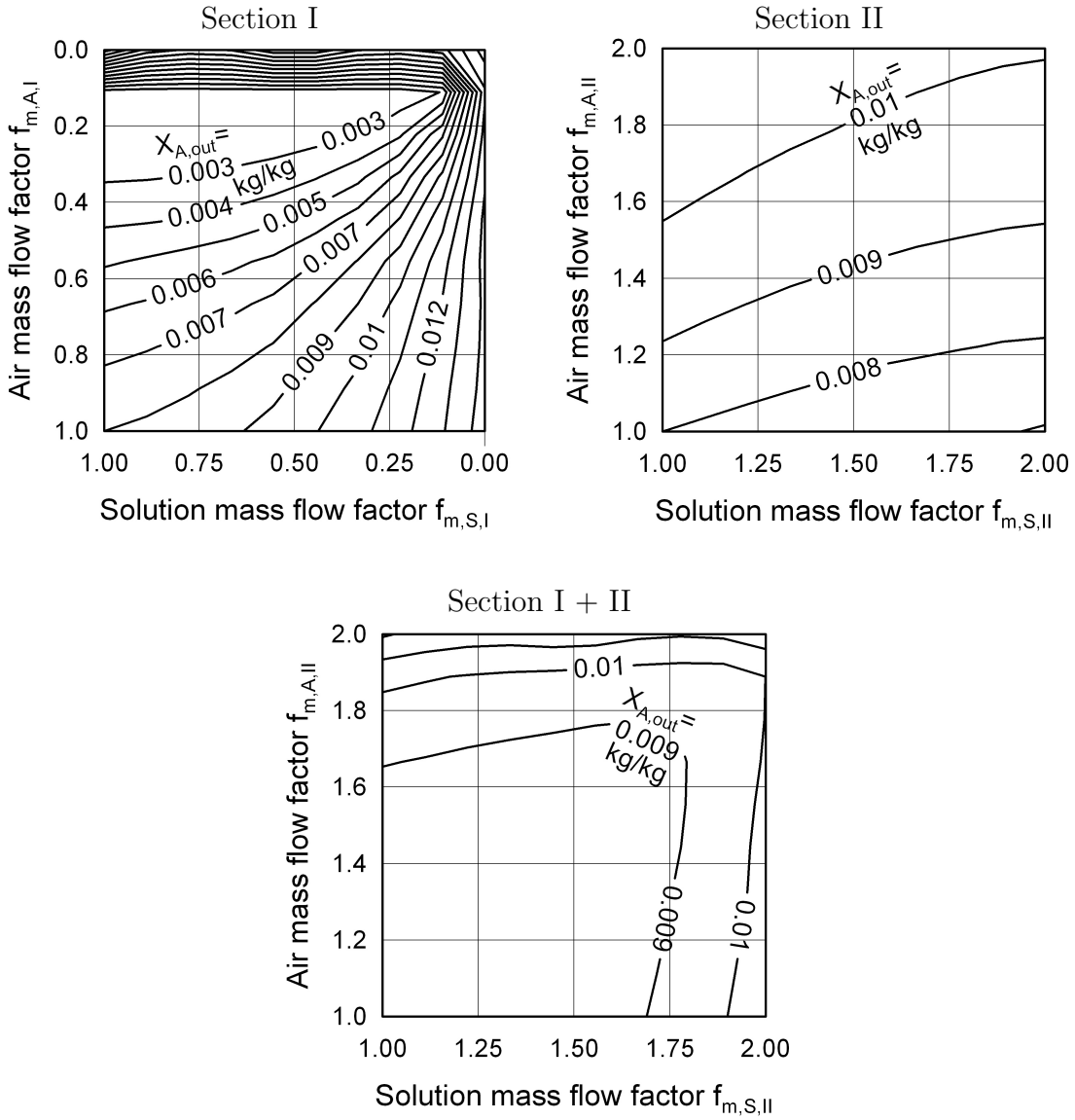

Figure 5.18: *Simulated outlet humidity ratio for case A, co-correlation of the maldistribution of air flow and solution flow*

In case of co-correlation of the maldistribution of air flow and solution flow, mass flow factors of up to $f_{\dot{m},A,I} > 0.4$ ($f_{\dot{m},A,II} < 1.6$) and $f_{\dot{m},S,I} > 0.4$ ($f_{\dot{m},S,II} < 1.6$) can be tolerated.

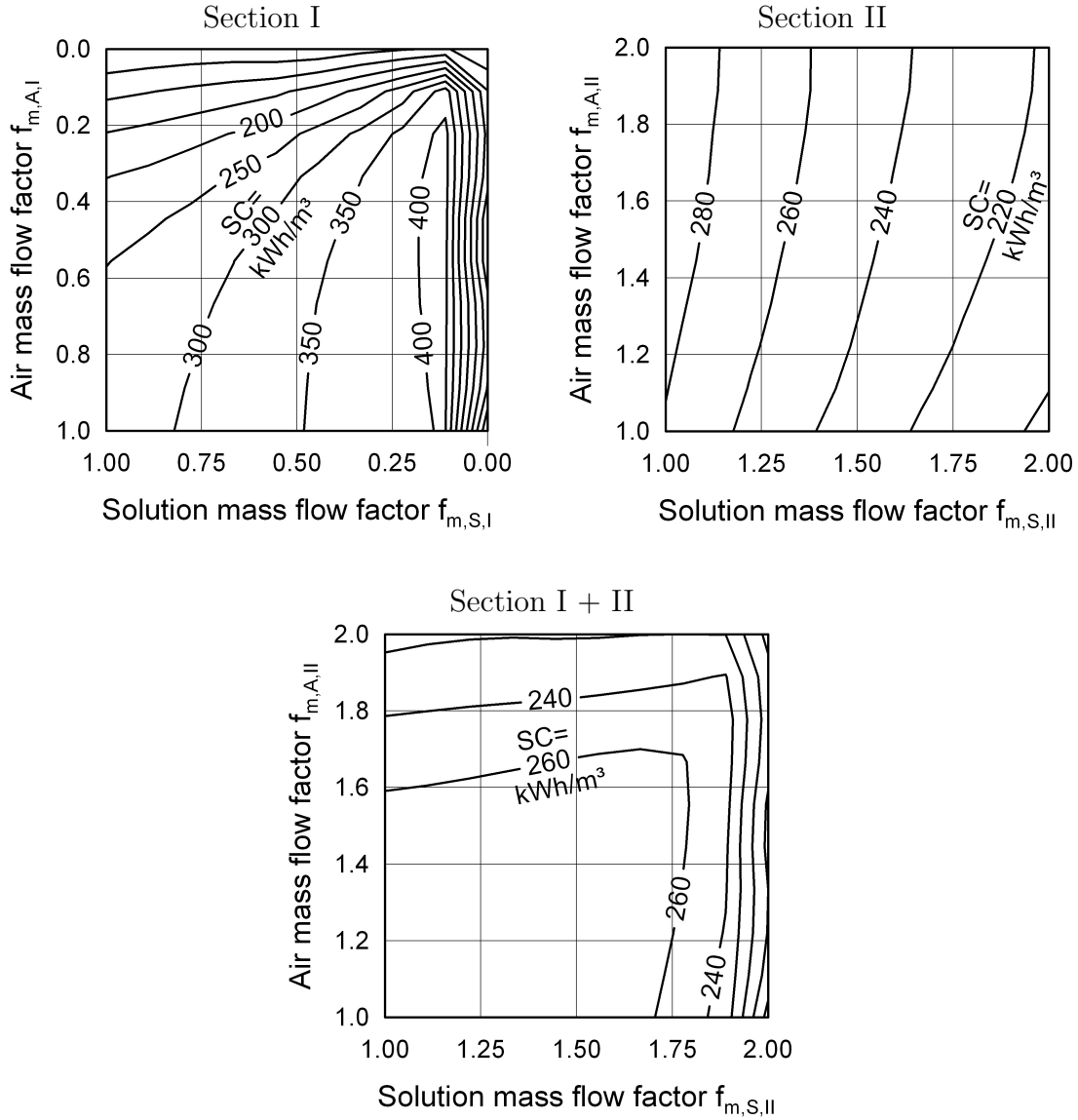

Figure 5.19: *Simulated energy storage capacity for case A, co-correlation of the maldistribution of air flow and solution flow*

Case B: anti-correlation of the maldistribution of air flow and solution flow

In case B, section I has a reduced gas load and an increased liquid load. The mass flow factor of air is smaller than 1 while the mass flow factors of the solution is greater than 1. Consequently, the outlet humidity ratio in section I is always lower than the design outlet humidity ratio. The gas load of section II is higher than in the reference case and the liquid load is lower. The mass flow factor of air is greater than 1 and the mass flow factor of the solution is smaller than 1. This leads to an outlet humidity ratio in section II that always exceeds the design outlet humidity ratio.

Figure 5.20 shows the individual outlet humidity ratios for section I and II and the combined performance of both sections and Figure 5.21 the according storage capacities.

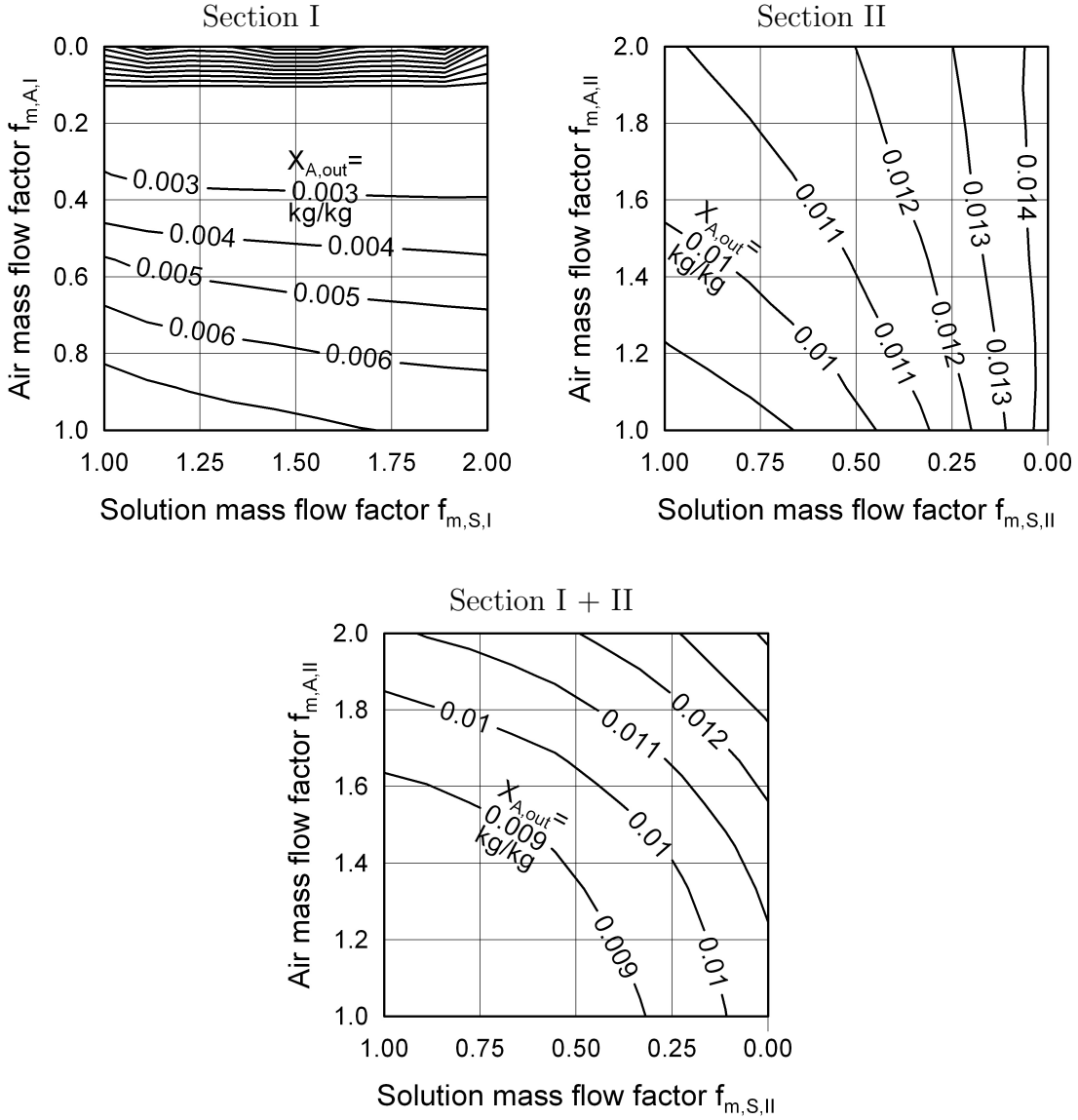

Figure 5.20: *Simulated outlet humidity ratio for case B, anti-correlation of the maldistribution of air flow and solution flow*

In case of anti-correlation of the maldistribution of air flow and solution flow, mass flow factors of up to $f_{\dot{m},A,I} > 0.6$ ($f_{\dot{m},A,II} < 1.4$)and $f_{\dot{m},S,I} > 0.6$ ($f_{\dot{m},S,II} < 1.4$) can be tolerated.

Figures 5.18 and 5.20 prove that a simultaneous maldistribution of air and solution flow with a co-correlation has less influence on the outlet humidity ratio of both sections than a simultaneous maldistribution of air and solution flow with an anti-correlation.

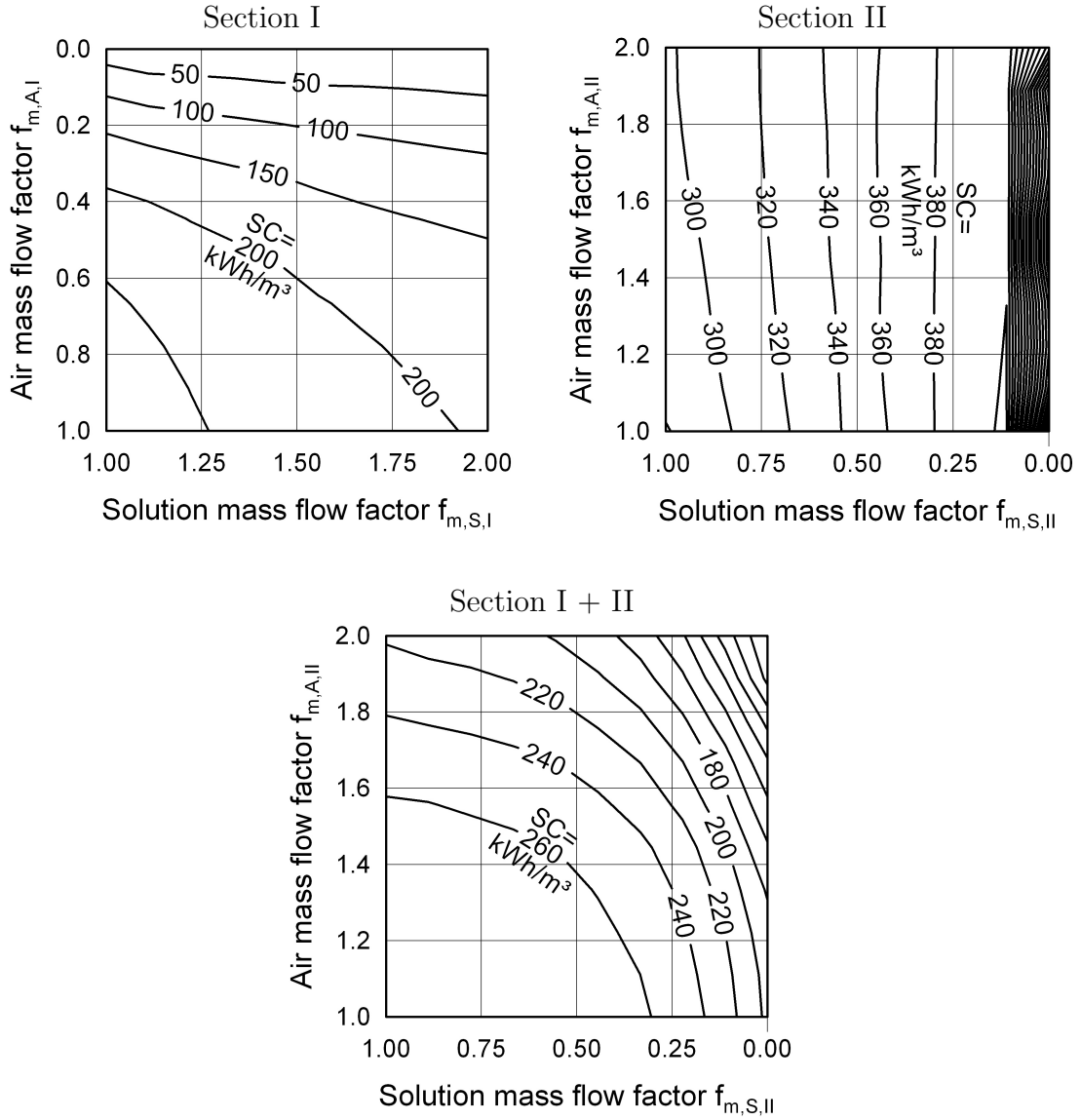

Figure 5.21: *Simulated energy storage capacity for case B, anti-correlation of the maldistribution of air flow and solution flow*

Figures 5.19 and 5.21 demonstrate the same trend for the storage capacity. The resulting energy storage capacity of both sections is more sensitive to a simultaneous maldistribution with an anti-correlation (case B) than to a simultaneous maldistribution with a co-correlation (case A).

Division of the exchange plate into a section without any solution flow and one with the total solution flow and variation of the exchange plate height to meet the reference outlet humidity ratio

Again, the previous calculations base on the assumption that - unless $f_{\dot{m},S,I} = 0$ - the distribution device always distributes some solution evenly on section I. Yet, some

parts of the exchange surface might not be wetted at all by the solution and remain dry during the absorption process. Consequently, the division of the exchange surface into an always completely dry fraction (section I) and an always completely wetted fraction (section II) and a simultaneous maldistribution of the air flow best represent this operating condition. As explained in subsection 5.2.1, this operating condition corresponds with a simulation of the worst case performance of a low-flow LDCS.

The fraction of dry surface f_{dry} specifies the maldistribution of the solution flow $f_{mal,S}$ and varies between 0 and 0.5. The air mass flow factor $f_{\dot{m},A}$ specifies the maldistribution of the air flow and the upper limit for the air mass flow factor is set to the value of 2, according to the previous calculations.

As an anti-correlation of the maldistribution of air flow and solution flow is more critical than a co-correlation, only anti-correlation of the maldistribution of air flow and solution flow is simulated. Because of the anti-correlation the air mass flow factor for section I always has to be higher than 1 ($f_{\dot{m},A,I} > 1$) and the air mass flow factor for section II always has to be lower than 1 ($f_{\dot{m},A,II} < 1$). For this simulation, the air mass flow factor for section I always equals 2 ($f_{\dot{m},A,I} = 2$) and equation 5.8 specifies the resulting air mass flow factor for section II.

$$f_{\dot{m},A,II} = \frac{1 - f_{\mathrm{dry}} \cdot f_{\dot{m},A,I}}{1 - f_{\mathrm{dry}}} \tag{5.8}$$

Figure 5.22 shows how the required height of the exchange plates increases with an increasing fraction of dry surface and simultaneous maldistribution of the air flow.

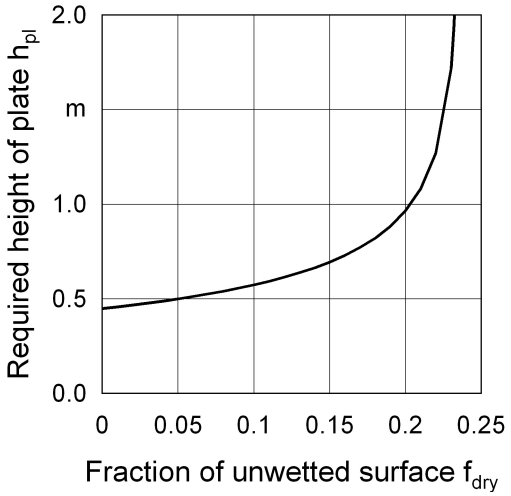

Figure 5.22: *Required height of the absorption plate for anti-correlated maldistribution of air and solution flow with $f_{\dot{m},A,I} = 2$ and as function of the fraction of dry surface*

For fractions of unwetted surface of up to 15%, the lack of wetted exchange plate can be compensated for by an increase of the height of the exchange plate that roughly

corresponds to four times the fraction of uncooled surface. For $f_{\mathrm{dry}} = 15\%$, e.g., the required additional height is 60% of the reference height. With increasing f_{dry}, however, the requested outlet humidity ratio is harder to obtain and for $f_{\mathrm{dry}} = 20\%$, an exchange plate with 2.2 times the height of the reference height is required. For solution maldistribution factors above 23%, the absorption device cannot provide air with the required outlet humidity any more. Figure 5.23 shows the corresponding McCabe-Thiele diagram.

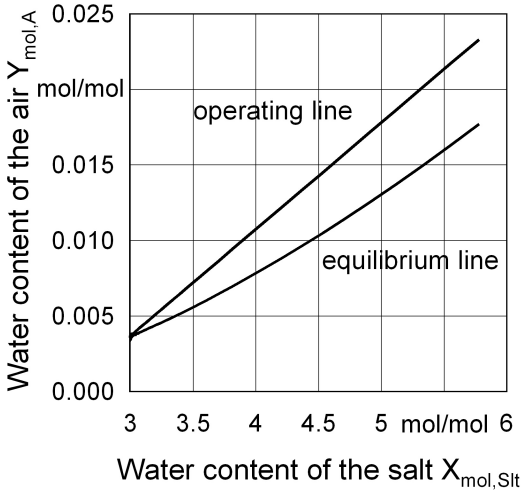

Figure 5.23: *McCabe-Thiele diagram for section II with* $f_{dry} = 0.23$

Under normal operating conditions, maldistribution of cooling water, air and solution flow occur. To compensate for the maldistribution of the cooling water, the height of the reference exchange plate has to be increased according to the expected or experimentally determined maldistribution of the cooling water flow ranging between 15% and 20%, as explained in section 5.2.3.

Concerning the maldistribution of air flow and solution flow, simulations show that an anti-correlation of the maldistribution is more severe than a co-correlation. With an expected existing air mass flow factor of about 2, the required outlet humidity ratio can be provided by the exchange plate if the fraction of dry surface of the exchange plate is lower than 23% and the height of the exchange plate is augmented accordingly.

The previous simulation proves that the distribution of the solution flow is the crucial factor for the performance of low-flow LDCS. The required height of the exchange plate increases rapidly with $f_{\mathrm{dry}} > 0.2$, thus, the fraction of dry surface should be well below 20%. Therefore, a reliable distribution device for the solution is indispensable for a good performance of a low-flow LDCS and an efficient energy storage in low-flow LDCS. The next chapter deals with the development of such a reliable distribution device for low liquid desiccant flows.

Chapter 6

Liquid Desiccant Distributors for Low Liquid Flows

This chapter outlines the development and the evaluation of distributors for the liquid desiccant under the given low-flow boundary condition. At first, it explains the requirements for the distributor and the design approaches. Then, it introduces the experimental setup with the corresponding data acquisition and data analysis. Finally, it describes the evaluated distributors and the experimental results of the distributor tests are presented and discussed.

6.1 Distributor Development

6.1.1 Requirements for the Distributor

The requirements and boundary conditions for the solution distributor development were

- a high solution distribution factor $f_{dis,S} \geq 85\%$, i.e. $f_{\mathrm{dry}} \leq 15\%$,
- the suitability for low specific volume flows of the solution $\dot{v}_S \approx 0.23$ l/(h m), $\dot{v}_S \approx 6.5 \cdot 10^{-8}$ m^3/(s m), and
- the suitability for attaching it to the existing heat and mass transfer plates or for integrating it into the existing heat and mass transfer plates.

The calculations in section 5.2 prove that the even distribution of the solution flow on the heat and mass transfer plates is the crucial factor for the performance of low-flow liquid desiccant cooling systems. Insufficient wetting of the plate surface leads to performance losses and the required outlet humidity ratio is harder to obtain with an

increasing fraction of dry surface f_{dry}. If the fraction of dry surface of the exchange plate is higher than 23%, under the given reference conditions, the required outlet humidity ratio can not be provided at all by increasing the height of the exchange plate. $f_{\mathrm{dry}} = 20\%$ already requires an exchange plate with 2.2 times the height of the reference height and for $f_{\mathrm{dry}} = 15\%$, the required additional hight is still 60% of the reference height. Thus, the distributor for the solution flow had to meet the strict requirement of ensuring a distribution factor for the solution of at least 85%

Another key parameter for the distributor development was the specific volume flow of solution $\dot{v}_S$, defined as the solution flow that the distributor has to distribute evenly on each side of the exchange plate per width of the exchange plate, see equation 3.64. The specific volume flow of solution $\dot{v}_S$ for the reference conditions stated in subsection 5.1.2 was $\dot{v}_S = 6.5 \cdot 10^{-8}$ m^3/(s m).

A design boundary condition was the requirement that the distributor had to be suitable for attaching to the existing heat and mass transfer plates. Moreover, the distributor dimensions could not exceed the dimensions of the heat and mass transfer plates. For the existing heat and mass transfer plates, the thickness of the the distributor was limited to 5 mm and the width could not exceed 1 m. The height was preferably below 10% of the height of the complete heat and mass transfer plate.

The mounting of a separately manufactured distribution device causes a horizontal transition section between distributor and plate and possibly leads to a deterioration of the distribution of the solution on the plate. This apparent disadvantage is true for all separate distributors that need to be fixed on the exchange plate. An integration of the distributor into the existing heat and mass transfer plates was identified as a promising approach to avoid the difficulties involved with separate distributors. In the case of the integrated distributor, the upper part of the heat and mass transfer plate consists of the distribution device and the lower part provides the cooled exchange surface for the dehumidification process. Yet, a disadvantage of the integration of the distributor into the plate is the fact that the internal structure of the exchange plate presets the internal dimensions of the distributor.

6.1.2 Design Approaches

Figure 6.1 shows a schematic of a distributor. It consists of one or two inlets, internal partitions that form hollows or channels that pass the solution to the outlets, and various outlets.

If the analyzed distributor had one inlet, it was located in the center of the distributor. In case of two inlets, they were located at both ends of the distributor. The outlets were located equidistant and the internals of the distributor had to ensure an even feeding of the outlets.

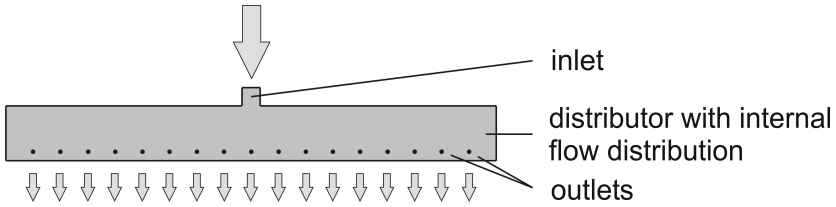

Figure 6.1: *Schematic of a distributor*

Number of outlets

The number of outlets depends on the spreading of the solution on the surface, i.e. the surface tension of the solution and the surface structure of the exchange plate. A better spreading of the solution, expressed by the width of a vertical section of the exchange plate wetted by the solution of one outlet, lowers the number of required outlets. If the solution of one outlet wets a vertical section of the exchange plate with a width of e.g. 10 mm well, 100 outlets are required per meter distributor width. Increasing the width of the vertical section wetted by the solution of one outlet to 20 mm leads to a reduction of the number of required outlets to 50 per meter distributor width. On a plain PP-surface, the liquid desiccant droplets of one outlet trickle down wetting a vertical section of the exchange plate with a width between 3 to 5 mm. Without a change in surface structure, a distributor for a plain PP-plate theoretically requires at least 250 outlets for a proper wetting of the exchange plate.

Even feeding of the outlets

To provide an even distribution of the solution on the exchange surface, the amount of solution flowing out of each outlet has to be the same. Thus, the internal sections or channels of the distributor have to feed the outlets evenly. The fraction of solution that flows through an individual section or channel of the distributor adjusts according to the pressure drop of this individual path. As all paths through the distributor experience the same pressure drop, all paths through the developed distributors had to be shaped in a way that their pressure drops led to the same volume flow for each path.

A good approach to guarantee the same specific pressure drop for a given volume flow between inlet and outlet for any path through the developed distributor was to design a distributor that possessed preset and specified internal paths, all with the same length and dimensions, and each leading to one outlet. The total pressure drop of the distributor was predominantly defined by the shape of these paths. Compared to the pressure drop of these paths, the pressure drop of the outlet became negligible. Therefore, pressure drop differences of the outlets became irrelevant and the definite internal paths ensured the even feeding of the outlets.

Another approach to ensure an even distribution of the fluid was to include an internal pressure drop producer in the developed distributors that caused a high specific pressure drop in each path and furthermore the same additional pressure drop in each path. The total pressure drop of these distributors was predominantly defined by this pressure drop producer. A very small cross sectional area of the outlets was selected as this leads to a high pressure drop at the outlets. Consequently, the pressure drop differences between the individual internal paths of the solution in the distributor became irrelevant compared to this high and definite pressure drop. In this case, the very small cross sectional area of the outlets ensured the even feeding of the outlets.

Therefore, the alternatives for generating an even distribution of the solution were

- definite internal distribution channels that account for the pressure drop and a negligible pressure drop at the outlets or
- distributor outlets that account for the pressure drop and a minor pressure drop inside the distributor.

These two approaches are referred to as **channel concept** and **outlet concept**.

Channel concept

A distributor based on the channel concept offers internal distribution channels that specify various paths of the same length and the same cross-section to feed the outlets. To ensure an even feeding of the outlets by means of specified paths, a promising approach is to divide the inlet flow into two flows and subsequently divide these flows into two again and those into two again until the number of flows corresponds with the number of required outlets. Figure 6.2 shows an example of this channel concept also called bisection concept.

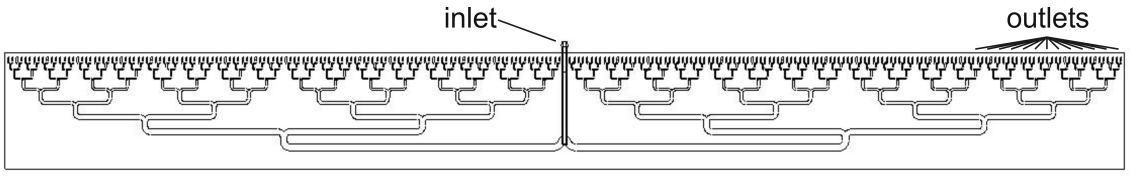

Figure 6.2: *Example of a distributor with channel concept*

Outlet concept

A distributor based on the outlet concept possesses outlets with a very small cross sectional area so that the pressure drop for the solution caused by the outlets is much higher than the pressure drop caused inside the distributor. The inside of the distributor does not need to specify paths but consists of an internal trough completely

filled with solution. Depending on the thickness of the distributor walls, distributors with outlet concept can require additional cross-beams as interconnections between the walls to stabilize the trough.

An advantage of the outlet concept is the fact that it can easily be integrated into the existing heat and mass transfer plates. This avoids a transition section between distributor and plate that can lead to a deterioration of the distribution of the solution on the plate. Figure 6.3 shows an example of a distributor with outlet concept integrated into a heat and mass transfer plate.

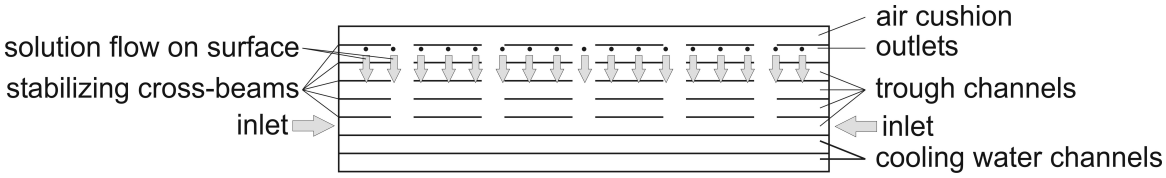

Figure 6.3: *Example of a distributor with outlet concept integrated into the a heat and mass transfer plate*

6.2 Distributor Evaluation

This section presents the experimental setup for the distributor evaluation with its corresponding data acquisition and data analysis.

6.2.1 Experimental Setup

As explained in section 6.1, the solution distribution factor $f_{dis,S}$ specifies the fraction of wetted surface and characterizes the quality of a distributor. The distribution factor results from analyzing the individual amounts of liquid that pass individual sections of the distributor. Yet, in structured packings it is not possible to determine the local liquid flows directly without disturbing the interaction of gas and liquid flow. Therefore, collecting the liquid underneath the packing is a common method to make accessible the distribution of the liquid flow. The experimental facility for the determination of the distribution factor of the developed distributors also utilized this method.

The experimental facility divided the distributor into vertical sections and collected the solution from each vertical section as a sample while the distributor operated with the design volume flow of the solution. Weighing the samples and evaluating the sample masses yielded the distribution factor, see subsection 5.1.1.

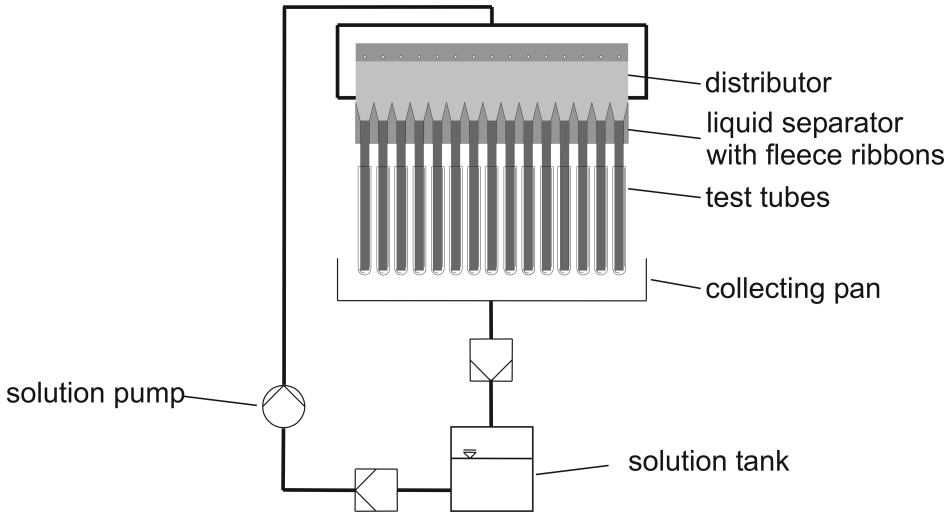

Figure 6.4: *Schematic of the experimental setup for the distributor evaluation*

Figures 6.4 and 6.5 show the experimental setup for the distributor evaluation. The main components of the testing facility were

- two dosing pumps for the solution,
- two comb-shaped liquid separators,
- a test tube rack with 128 test tubes à 25 ml,
- a support frame for clamping one or two distributors, one liquid separator, and the test tube rack and
- a collecting pan.

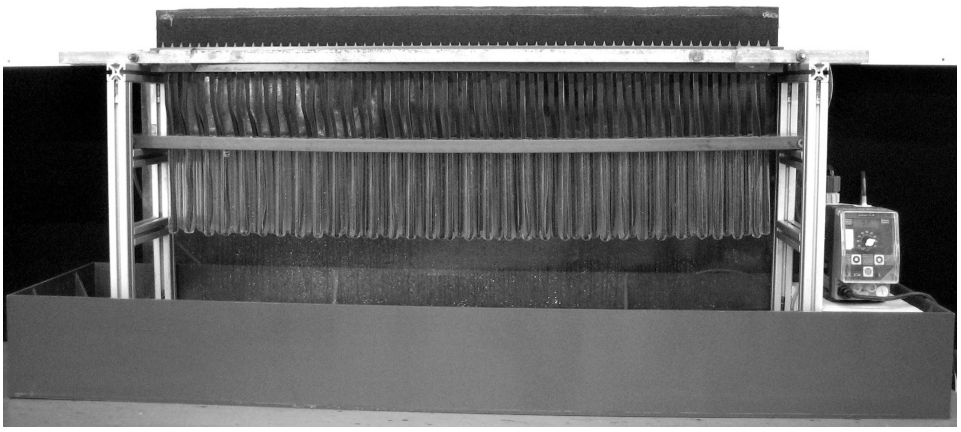

Figure 6.5: *Picture of the experimental setup for the distributor evaluation*

Two solenoid-driven diaphragm dosing pumps by ProMinent were available for the distributor tests. Depending on the design of the distributor, the solution pump fed either one single inlet or two inlets. The pumping parameters stroking rate and stroke length defined the pattern of the distributor feeding. The stroking rate could be varied between 1 and 120 strokes per minute and the stoke length between 1 and 100% of the maximum length. According to the manufacturer specification, pump *Gamma/5* operated in the volume flow range of up to 17.4 l/h. This pump delivered 2.4 ml per stroke at a maximal counter pressure of 3.5 bar and 2.5 ml per stroke at a counter pressure of 2 bar. The second pump, *Gamma/4*, operated in the volume flow range of up to 7.7 l/h. This pump delivered 1.1 ml per stroke at a maximal counter pressure of 3.5 bar and 1.2 ml per stroke at a counter pressure of 2 bar.

The support frame was fabricated of alloyed aluminum profiles that withstood the corrosive solution. It provided mounting clamps for one or two distributors and the liquid separator and struts that holded the test tube rack. The mounting positions for the distributors were labeled A and B. If only one distributor was tested, it was mounted in experimental position A. Figure 6.6 shows a schematic of the distributor mounting in the experimental setup. The mounting clamps also allowed to mount the distributor in the experimental position A 2 mm higher than the distributor in the experimental position B to compare the performance of two neighboring distributors operating simultaneously but mounted at slightly different heights.

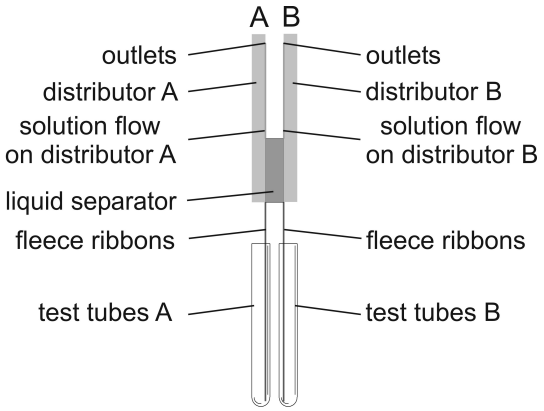

Figure 6.6: *Side view of the positions of the distributors in the experimental setup*

Two different types of liquid separators that had the form of a widetooth comb were available for the evaluation of distributors: one with flexible tubes and one with fleece ribbons. The selection of the liquid separator depended on the surface of the distributor and the type of experiment. The **liquid separator with flexible tubes** was suitable for the evaluation of the first development stages of a distributor. It allowed to analyze the distribution factor of the outlets and of distributors without any coating on the surface. As the solution wetted the PP-surface insufficiently, the

surface of the distributors was usually coated to improve the spreading of the solution. The coated distributors tested in this research were all coated with a flock-coating. The fibers of the flock-coating were approximately perpendicular to the distributor surface and improved the spreading of the solution, see subsection 6.5.2. The **liquid separator with fleece ribbons** was suitable for studying the distributors with a flock-coated surface.

Figure 6.7 shows a liquid separator with flexible tubes that was suitable for the evaluation of distributor outlets and uncoated distributors. In the experimental setup, the liquid separator was pressed against the distributor, split the liquid film on the distributor surface of the into vertical sections and passed the liquid on to the flexible tubes. Each flexible tube was inserted into one of the test tubes. As the liquid separator was pressed against the distributor, no liquid could trickle through any gap between liquid separator and distributor without being collected.

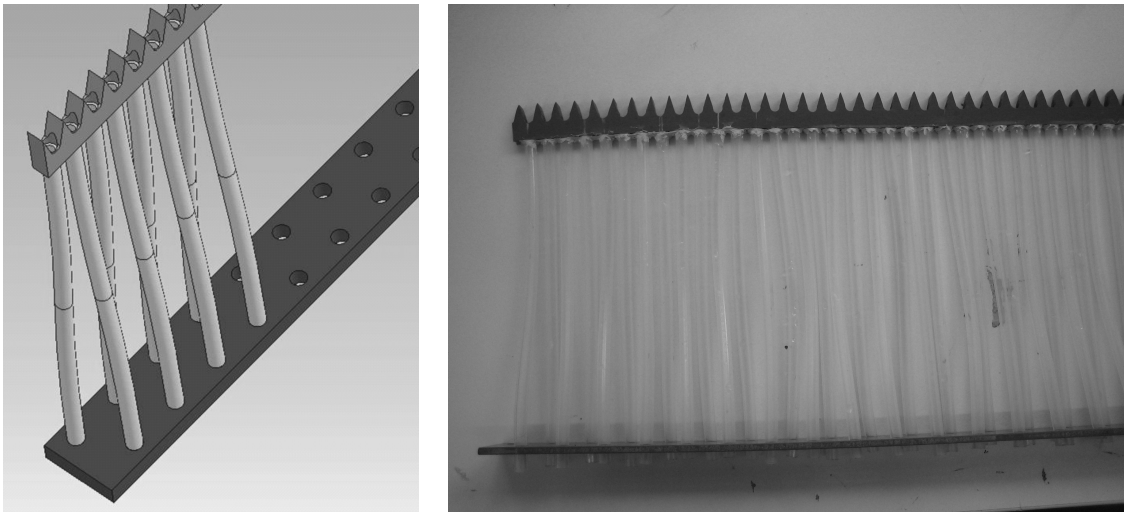

(a) (b)

Figure 6.7: *Liquid separator with flexible tubes (a) schematic drawing (b) manufactured device*

This separator could be positioned horizontally at any height of the distributor. Positioned closely underneath the outlets, it collected the liquid directly from the outlets. As the number of flexible tubes corresponded to the number of outlets, each test tube collected the liquid flows from an individual outlets allowing the analysis of the distribution factor of the outlets.

Figure 6.8 shows the liquid separator with fleece ribbons that was suitable for the evaluation of distributors with a flock-coating as the fleece carried on very well the liquid from the flock-coated surface to the test tubes. Analogously to the liquid separator with flexible tubes, it was pressed against the distributor, split the liquid film on the surface of the distributor into vertical sections and passed the liquid on

to the fleece ribbons. Each fleece ribbon was inserted into one of the test tubes and touched the ground of the test tube.

Figure 6.8a displays the slots for the fleece ribbons on both sides of the liquid separator. To prevent an incising of the fleece ribbons and a retaining of solution in the upper part of the fleece ribbons, this liquid separator could not be pressed as tightly to the distributor as the liquid separator with flexible tubes. This led to a trickling of the solution through the flock-coating without being collected in the test tubes if the bottom of the liquid separator was not aligned with the bottom of the distributor. An exact aligning of the lower edge of the liquid separator with the lower edge of the distributor avoided any trickling of the solution through the flock-coating without being collected in the sample mass.

An advantage of the liquid separator with fleece ribbons was that it allowed to study two distributors at the same time. It provided 128 fleece ribbons, 64 on each side. The shape of this liquid separator ensured that the fleece ribbons did not pass any solution from the distributor in the experimental position A to the distributor in the experimental position B and vice versa.

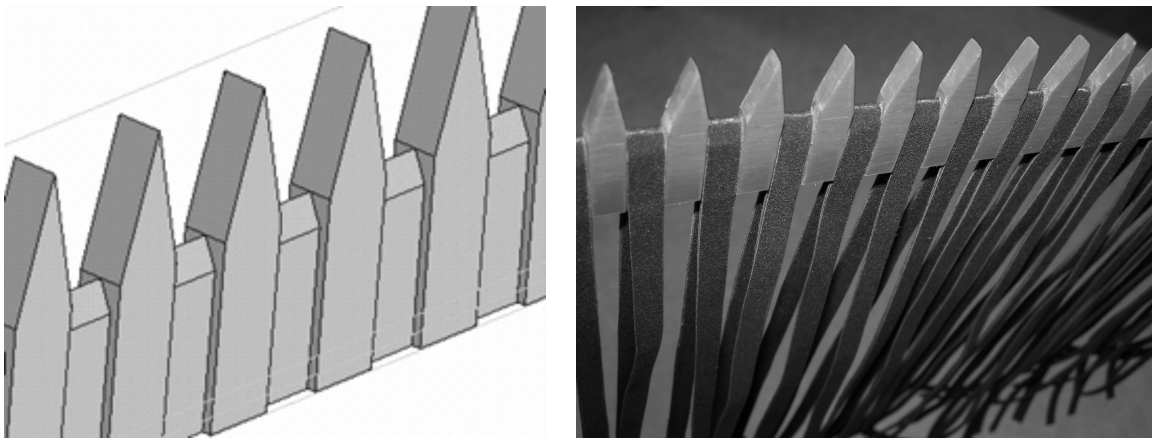

(a) (b)

Figure 6.8: *Liquid separator with fleece ribbons (a) schematic drawing of the liquid separator (b) manufactured device with fleece ribbons*

The test tube rack consisted in a mount made of corrosion-resistant PVC that held 128 standard glass test tubes with a volume of 25 ml each.

The support frame for distributor and test tube rack was positioned in a collecting pan made of corrosion-resistant PVC. This vat ensured a safe operation of the experimental facility also in case of distributor leakage because it fed spilled solution back into the solution tank.

The concentration of the solution in the tank was not constant because the experiment was setup in a laboratory without climate control and the solution was in contact with

the air in the laboratory. Absorption processes took place until the partial pressure of the solution and the partial pressure of the ambient water vapor were in equilibrium. As the water content of the air varied over the year and all the experiments were carried out with solution in equilibrium with the ambient air, the salt concentration lay between 27% in summer and 33% in winter.

Applying solution with the reference concentration of 44%, see subsection 3.3.1, for the experiments was not recommendable for two reasons. First, the absorption process is so quick that the solution would have reached the equilibrium concentration already during the start-up phase. Only a continuous reconcentration of the solution would have ensured the high reference concentration of 44%. Second, the distribution of the concentrated solution was easier than the distribution of the diluted solution. If the distributor met the distribution factor requirement for the diluted solution it also spread the concentrated solution well.

6.2.2 Test Procedure

All experiments were conducted according to a detailed test procedure check list to ensure comparability of the experimental results.

At first, some preliminary steps were necessary before starting an experiment. The experimental facility had to be inspected for broken or cracked glass test tubes that needed to be replaced by new ones. The 128 test tubes were labeled to define their position: A1-A64 and B1-B64. The individual masses of the empty test tubes were determined and fed into a spreadsheet. Covering the test tubes prevented them from collecting any solution beforehand.

As previously explained, the surface of the distributor and the type of experiment determined the appropriate liquid separator. The selected liquid separator was mounted together with the distributor in the support frame. After connecting the feed line to the distributor inlets, the solution pump was turned on. The pumping parameters stroke length and stroking rate were adjusted if they had already been defined for the experiment. Otherwise, they needed to be determined according to the mass flow specification for the experiment.

The adjustment of the stroke length was critical because a too high stroke length could provoke a spraying of the solution out of the outlets directly into the air stream rather than a trickling of the solution down the distributor surface. Therefore, the stroke length was selected at first and set in such a way that it avoided any spraying of solution for sure. Subsequently, the stroking rate was set accordingly to meet the mass flow requirements for the given pressure drop caused by the individual distributor. The set of pumping parameters also formed part of the name of the experiment. To test the distributor for the same mass flow yet with another set

of pumping parameters, the stroking length was lowered and the stroking rate was increased in accordance.

To analyze exclusively the distribution factor of the outlets or of a distributor without any coating on the surface, the distributor operated with the set mass flow for at least a day before its performance data were measured.

To evaluate a distributor with a flock-coated surface, the stroking rate was increased by a factor of ten to activate the distributor surface. As the high mass flow wetted the surface of the distributor better than the low mass flow, this corresponded to the start-up phase of full-scale equipment. The distributor operated at least one day with the high mass flow before the mass flow was reduced to the previously selected test conditions. Then, the distributor operated at least four hours with the design mass flow before its performance data were measured.

At the start of each experiment, the time was set to 0, the test tubes were uncovered and each flexible tube or fleece ribbon was inserted into the corresponding test tube.

During the experiment, the test tubes slowly filled up with solution. The liquid levels of the test tubes for distributors with a low distribution factor differed greatly while distributors with a high distribution factor filled the test tubes almost equally.

The experiment ended when one glass tubes completely filled up with solution. As the relative amounts of solution in each glass already defined the distribution factor, there was no need for the exact same amount of liquid in the fullest test tube to determine the end point of each experiment. This tube had to be well filled but the exact amount could vary slightly from experiment to experiment. Because of the low specific solution flows, one experiment with a good distributor lasted up to five hours.

Once the first test tube filled up, all fleece ribbons or tubes were withdrawn at the same time and their ends needed to point away from the test tubes because they still spilled solution droplets. The time was documented as end time of the experiment. If a further experiment was planned with the same distributor the solution pump kept running without interruption and the pumping parameters were adjusted if necessary. Otherwise, the pump was turned off.

6.2.3 Data Acquisition

The data acquisition consisted of a precision scale by Sartorius. It measured the individual masses of the empty and the filled test tubes with a precision of $\pm$ 0.1 g leading to a maximum error in the distribution factor of $\pm$ 0.2 percentage points.

After withdrawing the fleece ribbons or flexible tubes from the test tubes, the test tubes were weighed one after another and their masses were fed into the experiment's spreadsheet.

6.2.4 Data Analysis

The data analysis consisted in analytical and graphical evaluation of the experiment. The distribution factor achieved by the distributor under the given operating conditions was the main result of the data analysis.

The evaluation data file generated for the data analysis provided different spreadsheets that listed and evaluated the performance data. It also provided graph templates that plotted the results for each experiment automatically. Special macros in the evaluation data file were programmed to automate the evaluation of the data.

The first spreadsheet listed the masses of the empty test tubes and the assigned operating conditions of the experiment such as mass flow and the pumping parameters stroke length and stroking rate.

The second spreadsheet served for entering the experimental data, i.e. the masses of the filled test tubes, the date, and the start and the end time of the experiment. It calculated the mass of the liquid in each test tube and, for the purpose of revision, the mass flow based on total collected liquid and the duration of the experiment.

The third spreadsheet rearranged the samples masses in ascending order and related the individual masses to the fraction of the total width of the exchange plate. Thus, this spreadsheet listed the masses of the rearranged samples as function of the dimensionless exchange plate width.

The fourth spreadsheet divided the rearranged samples masses by the total mass of the liquid and provided the fraction of liquid that had been collected on the surface as function of the dimensionless exchange plate width. Integrating this function and relating it to the value for the ideal distribution, 0.5, determined the distribution factor of the distributor for the operating conditions, the main result of each experiment.

The evaluation data file also provided two graph spreadsheets that displayed the results for each experiment automatically. The first graph spreadsheet plotted the masses of the liquid in the filled test tubes as function of the sample number. Figure 6.9 shows two examples of this plot. This chart reflected the impression of the filled test tubes and showed the exact position of the outlets with an increased or a diminished solution flow as it plotted the exact experimental data. The example plots clearly show that the mass of the fullest test tube, the one that accounted for the end of the experiment, could vary slightly from experiment to experiment.

Figure 6.10 shows the second graph spreadsheet. It plotted the fraction of liquid that had been collected as function of the dimensionless exchange plate width. This plot was based on the rearranged samples that each represented a section of the exchange plate.

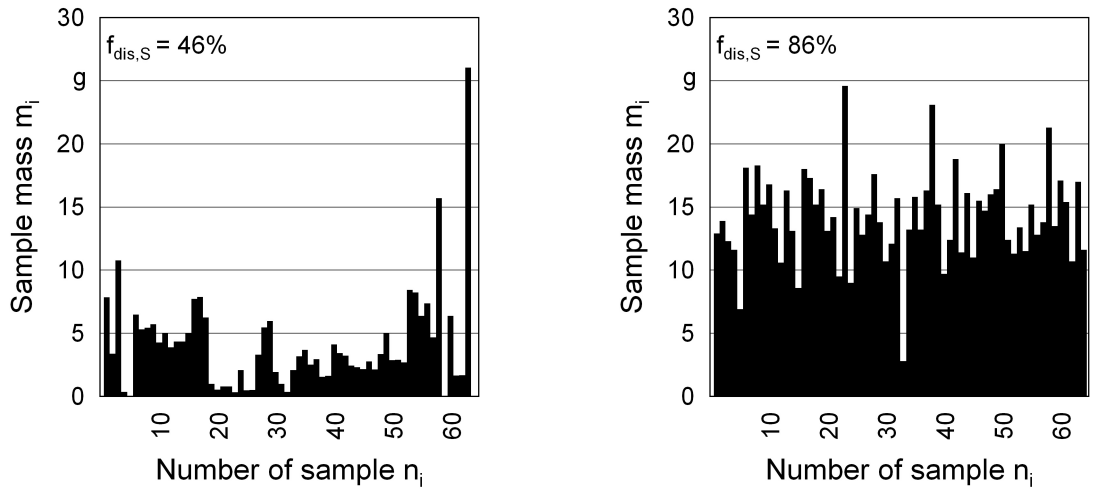

(a) (b)

Figure 6.9: *Example of the graphical evaluation of an experiment: masses of the liquid in the test tubes as function of the sample number (a) $f_{dis,S} = 46\%$ (b) $f_{dis,S} = 86\%$*

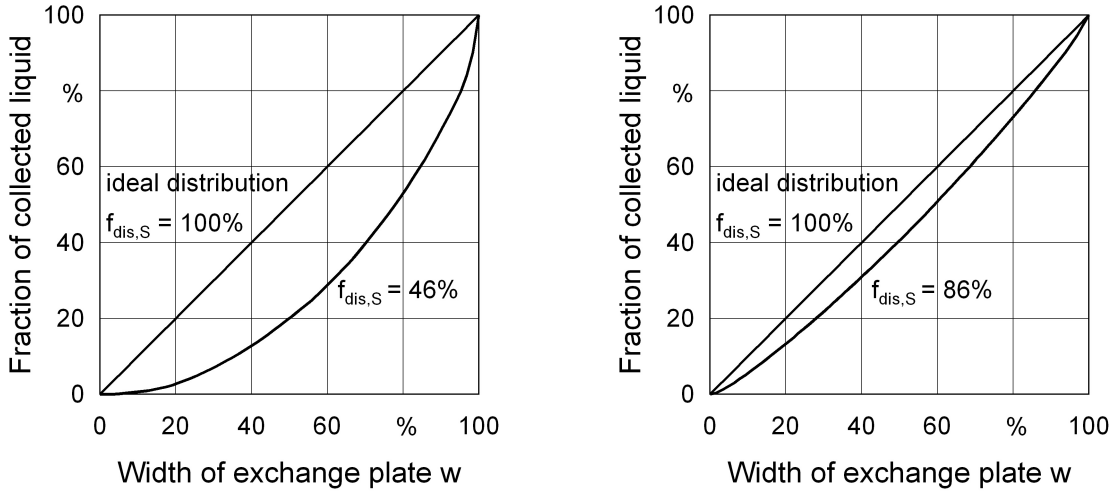

(a) (b)

Figure 6.10: *Example of the graphical evaluation of an experiment: fraction of collected liquid as function of the dimensionless exchange plate width (a) $f_{dis,S} = 46\%$ (b) $f_{dis,S} = 86\%$, for comparison, both graphs also include the line for ideal distribution ($f_{dis,S} = 100\%$)*

6.3 Evaluated Distributors

This section describes in detail the characteristics of the evaluated distributors that met the distribution requirements. Distributors with insufficient performance were tested only qualitatively and this section mentions them only for the sake of completeness but does not discuss them in detail.

Both alternative concepts for distributing the solution evenly, the channel concept and the outlet concept, were manufactured and tested. The evaluated distributors were either separate distribution devices or distribution devices already integrated into the existing heat and mass transfer plates. The separate distributors needed to be connected to the heat and mass transfer plates correctly in order to pass the evenly distributed solution properly to the cooled surface of the heat and mass transfer plates. The distributors integrated into the heat and mass transfer plates required no further connection to the plates.

According to the reference dimensions given in section 3.3.1, the width of the exchange plate w_{pl} was 1 m and therefore the width of a full-scale distributor was also 1 m. Due to material availability, the width of some of the evaluated full-scale distributors was only 0.98 m. Table 6.1 names the manufactured and tested distributors and classifies them according to their distribution concept.

Table 6.1: *Overview of the analyzed distributors*

Distributor Type	**Channel Concept**	**Outlet Concept**
separate distributor	SA, BS	RE1, RE2, RE3
integrated distributor	ML1, ML2	RE4, RE5, RE6, ML4

6.3.1 Distributors with Channel Concept

Separate and integrated distributors with channel concept were tested. The separate distributors had specially designed and dimensioned channels and were either manufactured as prototypes by milling or produced in large series by injection molding.

The distributors integrated into the heat and mass transfer plates had channels predominantly defined by the dimensions of the heat and mass transfer plates. These distributors were produced as prototypes by drilling.

Separate Distributors with Channel Concept

Two separate distributors with channel concept were analyzed: SA and BS. SA was a milled prototype and BS was a distributor fabricated in large quantities by injec-

tion molding. Both distributors applied the bisection concept explained in subsection 6.1.2. Both consisted of a base plate with the channels and the outlets for one side of the distributor and a top cover without channels that provided only the outlets for the other side of the distributor. As SA was just one of the prototypes that led to distributor BS, this subsection discusses only the more sophisticated distributor BS.

Distributor BS Figure 6.11 shows a schematic of the base plate of the distributor BS and also the side view of the distributor with the outlets to both sides.

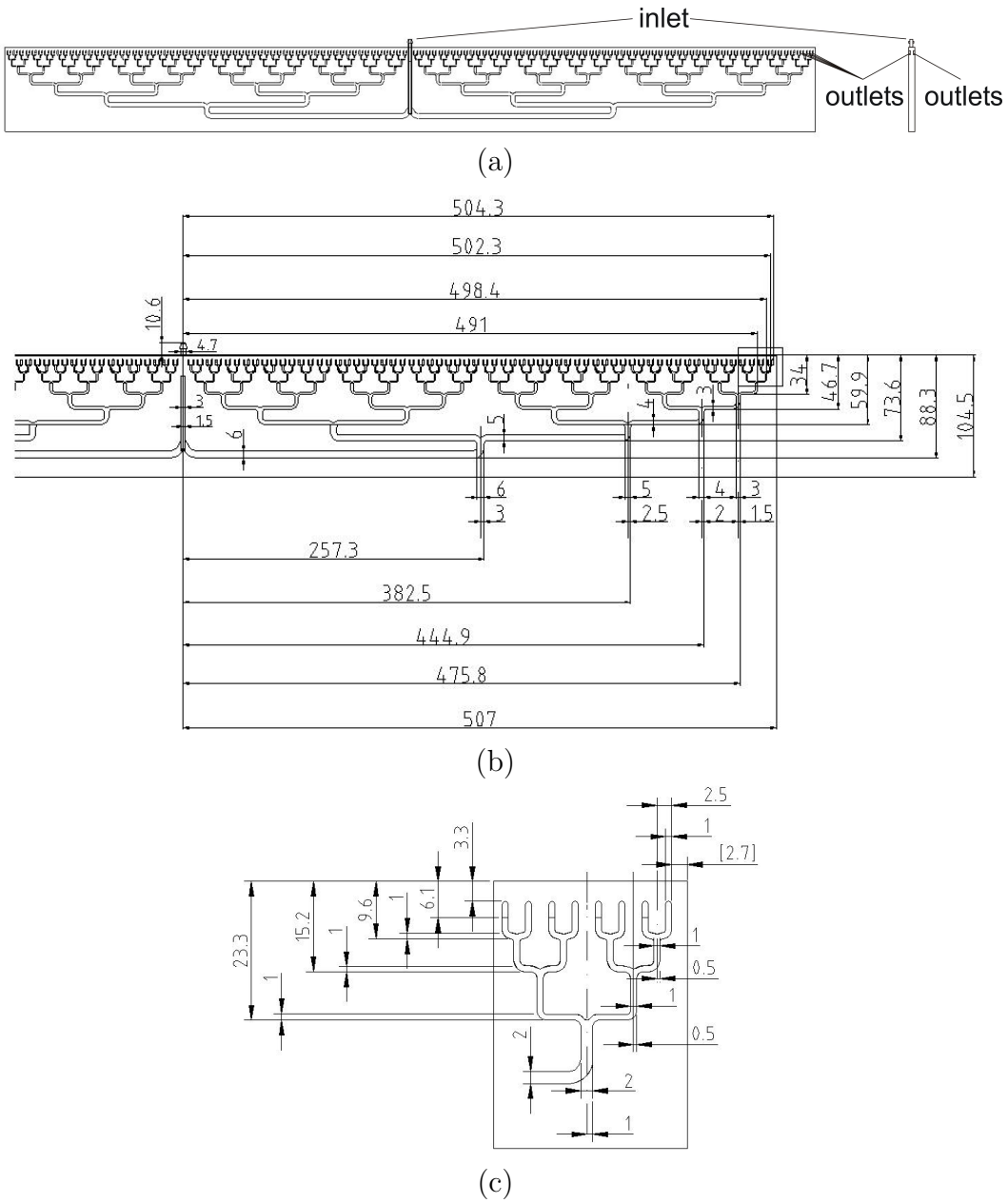

Figure 6.11: *Distributor BS (a) top & side view (b) detail base plate (c) detail outlets, dimensions are given in millimeters*

One inlet in the base plate fed the distributor BS and eight levels of flow division divided the inlet stream into 256 individual flows that fed the 128 outlets on each side of the distributor. As the distributor had a total width of 1 m, the distance between the outlets was approximately 7.8 mm.

In the structured packing of the absorber, both sides of the distributor operate and they both distribute the low specific mass flow rate of 0.29 kg solution per hour, per side and per meter distributor width evenly on the surface. The experimental setup, however, could not evaluate the solution distribution factor of both sides of the distributor at the same time. Therefore, the outlets of the side that was not tested had to be sealed before the other side of the distributor could be evaluated.

The low specific mass flow rate of 0.29 kg/(h m), i.e. $8.2 \cdot 10^{-5}$ kg/(s m), and a cross sectional area of each outlet of 2.5 mm^2 led to a mass flow rate per outlet of 2.3 g/h and a mean exit velocity at the outlets of $2.0 \cdot 10^{-4}$ m/s.

While the number of parallel channels increased with each level of flow division, the dimensions of the channels decreased according to the individual mass flows in each channel. To relate the pressure drop for each path through the distributor to the pressure drop caused by the distributor outlets, both fractions of the total pressure drop of the distributor were calculated for a continuous feeding of the distributor. For the mean mass flow rate of $8.2 \cdot 10^{-5}$ kg/(s m), the pressure drop for each path through the distributor was approximately 0.12 kPa and the pressure drop caused by the distributor outlets was far below 0.1 Pa. A mass flow rate of $4.2 \cdot 10^{-3}$ kg/(s m) corresponded to a continuous feeding with the maximum stroke intensity and led to a calculated pressure drop for each path through the distributor of approximately 7.5 kPa and a pressure drop caused by the distributor outlets of approximately 0.1 Pa. The relation of these values shows the implementation of the channel concept because the pressure drop at the outlets was much lower than the pressure drop inside the distributor. Yet, as the distributor was fed discontinuously, these figures only illustrate the relative importance of the fractions of the total pressure drop and the absolute values are of minor importance.

Integrated Distributors with Channel Concept

Two integrated distributors with channel concept were analyzed: ML1 and ML2. These prototypes were manufactured from the existing flock-coated heat and mass transfer plates with a thickness of 5 mm and both distributors measured 988 mm in width. Figure 6.12 shows the side view of such a plate that has been explained in further detail in subsection 3.3.1. The fibers of the flock-coating measured approximately 0.5 mm in length. Preliminary tests suggested that this flock-coating spread the solution flow from each outlet to a width of approximately 15 mm and therefore the distributors ML1 and ML2 each had 64 outlets.

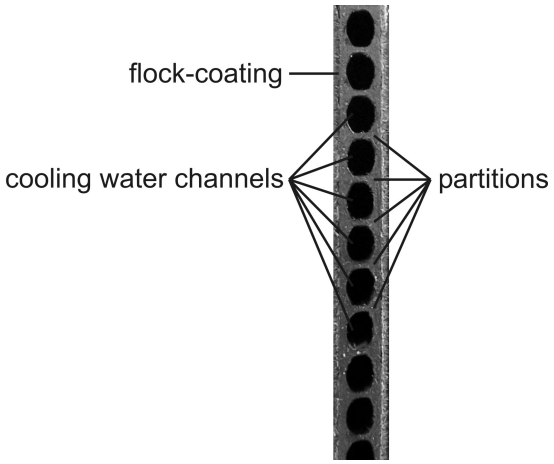

Figure 6.12: *Side view of the heat and mass transfer plate with flock coating*

Horizontal partitions divided the interior of the plates into parallel channels that usually served as cooling water channels for the internal cooling of the plate. For the integration of a distributor into the plates, however, these internal channels provided the horizontal channels of the channel concept. The vertical channels were drilled into the plates from the top of the distributor. To provide the projected flow division, the drills needed to be partially blocked again. The number of flow divisions depended on the number of the required outlets.

Distributor ML1 Distributor ML1 required six horizontal channels as minimum height. The lowest horizontal channel formed the inlet channel with inlets from both ends of the distributor. Between the first and the second horizontal channel, the first flow division took place. A drill in the center of the partition between the first and the second horizontal channel served as a T-piece. As the drilling was done from the top of the distributor, the partitions between the second and the sixth horizontal channel were also drilled. A plug sealed this upper part of the drill and thus prevented the solution from passing directly from the second horizontal channel to the upper horizontal channels. Figure 6.13 shows a schematic drawing of distributor ML1.

The second level of the flow division was accomplished between the second and the third horizontal channel. Two drills in the partitions between the second and the third horizontal channel served as a T-pieces, each in the center of the two stream sections. Again, the drilling was done from the top of the distributor and two plugs sealed the upper parts of these drills in the partitions between the third and the sixth horizontal channel.

The third level of the flow division between the third and fourth horizontal channel and the forth level of the stream partitioning between the fourth and the fifth

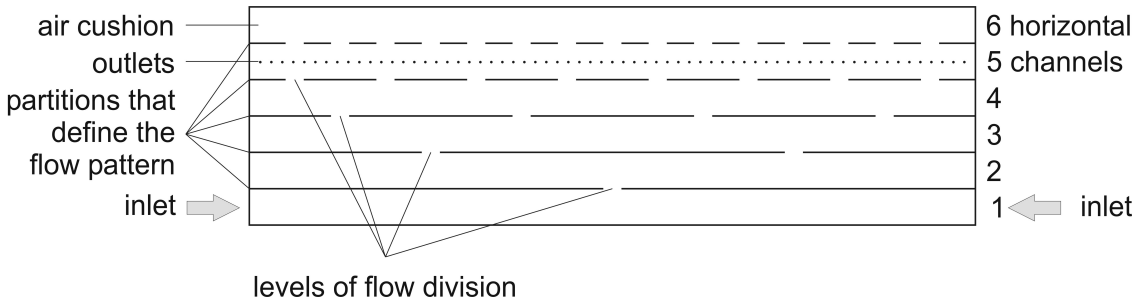

Figure 6.13: *Schematic drawing of distributor ML1*

horizontal channel were accomplished analogously by drilling four, respectively eight, drills in the partitions. The upper sections of the four drills of the third level of the flow division were subsequently plugged.

The distributor abstained from a fifth level of flow division because of the additionally required drills and plugs that would have over-complicated the manufacturing of the distributor. Thus, the solution entered the fifth horizontal channel by eight inlets and fed the 64 outlets in this channel, the therefore also so-called outlet channel.

The sixth horizontal channel was not filled with solution but with air providing an air cushion. The upper section of the eight drills of the fourth level of the flow division remained unplugged and connected the outlet channel with the air cushion. This air cushion lessened the stroking impulse from the pump and prevented the solution from squirting out of the outlets directly into the air stream. Zero carry-over of the solution is one of the crucial requirements for liquid desiccant cooling systems. Thus, the distributor had to ensure a proper trickling of the solution along the heat and mass transfer plates and had to avoid any spraying or squirting of the solution into the air stream.

In addition to the six horizontal channels that the distributor ML1 required as minimum height, two further horizontal channels below the distributor were not used for the cooling water circulation. Thus, the overall height of the distributor corresponded to the height of eight horizontal channels, i.e. 48 mm in the case of the existing flock-coated heat and mass transfer plates.

The additional horizontal channels below the distributor provided a security barrier between the solution and the cooling water. If a drill damaged the lower part of the inlet channel due to improper drilling, the heat and mass transfer plate could still be used. In this case, the channel below the inlet channel filled with solution as well and then remained inactive. Without this security barrier, an improper drilling of the central drill of the distributor would inevitably disable the heat and mass transfer plate. Yet, this consideration was only of importance for the prototype production

with limited resources. Under real production conditions, the security barrier could be diminished to one horizontal channel or even be omitted. This would reduce the total height of the distributor from 48 mm to 42 mm or even 36 mm.

The flock-coating of the heat and mass transfer plates allowed a distance between the outlets of 15 mm and therefore distributor ML1 had 64 outlets. The distance between the left-most outlet and the left border of the distributor was 21.5 mm and between the right-most outlet and the right border was also 21.5 mm. The diameter of the outlets of 1 mm led to a mass flow per outlet of 4.5 g/h and a mean exit velocity at the outlets of $1.3 \cdot 10^{-3}$ m/s.

Testing the distributor ML1, see subsection 6.4.1, showed that both ends of the distributor were favored in terms of liquid distribution. As the solution had to make up to three U-turns to reach the middle of the distributor and only one U-turn to reach the ends of the distributor, the inertia of the solution favored the ends of the distributor. Distributor ML2 avoided this problematic flow pattern.

Distributor ML2 The design of distributor ML2 was based on the geometry of distributor ML1 but it improved the flow pattern of the solution. Figure 6.14 shows the schematic diagram of distributor ML2 that extended the dimensions of the flow divisions. An additional channel before the stream partitioning aligned the streams vertically and thus the U-turns were divided into two 90°-bends.

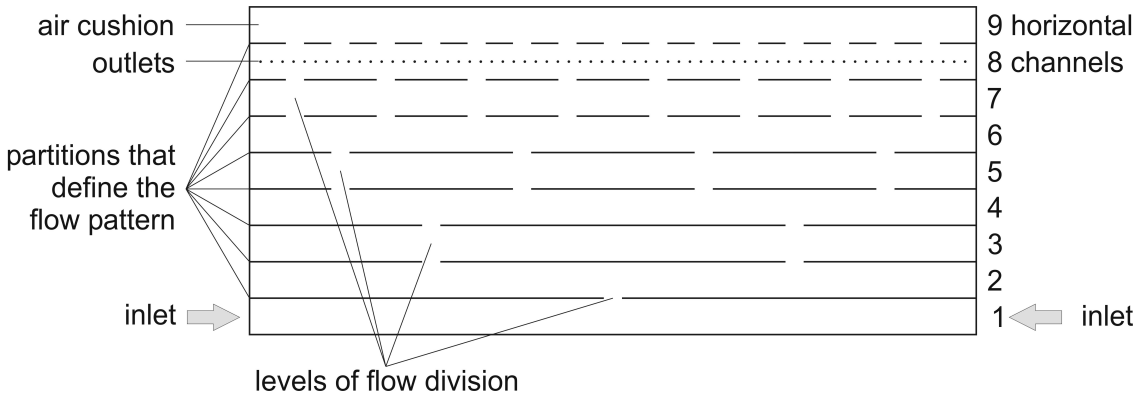

Figure 6.14: *Schematic drawing of distributors ML2a and ML2b*

Analogously to distributor ML1, distributor ML2 also possessed four levels of the flow division. The additional channel before the second, third, and fourth level of flow division led to a minimum height of the distributor ML2 of nine horizontal channels. Due to the geometry of the first level of flow division, this level of flow division did not require an additional channel to align the flows vertically.

The ninth and therefore upper horizontal channel also provided an air cushion to lessen the stroking impulses from the pump and to prevent the solution from squirting directly into the air stream.

Two additional horizontal channels below distributor ML2 without cooling water circulation served as security barrier between the solution and the cooling water. Thus, the overall height of the distributor ML2 corresponded to the height of eleven horizontal channels, i.e. 66 mm in the case of the existing flock-coated heat and mass transfer plates. Again, under real production conditions this height could be reduced to 60 mm or even 54 mm by diminishing the security barrier to only one horizontal channel or omitting even both security horizontal channels.

Four versions of distributor ML2 existed: ML2a, ML2b, ML2c, and ML2d. They differed in diameter and position of the outlets in the horizontal channel, see Table 6.2. Figure 6.15 shows the position of the outlets for the distributors ML2c and ML2d.

Table 6.2: *Versions of distributor ML2*

Distributor Version	**Diameter of the Outlets**	**Vertical Position of the Outlets**
ML2a	1 mm	center of the horizontal channel
ML2b	1.5 mm	center of the horizontal channel
ML2c	0.55 mm	top of the horizontal channel
ML2d	1 mm	top of the horizontal channel

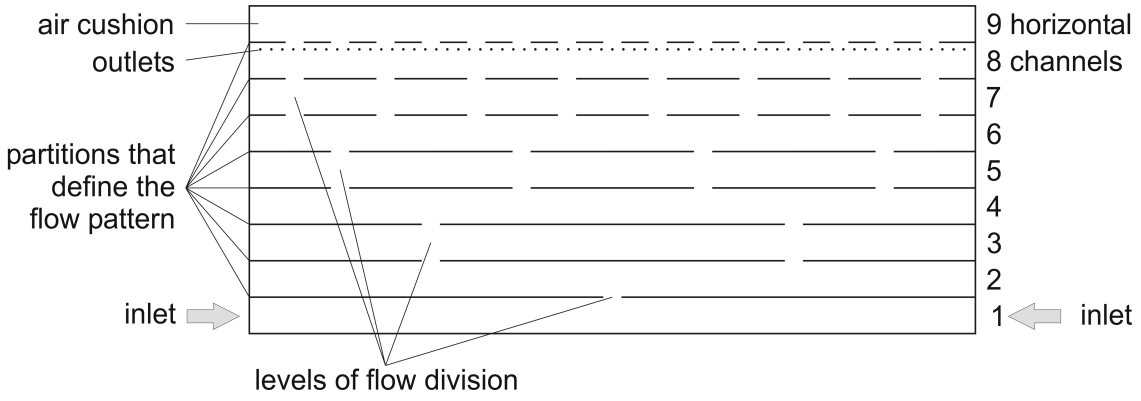

Figure 6.15: *Schematic drawing of distributors ML2c and ML2d*

The 64 outlets of distributor ML2 were located at a distance between the outlets of 15 mm and for the design mass flow rate of $8.2 \cdot 10^{-5}$ kg/(s m), the mass flow per outlet was 4.5 g/h. Again, the distance between the left-most outlet and the left border of the distributor was 21.5 mm and between the right-most outlet and the right border was also 21.5 mm.

The diameter of the outlets of 1 mm of the distributor versions ML2a and ML2d led to a mean exit velocity at the outlets of $1.3 \cdot 10^{-3}$ m/s. The larger diameter of the outlets of 1.5 mm of the distributor version ML2b decreased the mean exit velocity at the outlets to $5.7 \cdot 10^{-4}$ m/s and the smaller diameter of the outlets of 0.55 mm of the distributor version ML2c increased the mean exit velocity at the outlets to $4.2 \cdot 10^{-3}$ m/s.

6.3.2 Distributors with Outlet Concept

Separate and integrated distributors with outlet concept were tested. The separate distributors were designed as prototypes for preliminary studies of the outlet concept. They were based on the results of a previous research project [Lävemann *et al.* 1996] that applied microporous flexible tubes as separate distributions devices with outlet concept.

The design of the distributors with outlet concept that were integrated into the heat and mass transfer plates was also predominantly defined by the dimensions of the heat and mass transfer plates, yet the feeding of the outlets varied as well as their position and diameter. These integrated distributors were also produced as prototypes by drilling.

Separate Distributors with Outlet Concept

Three separate distributors with outlet concept were analyzed: RE1, RE2, and RE3. They were all milled and drilled prototypes consisting of a back plate and top cover. The back plate was milled in such a way that it provided an inner trough that filled with solution before the solution reached the outlets. As the connection between separate distributors and the heat and mass transfer plates proved to be difficult, those prototypes served only for preliminary studies on the outlet dimensions. They were not intended to be connected to the heat and mass transfer plates. Therefore, the outer dimensions did not have to be on par with the thickness of the given heat and mass transfer plates. The thickness of back plate and top cover added up to 6 mm and the inner trough of the distributors had a thickness of 2 to 3 mm.

Distributor RE1 Distributor RE1 was a prototype of 500 mm width. Figure 6.16 shows a schematic of this distributor that consisted of a PVC back plate and an acrylic glass top cover. This transparent cover allowed to see the solution flow inside the distributor.

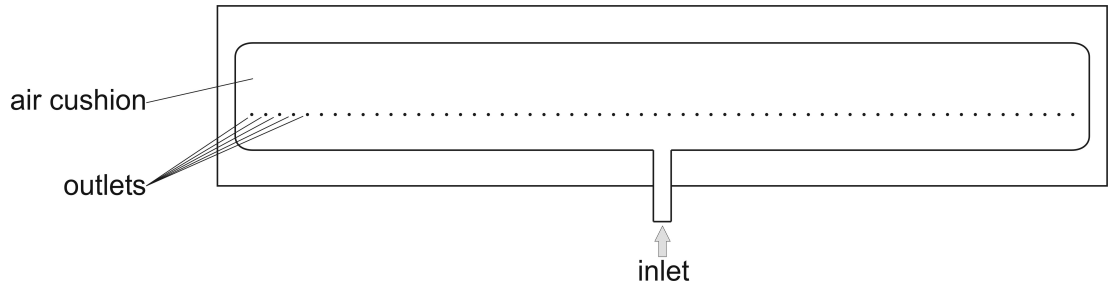

Figure 6.16: *Schematic drawing of distributor RE1*

The inner trough of the distributor had a thickness of 2 mm and a height of 60 mm. One inlet located at the bottom end in the center fed the distributor. 60 outlets were located at a distance of 20 mm from the bottom of the trough. They had a diameter of 1 mm and were located equidistantly with a distance of 7.8 mm. This distance corresponded to the distance of the outlets of the separate distributor with channel concept BS. For the design mass flow, the mass flow per outlet was 2.4 g/h and the mean exit speed at the outlets was $6.8 \cdot 10^{-4}$ m/s. The air cushion above the outlets of the distributor measured approximately 480 mm in width, 40 mm in height, and 2 mm in thickness.

Distributor RE2 Distributor RE2 was a full-scale prototype of 1000 mm width. It was based on the main design features of distributor RE1 and also consisted of a PVC back plate and an acrylic glass top cover. Figure 6.17a illustrates this distributor in a schematic. Figure 6.17b shows a picture of the back plate this distributor and Figure 6.17 pictures a detail of the distributor with its acrylic glass top cover.

Diameter and distance of the 127 outlets were the same as for RE1. A 128th outlet could not be drilled because this distributor design required a frame around the trough for assembling back plate and top cover. The height of the inner trough was kept while the thickness of the inner trough was increased to 3 mm. This dimension corresponded to the diameter of the cooling water channels in the given heat and mass transfer plates. For the design mass flow, the mass flow per outlet was 2.3 g/h and the mean exit speed at the outlets was $6.4 \cdot 10^{-4}$ m/s. The height of the air cushion above the outlets was reduced to only 13 mm to see whether a reduction of this attenuation effected the performance of the distributor. The height of 13 mm corresponded to the height of two horizontal channels in the existing heat and mass transfer plates.

One inlet located at the bottom end in the center fed the distributor. Yet, distributor RE2 combined the outlet concept with the bisection concept. Before entering the inner trough of the distributor, the solution was divided into four flows by two levels of the flow division.

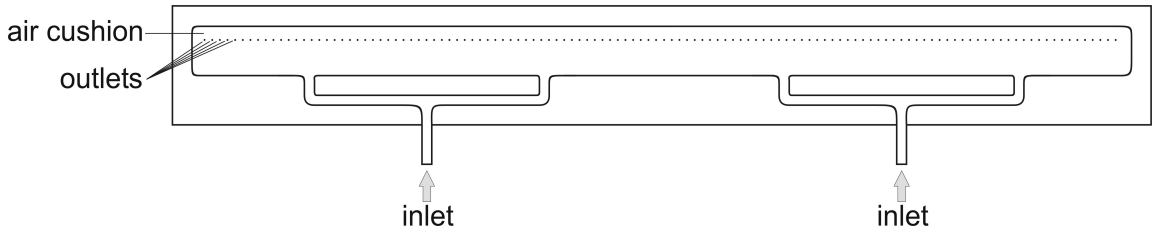

(a)

(b)

(c)

Figure 6.17: *Distributor RE2 (a) schematic (b) picture of the back plate (c) picture of one inlet section of the distributor with top cover*

Distributor RE3 Distributor RE3 was also a full-scale prototype of 1000 mm width that was based on the main design features of distributor RE2. It consisted of a back plate and a top cover both made of acrylic glass. The height of the air cushion above the outlets, the thickness of the inner trough, and diameter and distance of the 127 outlets were the same as for distributor RE2. Therefore, design mass flow per outlet and mean exit speed at the outlets were also the same as for distributor RE2. Figure 6.18 shows that the distributor RE3 possessed three levels of the flow division. Before entering the inner trough of the distributor, the solution was divided into eight flows.

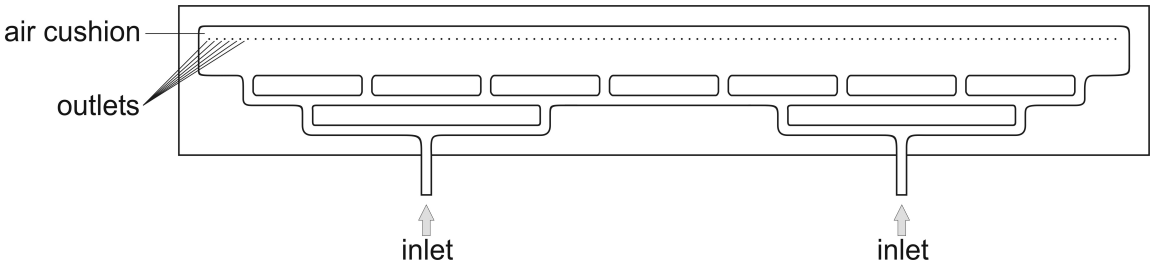

Figure 6.18: *Schematic drawing of distributor RE3*

Integrated Distributors with Outlet Concept

Based on the results of the preliminary studies on the outlet concept, four distributors with outlet concept integrated into the heat and mass transfer plates were analyzed: RE4, RE5, RE6 and ML4. Base material for distributors were the existing heat and mass transfer plates both with and without flock-coating on the surface. They were produced as prototypes mainly by drilling.

Distributor RE4 Distributor RE4 was a prototype of 460 mm width. Base material of the distributor was one of the existing heat and mass transfer plates with flock-coating. Two inlets on both sides of the bottom end fed the distributor. The partitions that defined the individual horizontal channels were almost completely removed to form the inner trough of this distributor. Only the outer 20 mm of the partitions remained on each side to stabilize the distributor. The inner trough had the dimensions of 7 horizontal channels, i.e. approximately 420 mm in width, 42 mm in height, and 3 mm in thickness. The outlets were drilled into the sixth horizontal channel and the seventh horizontal channel provided the air cushion with a height of 5 mm. Figure 6.19 shows that the distributor RE4 had no level of flow division and analogously to distributor RE1 the solution flowed directly into the trough.

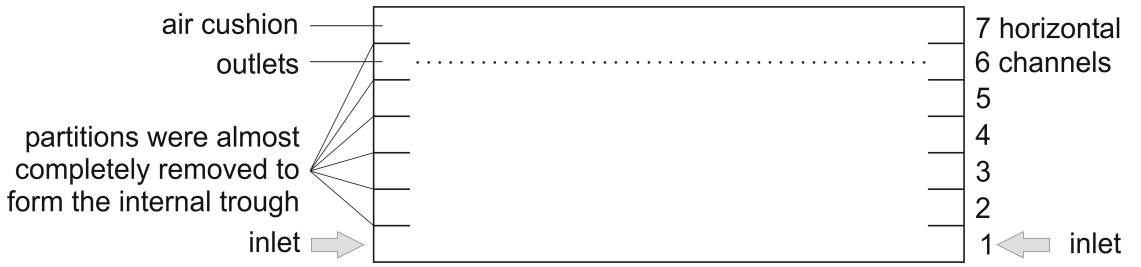

Figure 6.19: *Schematic drawing of distributor RE4*

As the distributors RE1-RE3, the 54 outlets of this distributor also had a diameter of 1 mm and a distance of 7.8 mm. The design mass flow per outlet was 2.6 g/h and the mean exit speed at the outlets was $6.9 \cdot 10^{-4}$ m/s. The flock-coating remained on the complete surface of the distributor.

The evaluation of distributor RE4 brought forward two problems. Keeping the flock-coating around the outlets enabled the flock fibers to suck the solution directly from the outlets instead of only passing on the solution that has exited the outlets. This led to different mass flows per outlet. Removing the partitions completely to get the inner trough of the distributor RE4 resulted in a lack of stability. Distributor RE5 avoided both problems, the flock-coating was removed from the outlets and the internal partitions of distributor RE5 were only partially removed.

Distributor RE5 Distributor RE5 was a prototype of 490 mm width. To form the inner trough of the distributor RE5, the partitions were only partially removed by drilling 7 drills from the top of the distributor to connected the horizontal channels. Figure 6.20 shows a schematic of distributor RE5.

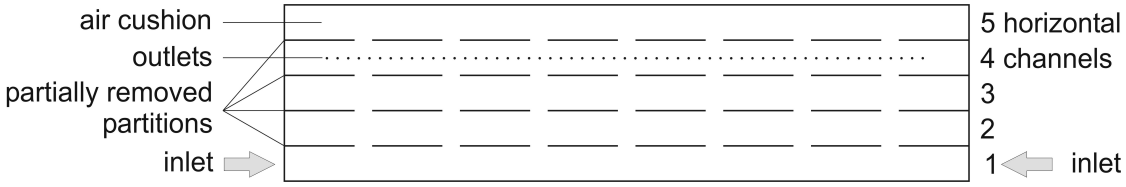

Figure 6.20: *Schematic drawing of distributor RE5*

The diameter of the drills was 3 mm and their distance was 60 mm. The distance between the left-most drill and the left border of the distributors was 65 mm and between the right-most drill was also 65 mm. The drills connected the upper five horizontal channels. After the drilling from the top end of the distributor, this top end was sealed again. Though the partial removing of the partitions did not provide a real trough, this geometry of connected horizontal channels is referred to as the inner trough of the distributor. The inner trough of distributor RE5 had the dimensions of approximately 470 mm in width, 29 mm in height, and 3 mm in thickness including the air cushion of a height of 5 mm. Distributor RE5 also had no level of flow division and the solution flowed directly into the inner trough.

The diameter of 1 mm and the distance of 7.8 mm of the 61 outlets were the same as for distributors RE1-RE4. The design mass flow per outlet was 2.3 g/h and the mean exit speed at the outlets was $6.5 \cdot 10^{-4}$ m/s.

To prevent the flock-coating from sucking the solution directly from the outlets, the flock-coating on the plate was removed from the upper 14 mm of this distributor. Therefore, different flock structures around the outlets did not lead to differences between the mass flows exiting the outlets. Individual droplets of solution exited the outlets and subsequently the flock-coating passed them on, providing a solution film on the surface.

Distributor RE6 Distributor RE6 was an almost full-scale prototype of 980 mm width that was based on the design of distributor RE5. 13 drills of diameter of 3 mm and a distance of 49 mm connected the upper five horizontal channels. The distances between the left-most drill and the left border of the distributors and the right-most drill and the right border of the distributor were also 49 mm. Analogously to distributor RE5, the top end of the distributor was sealed again after the drilling. The inner trough of distributor RE6 had the dimensions of approximately 970 mm, 29 mm, and 3 mm including the air cushion of a height of 5 mm. Distributor RE6 also had no level of flow division.

The diameter of the 118 outlets was 1 mm, the same as for distributors RE1-RE5. Their distance slightly increased to 8.2 mm. The design mass flow per outlet was 2.4 g/h and the mean exit speed at the outlets was $6.8 \cdot 10^{-4}$ m/s. Again, the flock-coating on the plate was removed from the upper 14 mm of this distributor.

As the three outer outlets at both sides of the distributor were located too close to a main drill, they tended to spray solution into the air stream due to kinetic effects. Therefore, they were sealed and only 112 outlets remained active during the tests.

Distributor ML4 Distributor ML4 was also an almost full-scale prototype of 980 mm width. It is based on the design of distributor RE6 and the results from the evaluation of distributor ML2. 16 drills from the top of the distributor connected the individual horizontal channels. The diameter of the drills was 3.2 mm and their mean distance was 58 mm. The inner trough of distributor ML4 had a width of approximately 970 mm and a thickness of 3 mm.

Three versions of distributor ML4 existed: ML4a, ML4b and ML4c. They differed in the number of horizontal channels connected by the drills, see Table 6.3. Figure 6.21 shows schematics of the three versions of distributor ML4.

Table 6.3: *Versions of distributor ML4*

Distributor Type	Connected Horizontal Channels	Height of the Inner Trough
ML4a	3	17 mm
ML4b	4	23 mm
ML4c	6	35 mm

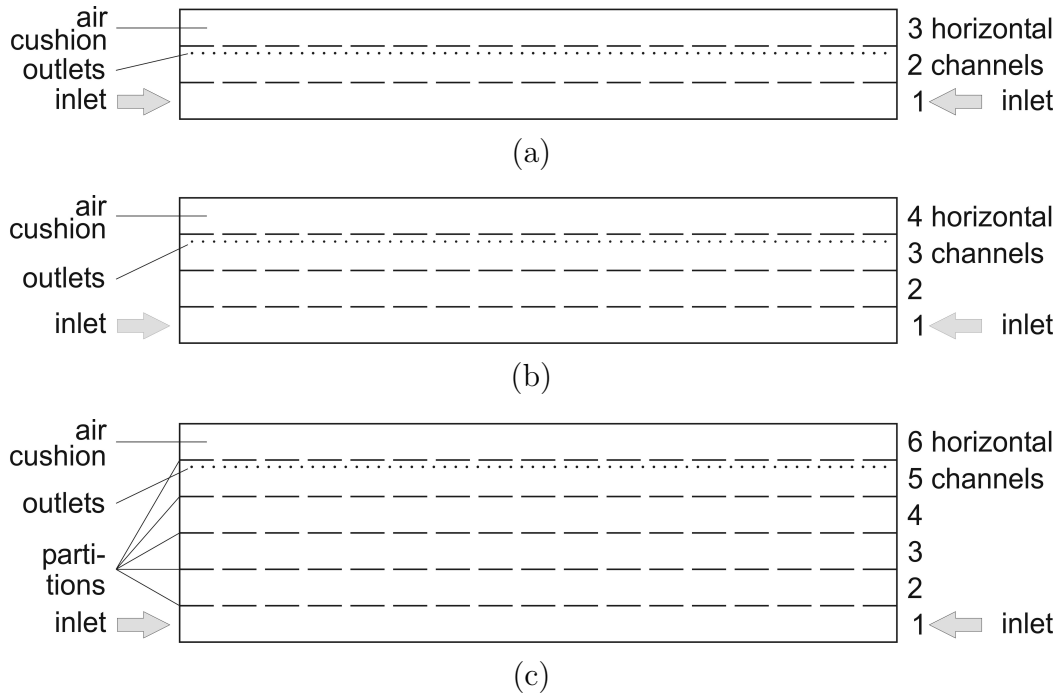

Figure 6.21: *Schematic drawing of distributor ML4 (a) ML4a (b) ML4b (c) ML4c*

The top horizontal channel of the internal trough provided the air cushion of a height of 5 mm. Distributor ML4 also had no level of stream partitioning and the solution flowed directly into the inner trough. As the distributors ML1 and ML2, distributor ML4 possesses 64 outlets located at a distance of 15 mm.

The diameter of the outlets was reduced to 0.55 mm, the outlet diameter of distributor ML2b that showed the best performance concerning the integrated distributors with channel concept, see subsection 6.4.1. This smaller diameter of the outlets led to a mean exit speed at the outlets of $4.2 \cdot 10^{-3}$ m/s. As for all ML distributors, the flock-coating on the plate was completely removed.

6.4 Results of the Distributor Evaluation

This section describes in detail the results of the quantitative distributor analysis and presents the experimental data of selected test runs graphically.

Distributors that obviously showed an insufficient performance were tested only qualitatively and no distribution factor was determined. Table 6.4 summarizes the analyzed distributors. An italic print of the distributor name indicates that the distributor had been analyzed only qualitatively. A bold print of the distributor name indicates that the distributor had been evaluated quantitatively.

Table 6.4: *Overview of the distributor analysis*

Distributor Type	**Channel Concept**	**Outlet Concept**
separate distributor	**SA**, **BS**	*RE1*, **RE2**, *RE3*
integrated distributor	**ML1**,**ML2**	*RE4*, *RE5*, **RE6**, **ML4**

The distributors with the flock-coating of the surface, i.e. SA, BS, RE2, and RE6, were analyzed with the liquid separator with fleece ribbons. The distributors without the flock-coating, i.e. ML1, ML2, and ML4, were tested with the liquid separator with flexible tubes. As the liquid separator with flexible tubes could be positioned horizontally at any height of the distributor and could collect the liquid directly from the outlets, the experiments with ML1, ML2, and ML4 directly analyzed the distribution factor of the outlets.

6.4.1 Distributors with Channel Concept

Separate Distributors with Channel Concept

The evaluation of the available distributors with channel concept SA and BS focused on varying the operating conditions and identifying the optimal operating conditions. Distributor geometry, outlet geometry or coating of the existing distributors were not altered for these tests.

Distributor SA As distributor SA had been evaluated in an earlier research project and the results led to the improved concept of the distributor BS, the evaluation of distributor SA in this research was mainly for testing the experimental setup. The distribution factors measured with distributor SA ranged between 65% and 69%, far below the required distribution factor of 85%. For two test runs, Figure 6.22 plots the relative filling levels of the test tubes as function of the sample number.

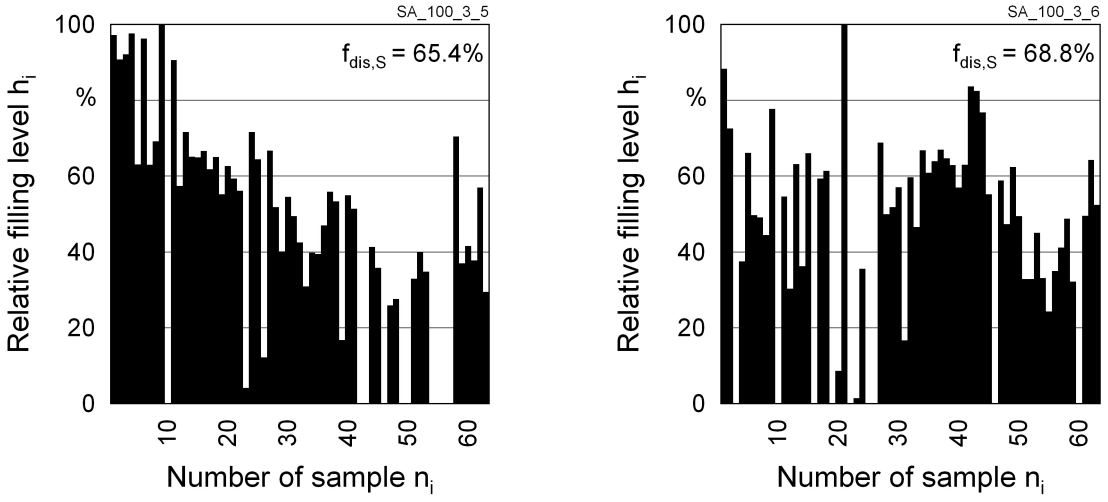

(a) (b)

Figure 6.22: *Performance of distributor SA: relative filling levels of the test tubes for two test runs (a) SA_100_3_5 (b) SA_100_3_6*

Distributor BS Distributor BS had not been evaluated quantitatively to such a detailed level in any earlier research program. This research carried out 44 experiments with a number of the available distributors of type BS. Due to the flock-coating of the surface of the BS-distributors, the liquid separator with fleece ribbons was applied. Therefore, each experiment could analyze two BS-distributors at the same time, one in the mounting position A and the other in the mounting position B of the experimental set-up.

The main objectives of the experiments were:

- evaluation and comparison of the performance of base plate and top cover of distributor BS
- variation of the operating conditions to identify the best operating conditions
- variation of the distributor mounting and alignment to identify the allowable tolerances for the distributor mounting
- evaluation of a number of distributors of the same type fabricated in large quantities to compare their solution distribution factors

Performance of base plate and the top cover of distributor BS

The distributor type BS consisted of a base plate and a top cover both produced by injection molding that were glued together to form the distributor BS. As both elements provided outlets and subsequently desiccant solution for both sides of the plate, an important first test series quantified the performance of base plate and top

cover of distributor BS and their possible performance differences for given operating conditions, i.e. the same pumping parameters stroke length and stroking rate. Table 6.5 lists the experimental data.

Table 6.5: *Performance of base plate and the top cover of distributor BS, pump: Gamma/5, stroke length: 70%, stroking rate: 3/min*

Experiment No.	**Specific Mass Flow** kg/(h m)	**Part**	**Exp. Position**	**Distribution Factor** $f_{dis,S}$ %
BS_BP_70_3_1_A	0.28	base plate	A	80.7
BS_BP_70_3_2_A	0.28	base plate	A	82.7
BS_BP_70_3_1_B	0.28	base plate	B	73.9
BS_BP_70_3_2_B	0.28	base plate	B	72.5
BS_TC_70_3_1_A	0.27	top cover	A	68.5
BS_TC_70_3_2_A	0.27	top cover	A	72.9
BS_TC_70_3_1_B	0.27	top cover	B	78.5
BS_TC_70_3_2_B	0.27	top cover	B	81.1

The distribution factor for the base plate varied between 73% and 82% and the one for the top cover varied between 71% and 80%. Thus, the performance of the top covers was a little lower than the performance of the base plates. One reason for this was the fact that the outlets of the top cover did not always perfectly overlap with the ends of the channels provided by the base plate. Some outlets overlapped only partially with the channels provided by the base plate or they even did not coincide with the end of a channel at all. Figure 6.23 shows that for one top cover, the test tubes with sample numbers around 50 collected significantly less liquid. In the center of the distributor, top cover outlets and base plate channels always overlapped perfectly because both elements were aligned in the center and glued together from the center outwards.

Again, the measured solution distribution factors were all below the required distribution factor of 85%. Further analysis was required to find the best operating conditions and a promising approach was to evaluate the influence of the pumping parameters.

Variation of the operating conditions to identify the best operating conditions

The low specific solution mass flow of $\dot{v}_S \approx 2.3{\cdot}10^{-4}$ m^3/(h m) was crucial for reaching a high energy storage density. The pumping parameters stroke length and stroking rate defined the mass flow. To identify the best operating conditions, the pumping parameters stroke length and stroking rate were varied in one experimental series. This experimental series evaluated the influence of the pumping parameters on the performance of the top cover for three sets of stroke length and stroking rate.

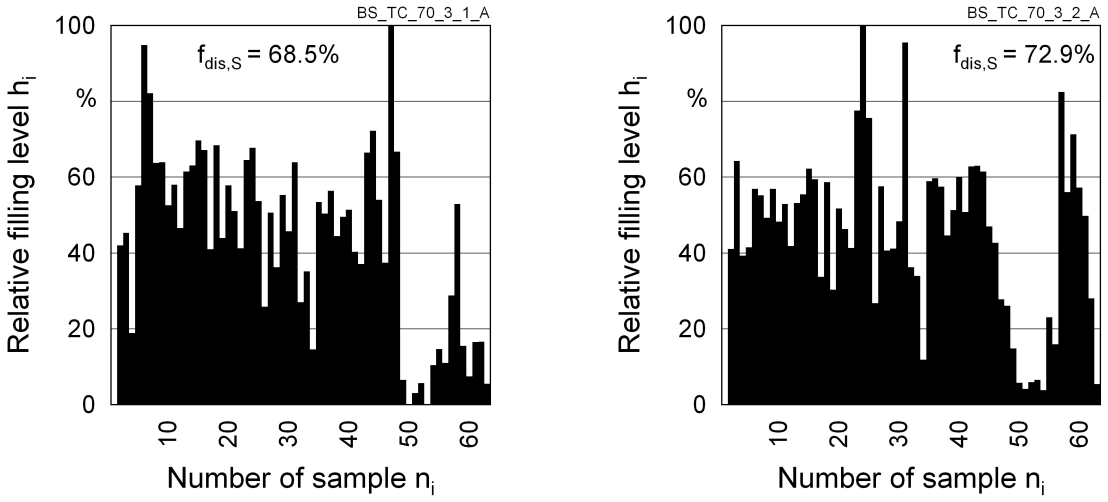

Figure 6.23: *Performance of the top cover of distributor BS: relative filling levels of the test tubes for two test runs (a) BS_TC_70_3_1_A (b) BS_TC_70_3_2_A*

To evaluate the best combination of the pumping parameters stroke length and stroking rate, the stroking rates were fixed to two, three and four strokes per minute and the stroke length was adjusted according the design mass flow, leading to stroke lengths of 100%, 70% and 40%.

As zero carry-over of the solution is one of the crucial requirements for liquid desiccant cooling systems, the stroke length was adjusted in such a way that any squirting or spraying of solution directly into the air stream was definitely avoided. Up to a stroke length of 100%, distributor BS did not spray any solution directly into the air stream but trickled it on the surface.

The experimental mass flows did not always meet the design mass flow because the stroking rate could only be varied in integers. As the analysis aimed at proving influences and dependencies rather than identifying exact distribution factors, the parameters leading to the mass flow closest to the design mass flow were selected for each experiment. Table 6.6 lists the experimental data.

The distribution factor for the top cover varied between 67% and 77% for a stroke length of 100%, and between 71% and 80% for a stroke length of 70%. This suggested that a shorter stroke length and a higher stroking rate led to a better distribution factor. For a stroke length of 40%, the distribution factor for the top cover varied between 78% and 87%. This agreed with the assumption that a shorter stroke length and a higher stroking rate led to a better distribution factor. A further increase of the stroking rate to five strokes per minute and simultaneous shortening the stroke length accordingly could not be tested because a stroke length below 30% was not recommended for the utilized solution pump.

Table 6.6: *Performance of the top cover of distributor BS with different sets of pumping parameters, pump: Gamma/5*

Experiment No.	**Specific Mass Flow** kg/(h m)	**Stroke Length** %	**Stroking Rate** 1/min	**Exp. Position**	**Distribution Factor** $f_{dis,S}$ %
BS_TC_100_2_1_A	0.24	100	2	A	64.3
BS_TC_100_2_2_A	0.24	100	2	A	70.4
BS_TC_100_2_1_B	0.24	100	2	B	74.3
BS_TC_100_2_2_B	0.24	100	2	B	79.8
BS_TC_70_3_1_A	0.27	70	3	A	68.5
BS_TC_70_3_2_A	0.27	70	3	A	72.9
BS_TC_70_3_1_B	0.27	70	3	B	78.5
BS_TC_70_3_2_B	0.27	70	3	B	81.1
BS_TC_40_4_1_A	0.26	40	4	A	77.4
BS_TC_40_4_2_A	0.26	40	4	A	77.7
BS_TC_40_4_1_B	0.26	40	4	B	87.7
BS_TC_40_4_2_B	0.26	40	4	B	86.9

Again, these solution distribution factors were almost all below the required one of 85%. For solution distribution factors below 77% and a simultaneous maldistribution of the air flow, the air dehumidification requirements for the LDCS can not be met any more, see subsection 5.2.4. Only the experiments with a stroke length of 40% led to a distribution factor above 85%. Thus, distributor BS could meet the requirement for the solution distribution factor but only for very specific operating conditions. Figure 6.24 plots the experimental data of the two best test runs.

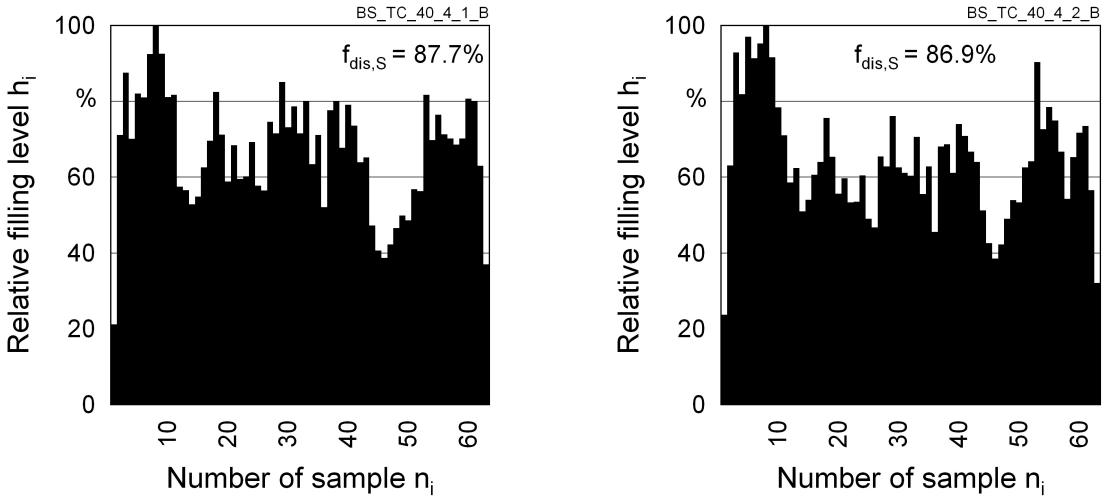

(a) (b)

Figure 6.24: *Performance of the top cover of distributor BS: relative filling levels of the test tubes for two test runs (a) BS_TC_40_4_1_B (b) BS_TC_40_4_2_B*

Variation of the mounting and the alignment of parallel distributors in a structured packing to identify their influence on the performance of the individual distributor

The previous experiments proved that the individual distributor BS met the requirements for the solution distribution factor only under very specific operating conditions. But even if the operating conditions met the specifications, the performance of an individual distributor within the structured packing of the absorber might not meet the requirements for the solution distribution factor. Improper mounting of the parallel heat and mass transfer plates that form for the structured packing of absorber can have a negative impact on the solution distribution factor. Also, the parallel distributors all need to be fed with the same specific solution mass flow. The following distributor mounting and alignment conditions had been varied to identify their influence on the performance of the individual distributor in the structured packing of parallel distributors in the absorber:

- poor matching of the distributors' feed lines and therefore a too low specific solution mass flow in some of the distributors
- poor horizontal alignment of the packing and therefore a slight slope
- poor alignment of neighboring distributors and therefore a slight difference in their vertical position

Under certain boundary conditions, such as poor matching of the distributors' feed lines and therefore different pressure drops in the feed lines of the distributors, the inlet solution flow into one distributor can be lower than the inlet solution flow into another distributor. Therefore, it was important to evaluate the influence of the specific solution mass flow on the solution distribution factor of the distributor BS.

Two experimental series compared the performance of both base plate and the top cover for two specific solution mass flows. The selected specific solution mass flows were the design mass flow of 0.29 kg/(h m) and half the design mass flow.

Again, the experimental mass flows did not always meet the specified mass flows because the stroking rate could only be varied in integers. As the analysis aims at getting an idea of the influences and dependencies rather than identifying exact distribution factors, again the parameters leading to the mass flow closest to the design mass flow were selected for each experiment. Tables 6.7 and 6.8 list the experimental data.

The distribution factor for the base plate varied between 59% and 72% for the design mass flow and between 54% and 60% for half the design mass flow. The decrease of the mass flow led to a decrease of the distribution factor of 5 to 12 percentage points.

Table 6.7: *Performance of the base plate of distributor BS with different mass flows, pump: Gamma/4, stroke length: 100%, stroking rates: 4/min and 2/min*

Experiment No.	**Specific Mass Flow** kg/(h m)	**Exp. Position**	**Distribution Factor** $f_{dis,S}$ %
BS_BP_100_4_1_A	0.23	A	59.4
BS_BP_100_4_2_A	0.23	A	58.5
BS_BP_100_4_1_B	0.23	B	74.7
BS_BP_100_4_2_B	0.23	B	68.3
BS_BP_100_2_1_A	0.12	A	56.5
BS_BP_100_2_2_A	0.12	A	52.1
BS_BP_100_2_1_B	0.12	B	60.3
BS_BP_100_2_2_B	0.12	B	60.5

Table 6.8: *Performance of the top cover of distributor BS with different mass flows, pump: Gamma/5, stroke length: 70%, stroking rates: 2/min and 1/min*

Experiment No.	**Specific Mass Flow** kg/(h m)	**Exp. Position**	**Distribution Factor** $f_{dis,S}$ %
BS_TC_70_2_1_A	0.25	A	57.8
BS_TC_70_2_2_A	0.25	A	58.9
BS_TC_70_2_1_B	0.25	B	56.3
BS_TC_70_2_2_B	0.25	B	55.8
BS_TC_70_1_1_A	0.13	A	57.8
BS_TC_70_1_2_A	0.13	A	57.7
BS_TC_70_1_1_B	0.13	B	46.3
BS_TC_70_1_2_B	0.13	B	45.8

The distribution factor for the top cover varied between 56% and 58% for the design mass flow and between 46% and 58% for half the design mass flow. This also proved that a lower specific solution mass flow lowers the distribution factor. The reduced mass flow in this test lowered the distribution factor up to 10 percentage points.

The experimental data clearly pointed out that the proper matching of the distributors' feed lines is crucial for the performance. Figure 6.25 plots the experimental data of two test runs of distributor BS with a reduced mass flow.

Another assembly specification is the requirement for an exact horizontal alignment of the structural packing in the absorber. For absorbers mounted on inclined roof tops, the exact horizontal alignment of the structural packing in the absorber casing might be done with less care. As the distributor had a width of 1 m, a maximum difference in the vertical position of both ends of the distributor of up to 10 mm was possible. This corresponded to a slope of the distributor of 0.6°.

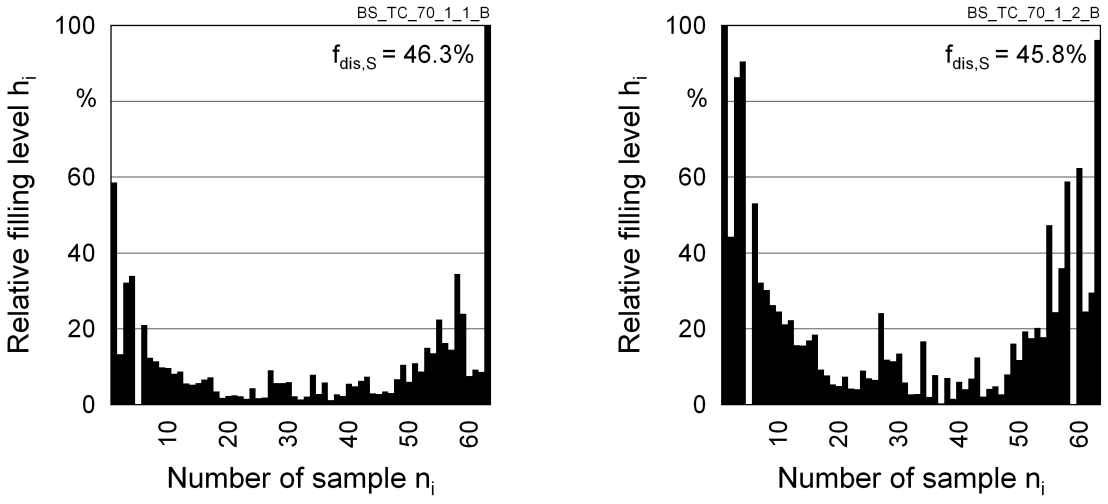

(a) (b)

Figure 6.25: *Performance of distributor BS for a reduced mass flow: relative filling levels of the test tubes for two tests (a) BS_TC_70_1_1_B (b) BS_TC_70_1_2_B*

One experimental series compared the performance of the top cover for two distributor alignments. The selected alignments were the horizontal design alignment of the distributor without any slope and the previously mentioned tilted alignment of the distributor with a slope of 0.6°. Table 6.9 lists the experimental data.

Table 6.9: *Performance of the top cover of distributor BS with different slopes of the distributor, pump: Gamma/5, stroke length: 40%, stroking rate: 4/min*

Experiment No.	**Slope** °	**Specific Mass flow** kg/(h m)	**Exp. Position**	**Distribution Factor** $f_{dis,S}$ %
BS_TC_40_4_1_A	0	0.26	A	77.4
BS_TC_40_4_2_A	0	0.26	A	77.7
BS_TC_40_4_1_B	0	0.26	B	87.7
BS_TC_40_4_2_B	0	0.26	B	86.9
BS_TC_40_4_1_A_incl	0.6	0.26	A	71.5
BS_TC_40_4_2_A_incl	0.6	0.26	A	69.2
BS_TC_40_4_1_B_incl	0.6	0.26	B	80.6
BS_TC_40_4_2_B_incl	0.6	0.26	B	78.0

The distribution factor for the top cover varied between 78% and 87% for the horizontal alignment and between 70% and 79% for the tilted alignment of the distributor with a slope of 0.6°. Therefore, the slope led to a decrease of the distribution factor of approximately 8 percentage points. This proved that the horizontal alignment of the distributor BS and consequently of the structural packing in the absorber casing is also of high importance.

A further specification for the assembly of the structured packing that might be implemented improperly and that can lead to performance losses is mounting the plates with the distributors horizontally aligned but at different heights, i.e. with a difference in their vertical position. As the assembly of the structured packing is done in a factory, a maximum difference in the vertical position of two neighboring distributors of 2 mm is possible.

One experimental series compared the performance of the top cover for two sets of relative distributor heights. In the first experimental setup, the distributors in the experimental positions A and B were located at the same height and two experiments were carried out with the design mass flow. Subsequently, the distributor in the experimental position A was located 2 mm higher than the distributor in the experimental position B and again two experiments were carried out with the design mass flow. Table 6.10 lists the experimental data.

Table 6.10: *Performance of the top cover of distributor BS at different heights, pump: Gamma/5, stroke length: 40%, stroking rate: 4/min*

Experiment No.	**Mounting Height** mm	**Specific Mass Flow** kg/(h m)	**Exp. Position**	**Distribution Factor** $f_{dis,S}$ %
BS_TC_40_4_1_A	0	0.26	A	77.4
BS_TC_40_4_1_B	0	0.26	B	87.7
BS_TC_40_4_2_A	0	0.26	A	77.7
BS_TC_40_4_2_B	0	0.26	B	86.9
BS_TC_40_4_1_A_incr	2	0.26	A	74.7
BS_TC_40_4_1_B	0	0.26	B	87.0
BS_TC_40_4_2_A_incr	2	0.26	A	73.7
BS_TC_40_4_2_B	0	0.26	B	84.3

The distribution factor difference between the distributors in the experimental positions A and B of approximately 10 percentage points in the first experimental setup with the same height of the distributors increased slightly to a distribution factor difference of 11 percentage points in the second experimental setup with the difference in height of 2 mm. Therefore, mounting neighboring distributors at slightly different heights did not have a strong influence on their distribution factors compared to the distribution factor differences between different distributors.

Evaluation of a number of distributors of the same type to compare their solution distribution factors

The multitude of available BS distributors that had been fabricated in large quantities allowed the evaluation of a number of these distributors to compare their solution distribution factors and to determine the reproducibility of the experimental data.

Each experiment tested two BS-type distributors at the same time, one in position A and the other one in position B of the experimental set-up. As all BS-type distributors were identical in design, the two solution distribution factors evaluated in one experiment should correspond approximately. Yet, the differences between the distribution factors for each experiment lay between 2 and 13 percentage points and on average at 8.8 percentage points. This shows that the measured distribution factors only gave the order of magnitude and range of the distribution factor but not an exact result. Further experiments would be necessary to evaluate the actual mean value for each experimental series. Yet, the existing analysis identified influences on the solution distribution factor of the distributor BS and determined the parameters that improve or worsen the performance of the distributor.

In summary, the experiments with the distributor BS proved that the distributor BS met the requirement for the solution distribution factor $f_{dis,S} \geq 85\%$ - but only under very specific operating conditions.

As the evaluated solution distribution factors were very close to the minimum solution distribution factor, the requirements for the proper connection between the separate distributors and the heat and mass transfer plates were very strict. The transition between distributor and plate could not degrade the distribution of the solution at all but had to pass the evenly distributed solution properly to the cooled surface of the heat and mass transfer plates. The fact that this proper connection is difficult to realize favors the concept of an integrated distributor.

Integrated Distributors with Channel Concept

Distributor ML1 Distributor ML1 integrated the bisection concept of distributor BS into the heat and mass transfer plates and avoided the requirement of a smooth transition between the separate distributor and the plate.

As the flock-coating of the heat and mass transfer plates had been removed to analyze the distribution factor directly at the outlets, all experiments with distributor ML1 were carried out with the liquid separator with flexible tubes.

Two experimental series studied the performance of distributor ML1 quantitatively. The first one evaluated the solution distribution factor of distributor ML1 for the design mass flow and the second one for twice the design mass flow. Table 6.11 lists the experimental data.

The performance of distributor ML1 lacked behind the expectations because the solution distribution factor lay only slightly above 50% for the design mass flow, see Figure 6.26. Even doubling the mass flow increased the solution distribution factor of distributor ML1 to only 56%.

Table 6.11: *Performance of the distributor ML1 for two solution mass flows, pump: Gamma/4, stroke length: 40%, stroking rates: 7/min and 15/min*

Experiment No.	**Specific Mass Flow** kg/(h m)	**Exp. Position**	**Distribution Factor** $f_{dis,S}$ %
ML1_c_40_7_2	0.25	A	50.3
ML1_c_40_7_3	0.25	A	50.8
ML1_c_40_15_2	0.55	A	55.8
ML1_c_40_15_3	0.55	A	56.5

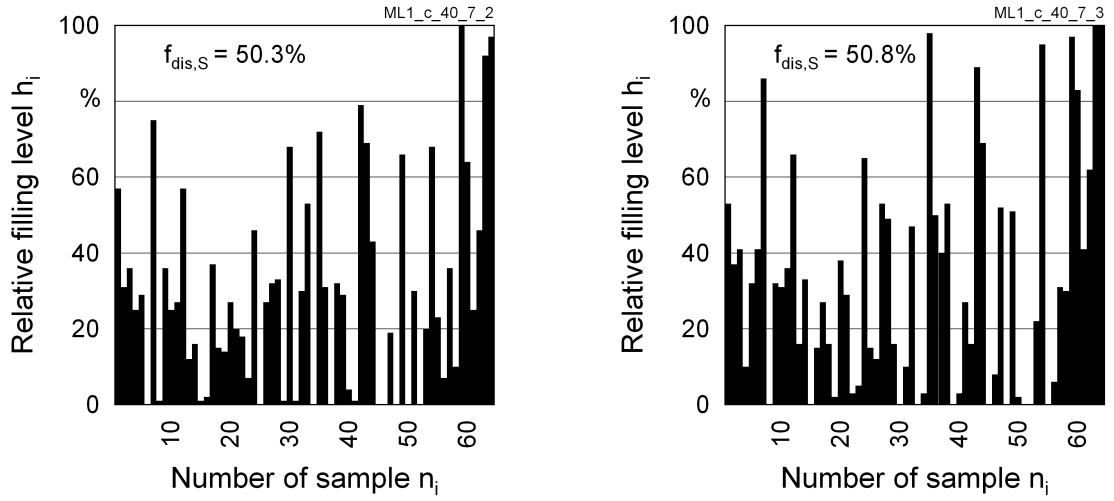

(a) (b)

Figure 6.26: *Performance of distributor ML1: relative filling levels of the test tubes for two test runs (a) ML1_c_40_15_2 (b) ML1_c_40_15_3*

The evaluation of the liquid levels of the individual samples showed that both ends of the distributor were favored in terms of the solution distribution. As the solution had to make up to three U-turns to reach the middle of the distributor and only one U-turn to reach the ends of the distributor, the inertia of the solution favored the ends of the distributor. Distributor ML2 avoided this problematic flow pattern.

Distributor ML2 Distributor ML2 improved the solution flow pattern of distributor ML1. Additional channels before the stream partitioning aligned the streams vertically and divided the U-turns into two 90°-bends.

13 tests evaluated the distribution factor of the four versions of distributor ML2 (ML2a, ML2b, ML2c and ML2d) that differed in the diameter and the position of the outlets in the horizontal outlet channel. Table 6.12 repeats the characteristics of the four versions of distributor ML2 and lists the test series carried out with them.

Table 6.12: *Characteristics and test series with the four versions of distributor ML2*

Distributor Version	Diameter of the Outlets	Vertical Position of the Outlets	Experimental Variations
ML2a	1 mm	center	specific mass flow
ML2b	1.5 mm	center	specific mass flow
ML2c	0.55 mm	top	specific mass flow, pumping parameters
ML2d	1 mm	top	specific mass flow, pumping parameters

The vertical position of the outlets in the horizontal outlet channel of the distributor **ML2a** was in the center of the horizontal channel and their diameter was 1 mm. Table 6.13 lists the data for the two sets of experiments that analyzed distributor ML2a for the design mass flow and for twice the design mass flow.

Table 6.13: *Performance of distributors ML2a for two solution mass flows, pump: Gamma/4, stroke length: 100%, stroking rates: 3/min and 7/min*

Experiment No.	Specific Mass Flow kg/(h m)	Outlet Diameter mm	Outlet Position	Distribution Factor $f_{dis,S}$ %
ML2a_c_100_3_1	0.22	1	center	57.5
ML2a_c_100_3_2	0.22	1	center	62.4
ML2a_c_100_7_1	0.55	1	center	67.2
ML2a_c_100_7_2	0.55	1	center	67.7

The performance of distributor ML2a was approximately 10 percentage points better than the performance of distributor ML1 but still far below the required 85%. For the design mass flow rate, the solution distribution factor lay at 60% and it lay at 67% for two times the design mass flow.

To study the influence of the outlet diameter, the diameter of the outlets of distributor ML2a was increased to 1.5 mm for distributor **ML2b**. Again, two sets of experiments evaluated the performance of the distributor ML2b quantitatively for the design mass flow and for twice the design mass flow to quantify the assumed decrease of the distribution factor due to the increase of the outlets' diameter. The experimental data in Table 6.14 indicate that the performance of distributor ML2b was 2 to 4 percentage points lower than the performance of distributor ML2a.

The position of the outlets of the distributors ML2a and ML2b could possibly explain the bad performance of the distributors. They were located in the center of the horizontal outlet channel. During the experiments, air bubbles were observed in the solution that remained behind the outlets and blocked them permanently. They neither deaerated through the outlets nor rose and merged with the air cushion.

Table 6.14: *Performance of distributor ML2b for two solution mass flows, pump: Gamma/4, stroke length: 100%, stroking rates: 3/min and 7/min*

Experiment No.	**Specific Mass Flow** kg/(h m)	**Outlet Diameter** mm	**Outlet Position**	**Distribution Factor** $f_{dis,S}$ %
ML2b_c_100_3_3	0.24	1.5	center	58.6
ML2b_c_100_3_2	0.24	1.5	center	57.4
ML2b_c_100_7_1	0.54	1.5	center	64.3
ML2b_c_100_7_2	0.54	1.5	center	62.6

To focus on the influence of the outlet diameter and outlet position, the diameter of the outlets of distributor **ML2c** was lowered to only 0.55 mm. Besides, the outlets were located at the top of the outlet channel to prevent the formation of air bubbles behind and above the outlets that could not be deaerated. Again, two sets of experiments evaluated the performance of the distributor ML2c quantitatively for the design mass flow and for twice the design mass. The experimental data in Table 6.15 prove that the performance of distributor ML2c was very close to the required solution distribution factor of 85%.

Table 6.15: *Performance of distributor ML2c for two solution mass flows, pump: Gamma/4, stroke length: 100%, stroking rates: 3/min and 6/min*

Experiment No.	**Specific Mass Flow** kg/(h m)	**Outlet Diameter** mm	**Outlet Position**	**Distribution Factor** $f_{dis,S}$ %
ML2c_t_100_3_1	0.23	0.55	top	84.2
ML2c_t_100_3_2	0.23	0.55	top	84.2
ML2c_t_100_6_1	0.47	0.55	top	84.2
ML2c_t_100_6_2	0.47	0.55	top	85.0

As the performance of distributor ML2c was very close to the required solution distribution factor of 85%, the analysis of the influence of the pumping parameters and identyfying the best operating conditions was the next step. Consequently, the next test series decreased the stroke length of 100% to 70% and 40% for both mass flows. Table 6.16 lists the experimental data.

The experimental results did not confirm the assumption that a shorter but more frequent stroke could improve the distribution factor. For the design mass flow, the distribution factor decreased from 84% for a stroke length of 100% to 80% for a stroke length of 70% and to 58% for a stroke length of 40%. Doubling the specific mass flow led to slightly higher distribution factors that also decreased with decreasing stroke

length from 85% for a stroke length of 100% to 81% for a stroke length of 70% and to 73% for a stroke length of 40%. Figure 6.27 plots the experimental data of the two best test runs of distributor ML2c.

Table 6.16: *Performance of distributor ML2c for different sets of pumping parameters, pump: Gamma/4*

Experiment No.	**Specific Mass Flow** kg/(h m)	**Stroke Length** %	**Stroking Rate** 1/min	**Distribution Factor** $f_{dis,S}$ %
ML2c_t_100_3_1	0.23	100	3	84.2
ML2c_t_100_3_2	0.23	100	3	84.2
ML2c_t_70_5_1	0.28	70	5	81.5
ML2c_t_70_5_2	0.28	70	5	78.6
ML2c_t_40_9_2	0.27	40	9	60.5
ML2c_t_40_9_3	0.27	40	9	56.4
ML2c_t_100_6_1	0.47	100	6	84.2
ML2c_t_100_6_2	0.47	100	6	85.0
ML2c_t_70_9_1	0.52	70	9	81.6
ML2c_t_70_9_2	0.52	70	9	79.4
ML2c_t_40_18_1	0.52	40	18	73.8
ML2c_t_40_18_2	0.52	40	18	72.6

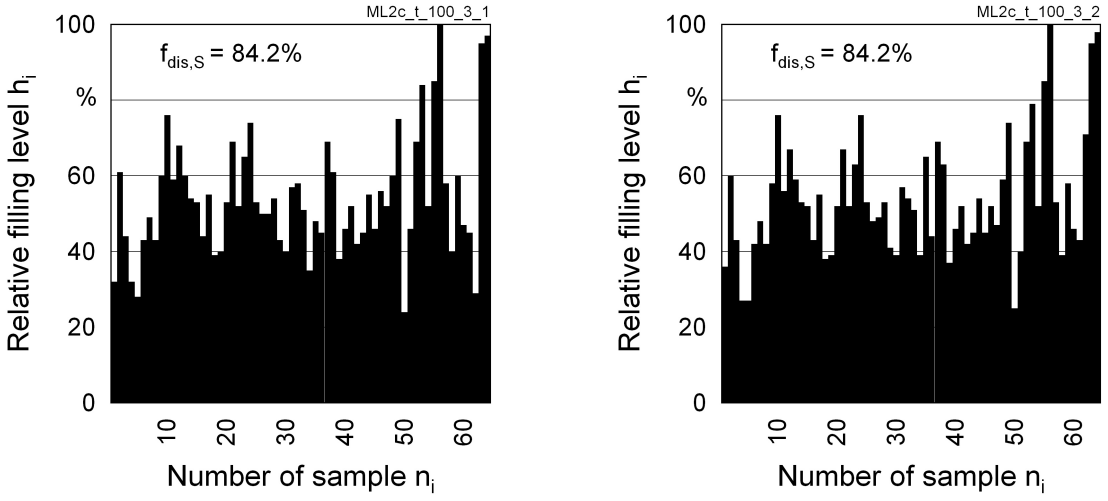

(a) (b)

Figure 6.27: *Performance of distributor ML2c: relative filling levels of the test tubes for two test runs (a) ML2c_t_100_3_1 (b) ML2c_t_100_3_2*

To separate the influence of the outlet diameter from the influence of the outlet position, distributor **ML2d** had the same outlet diameter as distributor ML2a, 1 mm, but the outlets were located at the top of the horizontal outlet channel. Again, two sets of experiments tested distributor ML2d and Table 6.17 lists the results.

Table 6.17: *Performance of distributor ML2d for two solution mass flows, pump: Gamma/4, stroke length: 100%, stroking rates: 3/min and 6/min*

Experiment No.	**Specific Mass Flow** kg/(h m)	**Outlet Diameter** mm	**Outlet Position**	**Distribution Factor** $f_{dis,S}$ %
ML2d_t_100_3_1	0.24	1	top	69.1
ML2d_t_100_3_2	0.24	1	top	68.5
ML2d_t_100_6_1	0.47	1	top	68.3
ML2d_t_100_6_2	0.47	1	top	68.9

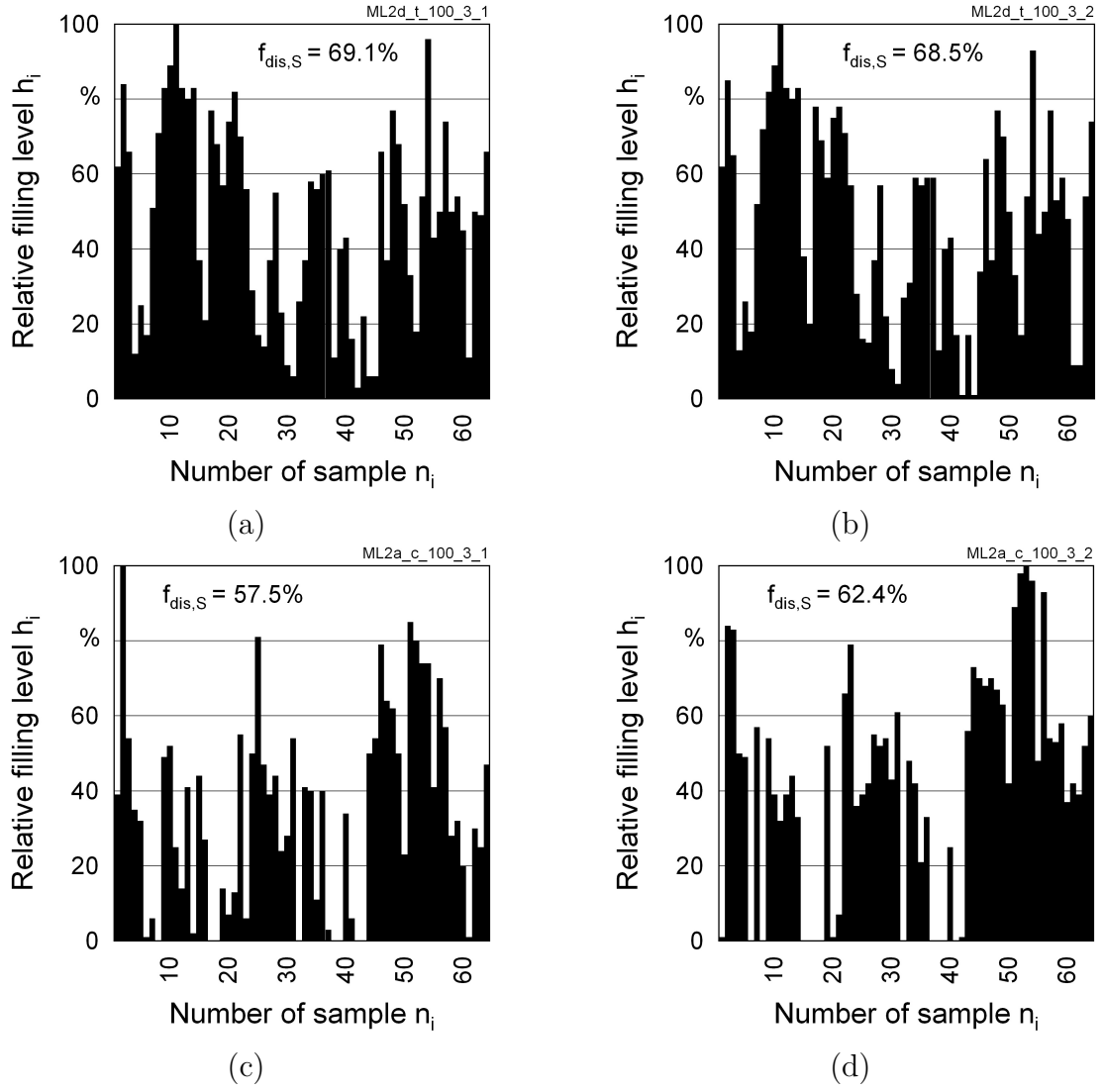

Figure 6.28: *Influence of the position of the outlets: outlets of distributor ML2d are located at the top of the horizontal outlet channel, outlets of distributor ML2a are located in the center of the outlet channel (a) ML2d_t_100_3_1 (b) ML2d_t_100_3_2 (c) ML2a_c_100_3_1 (d) ML2a_c_100_3_2*

For the same pumping parameters, the solution distribution factor of distributor ML2d lay at 69% for the design mass flow and was therefore approximately 9 percentage points better than the performance of distributor ML2a, see Figure 6.28. Yet, the solution distribution factor of distributor ML2d did not improve with an increase of the mass flow to twice the design mass flow and remained at 69%.

A possible reason for the improvement of the performance due to the position change of the outlets was that - if any - only small air bubbles could remain in the outlet channel behind the outlets and those could not block the outlets. In case of distributor ML2a, larger air bubbles remained in the outlet channel, blocked some outlets completely and thus decreased the solution distribution factor.

The change in position of the outlets improved the solution distribution factor by less than 10 percentage points, the change in outlet diameter improved the performance by approximately 15 percentage points. Therefore distributor ML2c could also be classified as distributor with outlet concept.

To prove the trend that a smaller stroke length decreased the distribution factor of the distributor type ML2, distributor ML2d was tested for the design mass flow yet with a stroke 40%. Table 6.18 compares these experimental results with the results for a stroke length of 100% and proves that the distribution factor decreased by 8 percentage points.

Table 6.18: *Performance of distributor ML2d for two sets of pumping parameters, pump: Gamma/4*

Experiment No.	**Specific Mass Flow** kg/(h m)	**Stroke Length** %	**Stroking Rate** 1/min	**Distribution Factor** $f_{dis,S}$ %
ML2d_t_100_3_1	0.24	100	3	69.1
ML2d_t_100_3_2	0.24	100	3	68.5
ML2d_t_40_9_1	0.28	40	9	61.8
ML2d_t_40_9_2	0.28	40	9	60.3

While further experiments would be necessary to evaluate the actual mean value for each experimental series, the existing analysis identified the main determining factor for the solution distribution factor of distributor ML2.

In summary, the experiments with distributor ML2 demonstrated that it was possible to successfully integrate the bisection concept into the heat and mass transfer plates. Yet, the requirement for the solution distribution factor could only be met for the small outlet diameter of 0.55 mm and under very specific operating conditions.

The experiments proved that the outlet diameter had the strongest influence and thus, distributor ML4 was built and tested, see subsection 6.4.2.

6.4.2 Distributors with Outlet Concept

Separate Distributors with Outlet Concept

Three separate distributors with outlet concept were built and tested: RE1, RE2, and RE3. Yet, only distributor RE2 was analyzed quantitatively.

Distributor RE2 Five tests assessed the performance of distributor RE2. The evaluation of distributor RE2 focused on varying the operating conditions and the alignment of the distributor. Table 6.19 lists the data for the first experimental series that tested RE2 with the design mass flow and different sets of pumping parameters.

Table 6.19: *Performance of distributor RE2, pump: Gamma/4*

Experiment No.	**Specific Mass Flow** kg/(h m)	**Stroke Length** %	**Stroking Rate** 1/min	**Distribution Factor** $f_{dis,S}$ %
RE2_100_2_1	0.23	100	2	87.3
RE2_100_2_3	0.23	100	2	87.4
RE2_70_3_1	0.25	70	3	86.9
RE2_70_3_2	0.25	70	3	86.2
RE2_50_4_1	0.21	50	4	82.3
RE2_50_4_2	0.21	50	4	86.4

The first test series showed that distributor RE2 provided the required distribution factor of 85% and that it was almost independent of the pumping parameters selection. It lay at 87% for the stroke lengths 100% and 70% and at 84% for a stroke length of 50%. Figure 6.29 plots the data of the test runs with a stroke length 100%.

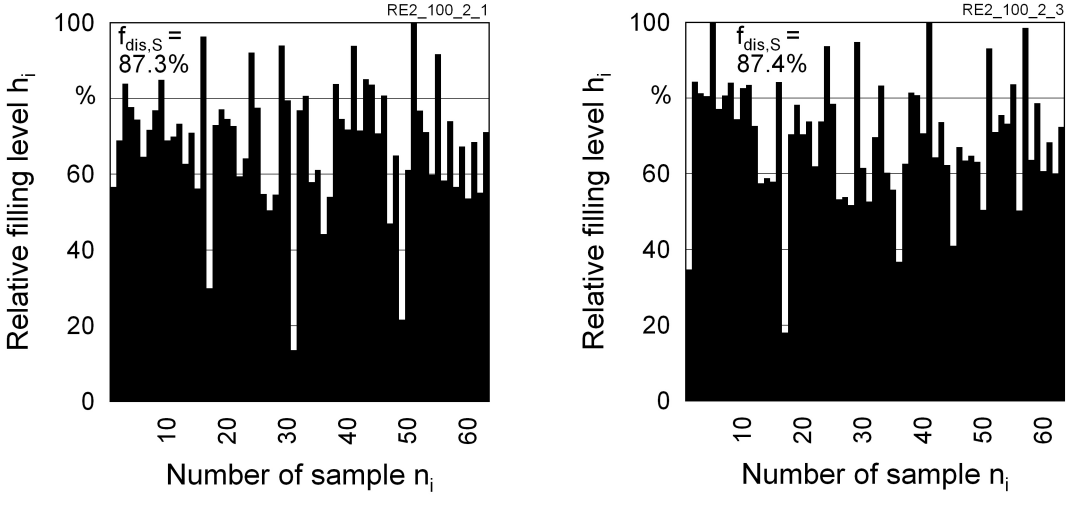

(a) (b)

Figure 6.29: *Performance of distributor RE2 (a) RE2_100_2_1 (b) RE2_100_2_3*

Distributor RE2 was also tested with a mass flow rate twice the design mass flow and as Table 6.20 shows, doubling the solution mass flow increased the solution distribution factor to 91%.

Table 6.20: *Performance of distributor RE2 with different mass flows, pump: Gamma/4, stroke length: 100%, stroking rates: 2/min and 4/min*

Experiment No.	**Specific Mass Flow** kg/(h m)	**Distribution Factor** $f_{dis,S}$ %
RE2_100_2_1	0.23	87.3
RE2_100_2_3	0.23	87.4
RE2_100_4_1	0.50	90.8
RE2_100_4_2	0.50	91.5

Analogously to the mounting test series with distributor BS, a further experiment evaluated the influence of a bad alignment of the distributor RE2 on its performance. Again, a slope of the distributor of 0.6° was tested. Table 6.21 compares the performance of a horizontally perfectly aligned distributor with a horizontally misaligned distributor with a 0.6° inclination.

Table 6.21: *Performance of distributor RE2 with different slopes of the distributor, pump: Gamma/4, stroke length: 100%, stroking rate: 2/min*

Experiment No.	**Slope** °	**Specific Mass Flow** kg/(h m)	**Exp. Position**	**Distribution Factor** $f_{dis,S}$ %
RE2_100_2_1	0	0.23	A	87.3
RE2_100_2_3	0	0.23	A	87.4
RE2_100_2_1_incl	0.6	0.24	A	88.0
RE2_100_2_2_incl	0.6	0.24	A	87.4

The experimental data showed that the inclination had no strong influence on the distribution factor. It remained in the same range of 87% to 88%. The experimental results agreed with the assumption that the performance of the distributor with outlet concept did not decrease because of the inclination. Even with a distributor inclination, the solution level rose above all outlets after the stroke from the pump as the air cushion compressed evenly. Only subsequently, as the air cushion released evenly, the solution exited the distributor uniformly through the outlets. For this level of inclination, the height difference of the outlets did not influence the distribution factor for this level of inclination.

Integrated Distributors with Outlet Concept

Four integrated distributors with outlet concept were built and tested: RE4, RE5, RE6 and ML4. Quantitatively, only distributors RE6 and ML4 were analyzed.

Distributor RE6 Out of the outer three outlets on both ends of distributor RE6, the distributor sprayed salt solution directly into the air stream rather than trickling it down the distributor surface. This resulted from the fact that both outer main vertical drills of distributor RE6 were located too close to the ends of the distributor and therefore to the inlets. Therefore, these outer three outlets on both ends of the distributor had to be sealed to prevent the spraying of the solution and only 112 outlets operated.

Due to the necessity for an alteration of the design of distributor RE6, only three experiments were carried out with distributor RE6. They evaluated the influence of the pumping parameters and tested the distributor for the design mass flow and twice the design mass flow. Table 6.22 lists the experimental data.

Table 6.22: *Performance of distributor RE6 with different mass flows and sets of pumping parameters, pump: Gamma/4*

Experiment No.	**Specific Mass Flow** kg/(h m)	**Stroke Length** %	**Stroking Rate** 1/min	**Distribution Factor** $f_{dis,S}$ %
RE6_40_4_1	0.21	40	4	79.3
RE6_40_4_2	0.21	40	4	82.4
RE6_85_3_1	0.30	85	3	79.6
RE6_85_3_2	0.30	85	3	90.3
RE6_85_4_1	0.46	85	4	87.9
RE6_85_4_2	0.46	85	4	87.5

For the design solution mass flow, the distribution factor lay at 85%. A lower stroke length of 40% and a higher stroking rate of 4 strokes per minute led to a solution mass flow of 0.21 kg/(h m) and this decreased the solution distribution factor to 81%. Figure 6.30 plots the corresponding experimental data. The solution distribution factor increased to 88% for a solution mass flow of 0.46 kg/(h m) accomplished by a stroke length of 85% and a stroking rate of 4 strokes per minute.

The experiments with distributor RE6 showed that the outlet concept could be integrated into the heat and mass transfer plates and that the distributor provided distribution factors in the demanded range. Still, the design of distributor RE6 had to be altered to prevent the solution carry-over into the air stream.

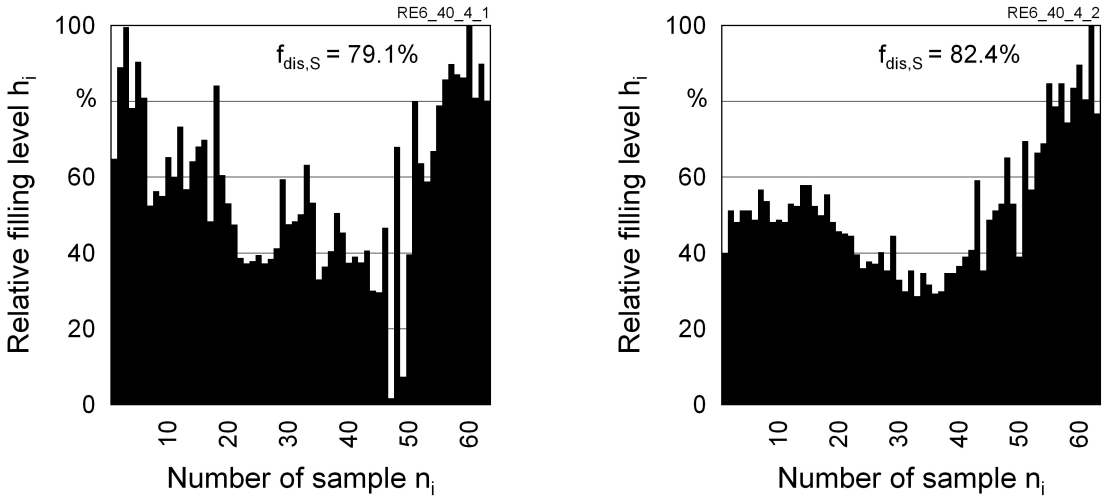

(a) (b)

Figure 6.30: *Performance of distributor RE6: relative filling levels of the test tubes for two test runs (a) RE6_40_4_1 (b) RE6_40_4_2*

Distributor ML4 Distributor ML4 avoided the small distance between the solution inlets and the outer vertical drills that caused problems with distributor RE6.

Five tests evaluated the distribution factor of the three versions of distributor ML4 (ML4a, ML4b and ML4c) that differed in the number of horizontal channels that formed the inner trough of the distributor. Table 6.23 repeats the characteristics of the three versions of distributor ML4 and lists the test series carried out with them. Table 6.24 lists the corresponding experimental data.

Table 6.23: *Characteristics and test series with the three versions of distributor ML4*

Distributor Version	Trough Channels	Trough Height	Experimental Variations
ML4a	3	17 mm	specific mass flow
ML4b	4	23 mm	specific mass flow
ML4c	6	29 mm	-

The test series with distributor ML4a showed that the solution distribution factor lay at 84% for the design mass flow and at 85% for twice the design mass flow. The additional horizontal channel in the trough of distributor ML4b slightly improved the distribution factor to 86% for the design mass flow and to 87% for twice the design mass flow. The solution distribution factor of ML4c lay at 78% for the design mass flow, 8 percentace points below the distribution factor of ML4b. Figure 6.31 plots the experimental data of the evaluation of distributor ML4b with the design mass flow.

Table 6.24: *Performance of distributors ML4a, ML4b and ML4c*

Distributor	**Experiment No.**	**Specific Mass Flow** kg/(h m)	**Stroke Length** %	**Stroking Rate** 1/min	**Distr. Factor** $f_{dis,S}$ %
ML4a	ML4a_t_25_14_1	0.27	25	14	84.0
	ML4a_t_25_14_3	0.27	25	14	83.9
	ML4a_t_25_26_1	0.51	25	26	84.8
	ML4a_t_25_26_2	0.51	25	26	84.1
ML4b	ML4b_t_25_12_1	0.27	25	12	86.4
	ML4b_t_25_12_2	0.24	25	12	85.5
	ML4b_t_25_22_1	0.45	25	22	86.9
	ML4b_t_25_22_2	0.44	25	22	86.5
ML4c	ML4c_t_30_8_1	0.23	30	8	77.5
	ML4c_t_30_8_2	0.24	30	8	77.9

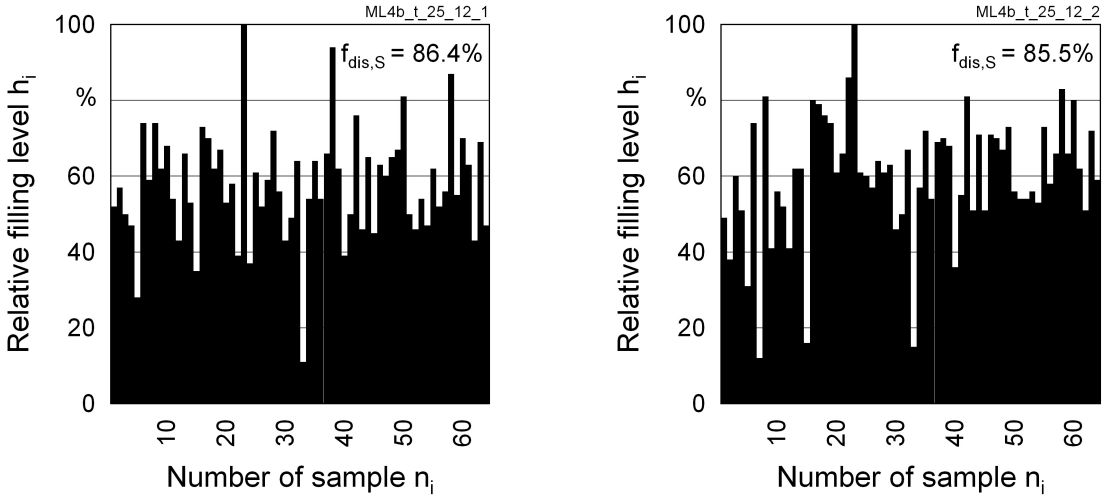

(a) (b)

Figure 6.31: *Performance of distributor ML4b: relative filling levels of the test tubes for two test runs (a) ML4b_t_25_12_1 (b) ML4b_t_25_12_2*

Comparing the all distributor experiments proved that distributor ML4b was the most suitable distributor. It provided the best experimental results and still had a relatively simple design. Figure 6.32 summarizes the experiments conducted with the specific design volume flow rate of the solution in the absorber $\dot{v}_S \approx 0.23$ l/(h m).

If this distributor ML4b is chosen for the absorber, the small diameter of the outlets requires routine maintenance of the equipment and especially continuous filtering of the solution to prevent the small outlets from clogging.

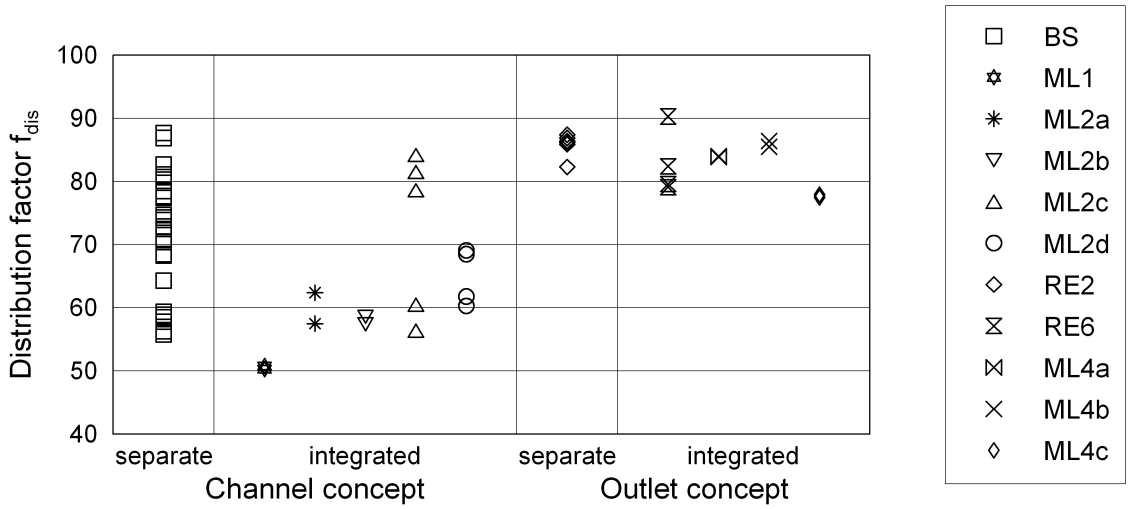

Figure 6.32: *Results of the distributor evaluation for the design solution flow*

6.5 Evaluation of the Most Promising Distributor with a Full-Scale Heat and Mass Transfer Plate

As a last step in the distributor testing, the best and yet simplest to build distributor ML4b was integrated into the upper part of a full-scale heat and mass transfer plate of 0.8 m height and 0.98 m width. This height resulted from increasing the reference height of a heat and mass transfer plate operating without maldistribution of 0.45 m, see subsection 5.1.2, by 60%, see subsection 5.2.4, because of the expected solution distribution factor of distributor ML4b of 85%, see subsection 6.4.2. Augmenting the height by an additional 10% to account for the possible fraction of the exchange plate without water cooling, see subsection 5.2.3, yielded the full-scale height of 0.8 m.

Two experimental series evaluated the solution distribution factor at the bottom of a heat and mass transfer plate. To see the exact solution rivulets on the surface, the flock-coating had been removed for the first experimental series. For the second one, the flock-coating remained on the plate. This second experimental series represented exactly the operating conditions of the distributor in combination with the plate in the absorber of the LDCS, yet without the air flow and the cooling water flow.

6.5.1 Heat and Mass Transfer Plate without Flock-Coating

Figure 6.33 shows a detail of the plain surface of the heat and mass transfer plate with the individual solution rivulets.

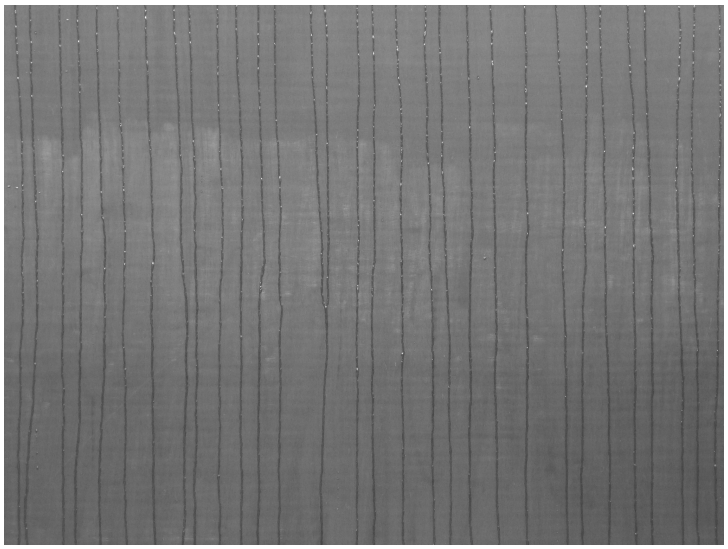

Figure 6.33: *Solution rivulets on the plain surface of the heat and mass transfer plate*

Most of the individual solution rivulets flowed in parallel and their distance roughly corresponded to the distance of the outlets of 15 mm along the complete height of the plate. Only some of the solution rivulets merged. The solution distribution factor at the bottom of the plain PP-plate allowed to find out the order of magnitude of this merging of the individual rivulets. Table 6.25 lists the parameters and results and Figure 6.34 plots the corresponding experimental data.

Table 6.25: *Performance of distributor ML4b with a full-scale and plain PP heat and mass transfer plate, pump: Gamma/4*

Experiment No.	**Specific Mass Flow** kg/(h m)	**Stroke Length** %	**Stroking Rate** 1/min	**Distribution Factor** $f_{dis,S}$ %
ML4b_FS_plain_21_14_3	0.25	21	14	65.2
ML4b_FS_plain_21_14_4	0.25	21	14	65.6

The solution distribution factor at the bottom of the heat and mass transfer plate lay at 65% and therefore about 20 percentage points below the solution distribution factor of distributor ML4b. The graphical presentation of the performance of distributor ML4b_FS_plain plotted in Figure 6.34 shows that eleven test tubes remained completely empty and did not fill with any solution. Therefore, eleven individual solution rivulets merged with a neighboring solution rivulet and did not fill their assigned test tubes.

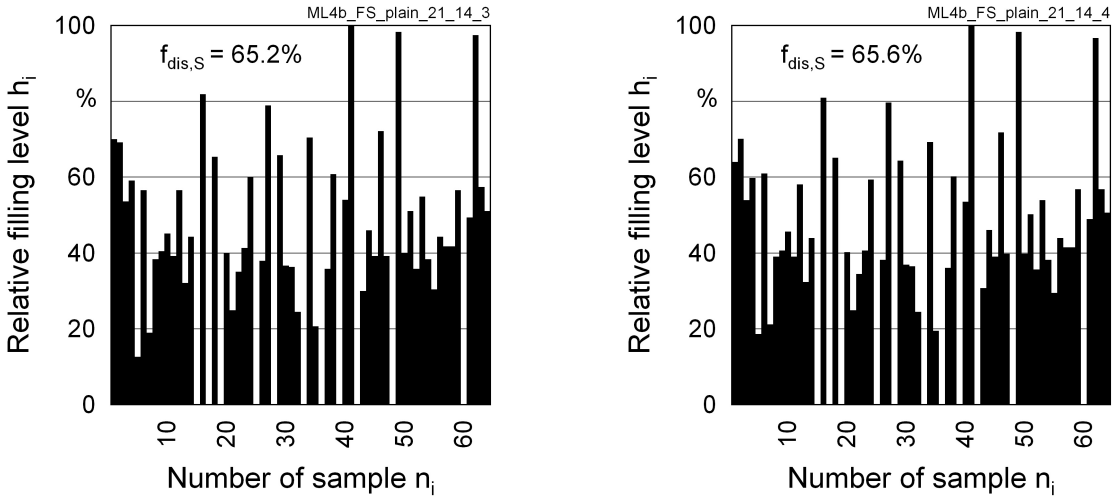

Figure 6.34: *Graphical presentation of the performance of distributor ML4b with a full-scale heat and mass transfer plate: solution distribution at the bottom of the PP-plate for two test runs (a) ML4b_FS_plain_21_14_3 (b) ML4b_FS_plain_21_14_4*

As the definition of the solution distribution factor considers an empty test tube as completely dry surface, these test tubes corresponded to a fraction of dry surface of 17%. Consequently, they already accounted for a decrease of the solution distribution factor of 17 percentage points though the upper part of the heat and mass transfer plate was wetted by solution before the rivulets merged.

Besides, this definition disregards the fact that on a plain PP-surface the rivulets wetted only a small fraction of the width they were ascribed to wet. Therefore, the second experimental series evaluated the solution distribution factor of distributor ML4b for a full-scale and flock-coated heat and mass transfer plate, the operating conditions of the distributor in combination with the plate in the absorber of a LDCS.

6.5.2 Heat and Mass Transfer Plate with Flock-Coating

Two sets of experiments analyzed the solution distribution at the bottom of the flock-coated heat and mass transfer plate with a height of 0.8 m. The first one evaluated the solution distribution factor of distributor ML4b for the design mass flow and the second one for twice the design mass flow. Table 6.26 lists the experimental data.

The solution distribution factor at the bottom of the flock-coated heat and mass transfer plate lay at 90% for the design mass flow and at 93% for twice the design mass flow. Therefore, the initial distribution of the solution on top of the plate with a distribution factor of $f_{dis,S} \approx 85\%$ did not degrade along the plate. The flock-coating also appeared to be suitable and visually, the surface always seemed well wetted.

Table 6.26: *Performance of distributor ML4b with a full-scale flock-coated heat and mass transfer plate, pump: Gamma/4*

Experiment No.	**Specific Mass Flow** kg/(h m)	**Stroke Length** %	**Stroking Rate** 1/min	**Distribution Factor** $f_{dis,S}$ %
ML4b_FS_flock_30_12_1	0.25	30	12	89.1
ML4b_FS_flock_30_12_2	0.25	30	12	88.9
ML4b_FS_flock_30_12_3	0.25	30	12	91.3
ML4b_FS_flock_30_12_4	0.25	30	12	91.0
ML4b_FS_flock_30_23_1	0.49	30	23	92.2
ML4b_FS_flock_30_23_2	0.49	30	23	93.4

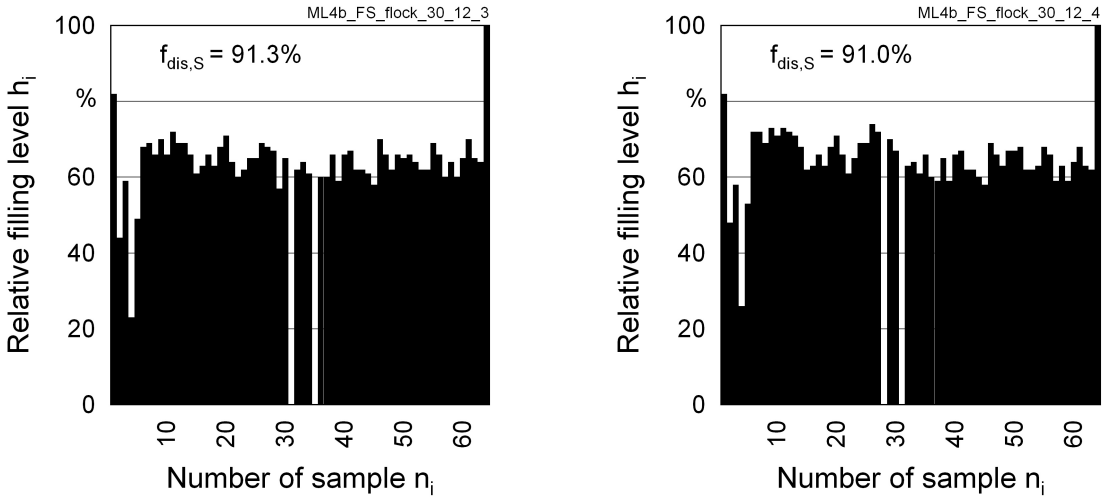

Figure 6.35: *Graphical evaluation of the performance of distributor ML4b with a full-scale heat and mass transfer plate: solution distribution at the bottom of the PP-plate for two test runs (a) ML4b_FS_flock_30_12_3 (b) ML4b_FS_flock_30_12_4*

The graphical evaluation in Figure 6.35 indicates that in both experimental runs two test tubes remained completely empty while the liquid levels in the other test tubes were roughly the same. As all distributor outlets were operating, clogging of two outlets was excluded as possible explanation. The maximum number of test tubes that remained empty in a ML4b_FS_flock experiment was three and in the other experiments only one or two test tubes did not contain any solution at all. As the position of the empty test tubes varied, a malfunction of the liquid separator with flexible tubes was also excluded as possible explanation. In a further research project, the solution flow within the flock-coating can be analyzed in more detail and the causes for the empty test tubes could be located and eliminated.

Chapter 7

Summary and Perspectives

Liquid desiccant cooling systems have a significant potential for replacing conventional vapor compression cooling systems. LDCS dehumidify the outside air by a liquid desiccant such as a concentrated lithium chloride solution and cool the dehumidified air by water evaporation. They require electricity only as auxiliary energy and do not contribute to the increasing peak electricity demand on hot days due to the growing number of installed air conditioning units.

Low temperature heat at a minimum temperature level of 70 °C drives them. This low temperature level favors heat sources not fully exploited yet such as waste heat, district heat or solar heat. Utilizing those heat sources can imply further benefits such as primary energy savings but can complicate the process engineering as they are not all continuous energy sources. Especially solar energy is a discontinuous energy source and therefore, a storage system is required to bridge the mismatch between energy demand and supply.

The volumetric energy storage capacity of a storage system is decisive for the size and the costs of the storage system. The higher this energy storage capacity is, the smaller is the storage system for the same energy content. For a given size of the storage system, the higher its energy storage capacity is, the longer it can provide driving energy for a device without the need of any additional supply.

In LDCS, the liquid desiccant itself can serve as storage medium. This is very efficient for storing energy for air dehumidification demands. Previous research verified that only a very low ratio of liquid desiccant flow to air flow leads to a sufficient energy storage in the liquid desiccant. The Bavarian Center for Applied Energy Research is developing a low-flow LDSC with energy storage driven by low temperature heat. The uniform distribution of the reduced desiccant flow, however, remains a technical challenge and no suitable distribution devices for the liquid desiccant are presently available.

The objective of the theoretical part of the present research is to analyze factors of influence on the achievable energy storage capacity in LDCS and to specify reasonable performance goals for the distribution of the process media. The objective of the experimental part is to develop a new liquid desiccant distributor that reliably meets the distribution quality required for efficient energy storage in the liquid desiccant.

The theoretical part deals with the development of a numerical model for the simulation of air dehumidification processes with a liquid desiccant, the regeneration processes of the liquid desiccant and air humidification processes in indirect evaporative coolers. The model was applied to simulate the performance of the two most common LDCS alternatives and to compare their energy storage capacities. The alternatives were the innovative low-flow LDCS and conventional high-flow LDCS that are available on the market. Figure 7.1 shows the results of the analysis of the feasible energy storage capacities for reference conditions for supply air and return air and two sets of ambient temperature and humidity conditions, representing moderate and tropical climates. The simulation clearly shows that the performance of the conventional high-flow system depends strongly on the outside humidity while it is almost independent from the ambient conditions for low-flow LDCS.

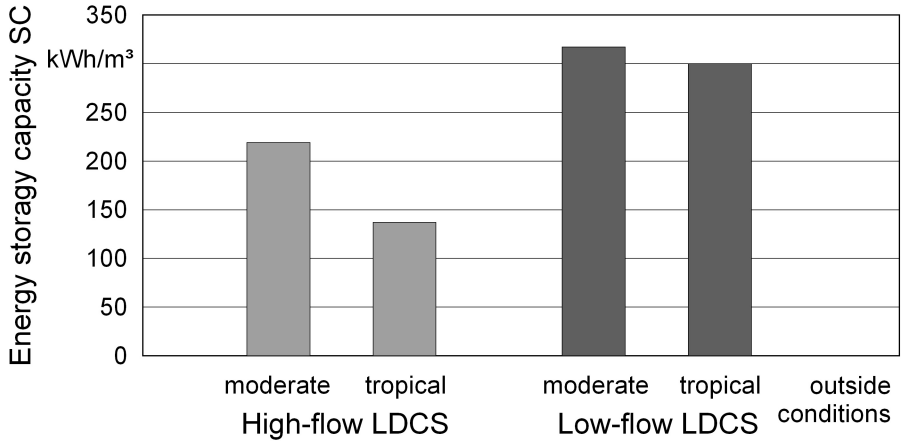

Figure 7.1: *Energy storage capacities for low-flow and high-flow LDCS for moderate and tropical reference conditions*

This research focuses on low-flow LDCS that offer the highest energy storage potential but require simultaneous cooling of the dehumidification process. This research determined the sensitivity of the energy storage capacity to maldistribution of cooling water flow, liquid desiccant flow and air flow. Maldistribution of the cooling water flow that leads to low fractions of the exchange plate without cooling water flow can easily be compensated by an increase of the height of the exchange plate, see subsection 5.2.3. Simulations show that simultaneous anti-correlated maldistribution of the liquid desiccant flow and the air flow is more severe than a co-correlated. For simulta-

neous anti-correlated maldistribution, an increase of the height of the exchange plate can compensate for a fraction of dry surface f_{dry} of up to 23% and an air bypass of 46% undehumidified air. But the required height of the exchange plate already increases rapidly with $f_{\mathrm{dry}} > 0.2$, see subsection 5.2.4. Therefore, the solution distributor in low-flow LDCS has to ensure a distribution factor of 85%, i.e. $f_{\mathrm{dry}} < 0.15$.

The experimental part of this research focuses on the analysis and further development of the solution distributors for low-flow LDCS. A new measuring system for the distribution of the solution was designed and constructed. The measuring system was tested by assessing distributors previously developed at the Bavarian Center for Applied Energy Research and the most promising distributor BS that had been utilized so far was tested for a wide range of operating conditions. This separate distributor meets the distribution requirement for the distributor itself but the transition between distributor and plate leads to a deterioration of the distribution of the solution on the plate. Therefore, the main task for the experimental development of a new liquid desiccant distributor was the integration of the distributor into the top of the heat and mass transfer plates. Base material for the development were the flock-coated heat and mass plates used for the structured packing of the absorber.

Both alternative concepts for evenly distributing the solution, the channel concept and the outlet concept, were manufactured and tested. The main design parameters were the outlet diameter and position. All distributors were tested for the design mass flow and twice the design mass flow in the absorber and various sets of operating conditions. Figure 7.2 summarizes the experiments conducted with the specific design volume flow rate of the solution in the absorber $\dot{v}_S \approx 0.23$ l/(h m).

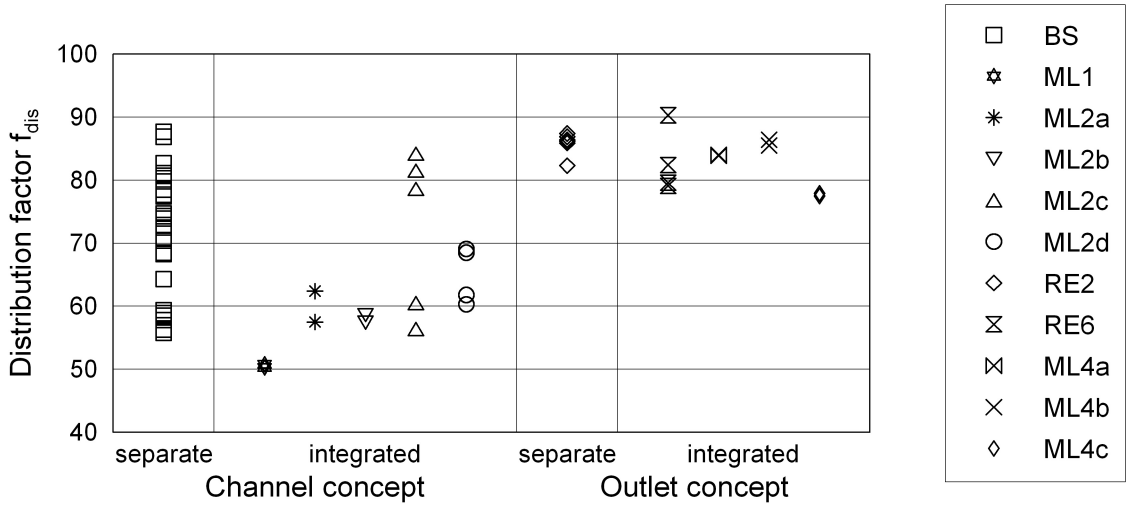

Figure 7.2: *Results of the distributor evaluation for the design solution flow*

Distributor ML4b proved to be the best and yet simplest to build distributor. It provides a solution distribution factor above the required 85% and its integration into the heat and mass transfer plate does not cause any problems.

As last step of the distributor development, distributor ML4b was integrated into the upper part of a full-scale flock-coated heat and mass transfer plate and the distribution of the solution was measured at the bottom of the plate.

At the bottom of the flock-coated heat and mass transfer plate, the solution distribution factor was as high as 90% for the design mass flow and at 93% for the double design mass flow. These results indicate that the initial distribution of the solution on top of the plate with a distribution factor of $f_{dis,S} \approx 85\%$ does not degrade along the plate. Therefore, distributor ML4b is proposed as most promising option for the distribution of the solution.

One main focus of future research will be testing the long term reliability of the distributor. The prototype distributor ML4b has been in operation for a month without interruption and without degradation of its performance but no long term experience is available yet. The small diameter of the wholes requires careful maintenance of the equipment and in turn especially continuous filtering of the solution to prevent the outlets from clogging.

Once the distributor proves to be reliable on a longer time-frame, considerations concerning production become the main research focus.

Bibliography

[AIL Research 2007]
AIL Research, Inc., Princeton, <http://www.ailr.com>, viewed 10 July 2007.

[Alizadeh and Saman 2002a]
Alizadeh, S.; Saman, W.: Modeling and Performance of a Forced Flow Solar Collector/Regenerator Using Liquid Desiccant, *Solar Energy*, vol. 72, no. 2 (2002) 143-154.

[Alizadeh and Saman 2002b]
Alizadeh, S.; Saman, W.: An Experimental Study of a Forced Flow Solar Collector/Regenerator Using Liquid Desiccant, *Solar Energy*, vol. 73, no. 5 (2002) 345-362.

[ARI 2004]
Air-Conditioning and Refrigeration Institute, Inc.: *ANSI/ARI Standard 340/360: Performance Rating of Commercial and Industrial Unitary Air-Conditioning and Heat Pump Equipment*, Arlington, Virginia, 2004.

[ASHRAE 2001]
American Society of Heating, Refrigeration and Air-Conditioning Engineers, Inc.: *2001 ASHRAE Handbook Fundamentals*, ASHRAE, Atlanta, Georgia, 2001.

[Atkins 1994]
Atkins, P. W.: *Physical Chemistry*, Oxford University Press, Oxford, 1994.

[Bales *et al.* 2005]
Bales, C.; Drück, H.; Hadorn, J.-C.; Streicher, W.: Advanced Storage Concepts for Solar Houses and Low Energy Buildings - IEA-SHC TASK 32, in *Proc. Solar World Congress 2005*, Orlando, 2005.

[Bales 2006]
Bales, C.: Solar Cooling and Storage with the Thermo-Chemical Accumulator, in *Proc. EuroSun 2006*, Glasgow, 2006.

[Berliner 1976]
Berliner, P.: *Klimatechnik*, Vogel-Verlag, Würzburg, 1976.

[Berliner 1979]
Berliner, P.: *Psychrometrie*, Verlag C. F. Müller, Karlsruhe, 1979.

[Choi and Kimura 1989]
Choi, K.; Kimura, K.: Experiments of a Dryness Storage Tank in a Solar Heated Dehumidification/Drying System of Open Cycle Absorption Type, in *Proc. Clean and Safe Energy Forever*, Kobe, 1989.

[Collier 1979]
Collier, R.: Analysis and Simulation of an Open Cycle Absorption Refrigeration System, *Solar Energy*, vol. 23, no. 4 (1979) 357-366.

[Conde 2004]
Conde, M.: Properties of aqueous solutions of lithium and calcium chlorides: formulations for use in air conditioning equipment design, *Int. J. of Thermal Sciences*, vol. 43 (2004) 367-382.

[Factor and Grossman 1980]
Factor, H.; Grossman, G.: A Packed Bed Dehumidifier/Regenerator for Solar Air Conditioning with Liquid Desiccants, *Solar Energy*, vol. 24, no. 6 (1980) 541-550.

[Feldman *et al.* 1991]
Feldman, S.; Bacchus, R.; Marsala, J.; Popelka, A.: *Integrated Gas-Fired Desiccant Dehumidification Vapor-Compression Cooling System for Residential Application. Phase 3*, Final Report for TECOGEN Inc., Waltham, 1991.

[Fumo and Goswami 2002]
Fumo, N.; Goswami, D.: Study of an Aqueous Lithium Chloride Desiccant System: Air Dehumidification and Desiccant Regenerators, *Solar Energy*, vol. 72, no. 4 (2002) 351-361.

[Gandhidasan *et al.* 1979]
Gandhidasan, P.; Sriramulu, V.; Gupta, M.: Buoyancy Effects in a Solar Regenerator, *Solar Energy*, vol. 22, no. 1 (1979) 9-14.

[Gandhidasan *et al.* 1985]
Gandhidasan, P.; Ullah, M.; Kettleborough, C.: Analysis of Heat and Mass Transfer between a Desiccant-Air System in a Packed Tower, in *Proc. ASME Winter Annual Meeting*, Miami, 1985.

[Gandhidasan *et al.* 1986]
Gandhidasan, P.; Kettleborough, C.; Ullah, M.: Calculation of Heat and Mass Transfer Coefficients in a Packed Tower Operating with a Desiccant-Air Contact System, *J. Solar Energy Engineering*, vol. 108, no. 2 (1986) 123-128.

[Goswami 2000]
Goswami, D.; Kreith, F.; Kreider, J.: *Principles of Solar Engineering*, Taylor & Francis, Philadelphia, 2000.

[Grigull 1989]
Grigull, U.: *Properties of Water and Steam in SI-Units*, Springer Verlag, Berlin, 1989.

[Gröber *et al.* 1988]
Gröber, H.; Erk, S.; Grigull, U.: *Die Grundgesetze der Wärmeübertragung*, 3rd edn, Springer, Berlin, 1988.

[Grossman and Wilk 1994]
Grossman, G.; Wilk, M.: Advanced Modular Simulation of Absorption Systems, *Int. J. of Refrigeration*, vol. 17, no. 14 (1994) 231-244.

[Gupta and Gandhidasan 1978]
Gupta, M.; Gandhidasan, P.: Open Cycle 3-ton Solar Air-Conditioner: Concept Design and Cycle Analysis, in Proc. *SUN : Mankind's Future Source of Energy*, New Delhi, 1978.

[Haim *et al.* 1992]
Haim, I.; Grossman, G.; Shavit, A.: Simulation and Analysis of an Open Cycle Absorption System for Solar Cooling, *Solar Energy*, vol. 49, no. 6 (1992) 515-534.

[Hancocks 2003]
Hancocks, P.: Deregulation to blame for blackouts?, CNN, Atlanta, Georgia, <http://www.cnn.com/2003/WORLD/europe/09/29/italy.blackout.hancocks/>, viewed 15 March 2005.

[Hardon 2006]
Hardon, J.-C.: IEA Solar Heating and Cooling Programme - Task 32: Advanced Storage Concepts for Solar and Low Energy Buildings, in *Proc. ECOSTOCK*, Tenth International Conference on Thermal Energy Storage, Stockton, USA, 2006.

[Hauer 2007a]
Hauer, A.: Sorption Theory for Thermal Energy Storage, in *Thermal Energy Storage for Sustainable Energy Consumption*, ed H. Paksoy, Springer, Dordrecht, 2007.

[Hauer 2007b]
Hauer, A.: Adsorption Systems for Thermal Energy Storage - Design and Demonstration Projects, in *Thermal Energy Storage for Sustainable Energy Consumption*, ed H. Paksoy, Springer, Dordrecht, 2007.

[Hawlader *et al.* 1993]
Hawlader, M.; Novak, K.; Wood, B.: Unglazed Collector/ Regenerator Performance for Solar Assisted Open Cycle Absorption Cooling, *Solar Energy*, vol. 50, no. 1 (1993) 59-73.

[Heinrich 1997]
Heinrich, G.; Franzke, U.: *Sorptionsgestützte Klimatisierung: Entfeuchtung und DEC in der Klima-Kälte-Technik*, C. F. Müller Verlag, Heidelberg, 1997.

[Hellmann and Grossman 1995]
Hellmann, H.; Grossman, G.: Simulation and Analysis of an Open-Cycle Dehumidifier - Evaporator - Regenerator (DER) Absorption Chiller for Low Grade Heat Utilization, *Int. J. of Refrigeration*, vol. 18, no. 3 (1995) 177-189.

[Henning 2004]
Henning, H.: Solar Assisted Air-Conditioning of Buildings, in *Proc. EuroSun2004*, Freiburg, 2004.

[Hublitz *et al.* 2006]
Hublitz, A.; Lävemann, E.; Peltzer, M.: Solare sorptionsgestützte Klimatisierung eines Fabrikgebäudes in Singapur - erste Betriebserfahrungen, in *Proc. 16. Symposium Thermische Solarenergie*, Bad Staffelstein, 2006.

[IEA 2003]
International Energy Agency: *Cool Appliances, Policy Strategies for Energy Efficient Homes*, IEA Publications, Paris, 2003.

[Incropera *et al.* 2007]
Incropera, F.; DeWitt, D.; Bergmann, T.; Lavine, A.: *Fundamentals of Heat and Mass Transfer*, 6th edn, John Wiley & Sons, Inc., New York, 2007.

[IPCC 2007]
Intergovernmental Panel on Climate Change: *Climate Change 2007: The Physical Science Basis, Contribution of Working Group I to the Fourth Assessment Report of the Intergovernmental Panel on Climate Change*, Geneva, <http://www.ipcc.ch/>, viewed 21 May 2007.

[Jeffus 2004]
Jeffus, L.: *Refrigeration and Air Conditioning - An Introduction to HVAC/R*, Pearson Education, Upper Saddle River, New Jersey, 1997.

[Kakabaev and Khandurdiev 1969]
Kakabaev, A.; Khandurdiev, A.: Absorption Solar Refrigeration Unit with Open Regeneration of Solution, *Applied Solar Energy*, vol. 5, no. 4 (1969) 69-72.

[Kakabaev *et al.* 1972]
Kakabaev, A.; Klyshchaeva, O.; Khandurdiev, A.: Refrigeration Capacity of an Absorption Solar Refrigeration Plant with Flat Glazed Solution Regenerator, *Applied Solar Energy*, vol. 8, no. 2 (1972) 90-95.

[Kammermaier 2008]
Kammermaier, F.: *Maldistribution in Packungskolonnen*, Dissertation, Technische Universität München, München, 2008, to be published.

[Kapfhammer 1997]
Kapfhammer, C.: *Experimentelle Untersuchung und Bewertung von Austauschflächen für Sorptionsentfeuchter*, Diplomarbeit, Fachhochschule München, München, 1997.

[Kapur 1960]
Kapur, J.: A Report on the Utilization of Solar Energy for Refrigeration and Air-Conditioning Application, *Solar Energy*, vol. 4, no. 1 (1960) 39-47.

[Kato 2007]
Kato, Y.: Chemical Energy Conversion Technologies for Efficient Energy Use, in *Thermal Energy Storage for Sustainable Energy Consumption*, ed H. Paksoy, Springer, Dordrecht, 2007.

[Keßling 1997]
Keßling, W.: *Luftentfeuchtung und Energiespeicherung mit Salzlösungen in offenen Systemen*, VDI Verlag, Düsseldorf, 1997.

[Keßling *et al.* 1998]
Keßling, W.; Laevemann, E.; Kapfhammer, C.: Energy Storage for Desiccant Cooling Systems Component Development, *Solar Energy*, vol. 64 (1998) 209-221.

[Khelifa and Sizmann 1989]
Khelifa, N.; Sizmann, R.: Combined Open Loop Refrigeration and Air-Conditioning by Low Temperature Solar Process Heat, in *Proc. Clean and Safe Energy Forever*, Kobe, 1989.

[Khelifa *et al.* 1990]
Khelifa, N.; Lävemann, E.; Milasinovis, T.; Sizmann, R.: Raumklimatisierung im offenen Umlauf mit Niedertemperaturwärme, in *Proc. 7. Internationales Sonnenforum*, Frankfurt, 1990.

[Kourouma 1998]
Kourouma, S.: *Experimentelle Untersuchungen eines offenen Absorptionssystems zur Klimatisierung in tropischen Ländern*, Shaker Verlag, Aachen, 1998.

[Lävemann *et al.* 1993]
Lävemann, E.; Keßling, W.; Röhle, B.; Kink, C.: *Klimatisierung über Sorption*, Endbericht zur Phase I des Forschungsvorhabens Nr. 032 9151 B des BMFT, Fraunhofer Instituts für Solare Energiesysteme, Freiburg und Ludwig-Maximilians-Universität München, Sektion Physik, LS Prof. Sitzmann, München, 1996.

[Lävemann *et al.* 1996]
Lävemann, E.; Keßling, W.; Peltzer, M.: *Solarunterstützte Klimatisierung über Sorption*, Endbericht zur Phase II des Forschungsvorhabens Nr. 032 9151 F des BMBF, Bayerisches Zentrum für Angewandte Energieforschung e.V., München, 1996.

[Lävemann *et al.* 2006]
Lävemann, E.; Peltzer, M.; Hublitz, A.; Krönauer, A.; Raab, U.; Hauer, A.: Raumklimatisierung und Kältespeicherung in offenen Sorptionssystemen, in *Proc. Statusseminar Thermische Energiespeicherung - mehr Energieeffizienz zum Heizen und Kühlen*, Freiburg, 2006.

[Lenz *et al.* 1987]
Lenz, T.; Löf, G.; Patnaik, S.: *Design and Testing a Solar Cooling System Employing Liquid Desiccants: Dehumidifier Experiments in Colorado State University Solar House II: Final Report, 1986-1987*, Final Report for DOE Contract, FG03-86SF16306, Colorado State University, 1987.

[Löf 1955a]
Löf, G.: Cooling with Solar Energy, in *Proc. Congress on Solar Energy*, Tucson, 1955.

[Löf 1955b]
Löf, G.: House Heating and Cooling with Solar Energy, in *Solar Energy Research*, University of Wisconsin Press, Madison, (1955) 33-46.

[Lottner 2006]
Lottner, V.: IEA Implementing Agreement Energy Conservation Through Energy Storage - Overview, in *Proc. ECOSTOCK*, Tenth International Conference on Thermal Energy Storage, Stockton, USA, 2006.

[Lowenstein *et al.* 1988]
Lowenstein, A.; Marsala, J.; Spatz, M.; Feldman, S.; Tandler, J.: *Integrated Gas-*

Fired Desiccant Dehumidification Vapor-Compression Cooling System for Residential Application. Phase 1, Final Report for TECOGEN Inc., Waltham, 1988.

[Lowenstein and Dean 1992]
Lowenstein, A.; Dean, M.: The Effect of Regenerator Performance on a Liquid Desiccant Air Conditioner, in *ASHRAE Transactions*, vol. 98 (1992) 704-711.

[Lowenstein 1993]
Lowenstein, A.: Liquid Desiccant Air Conditioners, Refrigeration and Air-Conditioning, in *Proc. Non-Fluorocarbon Refrigeration and Air Conditioning Technology Workshop*, Breckenridge, 1993.

[Lowenstein 1994]
Lowenstein, A.: *Low-Flow Internally-Cooled Liquid-Desiccant Absorber*, United States Patent #5351497, US Patent and Trademark Office, 1994.

[Lowenstein *et al.* 1998]
Lowenstein, A.; Slayzak, S.; Ryan, J.; Pesaran, A.: *Advanced Commercial Liquid Desiccant Technology Development Study*, National Renewable Energy Laboratory, Golden, 1998.

[Lowenstein *et al.* 2005]
Lowenstein, A.; Marsala, J.; Spatz, M.; Feldman, S.; Tandler, J.: *High Efficiency Liquid-Desiccant Regenerator for Air Conditioning and Industrial Drying*, Final Report for US-Department of Energy DOE/GO/13170-1, Princeton, 2005.

[Lowenstein *et al.* 2006]
Lowenstein, A.; Slayzak, S.; Kozubal, E.; Feldman, S.; Tandler, J.: A Zero-Carryover Liquid Desiccant Air Conditioner for Solar Applications, in *Proc. ASME Internation Solar Energy Conference*, Denver, 2006.

[MacCracken 2006]
MacCracken, M.: Ice Thermal Storage and LEED Gold, in *Proc. ECOSTOCK*, Tenth International Conference on Thermal Energy Storage, Stockton, USA, 2006.

[Martin and Goswami 1999]
Martin, V.; Goswami, D.: Heat and Mass Transfer in Packed Bed Liquid Desiccant Regenerators - An Experimental Investigation, *J. Solar Energy Engineering*, vol. 121, no. 3 (1999) 162-170.

[Mehling and Cabeza 2007]
Mehling, H.; Cabeza, L.: Phase Change Materials and Their Basic Properites, In: *Thermal Energy Storage for Sustainable Energy Consumption*, ed H. Paksoy, Springer, Dordrecht, 2007.

[Mehling *et al.* 2007]
Mehling, H.; Cabeza, L.; Yamaha, M.: Application of PCM for Heating and Cooling in Buildings, In: *Thermal Energy Storage for Sustainable Energy Consumption*, ed H. Paksoy, Springer, Dordrecht, 2007.

[Mersmann *et al.* 2005]
Mersmann, A.; Kind, M.; Stichlmair, J.: *Thermische Verfahrenstechnik*, Springer-Verlag, Berlin, 2005.

[Mesquita *et al.* 2004]
Mesquita, L.; Thomey, D.; Harrison, S.: Modeling of Heat and Mass Transfer in Parallel Plate Liquid Desiccant Dehumidifier, in *Proc. EuroSun2004*, Freiburg, 2004.

[Mesquita and Harrison 2005]
Mesquita, L.; Harrison, S.: Non-Isothermal Flate-Plate Liquid Desiccant Regenerators: A Numerical Study, in *Proc. Solar World Congress 2005*, Orlando, 2005.

[Mullick and Gupta 1974]
Mullick, S.; Gupta, M.: Solar Desorption of Absorbent Solutions, *Solar Energy*, vol. 16, no. 1 (1974) 19-24.

[Munters 2007]
Munters GmbH, Hamburg, <http://www.munters-luftentfeuchtung.de>, viewed 21 May 2007.

[Nelson *et al.* 1986]
Nelson, D.; Wood, B.; Collier, R.: *Open-cycle Absorption Solar Cooling, Part II, Heat and Mass Transfer Analysis for Glazed Collector/Regeneration*, Final Report for DOE Contract, DOE AC03-84SF12223 N001, Arizona State University, 1986.

[Nelson and Wood 1990]
Nelson, D.; Wood, B.: Evaporation Rate Model for a Natural Convection Glazed Collector/Regenerator, *J. Solar Energy Engineering*, vol. 112, no. 1 (1990) 51-57.

[Niagara Blower Company 2007]
Niagara Blower Company, Buffalo, <http://www.niagarablower.com>, viewed 10 July 2007.

[Nordell and Skogsberg 2007]
Nordell, B.; Skogsberg, K.: The Sundsvall Snow Storage - Six Years of Operation, in *Thermal Energy Storage for Sustainable Energy Consumption*, ed H. Paksoy, Springer, Dordrecht, 2007.

[Novak *et al.* 1985]
Novak, K.; Wood, B.; Nelson, D.: Experimentally Determined Correlations for Solar Collector/Regenerator Heat and Mass Transfer, in *Proc. ASME Annual Winter Meeting*, Miami, 1985.

[Novak and Wood 1985]
Novak, K.; Wood, B.: Solar Collector/Regenerator Performance Based on Experimental Heat and Mass Transfer Correlations, in *Proc. Intersol 85*, Montreal, 1985.

[Novak *et al.* 1986]
Novak, K.; Wood, B.; Nelson, D.: *Open-cycle Absorption Solar Cooling, Part I, Combined Heat and Mass Transfer on an Open Flow Liquid Absorbent Solar Collector/Regenerator*, Final Report for DOE Contract, DOE AC03-84SF12223 N001, Arizona State University, 1986.

[Öberg and Goswami 1998]
Öberg, V.; Goswami, D.: Experimental Study of the Heat and Mass Transfer in a Packed Bed Liquid Desiccant Air Dehumidifier, *J. Solar Energy Engineering*, vol. 120, no. 4 (1998) 289-297.

[Okumiya and Paksoy 2006]
Okumiya, M.; Paksoy, H.: Sustainable Cooling with Thermal Energy Storage - From IEA ECES Annex 14 to IEA ECES Annex 20, in *Proc. ECOSTOCK*, Tenth International Conference on Thermal Energy Storage, Stockton, USA, 2006.

[Patnaik *et al.* 1990]
Patnaik, S.; Lenz, T.; Löf, G.: Performance Study for an Experimental Solar Open-Cycle Liquid Desiccant System, *Solar Energy*, vol. 44, no. 3 (1990) 123-135.

[Pesaran 1993]
Pesaran, A.: A Review of Desiccant Dehumidification Technology, in *Proc. Electric Dehumidification: Energy Efficient Humidity Control for Commercial and Institutional Buildings Conference*, New Orleans, 1993.

[Peng and Howell 1981]
Peng, C.; Howell, J.: Analysis and Design of Efficient Absorbers for Low-Temperature Desiccant Air-Conditioners, *J. Solar Energy Engineering*, vol. 103, no. 4 (1981) 331-338.

[Peng and Howell 1984]
Peng, C.; Howell, J.: The Performance of Various Types of Regenerators for Liquid Desiccants, *J. Solar Energy Engineering*, vol. 106, no. 2 (1984) 133-141.

[Perry 1998]
Perry, R.: *Perry's chemical engineers' handbook*, 7th edn, McGraw-Hill, New York, 1998.

[Recknagel 1997]
Recknagel, H.; Sprenger, E.; Schramek, E.: *Taschenbuch für Heizung + Klimatechnik*, R. Oldenbourg Verlag, München, 1997.

[Robinson 1978a]
Robinson, H.: Liquid Sorbent Solar Air-Conditioner, in *Proc. Miami International Conference: Alternative energy sources*, Washington D.C., 1978.

[Robinson 1978b]
Robinson, H.: Liquid Desiccant Solar Heat Pumps for Developing Nations, in *Proc. International Symposium, Workshop on Solar Energy*, Cairo, 1978.

[Robinson 1983]
Robinson, H.: Operational Experience with a Liquid Desiccant Heating and Cooling System, in *Proc. 18th International Energy Conversion Engineering Conference*, Orlando, 1983.

[Saman and Alizadeh 2001]
Saman, W.; Alizadeh, S.: Modeling and Performance Analysis of a Cross-Flow Type Plate Heat Exchanger for Dehumidification/Cooling, in *Solar Energy*, vol. 70, no. 4 (2001) 361-372.

[Saman and Alizadeh 2002]
Saman, W.; Alizadeh, S.: An Experimental Study of a Cross-Flow Type Plate Heat Exchanger for Dehumidification/Cooling, *Solar Energy*, vol. 73, no. 1 (2002) 59-71.

[Scalabrin and Scaltriti 1988]
Scalabrin, G.; Scaltriti, G.: Modeling and Experimental Analysis of an Efficient Absorber for Air Dehumidification, *Heat and Mass Transfer*, vol. 22 (1988) 111-124.

[Scalabrin and Scaltriti 1990]
Scalabrin, G.; Scaltriti, G.: A Liquid Sorption-Desorption System for Air Conditioning with Heat at Lower Temperature, *J. Solar Energy Engineering*, vol. 112, no. 2 (1990) 70-75.

[Siebe *et al.* 1986]
Siebe, D.; Wood, B.; Collier, R.: *Open-cycle Absorption Solar Cooling, Part III, Evaluation of Air-Conditioning Systems Utilizing Liquid Absorbents Regenerated*

by Solar Energy, Final Report for DOE Contract, DOE AC03-84SF12223 N001, Arizona State University, 1986.

[So'Brien and Satcunanathan 1989]
So'Brien, G.; Satcunanathan, S.: Performance of a Novel Liquid Desiccant Dehumidifier/Regenerator System, *J. Solar Energy Engineering*, vol. 111, no. 4 (1989) 345-352.

[Solid 2006]
Solarenergie Informations- und Demonstrationszentrum: *Marktübersicht Solarspeicher 2007*, Solarpraxis, Berlin, 2006.

[Steimle 2000]
Steimle, F.: *Handbuch Haustechnische Planung*, Karl Krämer Verlag, Stuttgart, 2000.

[Steinmann *et al.* 2005]
Steinmann, W.-D.; Eck, M.; Laing, D.: Solarthermal Parabolic Trough Power Plants with Integrated Storage Capacity, *Int. J. Energy Technology and Policy*, vol. 3, no. 1/2 (2005) 123-136.

[Stevens *et al.* 1989]
Stevens, D.; Braun, J.; Klein, S.: An Effectiveness Model of Liquid Desiccant System Heat/Mass Echange, *Solar Energy*, vol. 42, no. 6 (1989) 449-455.

[Stichlmair and Fair 1998]
Stichlmair, J.G.; Fair, J.R.: *Distillation*, WILEY-VCH, Weinheim, 1998.

[TEPCO 2003]
Tokyo Electric Power Company: *TEPCO ILLUSTRATED*, Corporate Communications dept., Tokyo, 2003.

[Ullah *et al.* 1988]
Ullah, M. ; Kettleborough, C. ; Gandhidasan, P.: Effectiveness of Moisture Removal for an Adiabatic Counterflow Packed Tower Absorber Operating with $CaCl_2$-Air Contact System, *J. Solar Energy Engineering*, vol. 111, no. 2 (1988) 98-101.

[Urbaneck *et al.* 2006a]
Urbaneck, T.; Schirmer, U.; Platzer, B.; Uhlig, U; Göschel, T.; Zimmermann, D.: Optimal Design of Chiller Units and Cold Water Storages for District Cooling Systems, in *Proc. ECOSTOCK*, Tenth International Conference on Thermal Energy Storage, Stockton, USA, 2006.

[Urbaneck *et al.* 2006b]
Urbaneck, T.; Platzer, B.; Schirmer, U.; Barthel, U.; Uhlig, U; Zimmermann, D.; Göschel, T.: Kältespeicher - Einsatz zur Optimierung der Energieversorgung, in *Proc. Statusseminar Thermische Energiespeicherung - mehr Energieeffizienz zum Heizen und Kühlen*, Freiburg, 2006.

[VDI 1997]
VDI-Wärmeatlas, 8th edn, VDI-Gesellschaft Verfahrenstechnik und Chemieingenieurwesen (GVC), Springer, Düsseldorf, 1997.

[Waide 2004]
Waide, P.: Keeping your cool: an overview of trends, in *Proc. Cooling Buildings in a Warming Climate*, Sophia Antipolis, France, 2004.

[Wille and Lottner 2006]
Wille, A.; Lottner, V.: R+D Programme on TES in Germany, in *Proc. ECOSTOCK*, Tenth International Conference on Thermal Energy Storage, Stockton, USA, 2006.

[Wood *et al.* 1983a]
Wood, B.; Siebe, D.; Novak, K.: *Performance Characteristics of Open-Flow Liquid Desiccant Solar Collector/Regenerator for Solar Cooling Applications, Part I, Two Dimensional Analysis of Heat and Mass Transfer for Open Flow Over Rough Inclined Surfaces* Final Report for DOE Contract, DOE AC03-82SF11691 N001, Arizona State University, 1983.

[Wood *et al.* 1983b]
Wood, B.; Siebe, D.; Applebaum, M.; Novak, K.; Ballew, L.: *Performance Characteristics of Open-Flow Liquid Desiccant Solar Collector/Regenerator for Solar Cooling Applications, Part II, System Simulation and Performance Measurements.*, Final Report for DOE Contract, DOE AC03-82SF11691 N001, Arizona State University, 1983.

[Yang and Wang 2001]
Yang, R.; Wang, P.: A Simulation Study of Performance Evaluation of Single-Glazed and Double-Glazed Collectors/Regenerators for an Open-Cycle Absorption Solar Cooling System, *Solar Energy*, vol. 71, no. 4 (2001) 263-268.

[Yang and Yan 1989]
Yang, R.; Yan, W.: Simulation Study for an Open Cycle Absorption Solar Cooling System Operated in Humid Areas, in *Proc. Clean and Safe Energy Forever*, Kobe, 1989.